CRANFIELD UNIVERSITY

SAMUEL THOMAS HOULKER

SCALE UP OF HOLLOW FIBRE MEMBRANE CONTACTORS FOR BIOGAS UPGRADING

SCHOOL OF WATER, ENERGY AND ENVIRONMENT
Cranfield Water Science Institute

EngD
Academic Year: 2014 - 2018

Primary Supervisor: Dr Ewan McAdam
Associate Supervisor: Dr Marc Pidou

March 2019
CRANFIELD UNIVERSITY

SCHOOL OF WATER, ENERGY AND ENVIRONMENT
Cranfield Water Science Institute

EngD

Academic Year 2014 - 2018

SAMUEL THOMAS HOULKER

SCALE UP OF HOLLOW FIBRE MEMBRANE CONTACTORS FOR BIOGAS UPGRADING

Primary Supervisor: Dr Ewan McAdam
Associate Supervisor: Dr Marc Pidou
March 2019

This thesis is submitted in partial fulfilment of the requirements for the degree of EngD

Abstract

Hollow fibre membrane contactors (HFMC) are a gas-liquid contacting technology suggested as a successor to existing gas-liquid absorption columns for the selective separation of carbon dioxide (CO_2) from biogas i.e. biogas upgrading, which in the United Kingdom (UK) is a rapidly expanding sector for renewable heat production. Current incentivisation schemes also encourage process innovation to reduce cost, and those that enable the revaluation of waste. In response to these drivers, this thesis firstly describes the implementability of HFMC as a successor technology to packed columns for biogas upgrading, due to its capability for process intensification, and subsequently introduces how to employ environmentally sourced ammonia to drive chemical absorption in HFMC, thereby extending process intensification, whilst also reducing aeration costs and through a unique contribution of the membrane, enables the crystallisation of ammonium bicarbonate which can increase value as a new product. This thesis has introduced an assessment of mass transfer in multi-module configurations to further intensify the process and demonstrated that when producing a high purity methane product, a simplified mass transfer model, based on the overall mass transfer coefficient, can be used to determine gas product quality, process scale and membrane configuration. Mass transfer behaviour in commercially favoured transverse flow HFMC modules was compared to parallel flow HFMC modules, typically used in laboratory investigation which are known to suffer from maldistribution, to enable the reconciliation of maldistribution with a description of parallel flow and the translation of the overall mass transfer coefficient across module scale. The resilience of HFMC to industrial conditions, including gas-phase contaminants such as particulates, was assessed at a WWTW, demonstrating the primary mechanism of fouling to arise from the absorbent, in particular biological adsorption and clogging of the shell-side, which is readily reversible through chemical cleaning. Integration of an NH_3 chemically reactive absorbent for the co-production of a high purity methane product and recovery of ammonium bicarbonate demonstrates that the reduction in specific nucleation rate and preferential crystal growth in HFMC protects the system from blocking by the reaction product, in contrast the high specific nucleation rate and subsequent agglomeration of the reaction product induces process blocking during column operation.

Keywords: multi-module design, maldistribution, cascade, dimensionless correlation, resistance, pre-filtration, membrane fouling, membrane crystallisation, ammonia, ammonium bicarbonate

Acknowledgments

Thank you to the Engineering and Physical Sciences Research Council, Northumbrian Water, Severn Trent and Anglian Water which provided both financial and practical support and interest that made this project possible. In particular, the industrial representatives Andrew Moore, Peter Vale and Adam Brookes for their enthusiasm and cooperation. I'd like to extend particular thanks to Tony Rutherford and Daniel Heron of Northumbrian Water for all their help onsite and for making me feel welcome.

At Cranfield I'd like to thank Ewan McAdam, for both his academic supervision and for forcing my personal development, I certainly owe him a lot. I'd also like to thank Marc Pidou for his enthusiasm and the rest of Cohort VI for their friendship. Additionally, I'd like to thank Mehrez Hermassi for his infinite patience in the lab and friendship.

At home I'd like to thank my parents for putting up with me for 3 months whilst I wrote this, my siblings for their proof reading and Anna and her family for the welcome distraction. Finally, Molly without whose influence this document would have been finished far sooner.

Table of Contents

List of Figures

Chapter 1

Chapter 2

Chapter 3

Chapter 4

Chapter 7

List of Tables

Notations

A	Correlation constant	-
A	Specific surface area	$m^2\ m^{-3}$
A_m	Membrane surface area	m^2
C	Concentration	$mol\ m^{-3}$
°C	Celsius	-
C*	Concentration at supersaturation	$mol\ /\ g\ L^{-1}$
C/C*	Supersaturation ratio	-
D_{st}	Diffusivity	$m^2\ s^{-1}$
d_h	Characteristic length	m
E	Enhancement factor	-
G	Crystal growth rate	$m\ s^{-1}$
Gz	Graetz number	-
$\Delta_{sol}H$	Enthalpy of dissolution	$J\ mol^{-1}$
H	Henry's constant	$mol\ L^{-1}\ atm^{-1}$
Ha	Hatta number	-
ID	Internal diameter	m
J	Flux	$mol\ m^2\ s^{-1}$
K	Kelvin	-
k_2	Second order rate constant	$m^3\ kmol^{-1}\ s^{-1}$
K_B	Nucleation rate constant	$No\ m^{-3-b}\ s^{-1+b}$
k_G	Gas mass transfer coefficient	$m\ s^{-1}$
K_G	kinetic rate constant for crystal growth	$kg^{-g}\ m^{3g+1}\ s^{-1}$
k_L	Liquid mass transfer coefficient	$m\ s^{-1}$
k_m	Membrane mass transfer coefficient	$m\ s^{-1}$
K_{OV}	Overall mass transfer coefficient	$m\ s^{-1}$
L	Contactor length	m
L_{eff}	Effective contactor length	m
L/G	Liquid to gas ratio	-

M	Mass	kg
OD	External diameter	m
P	Pressure	Bar
R	Ideal gas constant	J $mol^{-1}K^{-1}$
Re	Reynolds number	-
Sc	Schmidt number	-
Sh	Sherwood number	-
T	Time	s
Q_G	Gas flow rate	m^3 s^{-1}
Q_L	Liquid flow rate	m^3 s^{-1}
T	Temperature	°C / K
V_G	Gas velocity	m s^{-1}
V_L	Liquid velocity	m s^{-1}
η_{CO2}	CO_2 capture ratio	-
£	British pound	-
€	Euro	-

Greek symbols

α	Correlation constant	-
β	Correlation constant	-
γ	Correlation constant	-
μ	Dynamic viscosity	kg m^{-1} s^{-1}
ρ	Density	kg m^{-3}
σ	Standard deviation	-
φ	Fibre packing density	-

Abbreviations

AC	Activated carbon
ACS	Anhydrous calcium sulphate
AD	Anaerobic digestion
CAPEX	Capital expenditure
CCS	Carbon capture storage
CFD	Computational fluid dynamics
CfD	Contracts for difference
CHP	Combined heat and power
CLD	Chord length distribution
CNG	Compressed natural gas
CR-MCr	Chemically reactive membrane crystallisation reactor
EDX	Energy dispersive X-ray spectroscopy
EPSRC	Engineering and physical sciences research council
ESEM	Environmental scanning electron microscopy
FBRM	Focused beam reflectance measurement
FTIR	Fourier transform infrared spectroscopy
FTU	Formazin turbidity unit
GGCS	Green gas certification scheme
GDN	Grid distribution network
GEU	Grid entry unit
GC-MS	Gas chromatography-mass spectrometry
HFMC	Hollow fibre membrane contactor
HTU	Height of transfer unit
IBC	Intermediate bulk container
IEA	International energy association
KWh	Kilowatt-hour
LTS	Local transmission network
mol	Mole
NEA	Network entry agreement
NTS	National transmission system
NTU	Number of transfer units
NWS	Northumbrian water scientific services
OPEX	Operational expenditure
PTFE	Polytetrafluoroethylene
PP	Polypropylene

PVC	Polyvinyl chloride
PVM	Particle vision and measurement
REAL	Renewable energy assurance limited
RED2020	Renewable energy directive 2020
RES	Renewable energy source
RHI	Renewable heat incentive
RO	Renewables obligation
ROC	Renewable obligation certificate
RTD	Residence time distribution
RTFC	Road transport fuel certificate
RTFO	Road transport fuel obligation
SAZ	Silico aluminate zeolite
SEM	Scanning electron microscopy
STREAM	The industrial doctorate centre (IDC) for the water sector
TPH	Total petroleum hydrocarbons
UK	United Kingdom
UKAS	UK's national accreditation body
WWTW	Wastewater treatment works
VOC	Volatile organic compounds

Chemical formulae and speciation

CH_4	Methane
CO_2	Carbon dioxide
H_2O	Water
H_2S	Hydrogen sulphide
HCl	Hydrochloric acid
HCO_3^-	Bicarbonate ion
MEA	Monoethanolamine
NaOH	Sodium hydroxide
NH_3	Ammonia
NH_4^+	Ammonium ion
NH_4HCO_3	Ammonium bicarbonate

1 Introduction

1.1 UK water sector drivers toward technological innovation

The implementation of novel technological and engineering solutions to biogas upgrading within the United Kingdom (UK) water sector has progressed through two distinct drivers: (i) directly through the government launch of the Renewable Heat Incentive (RHI); and (ii) indirectly through market regulation by the water services regulation authority, Ofwat, who regulate each water utility's asset management plan (AMPs) over a five yearly cycle through imposed price reviews (PR) [1]. The most recent review, PR19, has emphasised the role of future challenges, in particular to the environment, resilience, innovation and affordability [1]. Simultaneously, UK climate change mitigation policies driven by the Renewable Energy Directive 2020 (RED2020) have resulted in the introduction of the RHI within the 2008 Energy Act [2–4], a tariff mechanism for the financial remuneration of renewable heat energy, incentivising biomethane as a renewable heat source for distribution in the national gas grid [5] over biogas combustion as a renewable electricity source [6–8]. Biogas produced from the anaerobic digestion of organic matter consists of a multicomponent gas, primarily methane (CH_4, 40-75%) and carbon dioxide (CO_2, 15-60%) with additional trace impurities such as siloxanes, hydrogen sulphide (H_2S) and water [9]. The process of biogas upgrading encompasses the selective bulk separation of CO_2 to produce a ≥98% CH_4 biomethane product and ancillary cleaning processes to ensure trace impurity removal and product quality [9–11]. By 2015, 159 sites in the water sector had an installed AD capacity to produce 195 MWe-equivalent [6], equivalent to 41% of total installed UK AD energy capacity. Overlap of regulatory and financial drivers in biogas upgrading therefore encourages investment in upgrading technology to produce biomethane (renewable heat) from existing and proposed biogas production (AD) sites. As a consequence of the tiered tariff regression mechanism, which offers greater financial reward to early adopters, absorption columns as a historically proven technology [9–14] represented low risk investment and fit for immediate purpose [14], despite disadvantages such as high capital expenditure (CAPEX), high operational expenditure (OPEX), biological fouling, H_2S corrosion and low input gas flexibility [9,13]. Within the UK water sector, water based physical absorption columns account for 85% of the reported biomethane installations, with an average treatment capacity of 880 $Nm^3 h^{-1}$ biogas [15] despite the specific investment cost for absorption columns only achieving an optima in economies of scale above 1500-2000 $m^3 h^{-1}$ [10,11]. A typical process layout for a WWTW operating biogas upgrading for injection into the natural gas grid can be seen in Figure 1.1. However, the RHI tariff guarantee for large scale plants ends 31st

December 2019 [16], as such process cost reduction and innovative operation within the Ofwat regulatory framework gains importance and value.

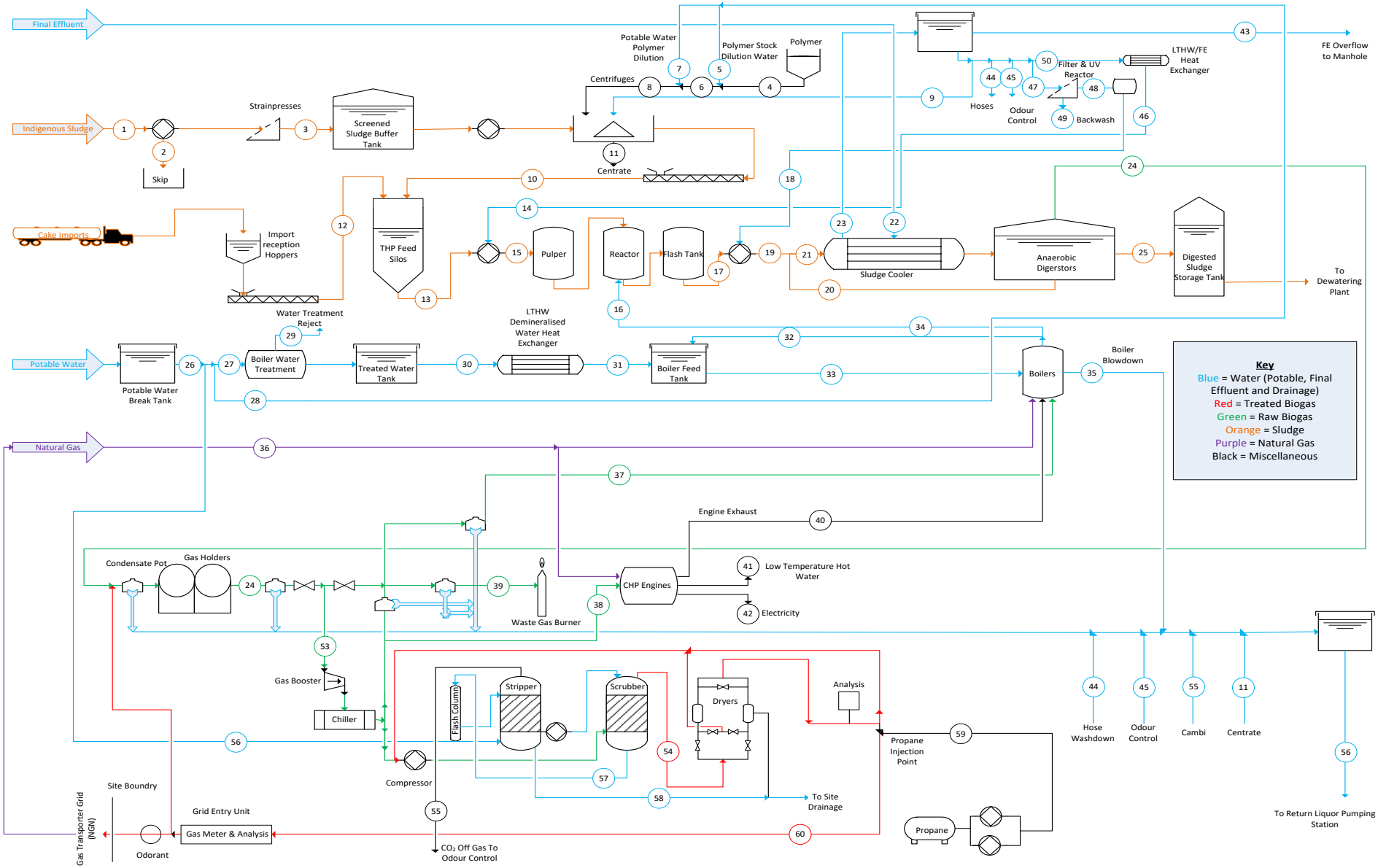

Figure 1.1 A typical process flow diagram of a biogas upgrading facility integrated into a wastewater treatment works operating anaerobic digestion.

1.2 Absorption technology and innovation

Absorption systems are subdivided into physical absorption systems, reliant on establishing a CO_2 concentration gradient and exploitation of the solubility difference between CO_2 and CH_4 for the selective absorption of CO_2 into the absorbent [9–14], typically under pressure [9–14], and chemically reactive absorption systems which employ a reversible chemical reaction to enhance mass transfer, intensifying the process to reduce process scale and increase removal efficiency [9–14]. The main advantages of physical absorption lie in the application of water, an easily accessible absorbent [13] and competitive 0.3 kWh Nm^{-3} biogas electricity demand [11] relative to commercial alternatives [11]. In contrast, chemical absorption systems offer greater removal efficiencies, lower power demand, and a further reduction in scale but at the cost of additional regenerative heat demand, 0.55 kWh Nm^{-3} biogas [11]. Unforeseen operational cost due to chemically induced corrosion and the loss of chemicals, due to their inherent volatility have also been noted [13]. An innovate engineering solution proposed for the water industry is the integration of gas-liquid absorption technology with a sustainable source of chemical enhancement to facilitate resource recovery and energy demand reduction, whilst reducing CAPEX for the absorption technology [17]. Thermally recovered aqueous free ammonia from WWTW return liquors, with an absorption capacity of 1.76 kg CO_2 kg NH_3^{-1}, has been demonstrated a potential sustainable source of chemical enhancement to further reduce process scale [17,19], which can use the chemically reactive CO_2–NH_3–H_2O system to precipitate a crystalline solid end product of ammonium bicarbonate (NH_4HCO_3) [17,18]. One direct advantage to conventional chemical scrubbers is that the solution regeneration stage is avoided. Furthermore, through the chemical recovery of ammonia from wastewater, the current biological nitrogen removal cost of £2.6 kg N^{-1}[19], accounting for 35% of WWTW energy cost via aeration [20] can be avoided, and the ammonium bicarbonate reaction product offers potential new value, as the price of this base product is around £99 kg^{-1} [17].

Hollow fibre membrane contactors (HFMC) are a prospective technology for the replacement of gas-liquid absorption columns and advantageous integration into a WWTW treatment process [17]. HFMC employ an absorption mechanism analogous to absorption columns with the high interfacial area of a microporous membrane barrier enabling 15 fold intensification factors relative to physical absorption in columns [16,21], reducing CAPEX for the core selective gas separation technology. Phase separation enabled by the membrane barrier can be further leveraged to control the precipitation and recovery of ammonium bicarbonate by limiting ammonia breakthrough into the gas-

phase and constraining crystal nucleation and growth at the micropore entrance [18,19] and maintain high purity methane [22,23]. This has led to the novel development of chemically reactive membrane crystallisation reactors (CR-MCr) to facilitate controlled recovery of crystalline ammonium bicarbonate precipitate using ammonia as an absorbent sustainably derived from wastewaters [18,19]. To ensure the economic viability of a gas-liquid separation process delivering value through the Renewable Heat Incentive, the intensification available through an HFMC based physical separation process has the potential to reduce both CAPEX and OPEX relative to current generation absorption columns, limiting the impact of a reducing RHI. Additional process intensification using sustainably derived ammonia further reduces cost whilst introducing an innovative mechanism for the recovery of ammonia (NH_4HCO_3) and energy demand reduction, valuable in realising PR19 goals.

1.3 HFMC or columns as facilitators of industrial biogas upgrading and ammonia recovery

Prior to water utility investment, it is necessary to estimate process size, process configuration and operational conditions at scale to complete an economic estimate. The design of gas-liquid absorption columns has already reached commercial maturity, thus size, cost and operational set points are available for biogas upgrading [9–11,24]. Whilst HFMCs have been applied commercially for specific gas-liquid applications (e.g. blood oxygenation during cardiothoracic surgery), membrane contactor technology has yet to reach commercial maturity for biogas upgrading. HFMC for biogas upgrading have been demonstrated [25], but studies have been limited to single stage modular laboratory scale contactors without direct consideration for how to translate into a configuration suitable for an industrial setting [21,26]. HFMC as a modular technology create the process length (L) required to reach a desired treatment capacity by supplementing individual transfer units (HTU) (HFMC modules) with additional transfer units (NTU) [27]. Application at scale is predicated on an understanding of HFMC multi-module design to attain a ≥98% CH_4 product gas purity. However, multi-module configurations have not been widely studied [25,28–30] and have focused on the maximisation of mass transfer over the control of gas product quality, an assessment of multi-module design and the impact of operational conditions to produce an industrially relevant gas quality is missing from the literature.

Commercial modules with a low treatment capacity suffer from maldistribution around the fibre bundle due to non-uniform fibre packing [31,32] but commercial modules with a high treatment capacity employ a different internal structure to overcome

maldistribution (Figure 1.2), the translation of multi-module design is limited by the impact of maldistribution [33–35] on performance. Small scale membranes in which most research is undertaken employ a shell-and tube design with absorbent directed to the well distributed fibre lumen at the cost of high pressure drop [26]. At industrial scale the internal architecture of modules changes, a shell-side disk baffle is employed to induce improved liquid-phase dispersion around the fibre bundle with reduced pressure drop, a consequence of which is enhanced mass transfer [26,36]. However variable shell-side maldistribution has resulted in over 30 descriptions for shell-side operation being developed [36], each with limited applicability. This ambiguity regarding the estimation of mass transfer across module scale, from lab-scale to industry, prevents academic process design outcomes from being directly applied to industry.

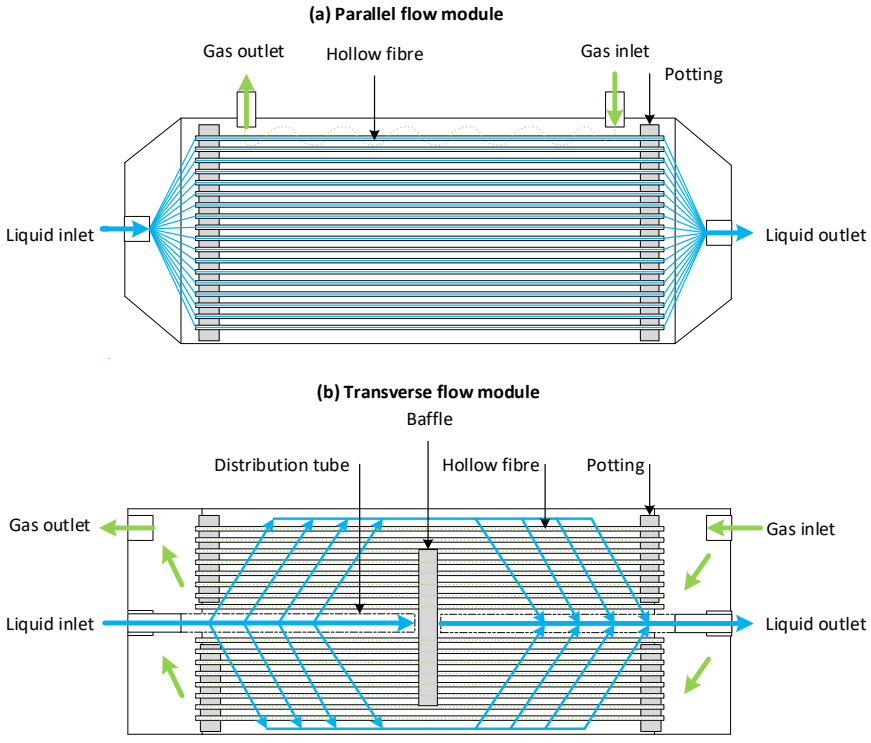

Figure 1.2 The liquid flow profiles which yield greatest membrane performance (a) liquid lumen-side in a parallel flow module (b) liquid shell-side in a transverse flow module.

Translation of design to industry faces the further challenge of additional gas (biogas) and fluid complexity (potable water) in industry relative to the de-ionised water and synthetic gas mixtures studied in laboratory investigation. Gas phase trace impurities, in particular particulates have been demonstrated to foul HFMC applied to carbon capture in flue gas [37–39] whilst liquid-phase biological fouling is encountered in traditional gas-liquid columns [40]. To date, only a single study into HFMC for industrial

biogas upgrading [41] has applied commercially available HFMC to industrial biogas, demonstrating the successful upgrading to ≥98% CH_4, but does not provide detailed investigation of long-term gas and liquid effects on separation robustness. Understanding the role of gas and liquid pre-treatment on membrane fouling is an important step toward a robust industrial process design.

The process intensification already facilitated by the introduction of HFMC can be further enhanced by a chemical reaction. Chemical enhancement by an ammonia absorbent (10M NH_3) is previously demonstrated in absorption columns exploiting ammonium bicarbonate precipitation to increase absorption capacity and reduce specific heat demand [42–46]. Whilst precipitation of ammonium bicarbonate has been demonstrated at commercial scale, the feasibility of ammonium bicarbonate recovery has not been investigated. A continuous biogas upgrading and ammonium bicarbonate recovery process from thermally recovered NH_3 in chemically reactive membrane crystallisation reactors (CR-MCr) has been developed to control the recovery of crystalline ammonium bicarbonate [18,19]. Control is achieved through lowering crystal nucleation rate by limiting the free ammonia concentration and recycling a low concentration (3.3 mol L^{-1}) ammonia absorbent. A relatively low concentration ammonia absorbent is coincident with the optimal concentration (2.5M NH_3) reported by Mani et al. [47] with respect to limiting ammonia slip and maximising CO_2 capacity for absorption columns. An investigation into controlled crystallisation for absorption columns, as existing assets at a WWTW and a commercial HFMC as a successor technology coupled with gas-phase treatment for high purity methane in a configuration suitable for industrial operation has not been undertaken in the literature.

1.4 Aims and objectives

The aim of this thesis is to demonstrate HFMC as a successor technology to existing gas-liquid absorption columns for industrial biogas upgrading by exploiting modularity to enhance performance and minimise cost. In doing so, the thesis seeks to understand how to translate laboratory scale data into commercial geometries to permit the projection of system scalability, whilst also establishing how commercially oriented HFMC geometries can incorporate the recovery of ammonium bicarbonate and simultaneously deliver the required gas phase quality.

To address the overall project aim, the following objectives have been developed:

1. Measure module performance for single and multi-module setup and analyse the impact of a changing dominant phase to mass transfer on the accuracy of an

overall resistance to mass transfer model, demonstrating validity for predicting multi-module performance for a high purity methane product.

2. Characterise the impact of shell-side maldistribution on mass transfer employing mean residence time as a surrogate for module geometry and hydrodynamic conditions to reconcile with an overall resistance to mass transfer model, enabling translation of mass transfer data from a maldistributed small-scale module to a well distributed larger scale module of industrial design.
3. Demonstrate membrane resilience to industrial operation at a WWTW and characterise the role of pre-filtration on enhancing resilience.
4. Demonstrate through comparison of HFMC and absorption column operation that controlled crystallisation and continuous operation is enabled by the unique nucleation and growth kinetics available through membrane crystallisation.
5. Characterise the economic factors underpinning biogas upgrading technology choice, scale of treatment capacity and the likely role of innovative solutions in the future UK biomethane market.

1.5 Thesis structure

Each thesis chapter has been formatted as a journal paper, with the four technical chapters (Chapters 2, 3, 4 & 5) addressing the established objectives (Figure 1.3). Chapter 2, "*Mass transfer in multi-module membrane contactor configurations for the production of high purity methane from biogas*" establishes the limitations to mass transfer in multi-module membrane contactor configurations, to determine how best to deliver high gas product purity from a concentrated CO_2 gas phase, using water absorption. Chapter 3, "*Translating shell-side mass transfer data across module architecture and scale*" investigates the influence of shell-side maldistribution to reconcile mass transfer between the two most commonly employed module geometries at laboratory and industrial scale, parallel flow and transverse flow. Chapter 4, "*Demonstration scale performance of a commercial hollow fibre membrane contactor for biogas upgrading at a wastewater treatment works*" applies HFMC to industrial biogas to enrich understanding of HFMC robustness to gas and liquid phase contaminants during industrial biogas upgrading. Chapter 5, "*Hollow fibre membrane contactors and absorption columns as crystallising reactors for a biogas upgrading – ammonium bicarbonate recovery system*" assesses the impact of membrane mediated nucleation on ammonium bicarbonate recovery whilst maintaining industrially relevant gas purity. Sam Houlker was lead author on all submissions and edited by Dr Ewan McAdam and

Dr Marc Pidou as supervisors. Data collection in Chapter 3 was supported by Alexandre Allemand as placement student, data collection at Howdon WWTW was facilitated and supported by Northumbrian water employees Tony Rutherford as sludge process optimisation controller, Daniel Herron as process support analyst and Andrew Moore as industrial supervisor, whilst data collection in Chapter 5 was supported by Dr Mehrez Hermassi. Chapter 6 "*Renewable energy policy and innovation in the UK biomethane sector*" discusses novel implementation methods by which reduced process cost can be achieved. Chapters 7 & 8 introduce an overall discussion of the thesis coupled with conclusions and proposed future work.

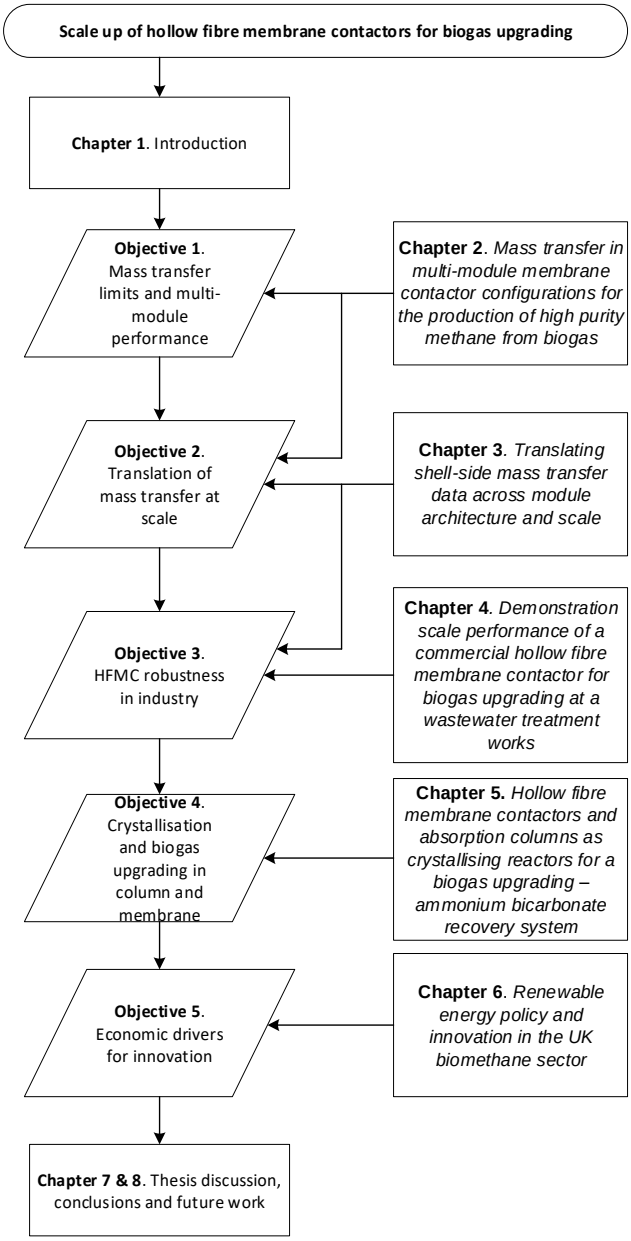

Figure 1.3 Thesis plan

References

[1] Ofwat, Delivering Water 2020 : Our final methodology for the 2019 price review, Birmingham, 2017. https://www.ofwat.gov.uk/publication/delivering-water-2020-final-methodology-2019-price-review/.(accessed November 17, 2018)

[2] T. Patterson, S. Esteves, R. Dinsdale, A. Guwy, An evaluation of the policy and techno-economic factors affecting the potential for biogas upgrading for transport fuel use in the UK, Energy Policy. 39 (2011) 1806–1816.

[3] T. Horschig, P.W.R. Adams, M. Röder, P. Thornley, D. Thrän, Reasonable potential for GHG savings by anaerobic biomethane in Germany and UK derived from economic and ecological analyses, Appl. Energy. 184 (2016) 840–852.

[4] P.M. Connor, L. Xie, R. Lowes, J. Britton, T. Richardson, The development of renewable heating policy in the United Kingdom, Renew. Energy. 75 (2015) 733–744.

[5] D. Thrän, E. Billig, J. Daniel-Gromke, J. Ponitka, M. Seiffert, T. Persson, M. Svensson, J. Balswin, L. Kranzl, F. Schipfer, J. Matzenberger, N. Devriendt, M. Dumont, J. Dahl, G. Bochmann, Biomethane Status and Factors Affecting Market Development and Trade, 2014. https://www.ieabioenergy.com/publications/biomethane-status-and-factors-affecting-market-development-and-trade/.

[6] Anaerobic Digestion and Biogas Association (ADBA), Anaerobic Digestion Market Report, London, 2015. http://adbioresources.org/library/market-report-july-2015.

[7] P.L. McCarty, J. Bae, J. Kim, Domestic Wastewater Treatment as a Net Energy Producer - Can This be Achieved?, Environ. Sci. Technol. 45 (2011) 7100–7106.

[8] K. Mizuta, M. Shimada, Benchmarking energy consumption in municipal wastewater treatment plants in Japan, Water Sci. Technol. 62 (2010) 2256–2262.

[9] E. Ryckebosch, M. Drouillon, H. Vervaeren, Techniques for transformation of biogas to biomethane, Biomass and Bioenergy. 35 (2011) 1633–1645.

[10] M. Miltner, A. Makaruk, M. Harasek, Review on available biogas upgrading technologies and innovations towards advanced solutions, J. Clean. Prod. 161 (2017) 1329–1337.

[11] F. Bauer, T. Persson, C. Hulteberg, D. Tamm, Biogas upgrading - technology overview, comparison and perspectives for the future, Biofuels, Bioprod. Biorefining. 7 (2013) 499–511.

[12] R. Muñoz, L. Meier, I. Diaz, D. Jeison, A review on the state-of-the-art of physical/chemical and biological technologies for biogas upgrading, Rev. Environ.

Sci. Biotechnol. 14 (2015) 727–759.

[13] I. Ullah Khan, M. Hafiz Dzarfan Othman, H. Hashim, T. Matsuura, A.F. Ismail, M. Rezaei-DashtArzhandi, I. Wan Azelee, Biogas as a renewable energy fuel – A review of biogas upgrading, utilisation and storage, Energy Convers. Manag. 150 (2017) 277–294.

[14] Q. Sun, H. Li, J. Yan, L. Liu, Z. Yu, X. Yu, Selection of appropriate biogas upgrading technology-a review of biogas cleaning, upgrading and utilisation, Renew. Sustain. Energy Rev. (2015) 521–532.

[15] International Energy Association Task 37, IEA Bioenergy Task 37 Upgrading Plant List 2017, (2017). http://task37.ieabioenergy.com/plant-list.html (accessed November 17, 2018).

[16] Department for Business Energy & Industrial Strategy, The Renewable Heat Incentive: A Reformed Scheme, 2016. https://www.gov.uk/government/uploads/system/uploads/attachment_data/file/577024/RHI_Reform_Government_response_FINAL.pdf.

[17] A. Mcleod, B. Jefferson, E.J. McAdam, Biogas upgrading by chemical absorption using ammonia rich absorbents derived from wastewater, Water Res. 67 (2014) 175–186.

[18] S. Bavarella, Chemically reactive membrane crystallisation reactor for CO_2 separation and ammonia recovery, PhD theis, Cranfield University, 2018.

[19] A. Mcleod, P. Buzatu, O. Autin, B. Jefferson, E. McAdam, Controlling shell-side crystal nucleation in a gas–liquid membrane contactor for simultaneous ammonium bicarbonate recovery and biogas upgrading, J. Memb. Sci. 473 (2015) 146–156.

[20] D. Rosso, L.E. Larson, M.K. Stenstrom, Aeration of large-scale municipal wastewater treatment plants : state of the art, Water Sci. Technol. 57 (2008) 973–978.

[21] B. Belaissaoui, J. Claveria-Baro, A. Lorenzo-Hernando, D. Albarracin, E. Chabanon, C. Castel, S. Rode, D. Roizard, E. Favre, Potentialities of a dense skin hollow fiber membrane contactor for biogas purification by pressurized water absorption, J. Memb. Sci. 513 (2016) 236–249.

[22] C. Makhloufi, E. Lasseuguette, J.C. Remigy, B. Belaissaoui, D. Roizard, E. Favre, Ammonia based CO_2 capture process using hollow fiber membrane contactors, J. Memb. Sci. 455 (2014) 236–246.

[23] Z. Cui, D. deMontigney, Experimental study of carbon dioxide absorption into

aqueous ammonia with a hollow fiber membrane contactor, J. Memb. Sci. 540 (2017) 297–306.

[24] F. Bauer, C. Hulteberg, T. Persson, D. Tamm, Biogas upgrading – Review of commercial technologies, 2013. http://www.sgc.se/ckfinder/userfiles/files/SGC270.pdf.

[25] A. Park, Y.M. Kim, J.F. Kim, P.S. Lee, Y.H. Cho, H.S. Park, S.E. Nam, Y.I. Park, Biogas upgrading using membrane contactor process: Pressure-cascaded stripping configuration, Sep. Purif. Technol. 183 (2017) 358–365.

[26] A. Sengupta, P.A. Peterson, B.D. Miller, J. Schneider, C.W. Fulk, Large-scale application of membrane contactors for gas transfer from or to ultrapure water, Sep. Purif. Technol. 14 (1998) 189–200.

[27] B.W. Reed, M.J. Semmens, E.J. Cussler, Membrane contactors, in: R.D. Nobel, A.S. Stern (Eds.), Membr. Sep. Technol. Princ. Appl., Elsevier, 1995: pp. 467–498.

[28] S. Boributh, W. Rongwong, S. Assabumrungrat, N. Laosiripojana, R. Jiraratananon, Mathematical modeling and cascade design of hollow fiber membrane contactor for CO_2 absorption by monoethanolamine, J. Memb. Sci. 401–402 (2012) 175–189.

[29] S. Boributh, S. Assabumrungrat, N. Laosiripojana, R. Jiraratananon, Effect of membrane module arrangement of gas-liquid membrane contacting process on CO_2 absorption performance: A modeling study, J. Memb. Sci. 372 (2011) 75–86.

[30] S. Atchariyawut, R. Jiraratananon, R. Wang, Mass transfer study and modeling of gas-liquid membrane contacting process by multistage cascade model for CO_2 absorption, Sep. Purif. Technol. 63 (2008) 15–22.

[31] M.J. Costello, A.G. Fane, P.A. Hogan, R.W. Schofield, The effect of shell side hydrodynamics on the performance of axial flow hollow fibre modules, J. Memb. Sci. 80 (1993) 1–11.

[32] I. Noda, D.G. Brown-West, C.C. Gryte, Effect of flow maldistribution on hollow fiber dialysis - experimental studies, J. Memb. Sci. 5 (1979) 209–225.

[33] E. Chabanon, E. Kimball, E. Favre, O. Lorain, E. Goetheer, D. Ferre, A. Gomez, P. Broutin, Hollow Fiber Membrane Contactors for Post-Combustion CO_2 Capture: A Scale-Up Study from Laboratory to Pilot Plant, Oil Gas Sci. Technol. – Rev. d'IFP Energies Nouv. 69 (2014) 1035–1045.

[34] E. Kimball, A. Al-azki, A. Gomez, E. Goetheer, N. Booth, D. Adams, D. Ferre, Hollow Fiber Membrane Contactors for CO_2 Capture : Modeling and Up-Scaling

to CO_2 Capture for an 800 MW e Coal Power Station, Oil Gas Sci. Technol. – Rev. d'IFP Energies Nouv. 69 (2014) 1047–1058.

[35] S. Zhao, P.H.M. Feron, L. Deng, E. Favre, E. Chabanon, S. Yan, J. Hou, V. Chen, H. Qi, Status and progress of membrane contactors in post-combustion carbon capture : A state-of-the-art review of new developments, J. Memb. Sci. 511 (2016) 180–206.

[36] S. Shen, S.E. Kentish, G.W. Stevens, Shell-Side Mass-Transfer Performance in Hollow-Fiber Membrane Contactors, Solvent Extr. Ion Exch. 28 (2010) 817–844.

[37] L. Zhang, R. Qu, Y. Sha, X. Wang, L. Yang, Membrane gas absorption for CO_2 capture from flue gas containing fine particles and gaseous contaminants, Int. J. Greenh. Gas Control. 33 (2015) 10–17.

[38] L. Zhang, B. Hu, H. Song, L. Yang, L. Ba, Colloidal Force Study of Particle Fouling on Gas Capture Membrane, Sci. Rep. 7 (2017) 1–11.

[39] L. Zhang, J. Li, L. Zhou, R. Liu, X. Wang, L. Yang, Fouling of Impurities in Desulfurized Flue Gas on Hollow Fiber Membrane Absorption for CO_2 Capture, Ind. Eng. Chem. Res. 55 (2016) 8002–8010.

[40] A. Håkansson, Preventing microbial growth on pall-rings when upgrading biogas using absorption with water wash, 2006. http://www.sgc.se/ckfinder/userfiles/files/SGC166.pdf.

[41] S. Vogler, A. Braasch, G. Buse, S. Hempel, J. Schneider, M. Ulbricht, Biogas conditioning using hollow fiber membrane contactors, Chemie-Ingenieur-Technik. 85 (2013) 1254–1258.

[42] V. Darde, K. Thomsen, W.J.M. van Well, E.H. Stenby, Chilled ammonia process for CO_2 capture, Int. J. Greenh. Gas Control. 4 (2010) 131–136.

[43] F. Kozak, A. Petig, E. Morris, R. Rhudy, D. Thimsen, Chilled Ammonia Process for CO_2 capture, Energy Procedia. 1 (2009) 1419–1426.

[44] V. Telikapalli, F. Kozak, J.F. Leandri, B. Sherrick, J. Black, D. Muraskin, M. Cage, M. Hammond, G. Spitznogle, CCS with the Alstom Chilled Ammonia Process Development Program - Field Pilot Results, Energy Procedia. 4 (2011) 273–281.

[45] O. Augustsson, B. Baburao, S. Dube, S. Bedell, P. Strunz, M. Balfe, O. Stallmann, Chilled Ammonia Process Scale-up and Lessons Learned, Energy Procedia. 114 (2017) 5593–5615.

[46] H. Yu, G. Qi, S. Wang, S. Morgan, A. Allport, A. Cottrell, T. Do, J. Mcgregor, L. Wardhaugh, P. Feron, Results from trialling aqueous ammonia-based post-combustion capture in a pilot plant at Munmorah Power Station : Gas purity and

solid precipitation in the stripper, Int. J. Greenh. Gas Control. 10 (2012) 15–25.

[47] F. Mani, M. Peruzzini, P. Stoppioni, CO_2 absorption by aqueous NH_3 solutions: speciation of ammonium carbamate, bicarbonate and carbonate by a 13C NMR study, Green Chem. 8 (2006) 995–1000.

2 Mass transfer in multi-module membrane contactor configurations for the production of high purity methane from biogas

Mass transfer in multi-module membrane contactor configurations for the production of high purity methane from biogas

S. Houlker[a], A. Brookes[b], A. Moore[c], P. Vale[d], M. Pidou[a], E.J. McAdam[a,*]

[a]Cranfield Water Science Institute, Cranfield University, Bedfordshire, UK
[b]Anglian Water, Thorpewood House, Peterborough, UK
[c]Northumbrian Water, Boldon House, Pity Me, Durham, UK
[d]Severn Trent Water, Coventry, UK
*Corresponding author: e.mcadam@cranfield.ac.uk

Abstract

In previous studies that have focussed on facilitating the physical absorption of carbon dioxide (CO_2) using single stage hollow fibre membrane contactors, the primary resistance to mass transfer is generally regarded to be the liquid phase, due to the limited solubility of the solvent. In this study, mass transfer was experimentally re-evaluated in single and multi-module configurations, for the production of high purity methane gas from a CO_2 rich binary gas (Biogas). For a single module configuration, it was determined that a low gas velocity (V_G <5.6x10^{-3} m s^{-1}) is required to favour gas product purity, which was coincident with gas-phase controlled mass transfer. Multi-module configurations were subsequently experimentally evaluated, which have not been widely reported upon in the literature. In multi-module configuration, whilst an increase in productivity was evidenced above that expected solely from the increase in contact area, the gas phase velocity had to be sustained within gas-phase controlled conditions to deliver the necessary gas product quality. The distinction in the governance of mass transfer identified in this study, to that of earlier studies, is the focus on optimising gas product quality rather than mass transfer. This was confirmed through extensive investigation of the liquid-gas ratio, where maximum overall mass transfer was facilitated at higher gas velocities and was predominantly liquid-phase controlled. A simplified mass transfer model was evaluated to estimate process configuration, based on the overall mass transfer coefficient. Comparison between modelled and experimental data determined from up to three membrane contactors in series, verified accurate description of mass transfer, provided the membranes were operating within the region of gas phase-controlled mass transfer, which is coincident with the production of high purity methane gas. The model validity was explained by the excess solvent flow associated with these conditions, which favours underutilisation of the solvents CO_2 loading limit. Importantly, this study demonstrates that scale-up of water-based membrane contactor configurations for the production of high purity product gas from a concentrated binary

gas can be achieved based on the overall mass transfer coefficient, a method which has been previously assumed to be limited to CO_2 separations utilising a chemical reaction.

Keywords: resistance, membrane module, in series configuration, biogas, scale-up, cascade

2.1 Introduction

Following launch of the 2009 Renewable Energy Directive by the European Union which set a renewable energy target of 20% by 2020 [1,2], there has been a marked increase in the production of biomethane from biogas. By 2016, over 162 installations were identified that comprised gas-liquid absorption columns for biomethane production, using water as the absorption solvent [3]. Whilst packed column technology has been commercially successful, the limited interfacial area per unit volume (up to 300 m^2 m^{-3}) results in substantial process scale [3,4,5]. Furthermore, phase dispersion within columns can introduce flooding, foaming and entrainment issues which limits operation to a narrow range of liquid to gas ratios (*L/G*), subsequently restricting capability for turn-up or turndown [6].

Hollow fibre membrane contactors (HMFC) employ an absorption mechanism analogous to gas-liquid absorption columns [7]. In this case, the membrane promotes phase separation, facilitating gas diffusion through the micropores. With no phase dispersion problems, a wider range of *L/G* ratios can be used, and has been shown to promote equivalent separation performance to columns using lower operational *L/G* ratios [5]. Two-film theory is employed to describe mass transfer in columns. For HFMCs, the membrane provides an additional resistance to mass transfer [8]:

$$\frac{1}{K_{OV}} = \frac{1}{k_g} + \frac{1}{k_m} + \frac{1}{k_l} \qquad \text{(Equation 2.1)}$$

Whilst the higher resistance results in lower mass transfer for HFMCs, the significant interfacial area per unit volume (up to 6000 m^2 m^{-3}) provides process intensification of over an order of magnitude versus packed columns [4].

At industrial scale, absorption columns for biogas are designed using transfer unit theory, where the challenge for the design engineer is to specify the correct height for the packed column to achieve the desired gas quality [9]. The column height (*L*) is given by the height of a transfer unit (HTU), multiplied by the number of transfer units (NTU):

$$L = HTU.NTU \qquad \text{(Equation 2.2)}$$

which can then be described by:

$$L = \left(\frac{V_G}{K_{ov}a}\right)\left\{\left(\frac{\frac{Q_L H}{Q_G}}{\frac{Q_L H}{Q_G}-1}\right) ln\left(\frac{C_{CO2,L,in}-HC_{CO2,G,in}}{C_{CO2,L,out}-HC_{CO2,G,out}}\right)\right\} \quad \text{(Equation 2.3)}$$

where K_{OV}, V_G and a within the left-hand term are the overall mass transfer coefficient (m s^{-1}), superficial gas velocity (m s^{-1}) and interfacial area (m^2 m^{-3}) respectively, representing one HTU. The braced right hand term represents the NTU, in which Q_L and Q_G are absorbent and feed flows, H is the Henry's constant, and $C_{CO2,G}$ and $C_{CO2,L}$ are the solute mole fraction in the feed and absorbent respectively [10]. The NTU is then defined by the number of units required in series to achieve a set treatment objective (or gas quality).

Due to the wide-scale industrial application of HFMC technology, there are numerous manufacturers now supplying HFMC modules of standard dimensions. This *de-facto* standardisation provides cost advantages through economies of scale, but also permits flexibility and cost efficiency during scale-up to cascade design [11]. At industrial scale, the number of HFMC modules in series (NTU, L) required to achieve a set treatment objective is also ascertained through transfer unit theory [12]. However, for most industrial HFMC applications, the extracting solvent flow is in excess, which is the absorbent in the case of CO_2 separation, and conforms to a limiting condition such that the overall solution can be reduced to [10,12,13]:

$$L = \left(\frac{V_G}{K_{ov}a}\right) ln\left(\frac{C_{CO2,G,in}}{C_{CO2,G,out}}\right) \quad \text{(Equation 2.4)}$$

which is often transformed to describe CO_2 capture ratio [10,13]:

$$\eta = 1 - exp\left(\frac{-K_{OV}aL}{V_G}\right) \quad \text{(Equation 2.5)}$$

Applying the overall mass transfer coefficient (K_{ov}) in this model is advantageous as it consolidates different mass transfer mechanisms into a single descriptor, making it simple to use [13] and requires only limited experimental information to facilitate estimation of scale, which is of practical significance to industry. Consequently, experimental determination of the mass transfer coefficient in a single module permits description of one HTU and can be subsequently used to estimate the NTU required. Whilst there are extremely few experimental examples of multi-module configuration analysis, Chabanon et al. [13] did employ this model for single module analysis and compared to more complex 1D, 1D-2D and 2D models. The authors identified the four

approaches to have similar fit efficiency to experimental carbon dioxide (CO_2) separation data ($C_{CO2,G,in}$, 5 to 15 vol% CO_2) produced from a single HFMC module in which chemical reaction was facilitated with Monoethanolamine (MEA). The same approach has been successfully used to estimate mass transfer between single modules of similar geometric construction [14], for the separation of dissolved oxygen in which sweep gas was applied in excess. Whilst extremely encouraging, the application of excess sweep gas or inclusion of a chemical reaction, are examples in which the extracting phase does not limit mass transfer, which conforms with the boundary conditions of the model [10,13].

Previous investigations of HFMC for CO_2 separation have primarily focussed on how changes to geometry [15–17], fibre packing [18–20] or solvent selection [21,22] enhance mass transfer in a single module (one HTU). To simplify analysis, pure CO_2 is commonly employed in the gas-phase, which implies that the overall resistance to mass transfer is then limited to the sum of $1/k_m$ and $1/k_l$ (Equation 2.1). Consequently, the gas phase resistance is generally either not reported or is assumed negligible (Table 2.1). Within these prescribed conditions, resistance to mass transfer is dominated by the liquid phase [23,24]. Liquid phase resistance has been particularly described for physical absorption using water, as commonly employed for biogas, due to the lower solvent loading that can be achieved when compared to chemically reactive solvents [7].

However, biogas is CO_2 rich (40-50 % v/v) and as the ambition is to achieve a high purity final gas product of greater than 98% CH_4 [7], the concentration driving force between the gas interface and bulk liquid is not constant but varies along the length of the module [25,26], which suggests that the gas phase should contribute to the overall resistance to mass transfer. Very few studies have reported gas-side mass transfer data for CO_2 separations when water was applied as the absorbent (Table 2.1). Dindore and Versteeg [27] suggested mass transfer was independent of gas velocity following analysis with a 30% CO_2 gas phase. Such observations have been similarly described elsewhere [23,29]. The limited impact from the gas phase could be due to the selection of prescriptive boundary conditions, with a primary focus on mass transfer optimisation in a single stage (HTU) rather than gas product quality (NTU). For example, Faiz et al. [29] noted that a change in gas velocity improved physical absorption from a 10% CO_2 gas mixture. Boributh et al. [30] used a modelling approach in one of the few examinations of multi-module configuration, to compare a ‘single-stage’ module and two modules in series. With two modules in series, when the gas flow rate was reduced to half, the gas phase resistance ($1/k_g$) increased to 12% of the overall mass transfer

coefficient ($1/K_{OV}$), which was around 45% higher than for the single-stage membrane [30–32]. These latter studies therefore suggest some discontinuity in the literature regarding the significance of the gas phase to mass transfer, the impact of which may well be exacerbated in biogas upgrading, being characterised by a higher CO_2 partial pressure and a more demanding CO_2 separation requirement (>95%).

The optimum commercial HFMC design is weighted on most mass transferred per unit cost [16,33], which infers a trade-off between mass transfer and gas product quality for each module. We propose that it is this relationship which has introduced discontinuity in the literature with respect to gas phase resistance, where the boundary conditions determined during single module optimisation for mass transfer may yield quite different data from those isolated for gas product quality in which more than one modular stage may be required. Furthermore, in a binary gas comprised of CO_2, the gas flow rate specified, and not just the gas-liquid ratio can also be expected to contribute toward mass transfer, whose governance over mass transfer has not been well examined. As such, a broad set of operational conditions must be evaluated before an optimum operating point can be determined. To compensate for gas product quality, membrane modules can be configured in-series (NTU). Whilst few experimental studies exist, through modelling, module configuration has been demonstrated to increase absorption beyond the increase in contact area [30,32,34], the impact of which requires elucidation to determine a modular configuration that can satisfy the gas product quality demanded, whilst delivering on mass transferred per unit cost. In this study, we therefore seek to establish the limitations to mass transfer in multi-module membrane contactor configurations, to determine how best to deliver high gas product purity from a concentrated CO_2 gas phase, using water absorption, which is one of the fastest growing areas for gas-liquid separation. Specific objectives are to: (i) evaluate mass transfer in a single module, to identify limiting behaviour across a broad range of gas velocities and gas-liquid ratios; (ii) appraise the advantage and transition in mass transfer behaviour for multi-module configurations, to achieve high product quality ($\eta_{CO2}, 0.98$); and (iii) determine the potential to estimate mass transfer across multi-module configurations using a simplified mass transfer model based on the overall mass transfer coefficient.

Table 2.1 Mass transfer data from hollow-fibre membrane contactor studies for CO_2 separation from water, providing membrane resistance, CO_2 flux and operating conditions.

Membrane		Configuration		Gas phase			Liquid phase		L/G[a]		CO_2 flux	Mass transfer (s m^{-1})			Ref.
Material	**Area/Pore size (m^2/μm)**	**Shell-side**	**Lumen-side**	**CO_2 (%)**	**Other**	**V_G (m s^{-1})**	**Type**	**V_L (m s^{-1})**	**Min.**	**Max.**	**J_{CO2} (x10^{-4}) (mol m^{-2} s^{-1})**	**$1/K_{OV}$**	**$1/k_g$**	**$1/k_m$**	
PVDF	0.08/0.5	Liquid	Gas	100	-	0.029-0.076	Water	0.133- 0.67	1.23	6.95	2-4.25	134352	(A/N)	53566	[35]
PP	0.213/(N/R)	Liquid	Gas	100	-	0.037-0.097	Water	0.133-0.63	1.35	7.59	0.75-1.1	331039	(A/N)	143406	
PTFE	0.044/20	Liquid	Gas	100	-	0.026-0.068	Water	0.167-0.75	1.15	6.47	1.25-3	400273	(A/N)	189049	
PVDF	0.00033/0.02	Liquid	Gas	100	-	(N/R)	Water	0.14-0.5	(N/R)	(N/R)	5.6-13.6	28589	(A/N)	7930	[36]
	0.00038/0.009	Liquid	Gas	100	-	(N/R)	Water	0.14-0.5	(N/R)	(N/R)	4-8.6	51101	(A/N)	18295	
	0.0004/0.011	Liquid	Gas	100	-	(N/R)	Water	0.14-0.5	(N/R)	(N/R)	4-6.4	67879	(A/N)	26558	
PVDF	0.019/0.2	Gas	Liquid	100	-	0.065	Water	0.9-2.2	0.74	1.81	10-14	22450	(A/N)	8082	[37]
MMM (PVDF&MMT)	0.0025/26	Gas	Liquid	100	-	0.017	Water	0.094-0.62	0.2	1.33	3-15	5910	(A/N)	N/R	
	0.0025/32	Gas	Liquid	100	-	0.017	Water	0.094-0.62	0.2	1.33	3-15	5110	(A/N)	N/R	
	0.0025/34	Gas	Liquid	100	-	0.017	Water	0.094-0.62	0.2	1.33	3-15	4830	(A/N)	N/R	
	0.0025/22	Gas	Liquid	100	-	0.017	Water	0.094-0.62	0.2	1.33	3-15	3440	(A/N)	N/R	
PEI	0.0063/0.026	Gas	Liquid	100	-	0.02	Water	0.47-2.8	0.25	1.5	4.5-7.5	(N/R)	(A/N)	31595	[38]
	0.0063/0.012	Gas	Liquid	100	-	0.02	Water	0.47-2.8	0.25	1.5	4-7	(N/R)	(A/N)	36210	
	0.0063/0.049	Gas	Liquid	100	-	0.02	Water	0.47-2.8	0.25	1.5	5-8.5	(N/R)	(A/N)	29625	
	0.0063/0.009	Gas	Liquid	100	-	0.02	Water	0.47-2.8	0.25	1.5	3-4	(N/R)	(A/N)	67563	
PVDF	0.0047/0.0078	Liquid	Gas	100	-	0.85	Water	0.004-0.035	0.31	2.5	3-7	(N/R)	(A/N)	33593	[39]
	0.0047/0.0096	Liquid	Gas	100	-	0.85	Water	0.004-0.035	0.31	2.5	3-8	(N/R)	(A/N)	12214	
PSF	0.0047/0.0061	Liquid	Gas	100	-	0.85	Water	0.004-0.035	0.31	2.5	3.8-5.5	(N/R)	(A/N)	89048	
	0.0047/0.0073	Liquid	Gas	100	-	0.85	Water	0.004-0.035	0.31	2.5	3.2-7.2	(N/R)	(A/N)	47541	
PP	1.5/(N/R)	Liquid	Gas	100	-	0.21	Water	(N/R)	0.59	1.64	12-25	(N/R)	(A/N)	5500-12000	[23]
A-Al_2O_3	0.00029/(N/R)	Gas	Liquid	100	-	0.026	Water	0.66-1.66	0.4	1	7.8	(N/R)	(N/R)	1748	[40]
	0.00055/(N/R)	Gas	Liquid	20	N_2	0.014-0.07	Water	0.24-1.18	0.2	5	2-4	(N/R)	(N/R)	(N/R)	
	0.00085/(N/R)	Gas	Liquid	20	N_2	0.017-0.08	Water	0.1-0.51	0.2	5	3-8	(N/R)	(N/R)	(N/R)	
PP	0.086/0.04	Gas	Liquid	20	N_2	0.054	Water	0.15-0.8	(N/R)	(N/R)	0.5-3	(N/R)	(N/R)	(N/R)	[41]
PPO (Dense Membrane Skin)	0.25/-	Liquid	Gas	30	CH_4	0.0031-0.011	Water	0.00011-0.00044	0.09	1.13	0.07-0.3	369004-1133787	1	1968	[42]
PVDF	0.019/0.2	Gas	Liquid	100	-	0.065	Water	0.6-2.5	2.4	10.5	10.4-15.2	36737	(N/R)	8082	[28]
				50	CH_4	0.065	Water	1.5-3	1.9	9.4	3.2-5.6	(N/R)	(N/R)	(N/R)	
				20	CH_4	0.065-0.13	Water	1.5-3	2.4	10.5	1.2-2.8	(N/R)	(N/R)	(N/R)	

Membrane materials: Polyvinylidene fluoride (PVDF), polypropylene (PP), Polytetrafluoroethylene (PTFE), Montmorillonite (MMT), mixed membrane material (MMM), Polyetherimide (PEI), Polysulfone (PSF), Polyphenylene Oxide (PPO)

2.2 Materials and methods

2.2.1 Experimental set-up

Synthetic biogas was prepared in-line by mixing methane (CH_4, 99.995%) and carbon dioxide (99.7%) (BOC gases, Ipswich, UK) using mass flow controllers with two prescribed flow rate ranges (0.01 - 1.0 L min^{-1} and 0.2 - 20 L min^{-1}, Roxspur Measurement and Control Ltd., Sheffield, UK) to provide combined flow rates between 50 and 4000 mL min^{-1} (Figure 2.1). The inlet gas phase either comprised of CO_2 (99.7%) or a 50/50 CH_4/CO_2 mixture maintained at a pressure of 0.5 BarG. Between one and three HFMCs were installed in series (Minimodule 1.7 X 5.5 G542, 3M Deutschland GmbH, Wuppertal, Germany). Each module comprised of 7400 microporous polypropylene fibres, with an outer diameter, inner diameter and fibre length of 300 µm, 220 µm, and 0.113 m respectively. The microporous fibres comprised a nominal pore size and porosity of 0.03 µm and 40% respectively. The total surface area for each module was 0.54 m^2 based on internal fibre diameter which provided an interfacial area per unit module of 3620 m^2 m^{-3}.

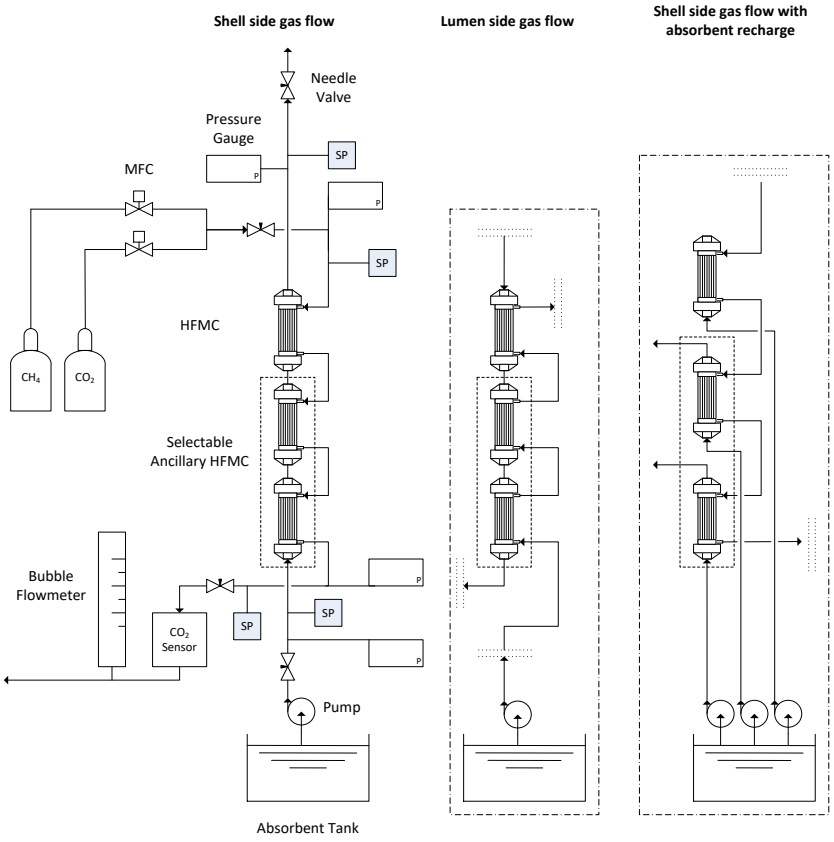

Figure 2.1 Schematic of experimental set up used for determining CO_2 capture, J_{CO2}, K_{OV} and constituent resistances under differing *L/G* set points.

Absorption solvent, de-ionised water (15MΩ cm), was stored in an 85 L PVC tank and was introduced in counter current mode using a peristaltic pump (up to 800mL min^{-1}, 520Du; from 800 to 3500 mL min^{-1}, 530S, Watson-Marlow Ltd, Falmouth, UK). The absorbent was primarily introduced onto the lumen-side, and flowed counter-current to the gas phase which flowed on the shell-side. Gas phase pressure drop on the shell-side in a single module was estimated to be less than 1 mBar using methods described elsewhere [13,43]. All experimentation was undertaken in temperature-controlled environment (20°C).

2.2.2 Analysis

Gas composition was determined using an in-line infrared CO_2 analyser (BCP-CO2, accuracy <0.5% full-scale, Bluesens gas sensor GmbH, Herten, Germany). Gas flow rate was measured by bubble flow meter (up to 300 mL min^{-1}, 50 mL, error ±2%, Restek, Bellefonte, USA; from 300-3000 mL min^{-1}, 1000 mL, Model 311, error ±2%, Blandford Forum, UK). All measurements were taken in triplicate once steady state had been achieved, limiting variation to combined instrument error (±2.5%). Carbon dioxide removal was analysed through mass balance[13]:

$$\eta = \frac{[(Q_{G,in} \times C_{G,in}) - (Q_{G,out} \times C_{G,out})]}{(Q_{G,in} \times C_{G,in})} \quad \text{(Equation 2.6)}$$

where η is the dimensionless CO_2 capture ratio, $Q_{G,in}$ and $Q_{G,out}$ are inlet and outlet gas flow rates respectively ($m^3\ s^{-1}$), and $C_{G,in}$ and $C_{G,out}$ are inlet and outlet gas phase concentrations respectively (mol m^{-3}). For each membrane process, absorbent flow rate was set up to a maximum Q_L of 2 L min^{-1}, which is the upper limit recommended by the manufacturer, and Q_G increased until there was no further discernible increase in η. Once η is determined, K_{OV} can be calculated from Equation 2.6. Carbon dioxide flux (J_{CO2}, mol $m^{-2}\ s^{-1}$) was calculated using:

$$J_{CO2} = \frac{[(Q_{G,in} \times C_{G,in}) - (Q_{G,out} \times C_{G,out})] \times 273.15 \times 1000}{(22.4 \times A_m \times T_G)} \quad \text{(Equation 2.7)}$$

where A_m refers to available membrane surface area for absorption (m^2),$C_{G,in}$ and $C_{G,out}$ are inlet and outlet gas phase concentrations respectively (volumetric ratio), 1000 a conversion from m^3 to L, 22.4 is the molar volume (L mol^{-1}) at 0 K, and T_G is gas temperature (K) [28]. The solubility limit for CO_2 (g_{CO2}/g_{H2O}) at 20°C and 0.5 BarG gas pressure was estimated using Henry's constant taken from the literature at 25°, with temperature dependence estimated using the Van't Hoff extrapolation [44,45]:

$$H^T = H^{\Theta} exp\left[\frac{\Delta_{sol}H}{R} \times \left(\frac{1}{T} - \frac{1}{T^{\Theta}}\right)\right] \quad \text{(Equation 2.8)}$$

Where H^T is Henry's constant at 20°C (mol L^{-1} atm^{-1}), H^{Θ} is Henry's constant at 25°C (mol L^{-1} atm^{-1}), $\Delta_{sol}H$ the enthalpy of dissolution (J mol^{-1}), R the ideal gas constant (J $mol^{-1}K^{-1}$), T and T_{Θ} are temperature and reference temperature respectively (K).

2.3 Results

2.3.1 Separation of carbon dioxide from a binary gas phase

CO_2 removal was evaluated initially with gas flowing on the shell side and subsequently with gas flowing on the lumen-side (Figure 2.2). In both cases, water was passed counter-current and on the opposing side of the membrane. With lumen-side gas flow, it was not possible to achieve an outlet CO_2 concentration below 20%, whilst for shell-side gas flow, an outlet CO_2 concentration approaching 0% was attained, and is similar to earlier studies in which shell-side gas flow was favourably demonstrated for parallel flow membrane contactors [46,47]. Subsequent experimentation was therefore conducted with shell-side gas flow.

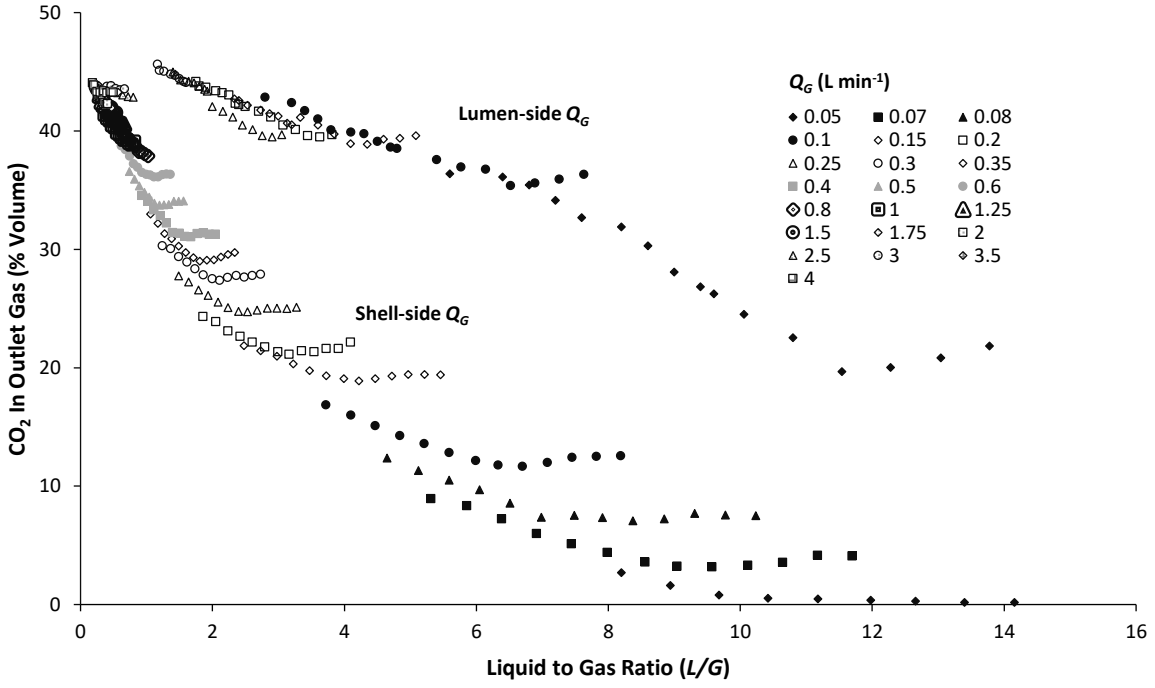

Figure 2.2 Comparison of the impact of lumen-side and shell-side gas flow on CO_2 gas outlet concentration (% vol.). Gas inlet, 50/50 CO_2/CH_4; Water as absorbent (20°C). Gas flow rate (Q_G) fixed between 0.05 and 4 L min^{-1}; for each fixed Q_G, liquid flow rate was varied between 0.28 and 2 L min^{-1}.

The influence of the liquid to gas ratio was investigated at differing gas velocities by initially fixing V_G and subsequently varying liquid flow rate (Figure 2.3). At the lowest V_G of 0.9x10^{-3} m s^{-1}, J_{CO2} was consistently recorded around 0.34x10^{-4} mol m^{-2} s^{-1} despite increasing *L/G* from 8 to 14. In contrast, for the intermediate range of gas velocities tested, the J_{CO2} profile at each V_G was characterised by an initial increase in J_{CO2}, followed by the onset of a plateau at higher *L/G* ratios. For the upper range of gas velocities tested (V_G, >55.8x10^{-3} m s^{-1}), J_{CO2} began to converge around a limit close to 3.5x10^{-4} mol m^{-2} s^{-1}, suggesting that J_{CO2} was dependent upon V_L but independent of V_G, at the upper V_G range tested (Figure 2.3, Inset). The boundary conditions that facilitated an upper limit for J_{CO2} corresponded to a low CO_2 capture ratio (Figure 2.4). To illustrate, a η_{CO2} of 0.12 was achieved when V_G and *L/G* were fixed at 74.4x10^{-3} m s^{-1} and 0.19 respectively. However, at the lowest V_G, a η_{CO2} approaching 1 was achieved, which is sufficient to achieve the gas-phase methane purity of 98% that is demanded for biogas grid injection [48].

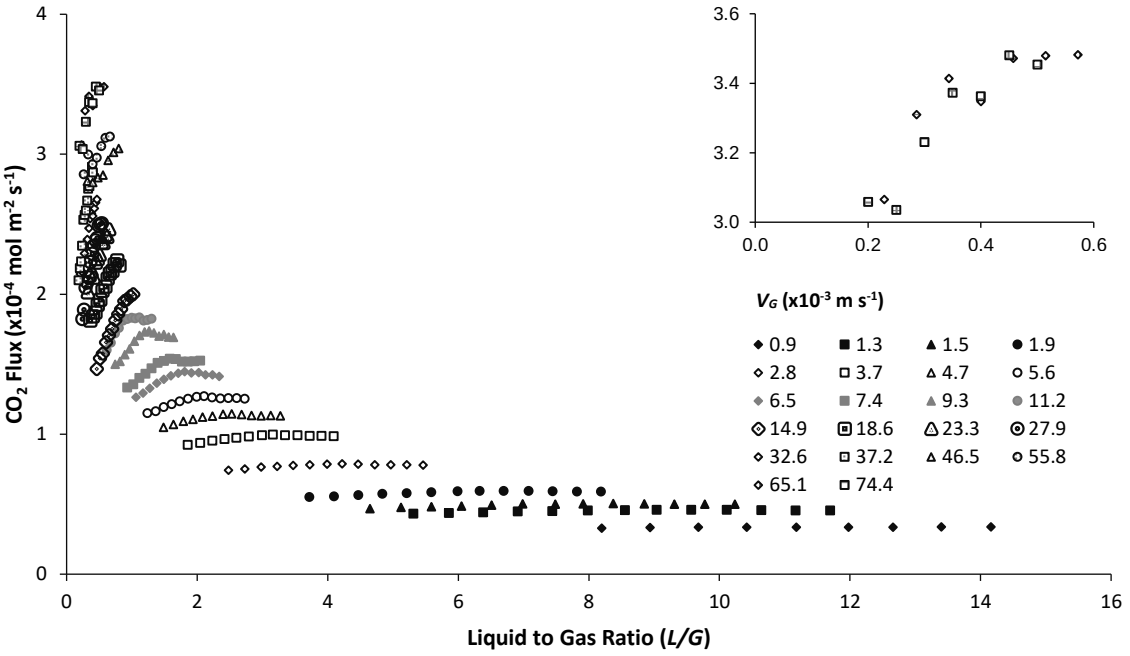

Figure 2.3 The impact of hydrodynamic conditions on CO_2 flux (J_{CO2}). Gas inlet, 50/50 CO_2/CH_4; Water as absorbent (20°C). Superficial gas velocity (V_G) was fixed between 0.0009 and 0.0744 m s^{-1}. At each fixed V_G, liquid velocity was varied between 0.0018 and 0.064 m s^{-1}). Inset: J_{CO2} data overlaid at the highest V_G tested therefore represent the maximum attainable J_{CO2} within a single module.

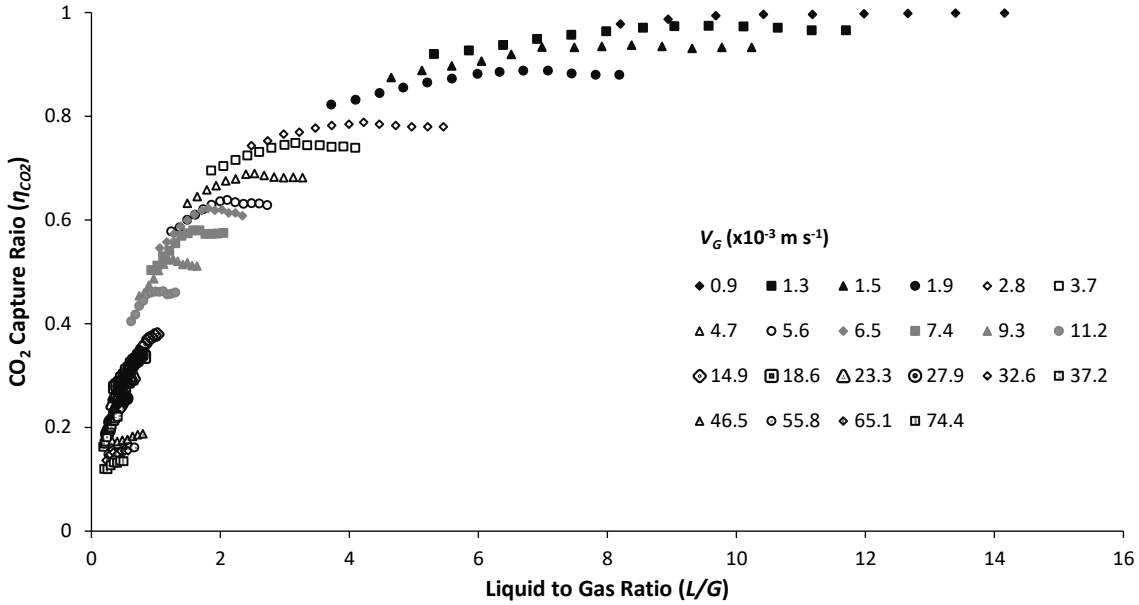

Figure 2.4 The effect of hydrodynamic conditions on the dimensionless capture ratio (η_{CO2}) within a single module. Gas inlet, 50/50 CO_2/CH_4; Water used as absorbent (20°C). Superficial gas velocity (V_G) was fixed between 0.0009 and 0.0744 m s^{-1}. At each fixed V_G, liquid velocity was varied between 0.0018 and 0.064 m s^{-1}).

2.3.2 Evaluation of mass transfer resistance

Overall resistance to mass transfer was first evaluated using pure CO_2 (Figure 2.5a). As the gas phase comprised of only one component, the gas phase resistance is assumed negligible and the overall resistance to mass transfer (Equation 2.1) can be described by the sum of liquid and membrane resistance [36]. Membrane resistance was subsequently determined with pure CO_2 as $1/k_m$ 2.7x10^{-4} s m^{-1} using the Wilson plot method (Figure 2.5a, inset), which permitted the liquid phase resistance to be determined ($1/k_l = 1/K_{ov} - 1/k_m$). For pure CO_2, as V_L was increased, $1/K_{ov}$ quickly reduced up until a plateau was reached, which began at around V_L 30x10^{-3} m s^{-1}. The $1/k_l$ corresponding to the plateau approached a minimum that was equal to 0.8x10^{-4} s m^{-1}.

Overall resistance for the binary gas was equivalent to that of pure CO_2 at the higher V_L range when V_G was fixed above 32.6x10^{-3} m s^{-1} (Figure 2.5a), suggesting that above this gas velocity, the gas phase resistance was negligible. This was subsequently confirmed by mass transfer analysis of the gas phase (Figure 2.5b). The gas phase resistance can be inferred from the difference in $1/K_{ov}$ between the pure CO_2 and binary gas mixture (Figure 2.5a). When V_G was below 5.6x10^{-3} m s^{-1}, $1/k_g$ dominated mass transfer. It was not until the upper limit for both V_G and V_L were simultaneously employed that membrane resistance dominated mass transfer (Figure 2.5c). To illustrate, at a fixed

V_G of 37.2x10^{-3} m s^{-1}, over 50% of $1/K_{ov}$ was attributable to $1/k_m$ once V_L increased above 14x10^{-3} m s^{-1}.

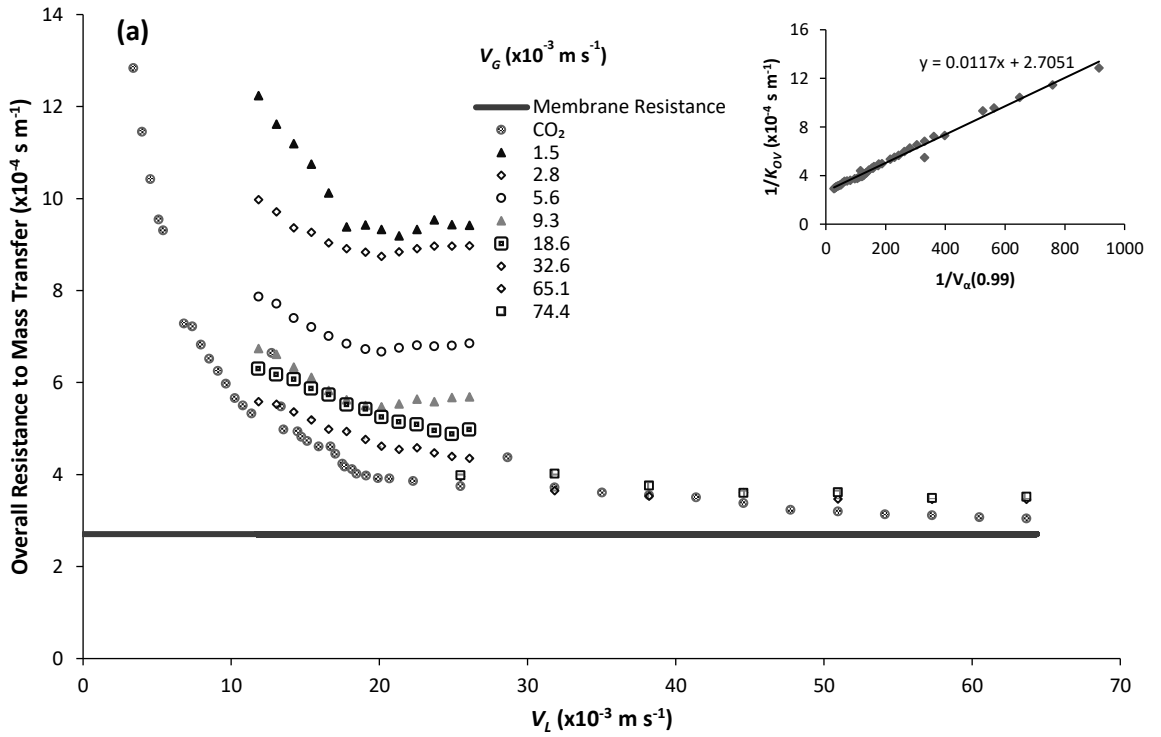

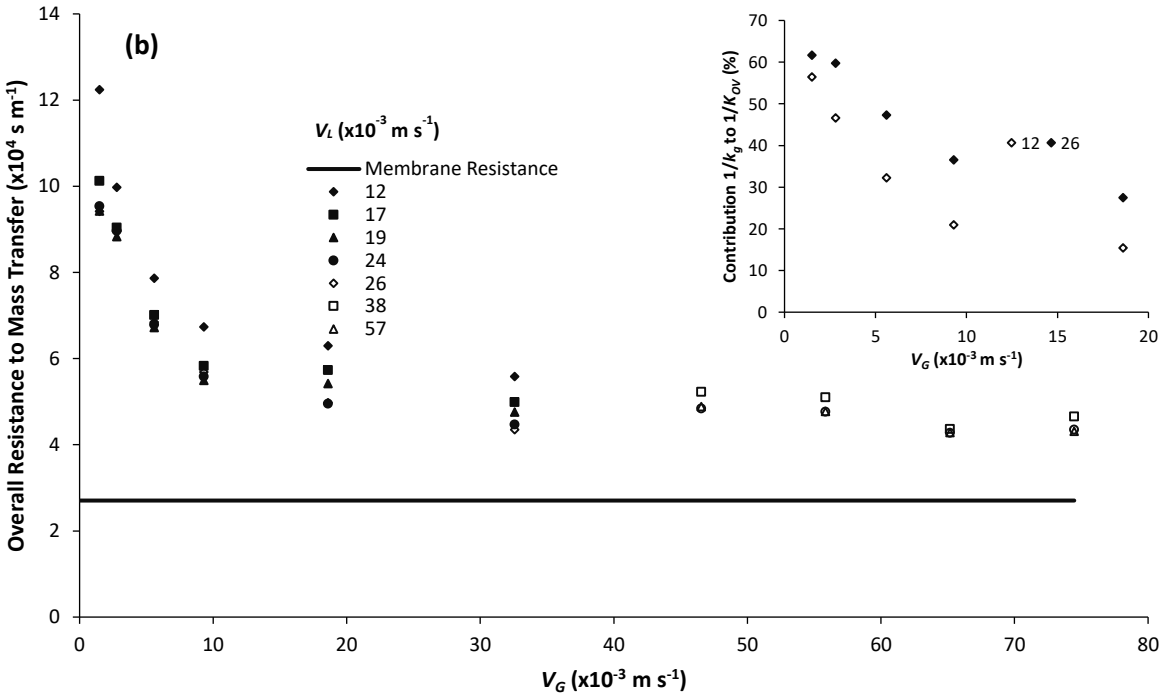

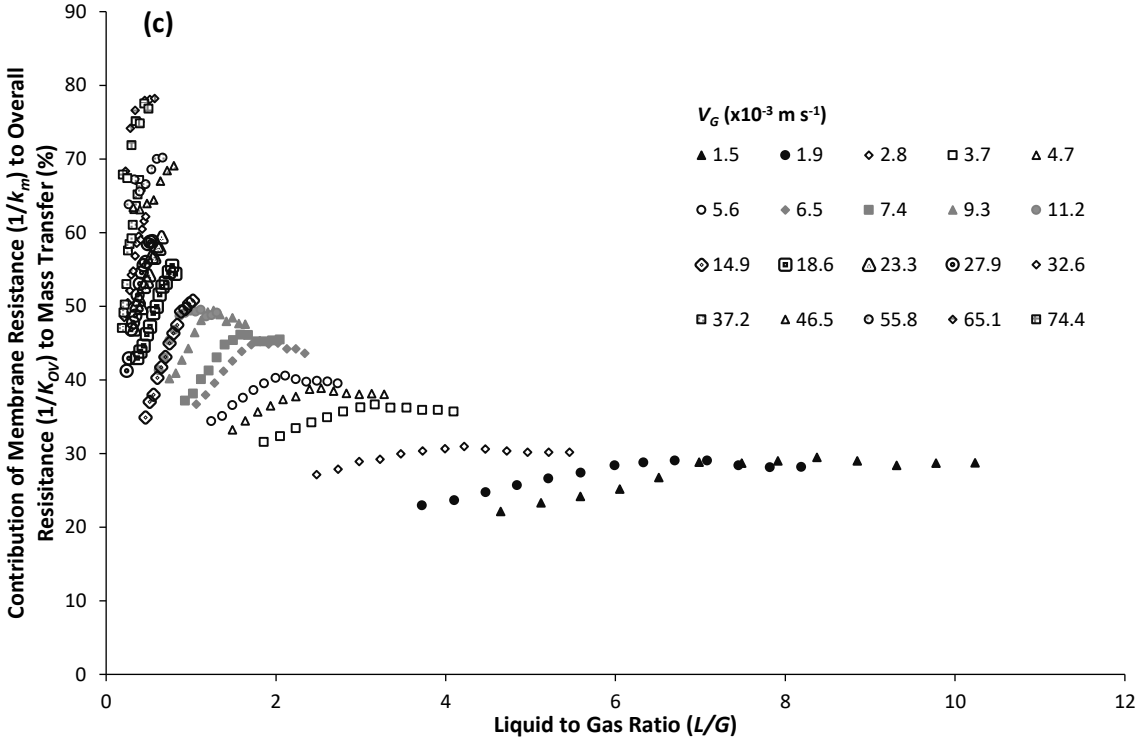

Figure 2.5 Resistance in series analysis undertaken on a single module. (a) Overall resistance to mass transfer for a 50/50 CO_2/CH_4 inlet gas. Data compared to 100% CO_2 inlet gas. Inset: Wilson Plot analysis using 100% CO_2 inlet gas, indicating $1/k_m$ of 27051 s m^{-1}. (b) Data analysed to identify gas phase contribution. Inset: relative contribution of gas phase resistance to $1/K_{ov}$. (c) Relative contribution of membrane resistance to the overall resistance to mass transfer. Water used as absorbent (20°C).

2.3.3 *Experimental assessment of hollow fibre membrane contactors in series*

The CO_2 capture ratio (η_{CO2}) was evaluated for one, two and three modules in series (Figure 2.1). In this configuration, the outlet gas and liquid from one module were applied to the subsequent module to extend process path length (Figure 2.6). Increasing the number of modules in series increased the η_{CO2} that could be attained at a fixed gas velocity. For example, at V_G 3.7x10^{-3} m s^{-1}, η_{CO2} increased from 0.75 to 0.94 for two modules and to 0.99 for three modules in series respectively. To attain the desired η_{CO2} of 0.98, a single module (L=0.113m) was limited to V_G <0.9x10^{-3} m s^{-1} and L/G ratio of 8. For comparison, using two (L=0.226m) and three (L=0.339m) modules in series to achieve η_{CO2} 0.98, V_G could be increased to 2.8x10^{-3} and 3.7 x10^{-3} m s^{-1} and L/G reduced to 4 and 2.2 respectively.

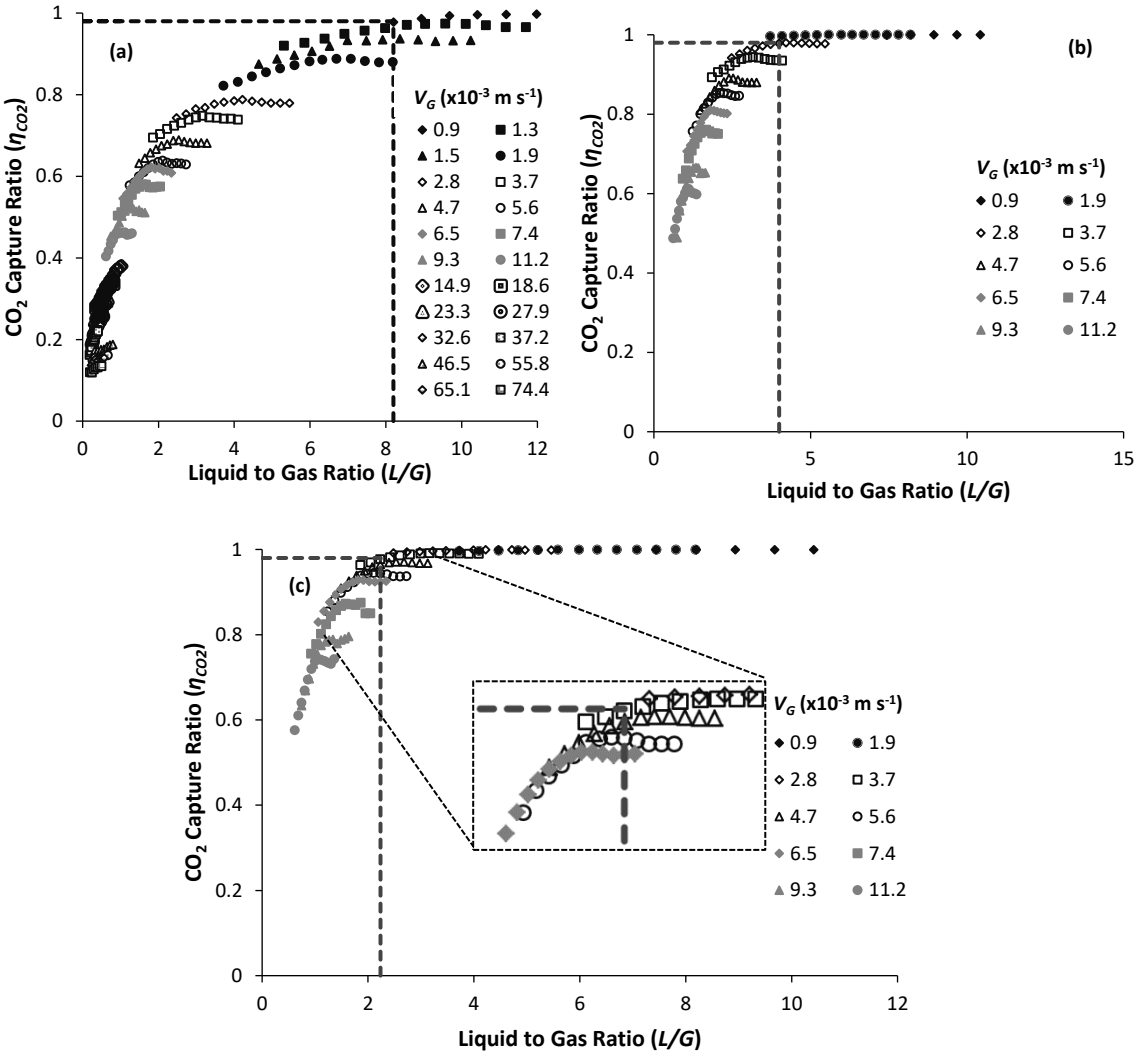

Figure 2.6 The impact of process length on CO_2 capture ratio: (a) one module, *L* 0.113m; (b) two modules in series, *L* 0.226m; and (c) three modules in series, *L* 0.339m. Superficial gas velocity was fixed between 0.0009 and 0.0744 m s^{-1}. For each V_G, liquid velocity was varied between 0.0018 and 0.064 m s^{-1}. Water used as absorbent (20°C).

2.3.4 An estimation of scale-up using the overall mass transfer coefficient

The applicability of the overall mass transfer coefficient for estimating η_{CO2} in multi-module configuration was undertaken using experimental data from a single module, and modelled η_{CO2} with a simplified equation to predict scale-up (Equation 2.5). The modelled output was then compared to experimental data of two and three modules in series (Figure 2.6) to test the model accuracy (Figure 2.7).

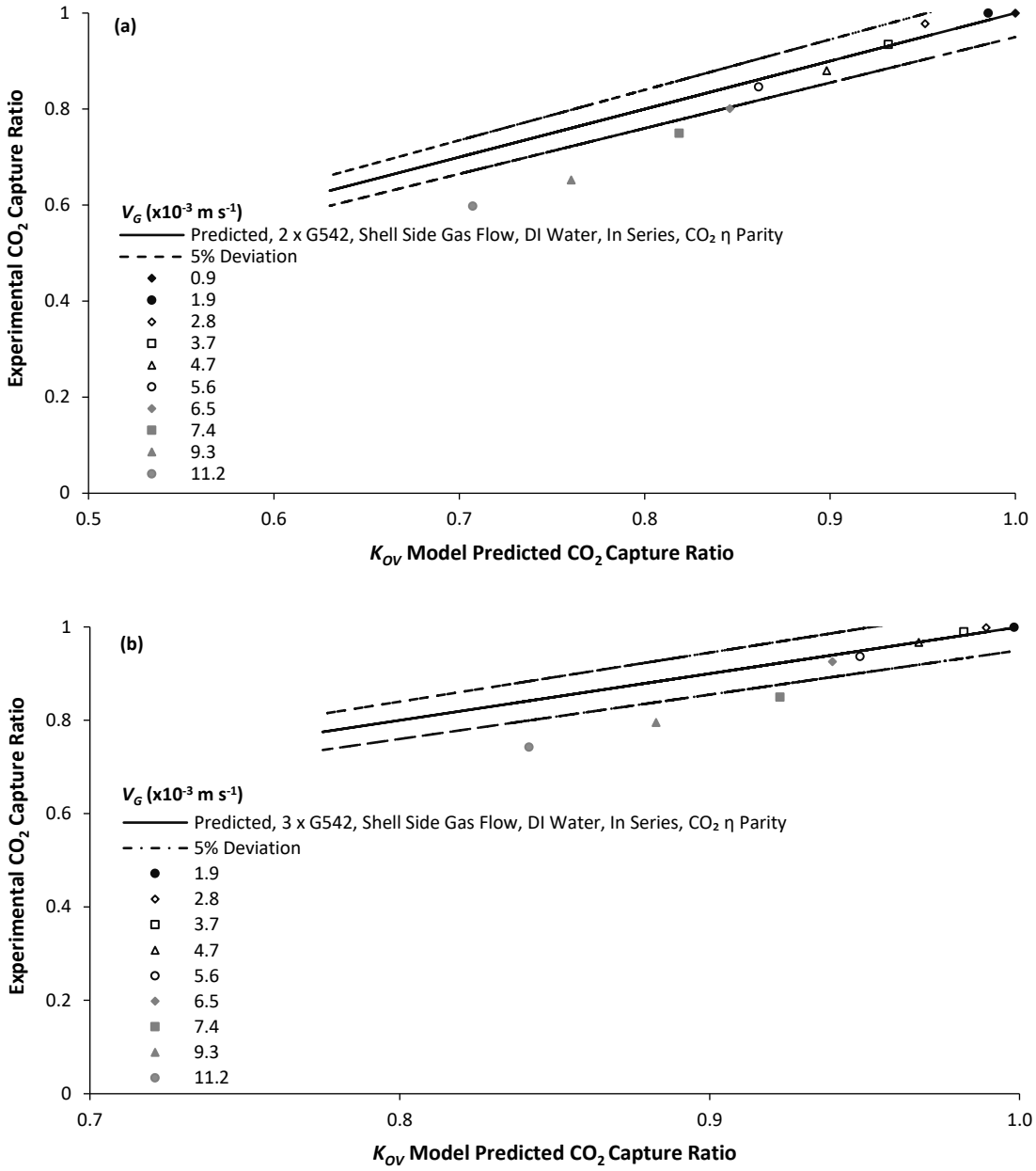

Figure 2.7 Parity plot of CO_2 capture ratio (η_{CO2}) estimated from a single module and compared to the η_{CO2} experimentally determined for: (a) two, and (b) three modules in series. Shell side gas flow; gas inlet, 50/50 CO_2/CH_4; water used as absorbent (20°C). Superficial gas velocity (V_G) was fixed between 0.0009 and 0.0744 m s^{-1}. At each V_G, liquid velocity was varied between 0.0018 and 0.064 m s^{-1}. The absorbent was fed in-series.

For two and three modules in series, the modelled data could accurately estimate mass transfer, and hence the η_{CO2} experimentally achieved, when V_G was less than 5.6x10^{-3} m s^{-1}. However, the estimated η_{CO2} tended away from the experimental data when V_G increased above 5.6x10^{-3} m s^{-1}, becoming more inaccurate as V_G increased. This corresponded to a CO_2 load in the liquid phase of 2.95x10^{-4} g_{CO2} g_{H2O}^{-1} (Figure 2.8),

or around 30% of the CO_2 solubility limit. Using the same in series configuration comprised of two and three modules, fresh absorbent was subsequently applied at each stage (absorbent recharge, Figure 2.1 and 2.9) to further evaluate the role of the liquid phase resistance on the estimation of mass transfer. Similar to classical shell-side absorbent flow, the estimated CO_2 capture ratio provided reasonable description of the experimental mass transfer data, for low V_G. However, the estimated mass transfer data was also considerably more accurate at the higher V_G in comparison to when the same absorbent was used. To illustrate, for two and three modules in series, the estimated η_{CO2} was within 5% of the experimentally determined η_{CO2} for the V_G range between 1.95×10^{-3} m s^{-1} and 14.95×10^{-3} m s^{-1}.

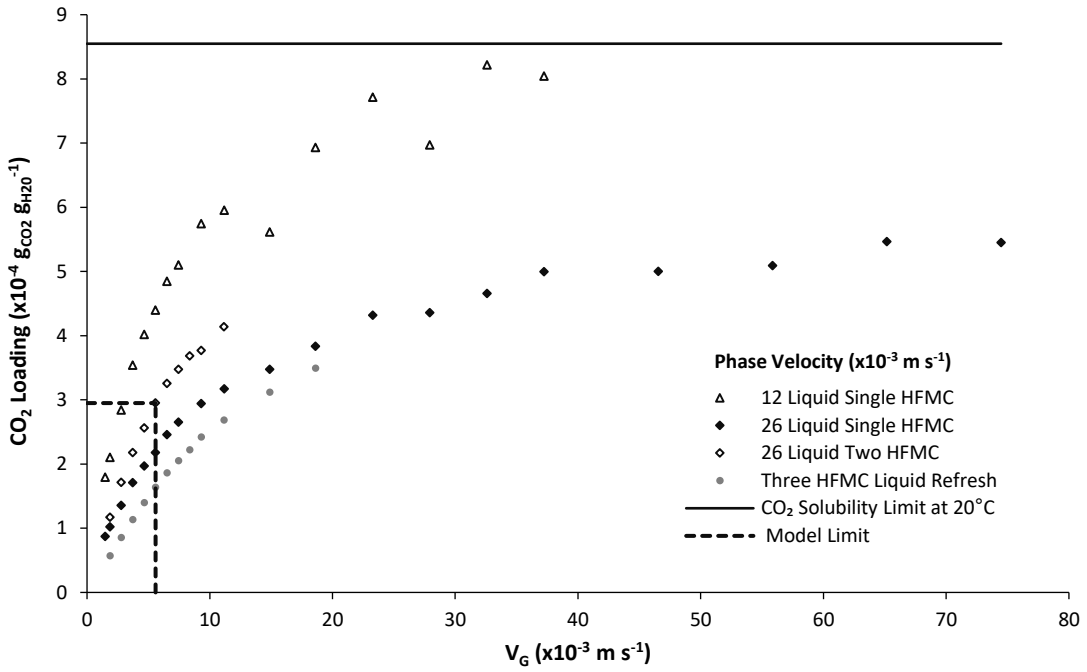

Figure 2.8 Liquid phase CO_2 loading (g_{CO2}/g_{H2O}) calculated for one and multiple HFMC (in series) at two liquid velocities (V_L, 0.012 and 0.026 m s^{-1}). The limiting gas phase velocity required to achieve a CO_2 capture ratio of 98 % (V_G of 0.0056 m s^{-1}) corresponded to a CO_2 loading of 2.95×10^{-4} g_{CO2} g_{H2O}^{-1}), well below the prescribed solubility limit.

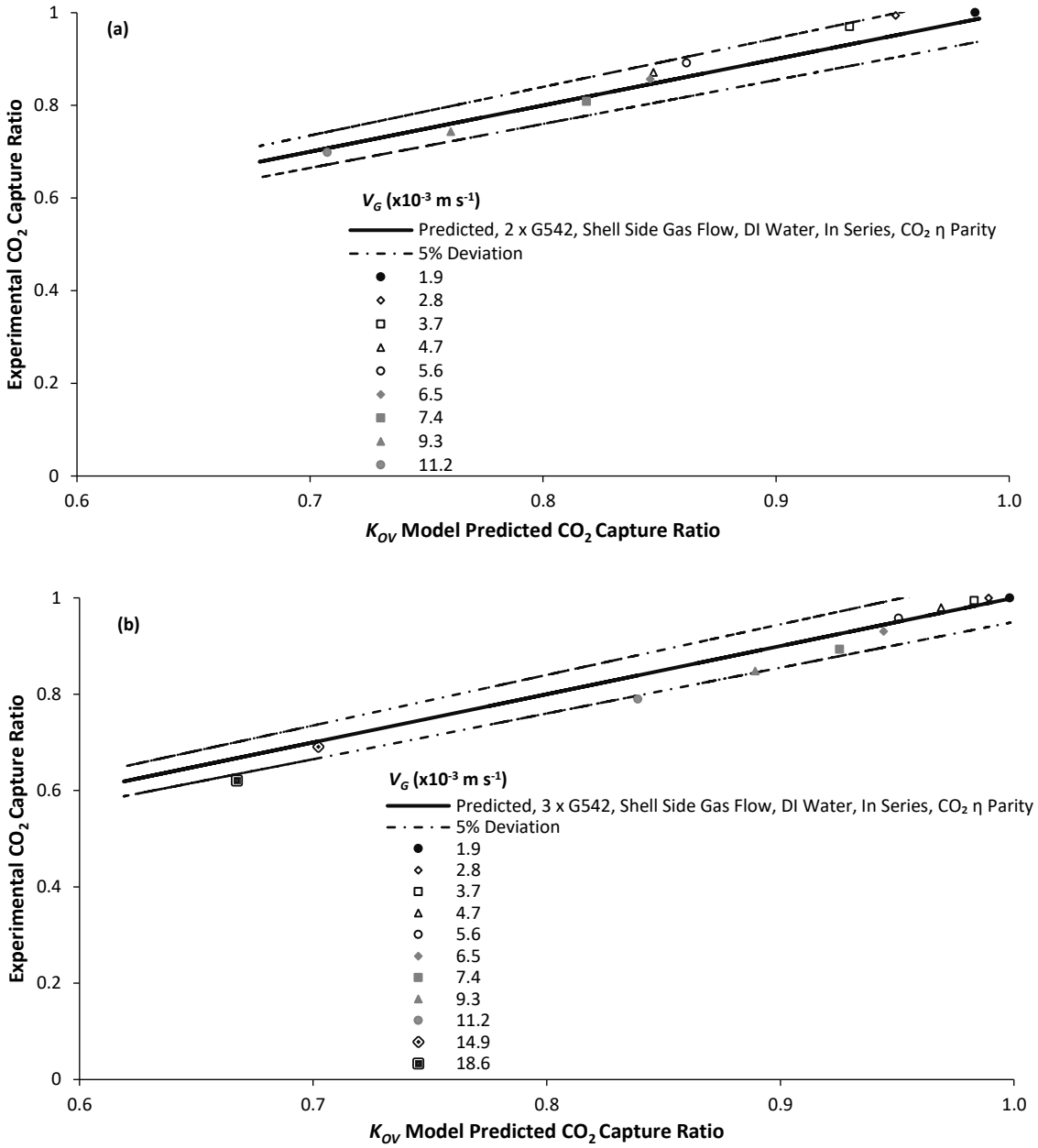

Figure 2.9 Parity plot of CO_2 capture ratio (η_{CO2}) estimated from a single module and compared to the η_{CO2} experimentally determined for: (a) two, and (b) three modules in series. Shell side gas flow; gas inlet, 50/50 CO_2/CH_4; water used as absorbent (20°C). Superficial gas velocity (V_G) was fixed between 0.0009 and 0.0744 m s^{-1}. At each V_G, liquid velocity was varied between 0.0018 and 0.064 m s^{-1}. Fresh absorbent was introduced into each module.

2.4 Discussion

A significant finding from this study is that mass transfer is primarily gas phase controlled when hydrodynamic conditions are instigated that favour the promotion of gas product purity in a concentrated binary gas. This re-evaluation of multi-module configured membrane contactors has demonstrated that process scale, and product quality, can be

satisfactorily estimated for water-based absorbents using a simplified mass transfer model, based on the overall mass transfer coefficient, which has been previously assumed to be limited to systems comprised of chemical reaction. When V_G was fixed at a velocity exceeding 47x10^{-3} m s^{-1} (Figure 2.3), CO_2 flux increased in response to an increase in liquid velocity until a plateau was reached. Such limiting behaviour has been similarly observed in the HFMC literature when using water as the solvent [7,28,35,38,39]. The driving force for CO_2 absorption is the concentration difference between the gas and liquid phase [8]. Consequently, increasing V_L reduced the CO_2 concentration gradient within the liquid phase boundary layer, helping to re-establish the concentration gradient and promote higher CO_2 flux [7,8]. Whilst such a trend ostensibly suggests that mass transfer is liquid phase controlled, it is evident that CO_2 flux increased upon increasing V_G (Figure 2.3). By increasing V_G, the gas phase residence time ($\tau = l/v$) reduced, which limited time for CO_2 transport from the bulk gas phase to the gas-membrane boundary. Consequently, higher gas velocities impose an increased average CO_2 partial pressure at the same total gas phase pressure, thereby promoting enhanced mass transfer [49,50].

Gas velocity was observed to enhance mass transfer up to around V_G 55x10^{-3} m s^{-1}, where J_{CO2} data began to converge around 3.5x10^{-4} mol m^{-2} s^{-1} (Figure 2.3). This indicates that the gas phase is less influential when operating HFMC within hydrodynamic conditions that favour mass transfer, which was subsequently confirmed by resistance in series analysis, whereby gas phase resistance ($1/k_g$) tended toward a minimum at low *L/G* ratio (Figure 2.5a and b). Within these conditions, mass transfer can therefore be primarily described as liquid phase controlled, which is in agreement with previous literature [21,23,51]. Process intensification is typically described in terms of average molar flux [48,44] which would infer that the optimum operating point in this study is around *L/G* 0.45. This is closely aligned to the *L/G* ratio typically specified in HFMC CO_2 separation studies that use water as the physical solvent (Table 2.1) and explains why the impact of gas phase resistance has previously been considered of negligible significance to mass transfer [24,28,36,38,39,52]. The practicable upper V_L limit for a single module was V_L 64 x 10^{-3} m s^{-1}, which corresponds to the maximum flow rate specified by the manufacturer [53] . During operation, at V_G above 65.1x10^{-3} m s^{-1}, an increase of between 26 and 64 x 10^{-3} m s^{-1} did not increase mass transfer (Figure 2.5b). This can be ascribed to the conditions for which both gas and liquid phase resistance are at a minimum, and membrane resistance begins to dominate mass transfer (Figure 2.5).

Notably, it is the lower V_G which favours gas product purity (Figure 2.4). Therefore, for a binary gas, it is the gas flow and not just the *L/G* applied that determines the relative resistance to mass transfer. The low gas velocity introduces longer gas phase residence time, which permits time for diffusion from the bulk to the boundary layer to initiate contact with the solvent [54]. As such, in the intermediate V_G range, gas-phase purity is also improved by increasing the *L/G* ratio, as this reduces the local CO_2 concentration gradient in the receiving liquid phase boundary layer [7]. However, for single module operation, it is only at the lowest gas velocity (V_G $0.9x10^{-3}$ m s^{-1}) where the final gas product achieves 98% CH_4, which is the target threshold identified for this application [48,55]. For gas velocities below V_G $5.6x10^{-3}$ m s^{-1}, CO_2 flux was independent of liquid velocity (Figure 2.3), coincident with a considerable increase in gas phase resistance (Figure 2.5a and b). Therefore, for the conditions that favour gas product purity, mass transfer is best described as gas-phase controlled [56]. It is proposed that when water is used to promote physical absorption in membrane contactors, gas phase resistance will inevitably provide a contribution for CO_2 binary gas applications, particularly when evaluated on an NTU rather than HTU basis. Whilst the gas phase resistance ($1/k_g$) contribution can be expected to be more significant for biogas upgrading due to the higher feed-side CO_2 concentration and final gas product standard that must be achieved relative to other CO_2 applications [57,58], several studies using chemically enhanced mass transfer have similarly identified a trade-off between CO_2 flux and CO_2 capture [57,59], which is consistent with this study where water is used as the solvent.

It was possible to achieve the desired CO_2 η of 0.98 at higher gas velocities within multi-module configurations (Figure 2.6). To illustrate, V_G increased from $0.9x10^{-3}$ m s^{-1} for one module to $2.8x10^{-3}$ and $3.7x10^{-3}$ m s^{-1}, and the *L/G* ratio necessary to deliver η 0.98, reduced from 8 to 4 and 2.2 for two and three modules in series respectively. Process intensification can be accounted for by the increased average CO_2 concentration gradient, which increased the K_{ov} [47,57], whilst the extended length provided the necessary gas phase residence time to achieve the desired separation. The transition from one to two modules doubled membrane area, and provided a three-fold increase in mass transfer, whilst also delivering the required capture ratio. This is analogous to observations of previous authors, who ascribe the enhancement to solvent mixing in the interstitial pipework, permitting redevelopment of the velocity and concentration profiles [32,34]. Zhang et al. [57] developed a model to describe CO_2 capture in water (physical absorption) and 2M Diethanolamine (chemical absorption). In their study, the authors noted the existence of an effective module length (L_{eff}), beyond

which CO_2 removal would be ineffective. This can be attributed to the preferential mass transfer of CO_2 within the initial fibre length (or module) being driven by the higher local concentration gradient [7]. In this study, this was evidenced by the inclusion of the third module, which provided comparatively less process intensification than inclusion of the second module in series (Figure 2.6c). For each configuration studied (one to three modules in series), a CO_2 η of 0.98 was identified for V_G below $5.6x10^{-3}$ m s^{-1}, which corresponded to a region where mass transfer was independent of V_L, similar to single module analysis (Figure 2.5 and Figure 2.6), and corresponded to liquid loading of $3x10^{-4}$ g_{CO2} g_{H2O}^{-1} (Figure 2.8) or around 35% of the loading limit. Within this gas velocity range, the η_{CO2} could be accurately predicted within multi-module configurations through analysis of the overall mass transfer coefficient (K_{ov}) from a single module, and using only gas-side data. An inherent assumption of the K_{OV} model is that the CO_2 concentration in the liquid phase is negligible such that the resistance of the liquid phase to mass transfer is neglected [13]. Whilst the liquid phase resistance was not negligible, the primary resistance was in the gas phase, which was sufficient to achieve reasonable model accuracy within the operational region that favours a high CO_2 capture ratio. This was corroborated by mass transfer analysis in which the absorption solvent was replenished at each stage (Figure 2.9). The region of gas phase-controlled mass transfer did not change but the introduction of new absorbent within each module reduced liquid phase resistance and increased modelling accuracy for operation at lower *L/G* ratios. Importantly, it is asserted that the K_{ov} model which is conveniently applied for the industrial design of membrane contactors, ordinarily operated with solvent flow in excess, can also be applied to binary gas separation in HFMC using water as the absorbent, which is presently one of the fastest growing areas for gas-liquid separation.

2.5 Conclusions

In this study, mass transfer can be described as gas phase controlled when modules are configured to facilitate high gas product quality in a CO_2 containing binary gas. Consequently, a simplified mass transfer model, based on the overall mass transfer coefficient, can be used to determine gas product quality, process scale and membrane configuration for water scrubbing of CO_2 from biogas. This demonstrates that the conventional industrial approach to modelling scale-up of membrane contactors is applicable for binary gas separation, even when the extracting solvent exerts resistance to mass transfer, but provided it is not the dominant resistance to mass transfer. Furthermore, since only gas phase data is required for modelling, the data requirement

to facilitate comprehensive process design is rationalised. Importantly this approach is valid to biogas upgrading, which is one of the fastest growing applications for gas-liquid contactors due to the Europe wide introduction of incentivisation, where water is the preferred absorption solvent. From the study several further conclusions can be drawn:

- For CO_2 separations generally, gas phase resistance can be expected to be more considerable than previously assumed in the literature, when the overall system is designed to determine the NTU required to achieve a prescribed gas product quality. This has been emphasised in this study, through the wider exploration of hydrodynamic conditions (i.e. changing gas flow rate and gas-liquid ratio), to revalue the significance of each contributing phase to mass transfer. In the case of applications such as biogas upgrading, characterised by a high CO_2 partial pressure and tightly defined final gas product quality, the gas phase resistance can be expected to present a higher proportion of overall resistance to mass transfer;
- Modelling scale-up of hollow fibre membrane contactors using the overall mass transfer coefficient is expectedly applicable to binary gas separations that must produce high purity gas since the extracting solvent must be in excess, defaulting to gas phase-controlled mass transfer, which conforms to the limit of the model;
- This simplified mass transfer analysis is applicable to conditions for which the gas-phase controls mass transfer but also for which the liquid phase resistance is not negligible (but rather not dominant);
- Configuring hollow fibre membrane contactors in series for binary gas separations is advantageous for capital cost, as an enhancement in mass transfer is evidenced that is greater than the sum of the membrane material added, however, there is a limiting effective length;
- Whilst configuring hollow fibre membrane contactors in series increased mass transfer, to achieve the necessary final gas phase product quality, the gas velocity range is limited to conditions in which the gas phase provides the principle resistance to mass transfer.

Acknowledgements

The authors would like to thank Anglian Water, Northumbrian Water and Severn Trent Water for their practical and financial support. We are also grateful for funding from the Engineering and Physical Sciences Research Council (EPSRC) which was provided through the STREAM Industrial Doctorate Centre. Enquiries for access to the data referred to in this article should be directed to: researchdata@ cranfield.ac.uk.

References

[1] P.M. Connor, L. Xie, R. Lowes, J. Britton, T. Richardson, The development of renewable heating policy in the United Kingdom, Renew. Energy. 75 (2015) 733–744.

[2] A. Hast, S. Syri, J. Jokiniemi, M. Huuskonen, S. Cross, Review of green electricity products in the United Kingdom, Germany and Finland, Renew. Sustain. Energy Rev. 42 (2015) 1370–1384.

[3] International Energy Association Task 37, IEA Bioenergy Task 37 Upgrading Plant List 2017, (2017). http://task37.ieabioenergy.com/plant-list.html (accessed November 17, 2018).

[4] C. Makhloufi, E. Lasseuguette, J.C. Remigy, B. Belaissaoui, D. Roizard, E. Favre, Ammonia based CO_2 capture process using hollow fiber membrane contactors, J. Memb. Sci. 455 (2014) 236–246.

[5] J. He, R.G. Arnold, A.E. Sáez, E.A. Betterton, W.P. Ela, Removal of Aqueous Phase Trichloroethylene Using Membrane Air Stripping Contactors, J. Environ. Eng. 130 (2004) 1232–1241.

[6] J. Elhajj, M. Al-hindi, F. Azizi, A Review of the Absorption and Desorption Processes of Carbon Dioxide in Water Systems, Ind. Eng. Chem. Res. 53 (2014) 2–22.

[7] S. Heile, S. Rosenberger, A. Parker, B. Jefferson, E.J. McAdam, Establishing the suitability of symmetric ultrathin wall polydimethylsiloxane hollow-fibre membrane contactors for enhanced CO_2 separation during biogas upgrading, J. Memb. Sci. 452 (2014) 37–45.

[8] Z. Cui, D. DeMontigny, CO_2 capture using hollow fiber membrane contactors, Carbon Manag. 4 (2013) 69–89.

[9] D. DeMontigny, P. Tontiwachwuthikul, A. Chakma, Comparing the Absorption Performance of Packed Columns and Membrane Contactors, Ind. Eng. Chem. Res. 44 (2005) 5726–5732.

[10] B.W. Reed, M.J. Semmens, E.J. Cussler, Membrane contactors, in: R.D. Nobel, A.S. Stern (Eds.), Membr. Sep. Technol. Princ. Appl., Elsevier, 1995: pp. 467–498.

[11] I. Iliuta, M.C. Iliuta, CO_2 Removal in Packed-Bed Columns and Hollow-Fiber Membrane Reactors . Investigation of Reactor Performance, Ind. Eng. Chem. Res. 54 (2015) 12455–12465.

[12] F. Wiesler, Membrane contactors: an introduction to the technology, Ultrapure

Water. (1996) 27–31.

[13] E. Chabanon, D. Roizard, E. Favre, Modeling strategies of membrane contactors for post-combustion carbon capture: A critical comparative study, Chem. Eng. Sci. 87 (2013) 393–407.

[14] A. Sengupta, P.A. Peterson, B.D. Miller, J. Schneider, C.W. Fulk, Large-scale application of membrane contactors for gas transfer from or to ultrapure water, Sep. Purif. Technol. 14 (1998) 189–200.

[15] P. Schöner, P. Plucinski, W. Nitsch, U. Daiminger, Mass transfer in the shell side of cross flow hollow fiber modules, Chem. Eng. Sci. 53 (1998) 2319–2326.

[16] S.R. Wickramasinghe, M.J. Semmens, E.L. Cussler, Better hollow fiber contactors, J. Memb. Sci. 62 (1991) 371–388.

[17] M. Yang, E.L. Cussler, Designing Hollow-Fiber Contactors, AIChE J. 32 (1986) 1910–1916.

[18] J.J. Cai, K. Hawboldt, M.A. Abdi, Contaminant removal from natural gas using dual hollow fiber membrane contactors, J. Memb. Sci. 397–398 (2012) 9–16.

[19] Y.Y. Wang, F. Chen, Y.Y. Wang, G. Luo, Y. Dai, Effect of random packing on shell-side flow and mass transfer in hollow fiber module described by normal distribution function, J. Memb. Sci. 216 (2003) 81–93.

[20] A. Bottino, G. Capannelli, A. Comite, R. Di, R. Firpo, CO_2 removal from a gas stream by membrane contactor, Sep. Purif. Technol. 59 (2008) 85–90.

[21] V.Y. Dindore, D.W.F. Brilman, F.H. Geuzebroek, G.F. Versteeg, Membrane – solvent selection for CO_2 removal using membrane gas – liquid contactors, Sep. Purif. Technol. 40 (2004) 133–145.

[22] S. Nii, H. Takeuchi, Removal of CO_2 and/or SO_2 from gas streams by a membrane absorption method, Gas Sep. Purif. 8 (1994) 107–114.

[23] M. Mavroudi, S.P. Kaldis, G.P. Sakellaropoulos, A study of mass transfer resistance in membrane gas-liquid contacting processes, J. Memb. Sci. 272 (2006) 103–115.

[24] S. Atchariyawut, C. Feng, R. Wang, R. Jiraratananon, D.T. Liang, Effect of membrane structure on mass-transfer in the membrane gas-liquid contacting process using microporous PVDF hollow fibers, J. Memb. Sci. 285 (2006) 272–281.

[25] Z. Zhang, Y. Yan, Y. Chen, L. Zhang, Investigation of CO_2 absorption in methyldiethanolamine and 2-(1-piperazinyl)-ethylamine using hollow fiber membrane contactors : Part C . Effect of operating variables, J. Nat. Gas Sci. Eng.

20 (2014) 58–66.

[26] W. Rongwong, S. Wongchitphimon, K. Goh, R. Wang, T. Bae, Transport properties of CO_2 and CH_4 in hollow fiber membrane contactor for the recovery of biogas from anaerobic membrane bioreactor effluent, J. Memb. Sci. 541 (2017) 62–72.

[27] V.Y. Dindore, D.W.F. Brilman, G.F. Versteeg, Hollow fiber membrane contactor as a gas–liquid model contactor, Chem. Eng. Sci. 60 (2005) 467–479.

[28] S. Atchariyawut, R. Jiraratananon, R. Wang, Separation of CO_2 from CH_4 by using gas–liquid membrane contacting process, J. Memb. Sci. 304 (2007) 163–172.

[29] R. Faiz, M.H. El-Naas, M. Al-Marzouqi, Significance of gas velocity change during the transport of CO_2 through hollow fiber membrane contactors, Chem. Eng. J. 168 (2011) 593–603.

[30] S. Boributh, S. Assabumrungrat, N. Laosiripojana, R. Jiraratananon, Effect of membrane module arrangement of gas-liquid membrane contacting process on CO_2 absorption performance: A modeling study, J. Memb. Sci. 372 (2011) 75–86.

[31] S. Boributh, S. Assabumrungrat, N. Laosiripojana, R. Jiraratananon, A modeling study on the effects of membrane characteristics and operating parameters on physical absorption of CO_2 by hollow fiber membrane contactor, J. Memb. Sci. 380 (2011) 21–33.

[32] S. Boributh, W. Rongwong, S. Assabumrungrat, N. Laosiripojana, R. Jiraratananon, Mathematical modeling and cascade design of hollow fiber membrane contactor for CO_2 absorption by monoethanolamine, J. Memb. Sci. 401–402 (2012) 175–189.

[33] J. Cookney, A. Mcleod, V. Mathioudakis, P. Ncube, A. Soares, B. Jefferson, E.J. McAdam, Dissolved methane recovery from anaerobic effluents using hollow fibre membrane contactors, J. Memb. Sci. 502 (2016) 141–150.

[34] S.-J. Kim, A. Park, S.-E. Nam, Y.-I. Park, P.S. Lee, Practical designs of membrane contactors and their performances in CO_2/CH_4 separation, Chem. Eng. Sci. 155 (2016) 239–247.

[35] S. Khaisri, D. DeMontigny, P. Tontiwachwuthikul, R. Jiraratananon, Comparing membrane resistance and absorption performance of three different membranes in a gas absorption membrane contactor, Sep. Purif. Technol. 65 (2009) 290–297.

[36] S. Atchariyawut, R. Jiraratananon, R. Wang, Mass transfer study and modeling of gas-liquid membrane contacting process by multistage cascade model for CO_2 absorption, Sep. Purif. Technol. 63 (2008) 15–22.

[37] M. Rezaei, A.F. Ismail, S.A. Hashemifard, G. Bakeri, T. Matsuura, Experimental study on the performance and long-term stability of PVDF/montmorillonite hollow fiber mixed matrix membranes for CO_2 separation process, Int. J. Greenh. Gas Control. 26 (2014) 147–157.

[38] M. Rahbari-Sisakht, A.F. Ismail, D. Rana, T. Matsuura, Effect of different additives on the physical and chemical CO_2 absorption in polyetherimide hollow fiber membrane contactor system, Sep. Purif. Technol. 98 (2012) 472–480.

[39] A.F. Ismail, A. Mansourizadeh, A comparative study on the structure and performance of porous polyvinylidene fluoride and polysulfone hollow fiber membranes for CO_2 absorption, J. Memb. Sci. 365 (2010) 319–328.

[40] H.J. Lee, E. Magnone, J.H. Park, Preparation, characterization and laboratory-scale application of modified hydrophobic aluminum oxide hollow fiber membrane for CO_2 capture using H_2O as low-cost absorbent, J. Memb. Sci. 494 (2015) 143–153.

[41] H. Zhang, R. Wang, D. Tee, J. Hwa, Theoretical and experimental studies of membrane wetting in the membrane gas-liquid contacting process for CO_2 absorption, J. Memb. Sci. 308 (2008) 162–170.

[42] B. Belaissaoui, J. Claveria-Baro, A. Lorenzo-Hernando, D. Albarracin, E. Chabanon, C. Castel, S. Rode, D. Roizard, E. Favre, Potentialities of a dense skin hollow fiber membrane contactor for biogas purification by pressurized water absorption, J. Memb. Sci. 513 (2016) 236–249.

[43] S. Rode, P.T. Nguyen, D. Roizard, R. Bounaceur, C. Castel, E. Favre, Evaluating the intensification potential of membrane contactors for gas absorption in a chemical solvent: A generic one-dimensional methodology and its application to CO_2 absorption in monoethanolamine, J. Memb. Sci. 389 (2012) 1–16.

[44] R. Sander, Compilation of Henry's law constants (version 4 . 0) for water as solvent, Atmos. Chem. Phys. 15 (2015) 4399–4981.

[45] F.L. Smith, A.H. Harvey, Avoid Common Pitfalls When Using Henry ' s Law, Chem. Eng. Prog. 103 (2007) 33–39.

[46] A. Gabelman, S. Hwang, Hollow fiber membrane contactors, J. Memb. Sci. 159 (1999) 62–106.

[47] Z. Cui, D. DeMontigny, Part 7: A review of CO_2 capture using hollow fiber membrane contactors, Carbon Manag. 4 (2014) 69–89.

[48] A. Mcleod, B. Jefferson, E.J. McAdam, Biogas upgrading by chemical absorption using ammonia rich absorbents derived from wastewater, Water Res. 67 (2014)

175–186.

[49] H.Y. Zhang, R. Wang, D.T. Liang, J.H. Tay, Modeling and experimental study of CO_2 absorption in a hollow fiber membrane contactor, J. Memb. Sci. 279 (2006) 301–310.

[50] Z. Cui, D. DeMontigny, Experimental study of carbon dioxide absorption into aqueous ammonia with a hollow fiber membrane contactor, J. Memb. Sci. 540 (2017) 297–306.

[51] W. Rongwong, S. Boributh, S. Assabumrungrat, N. Laosiripojana, R. Jiraratananon, Simultaneous absorption of CO_2 and H_2S from biogas by capillary membrane contactor, J. Memb. Sci. 392–393 (2012) 38–47.

[52] D. Albarracin Zaidiza, J. Billaud, B. Belaissaoui, S. Rode, D. Roizard, E. Favre, Modeling of CO_2 post-combustion capture using membrane contactors, comparison between one- and two-dimensional approaches, J. Memb. Sci. 455 (2014) 64–74.

[53] 3M, Membrane Contactor, (2017) 1–2. http://www.liquicel.com/product-information/data-sheets.cfm. (accessed May 15, 2017)

[54] A. Mansourizadeh, Experimental study of CO_2 absorption/stripping via PVDF hollow fiber membrane contactor, Chem. Eng. Res. Des. 90 (2012) 555–562.

[55] M. Persson, O. Jonsson, A. Wellinger, Biogas Upgrading To Vehicle Fuel Standards and Grid Injection, 2006. https://www.ieabioenergy.com/publications/biogas-upgrading-to-vehicle-fuel-standards-and-grid-injection/.

[56] A. Esquiroz-molina, S. Georgaki, R. Stuetz, B. Jefferson, E.J. Mcadam, Influence of pH on gas phase controlled mass transfer in a membrane contactor for hydrogen sulphide absorption, J. Memb. Sci. 427 (2013) 276–282.

[57] H. Zhang, R. Wang, D. Tee, J. Hwa, Modeling and experimental study of CO_2 absorption in a hollow fiber membrane contactor, J. Memb. Sci. 279 (2006) 301–310.

[58] D.A. Zaidiza, B. Belaissaoui, S. Rode, E. Favre, Intensification potential of hollow fiber membrane contactors for CO_2 chemical absorption and stripping using monoethanolamine solutions, Sep. Purif. Technol. 188 (2017) 38–51.

[59] N. Ghasem, M. Al-Marzouqi, A. Duidar, Effect of PVDF concentration on the morphology and performance of hollow fiber membrane employed as gas-liquid membrane contactor for CO_2 absorption, Sep. Purif. Technol. 98 (2012) 174–185.

3 Translating shell-side mass transfer data across module architecture and scale

Translating shell-side mass transfer data across module architecture and scale

S. Houlker[a], A. Allemand[b], A. Brookes[c], A. Moore[d], P. Vale[e], M. Pidou[a], E.J. McAdam[a,*]

[a]Cranfield Water Science Institute, Cranfield University, Bedfordshire, UK
[b] IMT Mines Alès, France
[c]Anglian Water, Thorpewood House, Peterborough, UK
[d]Northumbrian Water, Boldon House, Pity Me, Durham, UK
[e]Severn Trent Water, Coventry, UK
*Corresponding author: e.mcadam@cranfield.ac.uk

Abstract

Previous studies into the translation of shell-side mass transfer data from parallel flow modules to transverse flow modules have met with limited success, variation in shell-side distribution has prevented descriptions of shell-side flow from consistently quantifying the contribution of liquid-phase momentum mass transfer. However, describing shell-side flow as parallel flow has been shown to yield a better estimate of the contribution of momentum transfer in both architectures. In this study, shell-side maldistribution was experimentally measured by Residence Time Distribution (RTD) analysis and reconciled with a description of parallel flow to translate mass transfer data between the two module architectures, as the two most commonly employed geometries in commercial modules. Applying a description of parallel flow uncorrected for maldistribution, dimensionless correlations of Reynolds, Schmidt and Sherwood numbers indicate that both module architectures operate in the transition zone of mass transfer, however require differing correction factors to account for maldistribution. Employing mean average residence times experimentally derived from RTD analysis enables a single correction factor to describe mass transfer in both architectures, leading to the derivation of a dimensionless correlation applicable to both architectures: $Sh_s = 1.27Re^{0.793}Sc^{0.33}$. The impact of a gas-phase contribution to mass transfer resistance during the selective separation of CO_2 from biogas was experimentally measured as 8% of total resistance across varied liquid-gas ratios. Comparison between an integrated estimate of liquid-phase resistance, experimentally measured membrane resistance and an 8% gas-phase contribution within the resistance-in-series model and experimental data for 7 gas-phase velocities verified model accuracy. The successful translation of experimental mass transfer data across module architecture represents a powerful tool for module sizing, the development of cascade design and choice of optimal operational setpoints at industrial scale.

Keywords: shell-side mass transfer, maldistribution, dimensionless correlation, membrane module, biogas, scale-up

3.1 Introduction

Hollow fibre membrane contactors (HFMC) are a next generation gas-liquid absorption technology suitable for the selective separation of carbon dioxide from a multi-component gas mixture such as biogas, for the production of biomethane [1–6], or for carbon capture in flue gas [7–9]. Mass transfer of CO_2 from the gas phase into the liquid-phase is mediated by the large interfacial area of a microporous hydrophobic membrane [10,11]. The microporous membrane does not provide selectivity, instead enabling non-dispersive contact between the two fluids. It is the liquid phase which fosters selectivity through physical or chemical absorption [12].

At laboratory scale, considerable research has been undertaken on establishing the impact of different membrane material and absorbent liquid properties on the rate of CO_2 mass transfer [7,13,14]. The membrane contactor modular design ordinarily resembles a shell-and-tube heat exchanger design, where the two fluids pass counter-current in a parallel orientation with one fluid flowing through the shell and another within the lumen [15]. Whilst simple to produce, parallel flow membrane contactors suffer from channelling and maldistribution, particularly when high packing fractions are employed, and can be attributed to non-uniform fibre packing [16,17]. Consequently, for the evaluation of gas-liquid membrane contactors, the liquid phase is typically applied to the fibre lumen as this improves CO_2 mass transfer into the absorbent, but introduces a higher pressure drop and constrains the upper flowrate limit that can be achieved [15]. In contrast, industrial scale membrane contactors introduce transverse flow around a central tube and baffle arrangement to eliminate maldistribution, which improves shell-side mass transfer [15,18,19]. Liquid absorbent can therefore be introduced into the shell-side of the membrane contactor, which reduces associative pressure drop and increases the flow rate range that can be achieved. This provides further economic advantages, beyond the reduction in scale that is realised through the substantial increase in specific surface area in membrane contactors (around 7500 $m^2\ m^{-3}$) versus packed columns (around 250 $m^2\ m^{-3}$) [20,21].

Following laboratory investigation, it is useful to project technology feasibility at a scale equivalent to that seen in industrial applications. Dimensionless correlations based on the liquid-phase mass transfer coefficient have been successfully proposed for shell-side liquid flow in commercial scale transverse flow modules and have been validated for modules ranging from 1.2 m^2 HFMC to 104 m^2 HFMC [15,22]. However, a precise estimation for the liquid phase mass transfer coefficient within parallel flow membrane contactors, often the critical determining factor governing mass transfer resistance in

CO_2 absorption applications [7,18,23], is difficult to realise with shell-side liquid flow due to fluid maldistribution [7]. Consequently, it is difficult to project mass transfer within commercial scale transverse flow membranes based on the liquid-phase mass transfer coefficient realised in laboratory scale parallel flow membranes [13,16,23–25]. In seeking to reconcile mass transfer data between the two geometries, Shen et al. [23] collated over 30 shell-side mass transfer correlations and concluded that the distinction in overall mass transfer, was ostensibly the difference in liquid-phase velocity. The authors applied a description of shell-side parallel flow to both parallel and transverse flow modules with the derived liquid velocities subsequently providing a better correlative fit with experimental Sherwood numbers. However the presence of fibre non-uniformity introduces a degree of transverse flow across shell-side fibres as liquid seeks a preferential path through regions of lower packing density [16], limiting applicability of the Shen et al. [23] parallel flow assumption. Kavousi et al. [26] demonstrate that a computational fluid dynamic (CFD) model of liquid velocity in a 36 fibre bundle can compensate for maldistribution in shell-side flow, the study corroborates its findings with residence time distribution (RTD) analysis. The application of CFD within a larger fibre bundles is limited by the need for a description of fibre spacing [7], which is non-uniform in commercial modules [16,17]. RTD analysis represents an opportunity to experimentally measure maldistribution within a commercial range and reconcile with the description of parallel flow applied by Shen at al. [23], to translate mass transfer across module scale.

This study aims to reconcile mass transfer between the two most commonly employed module geometries, parallel flow and transverse flow, so that mass transfer analysis carried out on parallel flow can be used to estimate contactor size and operating conditions for commercial modules in an industrial setting. The objectives are to first limit mass transfer resistance to the liquid and membrane before introducing a gas phase resistance to simulate selective CO_2 separation from a multi-component gas mixture. Specific objectives include: (i) to evaluate liquid phase dominated mass transfer in a small-scale module (lumen-side liquid flow and parallel shell-side liquid flow) and larger scale baffled module (lumen-side liquid and transverse shell-side liquid flow); (ii) Undertake RTD analysis to calculate mean average residence time inclusive of maldistribution and derive a dimensionless correlation of mass transfer; and (iii) include gas-phase resistance to mass transfer within the developed dimensionless correlation and complete the resistance in series model for an overall mass transfer coefficient.

3.2 Materials and methods

3.2.1 Experimental set-up

Mass transfer rates in a small-scale gas-liquid contactor, a tube-in-shell design employing parallel flow and scaled design employing shell-side transverse flow around a central baffle (Figure 3.1) were measured (Figure 3.2).

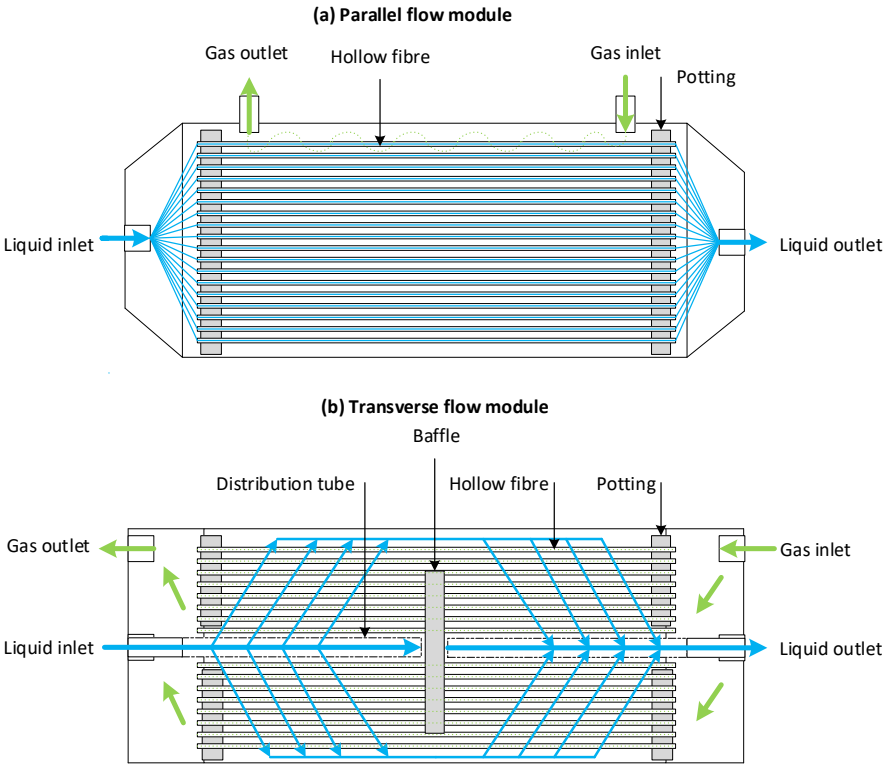

Figure 3.1 The liquid flow profiles which yield greatest membrane performance (a) liquid lumen-side in a parallel flow module (b) liquid shell-side in a transverse flow module

Absorption solvent, de-ionised water (15MΩ cm), was stored in an 85 L PVC tank and applied in counter current mode using a peristaltic pump (up 2000mL min^{-1}, 530S, Watson-Marlow Ltd, Falmouth, UK). The absorbent was selectively directed to the lumen-side and shell-side of each module (3M Deutschland GmbH, Wuppertal, Germany), and flowed counter-current to the gas phase. All experimentation was undertaken in a temperature-controlled environment (20°C) and module characteristics are listed in Table 3.1. Synthetic biogas (50/50 CH_4/CO_2) was prepared in-line by mixing methane (CH_4, 99.995%) and carbon dioxide (CO_2, 99.7%) (BOC gases, Ipswich, UK) using mass flow controllers (0.01 - 5.0 L min^{-1}, Roxspur Measurement and Control Ltd., Sheffield, UK) to provide combined flow rates between 0.05 and 4 L min^{-1} at a pressure of 0.5 BarG. The binary flow was directed to the lumen-side of a single parallel flow

module and to the lumen-side of a transverse flow module. When ensuring liquid phase control, the inlet gas phase comprised 99.7% carbon dioxide and a gas flow rate of 1.2 L min^{-1} was selectively directed to the shell-side or lumen-side of a parallel flow module and repeated in a transverse flow module. Gas flow rate was measured by bubble flow meter (up to 300 mL min^{-1}, 50 mL, error ±2%, Restek, Bellefonte, USA; from 300-3000 mL min^{-1}, 1000 mL, Model 311, error ±2%, Blandford Forum, UK). Gas composition was determined using an in-line infrared CO_2 analyser (BCP-CO2, accuracy <0.5% full-scale, Bluesens gas sensor GmbH, Herten, Germany) and a gas phase mass balance completed. Residence Time Distribution (RTD) analysis was completed by selectively applying absorption solvent, de-ionised water (15MΩ cm) to the shell-side or lumen-side of a parallel and transverse flow module. A 10g L^{-1} Sodium Chloride (NaCl, ≥99%) (Sigma-Aldrich Ltd, Dorset, UK) solution was prepared in de-ionised water and a 1mL volume of NaCl tracer was injected into the absorbent feed line 2 cm prior to the membrane inlet feed port.

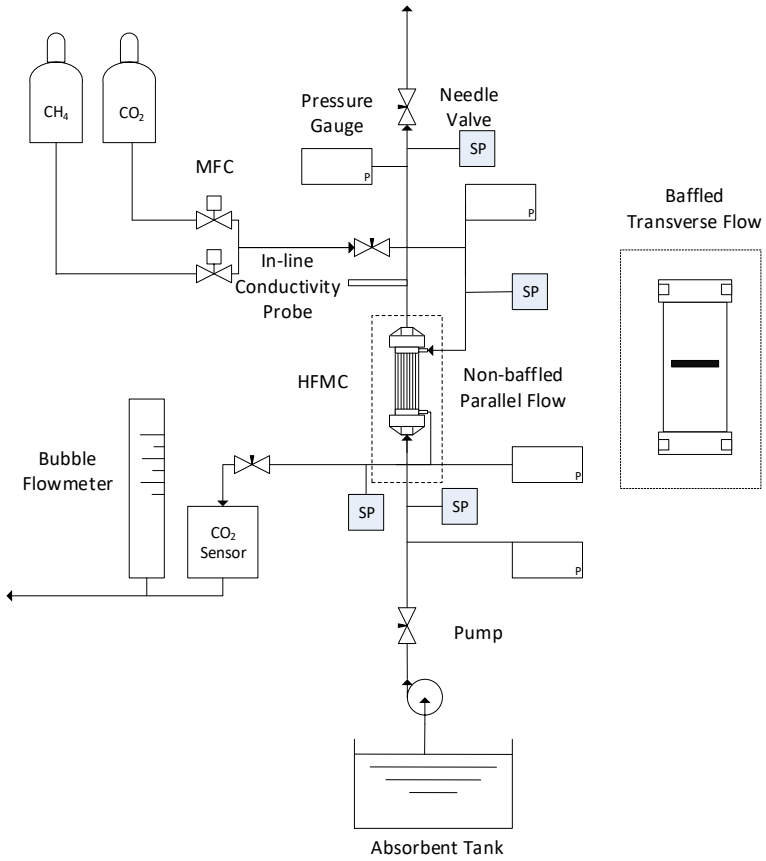

Figure 3.2 Schematic of experimental set up used for determining CO_2 capture, K_{OV}, constituent resistances and RTD derived mean residence times in both a non-baffled 0.5m^2 parallel flow HFMC and baffled 1.2m^2 transverse flow HFMC.

3.2.2 Analysis

The simplest description of mass transfer is the space-independent overall mass transfer coefficient (K_{OV}), this description of mass transfer has historically been applied in gas-liquid contacting [18,22,23,25,27–30] and has the benefit of including differing mass transfer mechanisms into a single overall parameter [24], enabling easy assessment of process performance. Within Equation 3.1, K_{OV} can be fitted once an experimental mass balance is undertaken.

$$L = \left(\frac{V_G}{K_{ov}a}\right)\left\{\left(\frac{\frac{Q_L H}{Q_G}}{\frac{Q_L H}{Q_G}-1}\right) ln\left(\frac{y_o - Hx_o}{y_l - Hx_l}\right)\right\} \quad \text{(Equation 3.1)}$$

Where K_{OV}, V_G and a within the left-hand term are the overall mass transfer coefficient (m s^{-1}), superficial gas velocity (m s^{-1}) and interfacial area (m^2 m^{-3}) respectively. The braced right hand term contains Q_L and Q_G as absorbent and feed flows, H is Henrys constant with x and y as the solute mole fraction in the feed and absorbent respectively [31]. Typically, for selective separation of carbon dioxide from a multi-component gas mixture, the liquid phase is applied in excess, conforming to a limiting condition, allowing CO_2 capture to be described in the form of Equation 3.2:

$$\eta = 1 - exp\left(\frac{-K_{OV}aL}{V_G}\right) \quad \text{(Equation 3.2)}$$

Experimentally, it may be determined through [24]:

$$\eta = \frac{[(Q_{G,in} \times C_{G,in}) - (Q_{G,out} \times C_{G,out})]}{(Q_{G,in} \times C_{G,in})} \quad \text{(Equation 3.3)}$$

where η is the dimensionless CO_2 capture ratio, $Q_{G,in}$ and $Q_{G,out}$ are inlet and outlet gas flow rates respectively (m^3 s^{-1}), and $C_{G,in}$ and $C_{G,out}$ are inlet and outlet gas phase concentrations respectively (mol m^{-3}). Overall resistance to mass transfer, defined as the reciprocal of the overall mass transfer coefficient can be separated into three constituent mass transfer domains within the resistance in series model [32,33].

$$\frac{1}{K_{OV}} = \frac{1}{k_g} + \frac{1}{k_m} + \frac{1}{k_l} \quad \text{(Equation 3.4)}$$

Individual resistances can be estimated through dimensionless analysis and combined to yield an overall resistance to mass transfer term, reducing the number of variables needed to estimate mass transfer [32,33] and permit the use of analogous correlations drawn from heat transfer literature [22,32–35]. In the case of physical absorption, liquid

phase resistance depends on hydrodynamic conditions and should remain unchanged at constant liquid flow rate [15,22,23,30]. Liquid-phase mass transfer for laminar flow conditions developed within the fibre lumen-side have been shown consistently well described by asymptotic correlation through the Lévêque solution [23,36,37], assuming well defined laminar flow of a Newtonian fluid in a smooth tube [7,33].

The Lévêque solution for Graetz numbers higher than 6:

$$Sh_t = \frac{k_t d_{in}}{D_{st}} = 1.62 Re^{\frac{1}{3}} Sc^{\frac{1}{3}} \left(\frac{d_{in}}{L}\right)^{\frac{1}{3}} \quad \text{(Equation 3.5)}$$

Graetz numbers less than 6:

$$Sh_t = \frac{k_t d_{in}}{D_{st}} = 0.5 ReSc \left(\frac{d_{in}}{L}\right) = 0.5 Gz \quad \text{(Equation 3.6)}$$

Sh, *Gz*, *Re* and *Sc* are the Sherwood, $Sh = \frac{K_{ov} d_h}{Dst}$, Graetz, $Gz = \frac{ReScd_h}{L}$, Reynolds, $Re = \frac{d_h V_L \rho}{\mu}$ and Schmidt numbers, $Sc = \frac{\mu}{\rho D}$ where V_L is liquid velocity (m s^{-1}), ρ is density of water (kg m^{-3}), μ is dynamic viscosity of water (kg m^{-1} s^{-1}), D_{st} is diffusivity of carbon dioxide in water (m^2 s^{-1}), L is effective fibre length (m) and d_h is hydraulic diameter (m). Within gas-liquid separation, such estimation is applicable to modules operating liquid lumen [23,38] and represent only the lower capacity end of a commercial module range [15]. Transition at larger module scale to liquid shell-side operation means shell-side mass transfer is key to estimating contactor performance at scale [7] however, shell-side mass transfer estimation is less well defined [23]. Choosing an appropriate shell side correlation for a desired application is problematic with module geometry, fibre packing density, inclusion of a liquid distribution channel and a transverse flow pattern introducing variables, when expressed as a dimensionless correlation as a function of *Sh*, the expression takes the general form [23]:

$$Sh_s = \frac{k_s d_h}{D_{st}} = A f(\varphi) \left(\frac{d_h}{L}\right)^{\alpha} Re^{\beta} Sc^{\gamma} \quad \text{(Equation 3.7)}$$

A, α, β, and *γ* are constants from the correlation of experimental data and *f*(*φ*) is a function of the packing fraction (*φ*) [23]. The Reynolds number exponent *β*, of Equation 3.7 is indicative of the mass transfer regime where the dimensionless ratio of momentum to diffusion mass transfer in the liquid phase is similarly dependent on liquid phase velocity [16], with laminar flow represented by *β* = 0.33, transition-zone by *β* = 0.5 to 0.8 and the turbulent regime by *β* = 0.8 to 1 [16,18,23].

When estimating mass transfer within the baffled structure of the transverse flow module, the membrane is considered as two modules in series, consistent with previous modelling approaches [15,22,23]. Velocity parameters (m s^{-1}) are assumed fully developed within the first module section, and as such based on the fibre effective length (L/2), whilst mean residence time (s) is calculated based on the fibre length (L). Shell-side and lumen-side hydraulic diameters within Figure 3.5 are calculated according standard approaches listed in the literature [23] whilst experimental values are used in Figure 3.8 and Figure 3.11, both conform to the general form [18]:

$$d_h = \frac{4\times(\text{cross}-\text{sectional area of flow})}{\text{total fibre circumference}} \quad \text{(Equation 3.8)}$$

Membrane resistance is directly measured through the application of a Wilson plot whilst gas and liquid phase velocity are calculated assuming parallel flow, as per the conclusions of Shen et al. [23] and used within experimental K_{OV} and Sherwood number calculations.

To consider parameters of non-ideal flow and changing module geometry, Residence Time Distribution (RTD) analysis was undertaken to determine the average liquid-phase residence time (s), as previously demonstrated in the literature [39–43]. The pulse method is employed, as described by Levenspiel 1999 [44]. Liquid-phase conductivity was measured by an inline platinum-cell conductivity probe (range 0–2000 uS cm^{-1}, accuracy ±10 µS cm^{-1}, response time 95% of full-scale in 5 seconds, Vernier, Beaverton, US). RTD derived lumen side volumes (parallel and transverse modules) were found 92% that of calculated volumes with a standard deviation of ±9% across test flow rates.

Area under the C_{pulse} curve (kg s m^{-3}) [44]:

$$A = \sum_i C_i \Delta t_i = \frac{M}{Q_L} \quad \text{(Equation 3.9)}$$

Mean of the C_{pulse} curve (s) [44]:

$$t_m = \frac{\sum_i t_i C_i \Delta t_i}{\sum_i C_i \Delta t_i} = \frac{V}{Q_L} \quad \text{(Equation 3.10)}$$

Where A is area under the curve (kg s m^{-3}), M is mass (kg), t_m is mean residence time (s), t_i is time entering (s), C_i is concentration entering (mol m^{-3}), V is volume (m^3) and Q_L liquid volumetric flow rate (m^3 s^{-1}). The method reported by Yang et al. [43] is applied to convert A and t_m to the dispersion number ($D/V_L L$) to describe axial mixing, where D is

the dispersion coefficient. RTD correction of gas and liquid phase residence time is applied to the experimental measurement of K_{OV} within Equation 3.2. Module characteristics and phase velocity parameters are experimentally determined from liquid-phase mean residence time (t_m) [24]: Liquid phase velocity (m s^{-1}) as $V_L = 0.5L/t_m$, shell-side and lumen-side volume (m^3) as $V = Q_L/t_m$ and cross-sectional area of flow (m^2) as $a = V/L$. Gas phase velocity (V_G) is estimated based on experimentally measured shell-side and lumen-side volumes within the RTD analysis, on the assumption of water as a non-compressible fluid. Hydraulic diameter (d_h) is based on the experimental cross-sectional area of flow (Equation 3.8) and incorporated in calculations of Reynolds number with corrected liquid-phase velocities. The corrected K_{OV} values are then subjected to a Wilson plot analysis of membrane resistance ($1/k_m$) applying corrected phase velocities. The experimentally measured $1/k_m$ is then subtracted from the measured $1/K_{OV}$ to yield a corrected $1/k_L$ value, consistent with the resistance in series model (Equation 3.4), and converted into an experimental Sherwood number. A logarithmic regression analysis of liquid phase Reynolds number versus experimental Sherwood number as per the method detailed by Ahmed et al. [45] is carried out to generate a Sherwood correlation in the general form of Equation 3.7.

3.3 Results and Discussion

3.3.1 Liquid-phase mass transfer coefficients

The liquid-phase mass transfer coefficient was evaluated through the introduction of pure CO_2, which then neglects the resistance to mass transfer provided by the gas phase. Carbon dioxide removal was evaluated initially with pure CO_2 flowing on the shell-side and subsequently on the lumen-side of both the parallel flow and transverse flow modules (Figure 3.3).

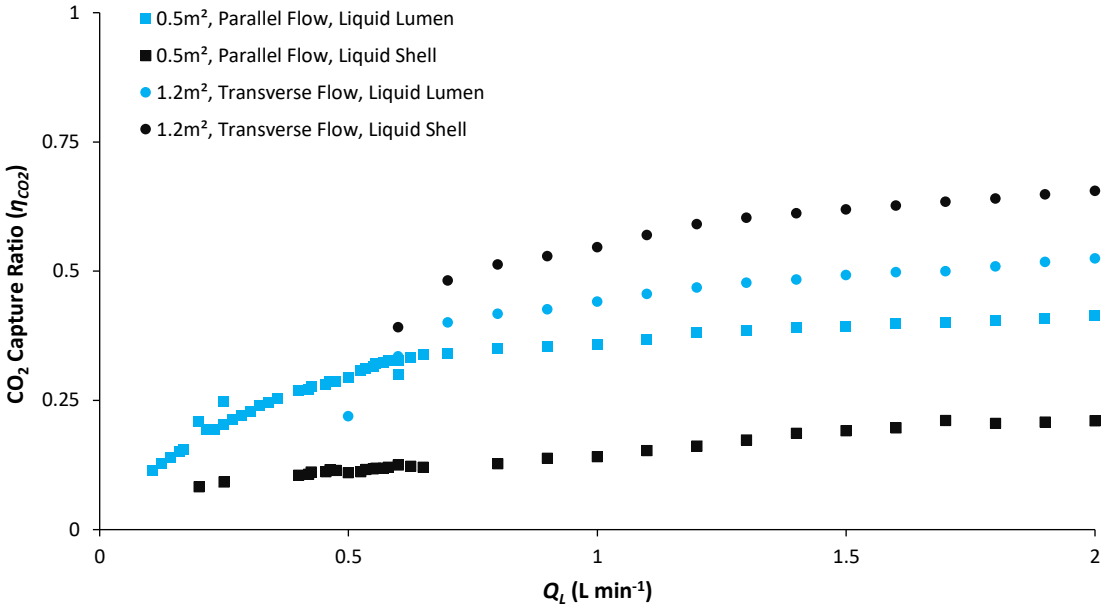

Figure 3.3 The impact of increased liquid flow rate, interfacial area (0.5m^2 and 1.2m^2) and liquid distribution (parallel flow or transverse flow) on CO_2 capture ratio (η_{CO2}). Inlet gas is 100% CO_2 at a fixed Q_G of 1.2 L min^{-1} and P_G of 0.5 BarG, deionised water was applied as absorbent (20°C) with Q_L varied between 0.1 and 2 L m^{-1} in single pass.

In both modules, de-ionised water was applied as the absorbent, flowing counter-current to the gas-phase (Figure 3.2). Within the parallel flow module at a maximum Q_L of 2 L min^{-1}, shell-side liquid flow achieved a CO_2 capture of 0.21 whilst lumen-side liquid flow achieved a maximum CO_2 capture of 0.41 (Figure 3.3). As example, at a fixed V_L of 0.012 m s^{-1} liquid shell-side achieved a CO_2 capture of 0.12 whereas liquid lumen-side achieved a CO_2 capture of 0.2, such results are consistent with literature assertions that a well distributed liquid flow within the fibre lumen encourages greater momentum mass transfer [15]. Within the transverse flow module at a maximum Q_L of 2 L min^{-1}, lumen-side liquid flow achieved a maximum CO_2 capture ratio of 0.52 whilst shell-side liquid flow achieved a maximum CO_2 capture of 0.65. As example, at a fixed V_L of 0.012 m s^{-1} liquid shell-side achieved a CO_2 capture of 0.59 whereas liquid lumen-side achieved a CO_2 capture of 0.26, this is due to enhanced liquid distribution around the fibre bundle eliminating dead zones and increasing the contribution of momentum mass transfer [15,33]. Notable within both modules is the asymptotic relationship of CO_2 capture with increased liquid-phase flow, consistent with a dominant liquid-phase resistance [36,46] whereby maximum momentum mass transfer is reached and at higher velocities [47]. Ahmed et al. [45] recommend the exclusion of membrane resistance from any empirical correlation of the liquid-phase mass transfer coefficient [45] as at infinitely high liquid

velocities there is theoretically no liquid-phase resistance, with membrane resistance to mass transfer then dominating [45]. Within this study membrane resistance was measured by Wilson Plot analysis (Figure 3.4) as 1511 s m^{-1} for 0.5m^2 parallel flow and 1391 s m^{-1} for 1.2m^2 transverse flow, similar to the 5000 s m^{-1} reported by Mavroudi et al. [28] for the same CO_2 absorption application within the same transverse flow module type and in line with other reported values (Chapter 2, Table 2.1). The liquid-phase mass transfer coefficient (k_L) was then determined from the overall mass transfer coefficient (K_{OV}) through resistance in series analysis (Equation 3.4).

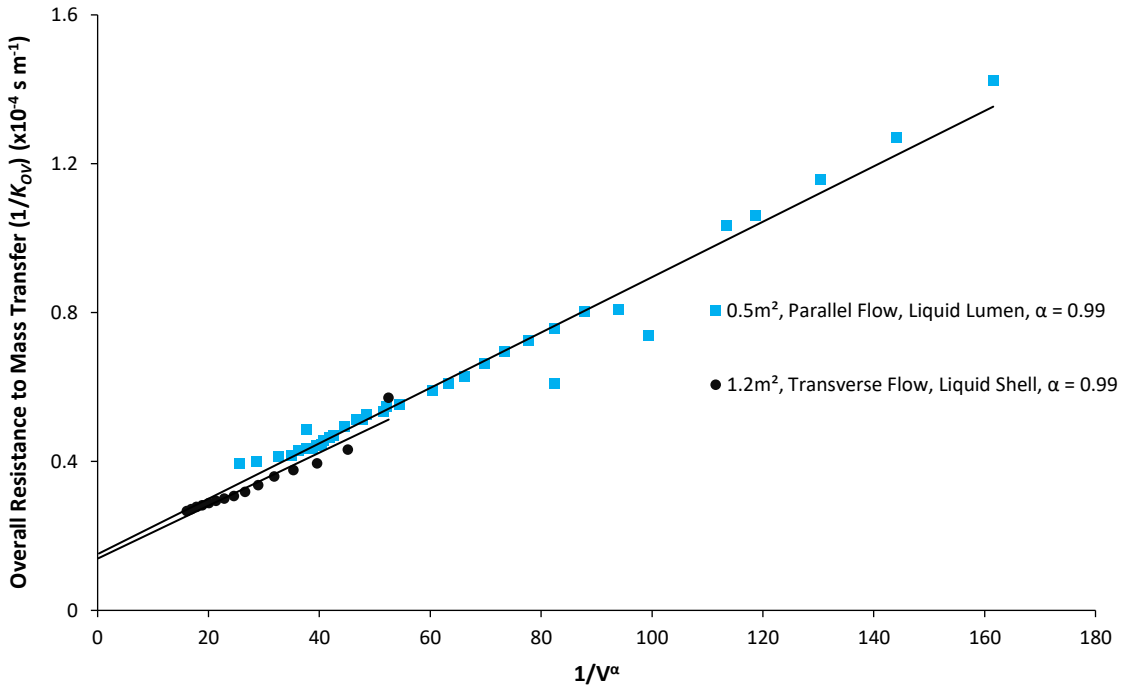

Figure 3.4 Wilson Plot analysis using 100% CO_2 inlet gas, indicating a 1/k_m of 1511 s m^{-1} for 0.5m^2 parallel flow liquid lumen-side and a 1/k_m of 1391 s m^{-1} for 1.2m^2 transverse flow liquid shell-side.

The resultant Sherwood numbers (*Sh*) for liquid lumen-side flow were found well described by the Graetz-Lévêque correlation in both parallel and transverse modules (Figure 3.5). Both module types employ the same membrane material and fibre characteristics (Table 3.1), 7400 fibres of 0.113 m length for the parallel flow module and 10200 fibres of 0.16 m length for the transverse flow module, as such similar liquid-phase distribution is present at both scales. In the lower Graetz number range, $Gz \leq 10$, the estimated and experimental *Sh* begin to deviate. This deviation from parity is noted in the existing literature and attributed to a strong mass transfer dependence on diffusion at the low *Gz* range [23,38]. Application of low *Gz* number correlations, 0.5*Gz* [23] and 0.36*Gz* [38] is shown accurate at low *Gz* numbers (Figure 3.5). The discontinuity of

lumen-side distribution in a multi-fibre bundle relative to a single fibre as studied by Wang et al. [38] can account for the variation between the two correlations. However, Wang et al.[38] studying the translation of mass transfer coefficients across differing characteristic length scales (d_h and L) note normalisation based on the Gz number [38],Figure 3.5 inset corroborates this assertion where Sh numbers for the two length scales display unity against corresponding Gz number in this study.

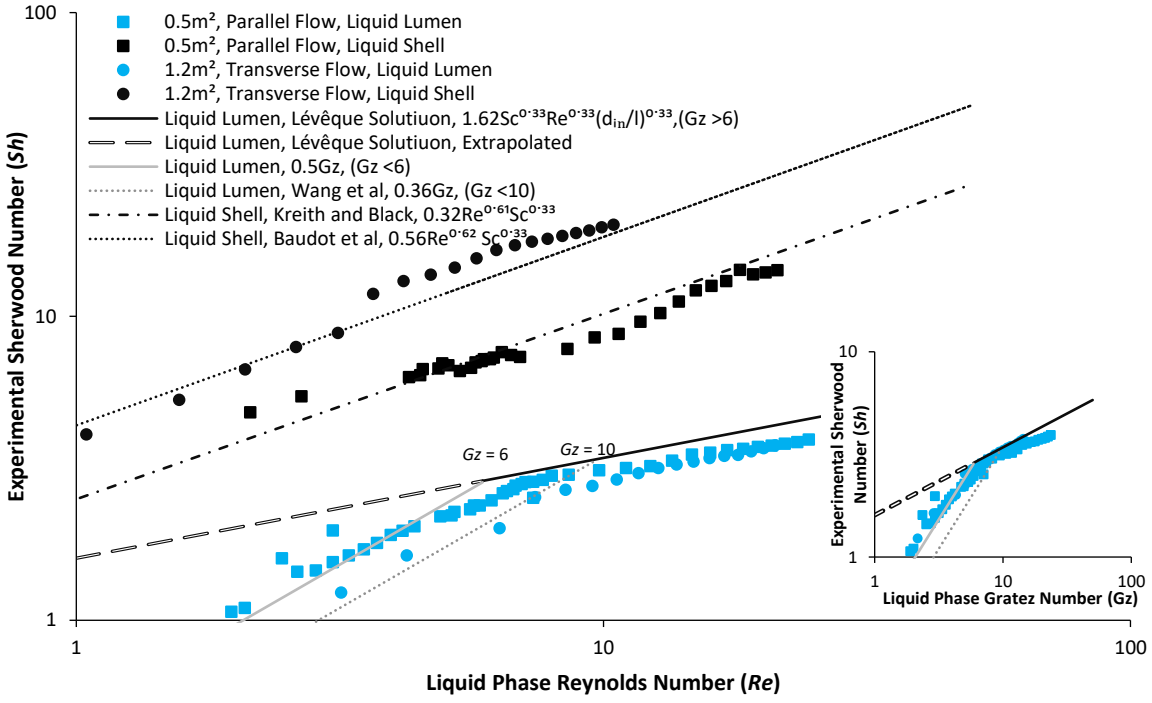

Figure 3.5 Empirical correlations for liquid phase mass transfer applied to differing hydrodynamic conditions and contact area (0.5m^2 and 1.2m^2) under identical operational conditions (Q_G, Q_L, P_G). The Lévêque solution was applied to lumen-side liquid flow at Gz>6 with 0.5Gz and the correlation of Wang et al. [38] for Gz<6. The correlations of Baudot et al. [49] and Kreith and Black. [32] were applied to shell-side liquid flow. Inlet gas is 100% CO_2 at a fixed Q_G of 1.2 L min^{-1} and P_G of 0.5 BarG, deionised water applied as absorbent (20°C) with Q_L varied between 0.1 and 2 L m^{-1} in single pass. Inset: Gratez number parity for lumen-side flow.

Experimental Sh numbers for liquid shell-side mass transfer were found to be increased by 50% in a transverse flow module relative to a parallel flow module at identical Reynolds numbers (Figure 3.5) and is attributed to enhanced liquid-phase distribution induced by the central baffle, consistent with the literature [15]. Sherwood's number (Sh) in the parallel flow module was found well described by the correlation proposed by Kreith and Black. [32]:

$$Sh = 0.32Re^{0.62}Sc^{0.33} \qquad \text{(Equation 3.11)}$$

which conforms with previous literature [35,48]. For shell-side flow within the transverse flow module (Figure 3.5), *Sh* was well described by the correlation proposed by Baudot et al. [49]:

$$Sh = 0.56Re^{0.63}Sc^{0.33} \quad \text{(Equation 3.12)}$$

The variable *A* parameter (Equation 3.7) between the two correlations, 0.32 for Kreith and Black and 0.56 for Baudot is a function of packing fraction [16], a lower packing fraction (as present in the parallel flow module) induces a greater degree of maldistribution [17] and contributes to a reduction in mass transfer and hence *A* parameter. The Reynolds number β exponent (Equation 3.7) within the Kreith and Black and Baudot correlations are 0.62 and 0.63 respectively, indicative of transition zone mass transfer with a degree of turbulence [16,23], in contrast to the laminar flow regime (Re < 2000) indicated by the *Re* range of 0.7 - 20 encountered in this study. However, the presence of fibre non-uniformity introduces areas of relatively low fibre packing where disproportionally high portions of flow enter, inducing local turbulence in otherwise laminar flow [16] and is prevalent throughout the literature [16,23]. In contrast the laminar flow conditions indicated by the $\beta = 0.33$ within the Graetz-Lévêque correlation are not subject to maldistribution. The dependence of the dimensionless ratio of momentum to diffusion mass transfer (*Sh*) on *Re* can therefore be expected to differ between lumen and shell side liquid flow due to the influence of maldistribution.

Interestingly, the Reynolds number exponent β, reported for transverse flow in commercially available modules tend to lie between 0.5 and 0.8 [23] and a similar β dependency is reported for parallel flow in randomly packed modules [23]. However, in correlations reported for the same commercially available baffled transverse flow module used in this study, β components differ between 0.3334 and 0.82 [15,22,28,49–51], depending on the description of liquid-phase velocity. When comparing the Kreith and Black and Baudot correlations, Zheng et al. [22] report their underprediction of mass transfer during transverse flow [22]. However, the study applies an assumption of radial liquid flow across the fibre bundle whereas Baudot et al. [49] originally applied a description of parallel flow [49], introducing a disparate response in liquid velocity. The successful application in this study is therefore attributed to the assumption of parallel flow in both modules as evidenced by Shen et al. [23] in providing the best description of the primarily laminar flow conditions present outside of local areas of turbulence. The similar β value of the Kreith and Black and Baudot correlations intimates that parallel and transverse flow modules have a similar *Sh* dependence on liquid-phase velocity [26].

This suggests that the introduction of a baffle does not alter the impact of liquid velocity on the mass transfer regime (β) but rather an enhancement of liquid-phase distribution eliminates the detrimental influence of maldistribution (A).

3.3.2 Residence Time Distribution analysis of maldistribution

Typically for modules of a similar fibre packing density (0.37 [52] for parallel flow and 0.45 [15] for transverse flow), dispersion characteristics can be expected to remain the same if fibre characteristics (Table 3.1) remain the same [53].

Table 3.1 Module characteristics

Characteristic	**Module Type**	
	Parallel flow	Transverse flow
Module ID (m)	0.0425*	0.05*
Shell-side baffle	No	Yes
Number of fibres	7,400[7]	10,200[6]
Contact area based on fibre ID	0.54+	1.2+
Fibre length (m)	0.113*	0.16*
Fibre ID	2.2×10^{-4}[52]	2.2×10^{-4}[15]
Fibre OD	3×10^{-4}[52]	3×10^{-4}[15]
Central distribution channel OD	N/A	0.022*
Lumen-side volume (m^3)	5.07×10^{-5}*	9.67×10^{-5}*
Shell-side volume (m^3)	9.51×10^{-5}*	1.08×10^{-4}*

*Experimentally measured +Calculated

This is evidenced in this study through characterisation of similar axial mixing through the dispersion number ($D/V_L L$) (Equation 3.9 & 3.10). During lumen-side flow for both the $0.5m^2$ parallel and $1.2m^2$ transverse modules (Figure 3.6) $D/V_L L$ ranges between 0.05 – 0.1 and 0.06 – 0.15 respectively whilst Re varied between 0.7 and 20, indicating limited deviation from plug flow [44]. This is corroborated by similar exit age distributions shifted left of a relative exit age of 1 [42–44]. Increase in the $D/V_L L$ above 0.01 and reduction of the dimensionless exit age distribution below an EΘ of 2.5 indicate mixing beyond the limits that a simple gaussian approximation would estimate [44]. Such deviation can be attributed to entrance effects in modules as a closed reactor, requiring a minimum entrance length before a flow pattern fully develops [16,44], independent of module length [16]. Accurate estimation of Sh within the Graetz-Lévêque correlation can be

attributed to similarly distributed laminar flow at both scales and resultant response in liquid phase momentum mass transfer to changing liquid velocity.

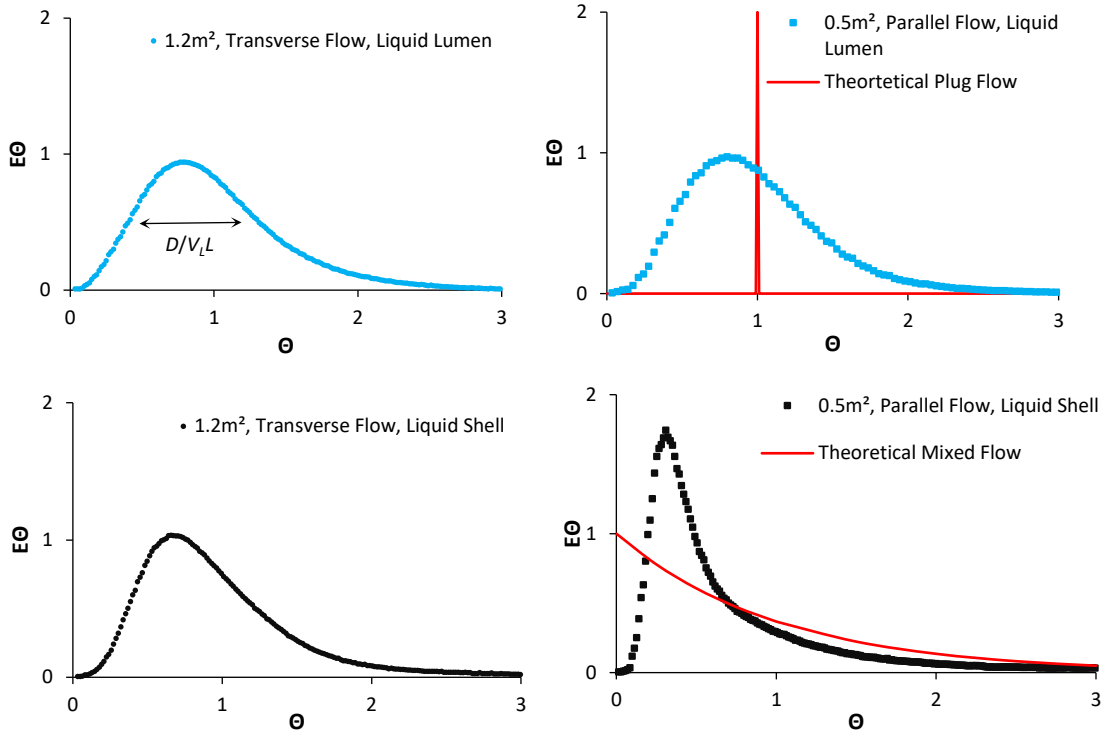

Figure 3.6 Residence Time Distribution (RTD) traces detailing maldistribution during parallel flow liquid shell-side operation where EΘ is the dimensionless exit age distribution and Θ the dimensionless mean residence time. Absorption solvent, deionised water and pulse tracer (1 mL volume of 10g L^{-1}NaCl), was selectively directed in single pass to the shell-side or lumen-side of both modules (1 L min^{-1}).

RTD analysis of shell-side flow demonstrates disparate traces between the parallel and transverse modules (Figure 3.6). Increased axial dispersion in the parallel flow module (D/V_LL range 0.3 – 0.5) indicates a large deviation from plug flow in the parallel module despite *Re* in the range of 2.3 to 7.3 , corroborated by the early exit age of 0.3 [44]. The reduction in D/V_LL with increased *Re* ,from 0.5 (*Re* = 2.3) to 0.3 (*Re* = 7.3) in this study, is noted in the literature [43] and is likely attributable to increased liquid pressure at elevated flow rate overcoming local pressure drop limitations in areas of high packing fraction, eliminating local transverse flow [16]. The analysis does not indicate the characteristic double peaks of parallel flow paths present during channelling [44]. However, previous tracer studies have attributed the deviation in plug flow to maldistribution caused by strong bypassing of the shell-side fluid [17,54,55]. It is likely that such maldistribution results in liquid entering the interstitial fibre spacing appearing as stagnant backwaters relative to the free-flowing volume between fibre bundle and module casing (shell-side), indicated by an early exit age (strong bypass) and long tail

representative of stagnation (interstitial volume). In contrast, the transverse module $D/V_L L$ (0.07 at Re = 7.8 to 0.17 at Re = 2.4), suggest the introduction of a central liquid distribution channel and baffle forces the liquid phase into contact with the fibre bundle, eliminating the free-flowing volume between fibre bundle and module casing and increasing the average shell-side residence time. The transverse flow module eliminates the early mean residence time peak (Figure 3.6) increasing the mean average residence time and reduces maldistribution as evidenced by the reduced $D/V_L L$ (0.07). The module then conforms to plug flow through the reactor with some axial mixing ($D/V_L L$ > 0.01) [55], corroborating the existence of a transition zone mass transfer regime, as indicated by similar β dependency [23] in both parallel and transverse flow modules (Figure 3.5). The introduction of a reduced average residence time by maldistribution in the parallel flow module relative to well distributed flow in a transverse module limits the translation of liquid-phase velocities between scale.

To account for maldistribution in the shell-side, the liquid-phase mean average residence time, t_m (s) for flow rates between 0.1 and 2 L min^{-1} were determined for both parallel and transverse flow modules from RTD analysis, in order to compare the resistance to mass transfer presented by the liquid phase by both modules within analogous conditions (Figure 3.7). The close fit of data around a linearised relationship indicates the translatability of mass transfer data across characteristic lengths [15], despite distinctions in liquid phase distribution (Figure 3.6). Applying the methodology of Ahmed et al. [45], a least square regression analysis was performed to develop an empirical correlation of mass transfer (Figure 3.8a) for Sherwood numbers derived from k_L that is capable of describing mass transfer in both geometries:

$$Sh_s = 1.27 Re^{0.793} Sc^{0.33} \qquad \text{(Equation 3.13)}$$

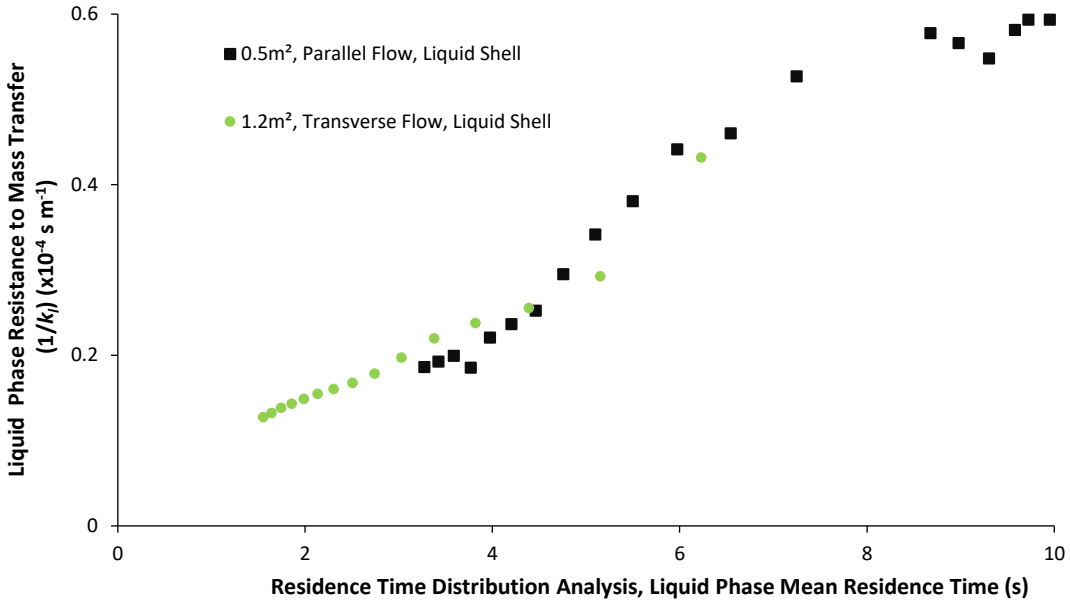

Figure 3.7 The impact of corrected liquid phase mean residence time on liquid phase resistance to mass transfer ($1/k_l$). Inlet gas is 100% CO_2 at a fixed Q_G of 1.2 L min^{-1} and P_G of 0.5 BarG, deionised water applied as absorbent (20°C) with Q_L varied between 0.1 and 2 L m^{-1} in single pass.

The derived Reynold's number exponent (β, 0.793), lies within the transition-zone of mass transfer [16], similar to previous correlations of Kreith and Black and Baudot, as expected by a D/V_LL greater than 0.01 [44]. Sengupta et al. [15] and Mavroudi et al. [28] apply the same transverse flow module to oxygen desorption and carbon dioxide absorption respectively [15,28]. At identical Reynolds numbers, assuming parallel flow, significant disparity is seen between the two studies (Figure 3.8b, inset). However, through correction of the residence time from data developed within this study, the mass transfer data is similarly comparable to that of this study (Figure 3.8b). The disparity between correlations of Reynolds and Schmidt to Sherwood number (Figure 3.8b, inset) within transverse flow modules can therefore be attributed to maldistribution of the liquid-phase and influence on liquid-phase momentum transfer.

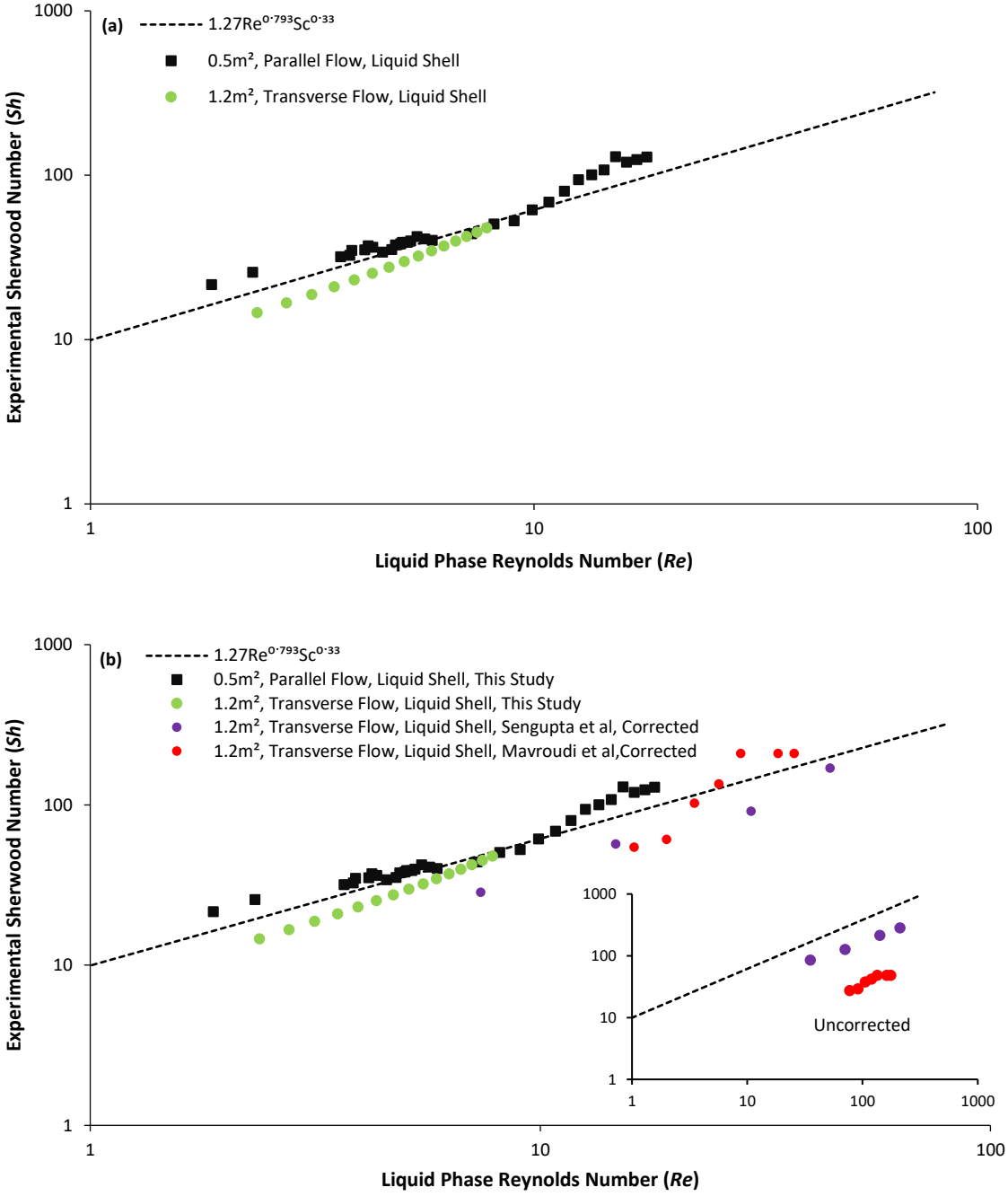

Figure 3.8 Derived empirical correlation (Sh = 1.27$Re^{0.793}Sc^{0.33}$) for residence time corrected liquid phase mass transfer applied for well distributed transverse and maldistributed parallel shell-side flow (a) parallel liquid shell-side flow and transverse shell-side liquid flow under identical operational conditions (Q_G, Q_L, P_G). Inlet gas is 100% CO_2 at a fixed Q_G of 1.2 L min^{-1} and P_G of 0.5 BarG, deionised water applied as absorbent (20°C) with Q_L varied between 0.1 and 2 L m^{-1}. (b) Derived correlation applied to residence time corrected literature data operating transverse shell-side liquid flow, Mavroudi et al. [28] and Sengupta et al. [15].

3.3.3 Evaluation of parallel flow and transverse flow geometries for binary gases

When applied to the separation of CO_2 from a binary gas mix such as biogas, the CO_2 partial pressure of 0.5 will reduce along the module length to a target of 0.02 at the membrane outlet [56]. Since the concentration difference between the two phases provides the driving force for separation [47], gas-phase resistance to mass transfer ($1/k_G$) can be expected to develop axially along the fibre length [57]. Mass transfer was therefore evaluated in both geometries with variable liquid to gas (L/G) ratios (Figure 3.9) for a 50/50 CO_2/CH_4 binary gas mixture, with the gas phase flowing counter-current in the lumen-side of both parallel and transverse flow modules. The asymptotic relationship of CO_2 capture with increased liquid-phase flow is evident for the transverse flow module (Figure 3.9b), achieving a <2%CO_2 (η_{CO2}, ~1) at a representative Q_L of 0.6 L min^{-1}. However, a linear relationship is evident for parallel flow, achieving a minimum CO_2 outlet concentration of 20% (η_{CO2}, 0.75). This is ascribed to the influence of maldistribution in reducing liquid-phase residence time and low liquid-phase flow (Q_L max = 600 mL min^{-1}) limiting achievable momentum mass transfer, Figure 3.3 indicates a Q_L of 1.5 L min^{-1} would be required to evidence maximum momentum transfer and asymptotic relationship.

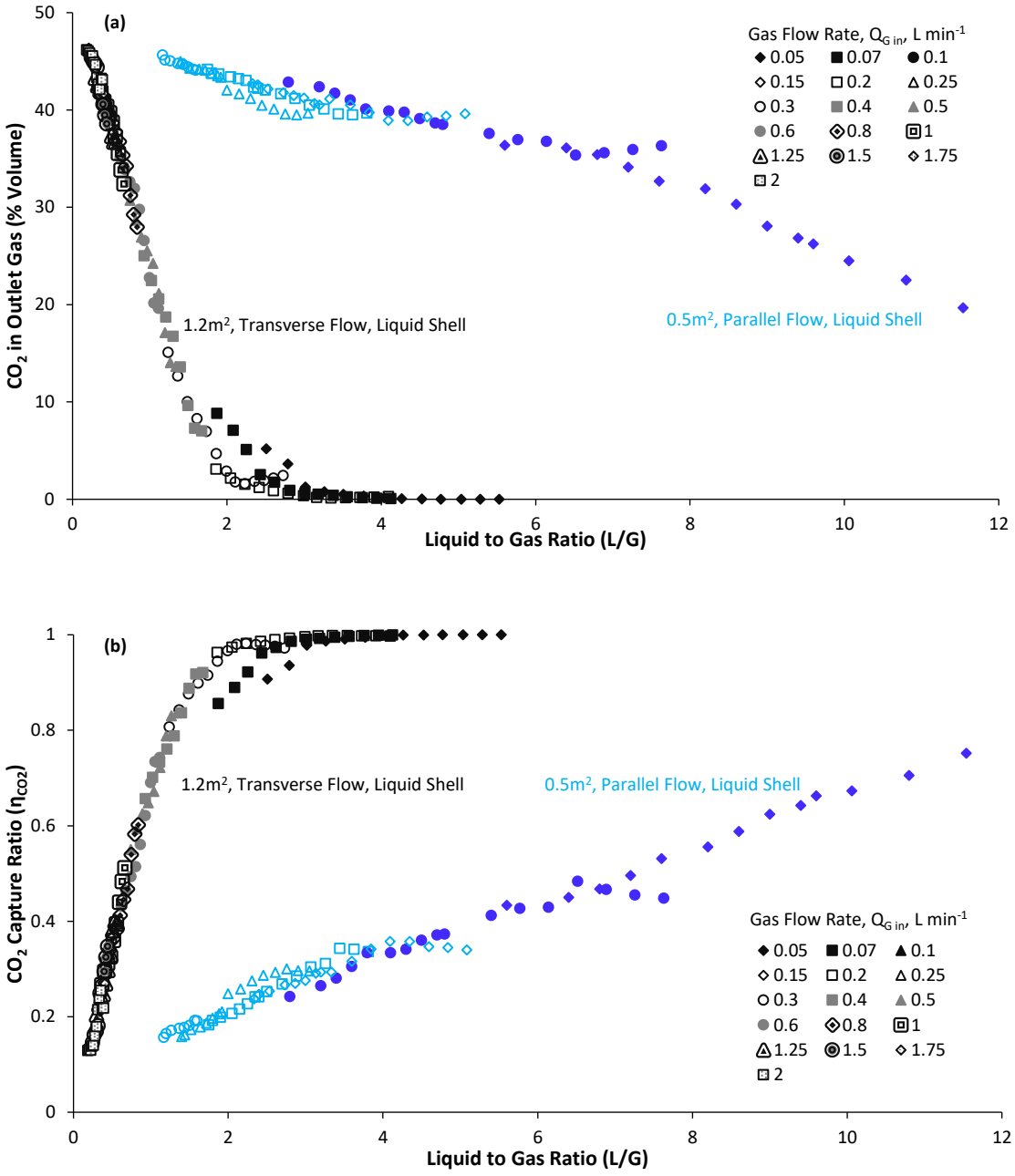

Figure 3.9 The positive impact of enhanced liquid distribution of transverse flow (1.2m^2) over parallel flow (0.5m^2) on the volumetric CO_2% in gas outlet and dimensionless capture ratio (η_{CO2}) applying a binary gas. (a) The influence of the liquid-to-gas ratio (Q_L/Q_G) on volumetric CO_2% in gas outlet (b) The influence of (Q_L/Q_G) on η_{CO2}. The inlet gas was a 50/50 CO_2/CH_4 at a P_G of 0.5 BarG with deionised water used as absorbent (20°C), gas flow rate (Q_G) was fixed between 0.05 and 2 L m^{-1}, at each fixed Q_G, liquid flow rate was varied between 0.1 and 2 L m^{-1}.

The contribution of $1/K_G$ to $1/K_{OV}$ is greatest at low gas-phase velocities (V_G) (Figure 3.10), coincident with greater CO_2 removal (Figure 3.9 a&b), contributing between 7% of $1/K_{OV}$ at a V_G of 0.09 m s^{-1} to 11% at a V_G of 0.035 m s^{-1}. The greater CO_2 removal at lower velocities reduces CO_2 partial pressure in the gas phase, reducing the

driving force for separation [47] and increasing gas-phase resistance. However, the correlation between reducing gas-phase velocity and increasing contribution to resistance to mass transfer is weak, with an R^2 value of 0.45 (Figure 3.10). Applying the gas-phase to the well distributed lumen side ensures a negligible role of gas-phase momentum transfer, the gas-phase diffusion coefficient is expected to be four orders of magnitude higher than the liquid phase [20,28], the contribution to mass transfer is therefore expected to be small and independent of velocity. This is in contrast to application of the gas-phase to the shell side where maldistribution reduces module performance [13,58]. As such, the gas-phase contribution to overall resistance to mass transfer is not expected to vary significantly with velocity and resistance in series analysis yields an average 8% contribution of $1/k_G$ to $1/K_{OV}$ (Figure 3.10), consistent with the 6 – 12% contribution reported by Boributh et al. [59].

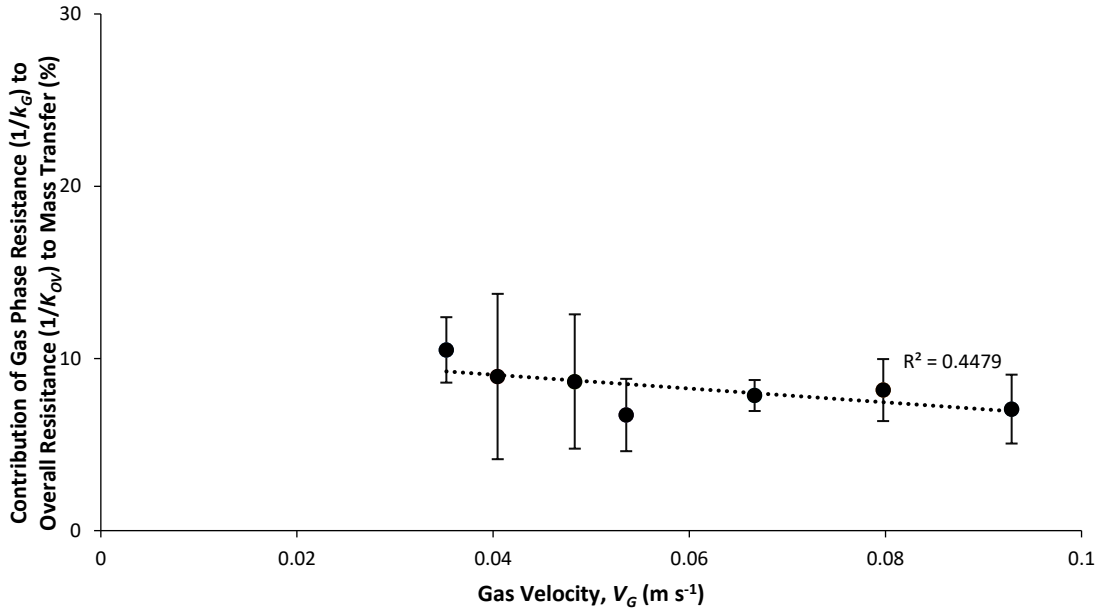

Figure 3.10 The decreasing contribution of gas phase resistance to the overall resistance to mass transfer when increasing gas phase velocity, the whiskers represent standard deviation. The inlet gas was a 50/50 CO_2/CH_4 at a P_G of 0.5 BarG with deionised water used as absorbent (20°C), gas flow rate (Q_G) was fixed between 0.05 and 2 L m^{-1}, at each fixed Q_G, liquid flow rate was varied between 0.1 and 2 L m^{-1}.

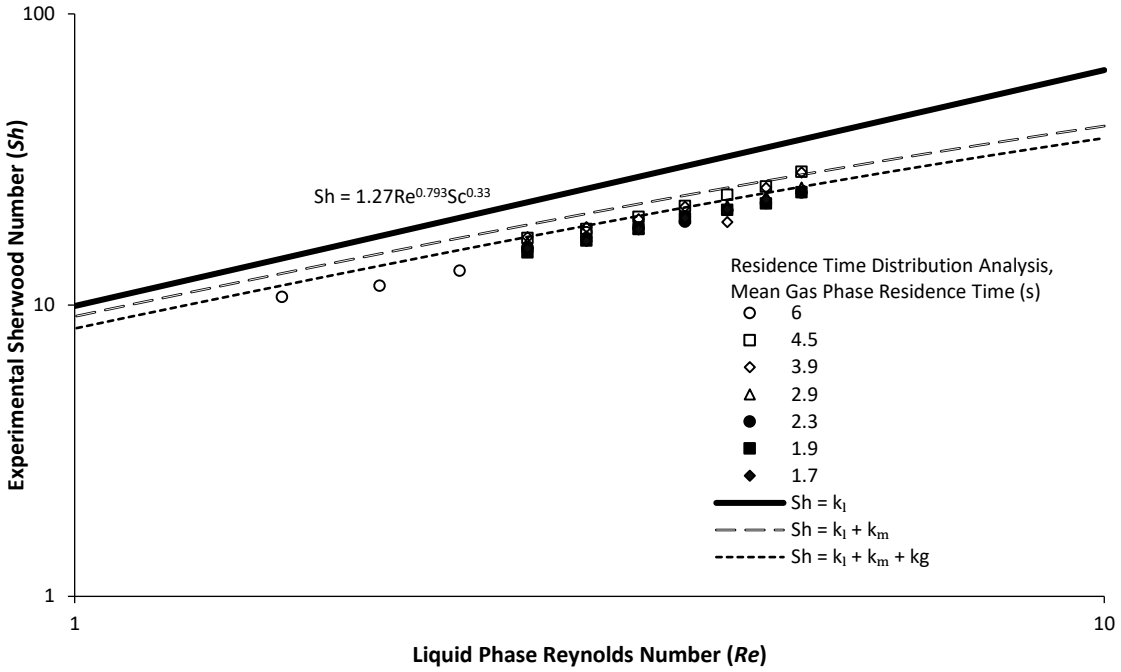

Figure 3.11 Derived empirical correlation ($Sh = 1.27Re^{0.793}Sc^{0.33}$) for liquid phase mass transfer applied to binary gas separation during transverse shell-side liquid flow. Sherwood number derived using k_l, $k_l + k_m$ and $k_l + k_m + k_g$ (K_{OV}). The inlet gas was a 50/50 CO_2/CH_4 at a P_G of 0.5 BarG with deionised water used as absorbent (20°C).

Incorporation of an 8% gas-phase contribution to the overall resistance to mass transfer, membrane resistance (Figure 3.4) and liquid phase resistance to mass transfer determined from Equation 3.13 into the resistance in series equation (Equation 3.4) yields a prediction of mass transfer in a transverse flow module applying liquid to the shell-side (Figure 3.11). The resultant Sherwood prediction line ($k_l + k_m + k_g$) demonstrates near unity with 7 distinct gas-phase velocities and increased predictive accuracy relative to estimations based on liquid and membrane resistances ($k_l + k_m$) and liquid phase resistances alone (k_l). Whilst the contribution of membrane resistance to overall mass transfer ranges between 72% ($V_L = 0.08$) and 2% ($V_L = 0.036$), the absolute resistance (1391 s m^{-1}) remains constant. The underlying assumption that gas-liquid separation is a predominantly liquid-phase controlled system, accounting for between 20% ($V_L = 0.08$) and 90% ($V_L = 0.036$) of overall resistance and the accurate translation of mass transfer across scales is predicated on accurate understanding of liquid-phase momentum transfer at a given flow rate is validated. The successful translation of experimental mass transfer data across disparate liquid-phase distribution and module architecture therefore represents a powerful tool for module sizing, the development of cascade design and choice of optimal operational setpoints at industrial scale.

3.4 Conclusions

Transition zone mass transfer is present in both parallel and transverse flow modules, the enhanced mass transfer present in the transverse flow module is attributed to a reduction in shell-side maldistribution. Subsequent reconciliation of shell-side maldistribution within a description of parallel flow through the application of mean average residence time, enables a single description of mass transfer to apply to both parallel and transverse module architectures. This represents the ability to translate mass transfer data from small-scale parallel flow modules as applied at the small-scale to transverse flow modules as applied at industrial scale. Importantly, it can be performed without lengthy CFD calculations and an extensive understanding of module fibre spacing. Consequently, optimal operational conditions, multi-module configurations and cost appraisal can be carried out at the small-scale and directly inform industrial practices. Furthermore, as a gas-phase contribution to mass transfer can be incorporated, the derived correlation can inform selective separation of CO_2 from a binary (biogas) mixture, an emerging industrial application for gas-liquid contactors.

Acknowledgements

The authors would like to thank Anglian Water, Northumbrian Water and Severn Trent Water for their practical and financial support. We are also grateful for funding from the Engineering and Physical Sciences Research Council (EPSRC) which was provided through the STREAM Industrial Doctorate Centre. Enquiries for access to the data referred to in this article should be directed to: researchdata@ cranfield.ac.uk.

References

[1] A. Mcleod, B. Jefferson, E.J. McAdam, Biogas upgrading by chemical absorption using ammonia rich absorbents derived from wastewater, Water Res. 67 (2014) 175–186.

[2] A. Park, Y.M. Kim, J.F. Kim, P.S. Lee, Y.H. Cho, H.S. Park, S.E. Nam, Y.I. Park, Biogas upgrading using membrane contactor process: Pressure-cascaded stripping configuration, Sep. Purif. Technol. 183 (2017) 358–365.

[3] Q. He, G. Yu, S. Yan, L.F. Dumée, Y. Zhang, V. Strezov, S. Zhao, Renewable CO_2 absorbent for carbon capture and biogas upgrading by membrane contactor, Sep. Purif. Technol. 194 (2018) 207–215.

[4] Z. Zhang, Y. Yan, L. Zhang, Y. Chen, J. Ran, G. Pu, C. Qin, Theoretical Study on CO_2 Absorption from Biogas by Membrane Contactors : Effect of Operating

Parameters, Ind. Eng. Chem. Res. 53 (2014) 14075–14083.

[5] P. Tantikhajorngosol, N. Laosiripojana, R. Jiraratananon, A modeling study of module arrangement and experimental investigation of single stage module for physical absorption of biogas using hollow fiber membrane contactors, J. Memb. Sci. 549 (2018) 283–294.

[6] B. Belaissaoui, E. Favre, Novel dense skin hollow fiber membrane contactor based process for CO_2 removal from raw biogas using water as absorbent, Sep. Purif. Technol. 193 (2018) 112–126.

[7] S. Zhao, P.H.M. Feron, L. Deng, E. Favre, E. Chabanon, S. Yan, J. Hou, V. Chen, H. Qi, Status and progress of membrane contactors in post-combustion carbon capture : A state-of-the-art review of new developments, J. Memb. Sci. 511 (2016) 180–206.

[8] A. Mansourizadeh, A.F. Ismail, Hollow fiber gas – liquid membrane contactors for acid gas capture : A review, J. Hazard. Mater. 171 (2009) 38–53.

[9] E. Chabanon, R. Bounaceur, C. Castel, S. Rode, D. Roizard, E. Favre, Pushing the limits of intensified CO_2 post-combustion capture by gas – liquid absorption through a membrane contactor, Chem. Eng. Process. Process Intensif. 91 (2015) 7–22.

[10] S. Heile, S. Rosenberger, A. Parker, B. Jefferson, E.J. McAdam, Establishing the suitability of symmetric ultrathin wall polydimethylsiloxane hollow-fibre membrane contactors for enhanced CO_2 separation during biogas upgrading, J. Memb. Sci. 452 (2014) 37–45.

[11] Z. Cui, D. DeMontigny, CO_2 capture using hollow fiber membrane contactors, Carbon Manag. 4 (2013) 69–89.

[12] S. Yan, M. Fang, W. Zhang, S. Wang, Z. Xu, Z.-Y. Luo, K.-F. Cen, Experimental study on the separation of CO_2 from flue gas using hollow fiber membrane contactors without wetting, Fuel Process. Technol. 88 (2007) 501–511.

[13] E. Chabanon, E. Kimball, E. Favre, O. Lorain, E. Goetheer, D. Ferre, A. Gomez, P. Broutin, Hollow Fiber Membrane Contactors for Post-Combustion CO_2 Capture: A Scale-Up Study from Laboratory to Pilot Plant, Oil Gas Sci. Technol. – Rev. d'IFP Energies Nouv. 69 (2014) 1035–1045.

[14] S.R. Wickramasinghe, M.J. Semmens, E.L. Cussler, Better hollow fiber contactors, J. Memb. Sci. 62 (1991) 371–388.

[15] A. Sengupta, P.A. Peterson, B.D. Miller, J. Schneider, C.W. Fulk, Large-scale application of membrane contactors for gas transfer from or to ultrapure water,

Sep. Purif. Technol. 14 (1998) 189–200.

[16] M.J. Costello, A.G. Fane, P.A. Hogan, R.W. Schofield, The effect of shell side hydrodynamics on the performance of axial flow hollow fibre modules, J. Memb. Sci. 80 (1993) 1–11.

[17] I. Noda, D.G. Brown-West, C.C. Gryte, Effect of flow maldistribution on hollow fiber dialysis - experimental studies, J. Memb. Sci. 5 (1979) 209–225.

[18] M. Yang, E.L. Cussler, Designing Hollow-Fiber Contactors, AIChE. J. 32 (1986) 1910–1916.

[19] K.L. Wang, E.L. Cussler, Baffled membrane modules made with hollow fiber fabric, J. Memb. Sci. 85 (1993) 265–278.

[20] B. Belaissaoui, J. Claveria-Baro, A. Lorenzo-Hernando, D. Albarracin, E. Chabanon, C. Castel, S. Rode, D. Roizard, E. Favre, Potentialities of a dense skin hollow fiber membrane contactor for biogas purification by pressurized water absorption, J. Memb. Sci. 513 (2016) 236–249.

[21] E. Brunazzi, G. Nardini, A. Pagliani, An economical criterion for packed absorption column design, Chem. Biochem. Eng. Q. 15 (2002) 199–206.

[22] J. Zheng, Z. Dai, F. Wong, Z. Xu, Shell side mass transfer in a transverse flow hollow fiber membrane contactor, J. Memb. Sci. 261 (2005) 114–120.

[23] S. Shen, S.E. Kentish, G.W. Stevens, Shell-Side Mass-Transfer Performance in Hollow-Fiber Membrane Contactors, Solvent Extr. Ion Exch. 28 (2010) 817–844.

[24] E. Chabanon, D. Roizard, E. Favre, Modeling strategies of membrane contactors for post-combustion carbon capture: A critical comparative study, Chem. Eng. Sci. 87 (2013) 393–407.

[25] S.R. Wickramasinghe, M.J. Semmens, E.L. Cussler, Mass transfer in various hollow fiber geometries, J. Memb. Sci. 69 (1992) 235–250.

[26] F. Kavousi, E. Syron, M. Semmens, E. Casey, Hydrodynamics and gas transfer performance of confined hollow fibre membrane modules with the aid of computational fluid dynamics, J. Memb. Sci. 513 (2016) 117–128.

[27] A. Bottino, G. Capannelli, A. Comite, R. Di, R. Firpo, CO_2 removal from a gas stream by membrane contactor, Sep. Purif. Technol. 59 (2008) 85–90.

[28] M. Mavroudi, S.P. Kaldis, G.P. Sakellaropoulos, A study of mass transfer resistance in membrane gas-liquid contacting processes, J. Memb. Sci. 272 (2006) 103–115.

[29] S.R. Wickramasinghe, M.J. Semmens, E.L. Cussler, Hollow fibre modules made with hollow fibre fabric, Membr. Technol. 84 (1993) 1–14.

[30] Q. Zhang, E.L. Cussler, Microporous Hollow Fibers for Gas Absorption I. Mass Transfer in the Liquid, J. Memb. Sci. 23 (1985) 321–332.

[31] B.W. Reed, M.J. Semmens, E.J. Cussler, Membrane contactors, in: R.D. Nobel, A.S. Stern (Eds.), Membr. Sep. Technol. Princ. Appl., Elsevier, 1995: pp. 467–498.

[32] F. Kreith, W.Z. Black, Basic Heat Transfer, Harper & Row, New York, 1980.

[33] V. Gekas, B. Hallström, Mass transfer in the membrane concentration polarization layer under turbulent cross flow 1. Critical literature review and adaption of existing Sherwood correlations to membrane operations, J. Memb. Sci. 30 (1987) 153–170.

[34] H. Mahmud, A. Kumar, R.M. Narbaitz, T. Matsuura, A study of mass transfer in the membrane air-stripping process using microporous polyproplylene hollow fibers, J. Memb. Sci. 179 (2000) 29–41.

[35] F.X. Pierre, I. Souchon, V. Athes-Dutour, M. Marin, Membrane-based solvent extraction of sulfur aroma compounds: Influence of operating conditions on mass transfer coefficients in a hollow fiber contactor, Desalination. 148 (2002) 199–204.

[36] H. Kreulen, C.A. Smolders, G.F. Versteeg, W.P.M. van Swaaij, Microporous hollow fibre membrane modules as gas-liquid contactors. Part 1. Physical mass transfer processes. A specific application: Mass transfer in highly viscous liquids, J. Memb. Sci. 78 (1993) 197–216.

[37] A. Gabelman, S. Hwang, Hollow fibre membrane contactors, J. Memb. Sci. 159 (1999) 62–106.

[38] C.Y. Wang, E. Mercer, F. Kamranvand, L. Williams, A. Kolios, A. Parker, S. Tyrrel, E. Cartmell, Tube-side mass transfer for hollow fibre membrane contactors operated in the low Graetz range, J. Memb. Sci. 523 (2017) 235–246.

[39] V.Y. Dindore, A.H.G. Cents, D.W.F. Brilman, G.F. Versteeg, Shell-side dispersion coefficients in a rectangular cross-flow hollow fibre membrane module, Chem. Eng. Res. Des. 83 (2005) 317–325.

[40] W. Zhang, Z. Hao, J. Li, J. Liu, Z. Wang, Z. Ren, Residence Time Distribution Analysis of a Hollow-Fiber Contactor for Membrane Gas Absorption and Vibration-Induced Mass Transfer Intensification, Ind. Eng. Chem. Res. 53 (2014) 8640–8650.

[41] J. Lemanski, G.G. Lipscomb, Effect of Shell-Side Flow on Hollow-Fibre Membrane Device Performance, AIChE J. 41 (1995) 2322–2326.

[42] Z. Ren, Y. Yang, W. Zhang, J. Liu, H. Wang, Modeling study on the mass transfer

of hollow fiber renewal liquid membrane : Effect of the hollow fiber module scale, J. Memb. Sci. 439 (2013) 28–35.

[43] Q. Yang, A. Drak, D. Hasson, R. Semiat, RO module RTD analyses based on directly processing conductivity signals, J. Memb. Sci. 306 (2007) 355–364.

[44] O. Levenspiel, Chemical Reaction Engineering, 3rd ed., John Wiley & Sons, 1999.

[45] T. Ahmed, M.J. Semmens, M.A. Voss, Oxygen transfer characteristics of hollow-fiber, composite membranes, Adv. Environ. Res. 8 (2004) 637–646.

[46] V.Y. Dindore, D.W.F. Brilman, G.F. Versteeg, Modelling of cross-flow membrane contactors : physical mass transfer processes, J. Memb. Sci. 251 (2005) 209–222.

[47] Z. Cui, D. DeMontigny, Part 7: A review of CO_2 capture using hollow fiber membrane contactors, Carbon Manag. 4 (2014) 69–89.

[48] S. Bocquet, F. Gascons Viladomat, C. Muvdi Nova, J. Sanchez, V. Athes, I. Souchon, Membrane-based solvent extraction of aroma compounds: Choice of configurations of hollow fiber modules based on experiments and simulation, J. Memb. Sci. 281 (2006) 358–368.

[49] A. Baudot, J. Floury, H.E. Smorenburg, Liquid-liquid extraction of aroma compounds with hollow fiber contactor, AIChE J. 47 (2001) 1780–1793.

[50] P. Schöner, P. Plucinski, W. Nitsch, U. Daiminger, Mass transfer in the shell side of cross flow hollow fiber modules, Chem. Eng. Sci. 53 (1998) 2319–2326.

[51] E.A. Fouad, H.J. Bart, Separation of zinc by a non-dispersion solvent extraction process in a hollow fiber contactor, Solvent Extr. Ion Exch. 25 (2007) 857–877.

[52] A. McLeod, B. Jefferson, E.J. McAdam, Quantifying the loss of methane through secondary gas mass transport (or 'slip') from a micro-porous membrane contactor applied to biogas upgrading, Water Res. 47 (2013) 3688–3695.

[53] Y. Wang, F. Chen, Y. Wang, G. Luo, Y. Dai, Effect of random packing on shell-side flow and mass transfer in hollow fiber module described by normal distribution function, J. Memb. Sci. 216 (2003) 81–93.

[54] A.F. Seibert, X. Py, M. Mshewa, J.R. Fair, Hydraulics and Mass Transfer Efficiency of a Commercial-Scale Membrane Extractor, Sep. Sci. Technol. 28 (1993) 343–359.

[55] J.J. Cai, K. Hawboldt, M.A. Abdi, Contaminant removal from natural gas using dual hollow fiber membrane contactors, J. Memb. Sci. 397–398 (2012) 9–16.

[56] E. Ryckebosch, M. Drouillon, H. Vervaeren, Techniques for transformation of biogas to biomethane, Biomass and Bioenergy. 35 (2011) 1633–1645.

[57] H. Zhang, R. Wang, D.T. Liang, J.H. Tay, Modeling and experimental study of CO_2

absorption in a hollow fiber membrane contactor, J. Memb. Sci. 279 (2006) 301–310.

[58] E. Kimball, A. Al-azki, A. Gomez, E. Goetheer, N. Booth, D. Adams, D. Ferre, Hollow Fiber Membrane Contactors for CO_2 Capture : Modeling and Up-Scaling to CO_2 Capture for an 800 MW e Coal Power Station, Oil Gas Sci. Technol. – Rev. d'IFP Energies Nouv. 69 (2014) 1047–1058.

[59] S. Boributh, S. Assabumrungrat, N. Laosiripojana, R. Jiraratananon, Effect of membrane module arrangement of gas-liquid membrane contacting process on CO_2 absorption performance: A modeling study, J. Memb. Sci. 372 (2011) 75–86.

4 Demonstration scale performance of a commercial hollow fibre membrane contactor for biogas upgrading at a wastewater treatment works

Demonstration scale performance of a commercial hollow fibre membrane contactor for biogas upgrading at a wastewater treatment works

S. Houlker[a], T.Rutherford[b], D.Herron[b], A. Brookes[c], A. Moore[b], P. Vale[c], M. Pidou[a], E.J. McAdam[a,*]

[a]Cranfield Water Science Institute, Cranfield University, Bedfordshire, UK
[b]Northumbrian Water, Boldon House, Pity Me, Durham, UK
[c]Anglian Water, Thorpewood House, Peterborough, UK
[d]Severn Trent Water, Coventry, UK
*Corresponding author: e.mcadam@cranfield.ac.uk

Abstract

Development of hollow fibre membrane contactors (HFMC) for bulk gas separation processes has focused primarily on synthetic gases, however industrial conditions are necessarily less controlled and operate on more complex gases and fluids than lab-scale studies. Limited demonstration studies into Carbon Capture Storage (CCS) and pre-filtered biogas upgrading have demonstrated industrial operation, however the robustness of membrane performance in the presence of trace impurities and moisture content of industrial biogas remains unknown. This study has employed a commercial transverse flow HFMC to the upgrading of industrial biogas from anaerobic digestion onsite at a wastewater treatment works (WWTW) operating a commercial gas-liquid absorption column for an extended 6-month operation period, sequentially stripping back gas-phase pre-treatment (activated carbon, molecular sieve and desiccant) until demonstrating operation on untreated biogas. The study demonstrates comparable CO_2 separation performance could be achieved for synthetic gas and industrial biogas, which simplifies considerations for scale-up, and that the primary mechanism for HFMC fouling in biogas upgrading is a combination of adsorption and clogging of the shell-side arising from the absorbent. Gas-phase impurities such as particulates, siloxanes and moisture content leading to capillary wetting are demonstrated not to limit industrial performance.

Keywords: industrial operation, biogas, pre-filtration, membrane fouling, wastewater treatment works

4.1 Introduction

Anaerobic Digestion (AD) at wastewater treatment works (WWTW) can recover 34% of the initial energy of raw wastewater as biogas [1]. When upgraded to biomethane (≥98% CH_4) it is an energy dense renewable heat source [2–4]. In the UK by the end of 2017, around 90 sites were producing biomethane, which was primarily facilitated through gas-liquid absorption columns at larger wastewater treatment installations [5,6]. Absorption columns are energy intensive, requiring up to 0.3 kWh Nm^{-3} biogas [7] and suffer from flooding, channelling and entrainment which limit their operational range [8]. Hollow fibre membrane contactors (HFMC) are a promising alternative to gas-liquid absorption as the membrane extends the range of operating conditions that can be applied, due to imparting a phase change between the liquid and gas, which eliminates flooding and entrainment [8–10] whilst the increased interfacial area introduces a 15 fold process intensification into the absorption column [11,12] which reduces process footprint, capital cost and energy demand.

Whilst much of the HFMC development has been undertaken on synthetic gases, several authors have sought to validate their robustness in an industrial setting with the use of real gases, with particular emphasis on their application to post combustion carbon capture storage (CCS) [13]. Pilot plant trials by Kværner Process Systems demonstrated sustained module performance for 7000h across 8 modules employing polytetrafluoroethylene (PTFE) fibres, with the longest running module operating for 5000h [14] on real industrial flue gas from natural gas combustion [15], which evidenced weight, footprint, operational and capital cost reduction versus packed columns [14,16]. Comite et al. [17] applied HFMC to pre-filtered industrial flue gases from a coal fired power station, and reported mass transfer data comparable to that derived on synthetic gas, which supports observations of Klaassen et al. [18] who did not observe a reduction in mass transfer over an operating period of 12 months on flue gas. Whilst successful, these examples primarily studied application to gases derived from natural gas combustion, or pre-filtered gases where particulates could be expectedly limited. Biogas can be conceived as a more complex gas mixture containing a broad spectrum of trace contaminants including: siloxanes, organic halides, microorganisms, terpenes, aldehydes & ketones, ammonia, particulates, pesticides & pharmaceuticals and moisture [19–23]. The introduction of such a complex mixture of trace determinants can be expected to increase the risk of membrane fouling or capillary wetting [24].

Particulate fouling was experienced for a polypropylene HFMC applied to unfiltered flue gas (Scholes et al. [25]), the authors reporting a visible build-up of fly ash

on the membrane after 60 hours of operation [25], which accords with observations from another study [26–28]. Several studies using both PTFE and PP HFMC have also inferred that gas phase fouling degraded mass transfer when applied to gas comprising SO_2, fine particulates, H_2O and CO_2 [26,28]. Consequently, whilst several studies report positively on the long-term demonstration in an industrial setting, evidence of deterioration in mass transfer during operation reported by other researchers, suggest there is some discontinuity in the literature, likely due to the changes in the composition of the gas. This is particularly important for biogas, since the gas is ostensibly more complex, yet the evaluation of commercially available membranes for biogas in an industrial setting has been studied significantly less. To our knowledge, Vogler et al. [29] are the only authors to report on the stability of HFMC for biogas upgrading in an industrial setting. Their system comprised potable water as the absorbent and pre-treatment using a carbon filter [29]. An important distinction between flue gas and biogas is also the risk of liquid side fouling by the absorption fluid, which has been observed to block packing media in classical gas-liquid absorption columns due to biological fouling introduced through regrowth, despite the deployment of potable water as the absorption solvent [23]. This study proposes to complement and build upon the limited existing literature on the testing of HFMC on real gases in an industrial setting, in order to enrich understanding with respect to HFMC robustness to gas and liquid phase contaminants, and specifically to evaluate commercially available HFMC for biogas upgrading. The specific objectives of the study are to: (i) evaluate the effect of gas phase contaminants on HFMC robustness through the inclusion and gradual removal of multi-media pre-filtration (activated carbon, a molecular sieve and a desiccant) which immediately protects the membrane from particulates, volatile organics and moisture; (ii) evidence the (in)significance of the liquid phase to sustaining the mass transfer of CO_2 from real gas; and (iii) determine the recoverability of membrane performance through standard cleaning protocols, following fouling.

4.2 Materials and methods

4.2.1 Experimental set-up

Biogas (CO_2: 34-39%) was taken from the primary biogas pipeline post chiller (Figure 4.1) and gas booster (up to 75mBar). Due to low gas pressure (9-44 mBar) post gas filtration, gas flow rate was maintained using an inline double-acting flow control valve (F.lli Tognella Spa, Rome, Italy) and manually corrected according to the inlet ST75V Mass Flow Meter (3.4-30 L min^{-1}, error±1.5, Fluid Components International LLC., San

Marcos, USA). Gas prefiltration was achieved using three VACU-GUARD 150 (Whatman International Ltd., Maidstone, UK) inline filters; activated carbon/PTFE membrane (AC) for particulate and siloxane removal, anhydrous calcium sulphate/PTFE membrane (ACS) for gas drying and silico aluminate zeolite/PTFE membrane (SAZ) as a molecular sieve. Gas and liquid pressure were measured using PX319 (0-10 BarG) series pressure transducers (Omega Engineering Ltd., Manchester, UK). Unfiltered or pre-filtered biogas was passed lumen side of a commercially available transverse flow HFMC, three EXF Series 2.5 x 8 3M Liqui-Cel membrane contactors (3M Industrial Group, Charlotte, USA) were tested. Each module comprised of 10200 microporous polypropylene X-50 fibres, with an outer diameter, inner diameter and fibre length of 300 µm, 240 µm, and 0.16 m respectively. The surface area of each module was 1.2 m^2 based on internal fibre diameter [30]. Potable water was stored in a 1 m^3 IBC tank and applied as absorbent to the shell side (0.6-9.5 L min^{-1}) in counter current mode using a peripheral pump (SP5/A, Lowara, Xylem Water Solutions UK Ltd., Axminster, UK). Liquid flow rate was measured using a FMG90 series electromagnetic flow meter (Omega Engineering Ltd., Manchester, UK). WWTW experimentation was undertaken in a non-controlled environment: ambient temperature (0 - 30°C), gas-phase pressure (0 – 80 mBar) and gas-phase composition (60 – 63% CH_4 v/v). Two modules were applied to WWTW biogas and potable water to investigate the impact of unfiltered biogas and potable water on membrane fouling. When investigating performance recovery post WWTW, synthetic biogas (50/50 and 60/40 CH_4/CO_2) was prepared in-line by mixing methane (CH_4, 99.995%) and carbon dioxide (99.7%) (BOC gases, Ipswich, UK) using mass flow controllers with two prescribed flow rate ranges (0.01 - 1.0 L min^{-1} and 0.2 - 20 L min^{-1}, Roxspur Measurement and Control Ltd., Sheffield, UK) to provide a combined flow rate between 0.05 and 3.5 L min^{-1} at a pressure of 0.1 BarG. Absorption solvent, potable water or de-ionised water (15MΩ), was stored in an 85 L PVC storage tank. Experimentation was undertaken in a temperature controlled (20°C) environment and carried out after 150 combined hours of on-site operation over 150 days with a third module applied to synthetic biogas, potable water and de-ionised water to investigate the impact of absorbent on membrane performance. Shell side membrane chemical cleaning was undertaken according to manufacturer guidelines [31] and consisted of a hydraulic cleaning step (75 min contact time, de-ionised water), a biological cleaning step (120 min contact time, 4% (w/w) NaOH) a second hydraulic clean (15 min contact time, de-ionised water), an inorganic cleaning step (120 min contact time, 3% (w/w) HCl), a

final hydraulic cleaning step (75 min contact time, de-ionised water) followed by a 90 minute gas drying step.

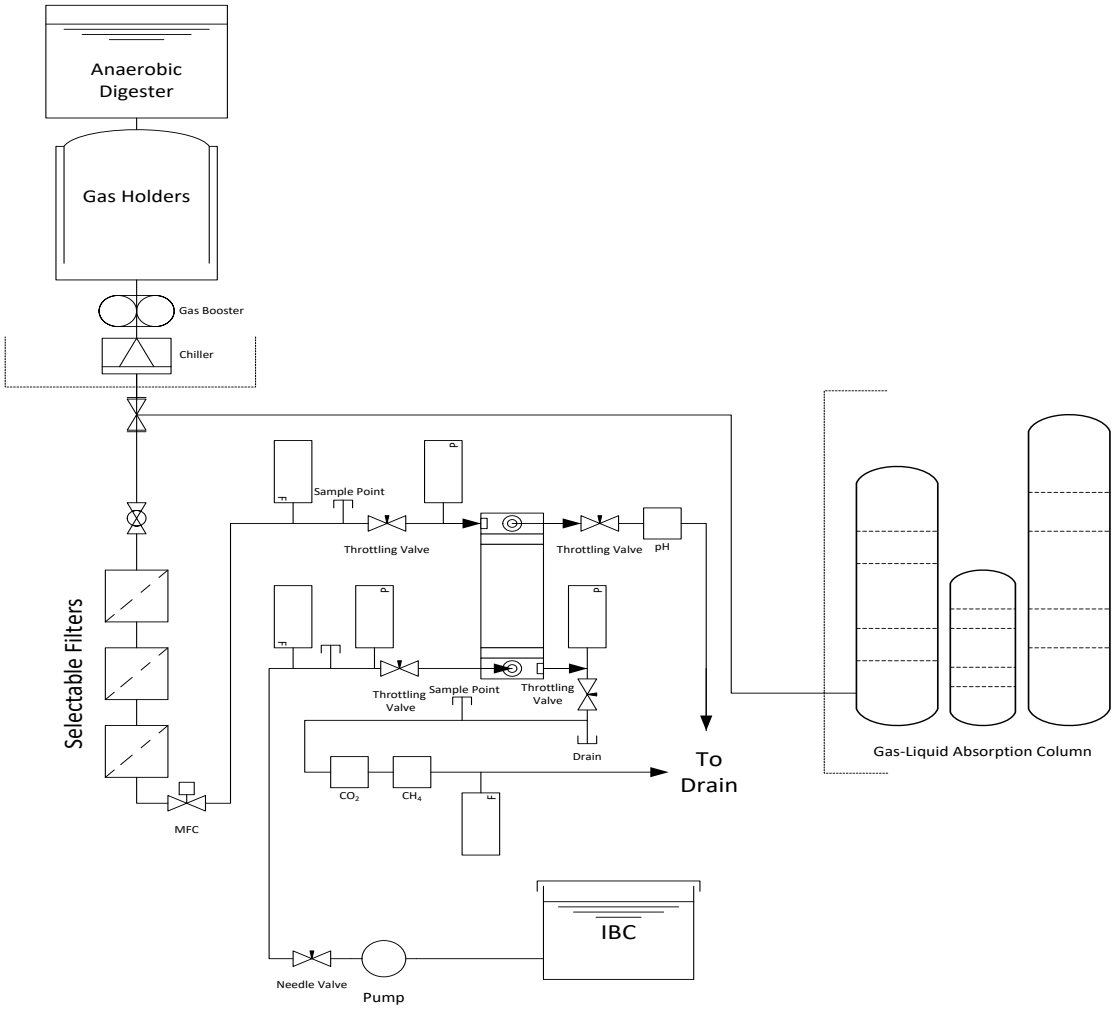

Figure 4.1 Schematic of experimental set up used for determining CO_2 capture under differing *L/G* set points and integration with existing absorption column upgrading system onsite at a WWTW.

4.2.2 Analysis

Process conditions were recorded, including inlet gas pressure (mBar) and ambient temperature (°C). Gas composition was determined using in-line infrared CO_2 and CH_4 analysers (BCP-CO2 or BCP-CH4, accuracy <0.5% full-scale, Bluesens gas sensor GmbH, Herten, Germany). Outlet gas flow rate was measured by a QuadraTherm 640i series in-line mass flow meter (1-30 L min^{-1}, error ±1.25%, Sierra Instruments, L Monterey, USA) utilising the QMix function to account for changing composition. Carbon dioxide removal was analysed through mass balance [32]:

$$\eta = \frac{[(Q_{G,in} \times C_{G,in}) - (Q_{G,out} \times C_{G,out})]}{(Q_{G,in} \times C_{G,in})}$$ (Equation 4.1)

where η is the dimensionless CO_2 capture ratio, $Q_{G,in}$ and $Q_{G,out}$ are inlet and outlet gas flow rates respectively (m^3 s^{-1}), and $C_{G,in}$ and $C_{G,out}$ are inlet and outlet gas phase concentrations respectively (mol m^{-3}). All gas mass flow data were standardised using normalised units (NL min^{-1}). When varying the *L/G* ratio, absorbent flow rate (Q_L) was fixed between 0.2 and 8 L min^{-1}, at each fixed Q_L, Q_G was fixed between 0.05 and 7 L min^{-1}. When maintaining a constant *L/G* at 0.29, Q_L was fixed at 1 L min^{-1} and Q_G at 3.5 L min^{-1}. GC-MS, total petroleum hydrocarbons (TPH) and gravimetric moisture analysis of raw biogas and prefiltered biogas was undertaken by Lucideon (Lucideon Ltd., Stoke-on-Trent, UK) using a UKAS accredited methodology. Gas samples were collected in 0.5L Tedlar bags and activated carbon tubes exposed to 15L (250 mL min^{-1}) of sample gas. Moisture content was assessed using gravimetric analysis of pre-weighed silica beads exposed to 15L (250 mL min^{-1}) of sample gas. Surface fouling was assessed through solvent extraction (dichloromethane) of volatile organic compounds and GC-MS analysis, undertaken by Northumbrian Water Scientific Services (NWSS, Tyne and Wear, UK) using a UKAS accredited methodology. Fourier transform infrared spectroscopy (Bruker Vertex 70, Bruker UK Limited, Coventry, UK) characterised membrane bound functional groups with environmental scanning electron microscopy (ESEM) and energy dispersive x-ray spectroscopy (EDX) (XL30 ESEM-FEG, Philips) determining bound inorganic compounds.

4.3 Results

4.3.1 Operational characteristics

Onsite (Figure 4.1) biogas variability: ambient temperature, *T* (°C), inlet gas pressure, P_{Gin} (mBar) and biogas composition $\%CH_{4in}$ (% CH_4) over 150 days of operation were recorded. *T* was measured between 10°C and 20°C for 74% of operation and P_{Gin} between 40 and 60 mBar for 91% of operation. However, $\%CH_{4in}$ was variable, only 13.9% of operational time fell within 60% - 63% CH_4 v/v target for operation, due to existing biogas upgrading practices onsite.

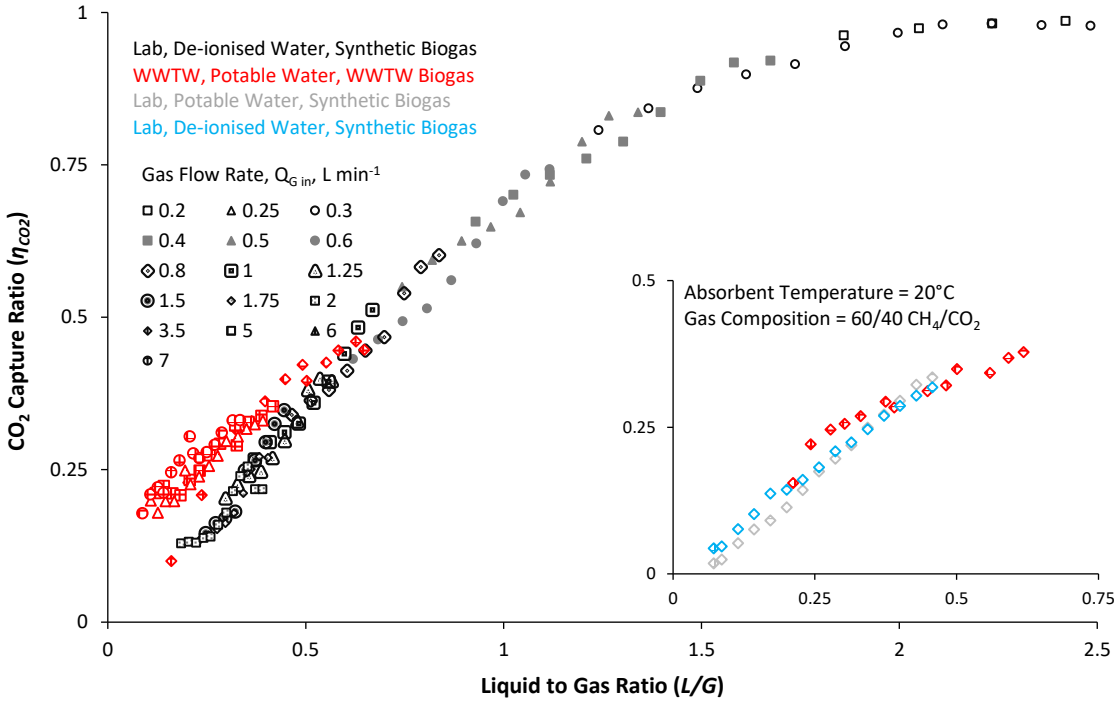

Figure 4.2 Comparative membrane performance under variable hydrodynamic conditions on synthetic and WWTW derived biogas, inset is the impact of de-ionised and potable water on membrane performance under more controlled conditions, *T* 20°C and 40/60 CO_2/CH_4 for both lab and WWTW operation. WWTW operation comprised potable water as absorbent at 14°C, Q_G was fixed between 0.05 and 7 L m^{-1}, at each fixed Q_G, Q_L was varied between 0.1 and 9.5 L m^{-1}. Lab operation comprised an inlet gas of 50/50 CO_2/CH_4 or 40/60 CO_2/CH_4, P_G 0.5 BarG and *T* 20°C at a fixed Q_G of 3.5 L min^{-1} and varied Q_L.

The operational hydrodynamic range (*L/G* ratio) was between 0.2 and 2.7 (Figure 4.2) with biogas flow capacity limited by gas-phase pressure drop, measured between 10 mBar (Q_G, 3.5L min^{-1}) and 33 mBar (Q_G, 7L min^{-1}), constraining upper gas flow rate to 7 L min^{-1}. Likewise, liquid-phase pressure drop was measured in the range of 0.01 Bar (0.5 L min^{-1}) and 1.75 Bar (9.5 L min^{-1}), limiting the upper flow rate to 9.5 L min^{-1}. Potable water and de-ionised water, applying synthetic biogas, yield comparable CO_2 capture ratios (η_{CO2}) for variable *L/G* ratios at a fixed Q_G of 3.5 L min^{-1} (Figure 4.2 inset). Potable water, applying pre-filtered biogas, yields comparable η_{CO2} under identical hydrodynamic conditions to synthetic biogas data (Figure 4.2), with statistical significance confirmed for a 60/40 CH_4/CO_2 gas (Figure 4.2 insert) using a *t*-test for independent samples where the null is zero, yielding a *t*-value of 0.7 against a *t*-critical of 2.1 and *p*-value of 0.5, indicating they are from the same population and therefore comparable. In both cases, observed CO_2 capture ratios increase with the *L/G* ratio in an asymptotic relationship. *L/G* overlap was achieved at differing absolute flow rates: Q_G between 0.05 L min^{-1} and 1.75 L min^{-1} for lab operation and Q_G between 3.5 L min^{-1} and 7 L min^{-1} for on-site

operation. At a fixed *L/G* of 0.29 (Q_G = 3.5 L min^{-1} and Q_L = 1 L min^{-1}) on-site performance is stable at an average η_{CO2} of 0.17 for a period of 115 days of potable water contact, after which the two modules begin to suffer a reduction in η_{CO2} to 0.08 (Figure 4.3).

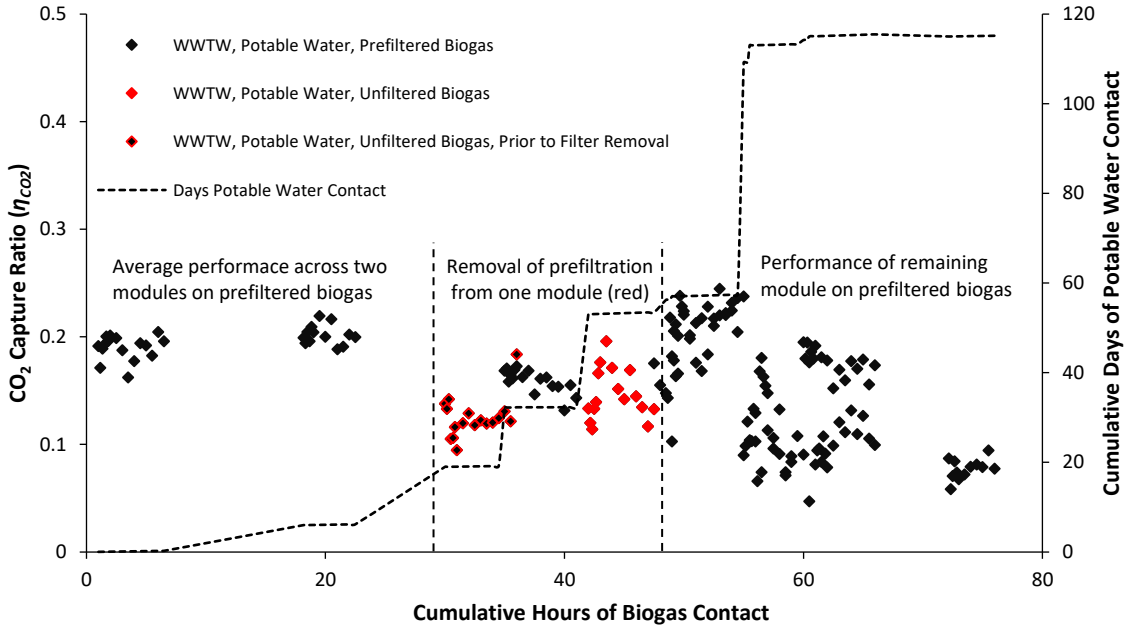

Figure 4.3 A long-term assessment of membrane performance stability on WWTW derived biogas and potable water. Detailed in black is performance average at comparable biogas contact hours for two modules operated on filtered biogas, at points where the hours of contact do not alight only one modules data set is displayed in the average. In red is performance data of a single module contacted with 2.8 Nm^3 unfiltered biogas (included in red outline with black centre is average CO_2 separation performance prior to unfiltered contact) after 42 hours of filtered biogas contact. Gas flow rate (Q_G) was fixed at 3.5 L m^{-1}and liquid flow rate (Q_L) at 1 L m^{-1}, performance loss is observed around 115 days of potable water contact.

Gravimetric analysis of raw and prefiltered biogas moisture content (Table 4.1) indicates the gas phase to have reached its moisture carrying capacity prior to the HFMC. Membrane drying by passing 90L of CO_2 through the fibre lumen and subsequent contacting of potable water and synthetic biogas, yields comparable η_{CO2} (Figure 4.4) to a fouled HFMC post operation at a WWTW.

Table 4.1 GC-MS analysis and moisture content of biogas pre and post filtration

Compound	**WWTW Biogas** mg m^{-3}	**+ACS**[1] mg m^{-3}	**+ACS, +SAZ**[2] mg m^{-3}
Carbon Disulphide	3.3	4.2	<1
Total Organo-Sulphur Compounds	5.3	4.2	<1
Total Volatile Organic Compounds	320	256	<100
Total Petroleum Hydrocarbons	187	117	35.1
	g m^{-3}	g m^{-3}	g m^{-3}
Moisture	19.7	26	17

[1]Anhydrous Calcium Sulphate [2]Silico Aluminate Zeolite

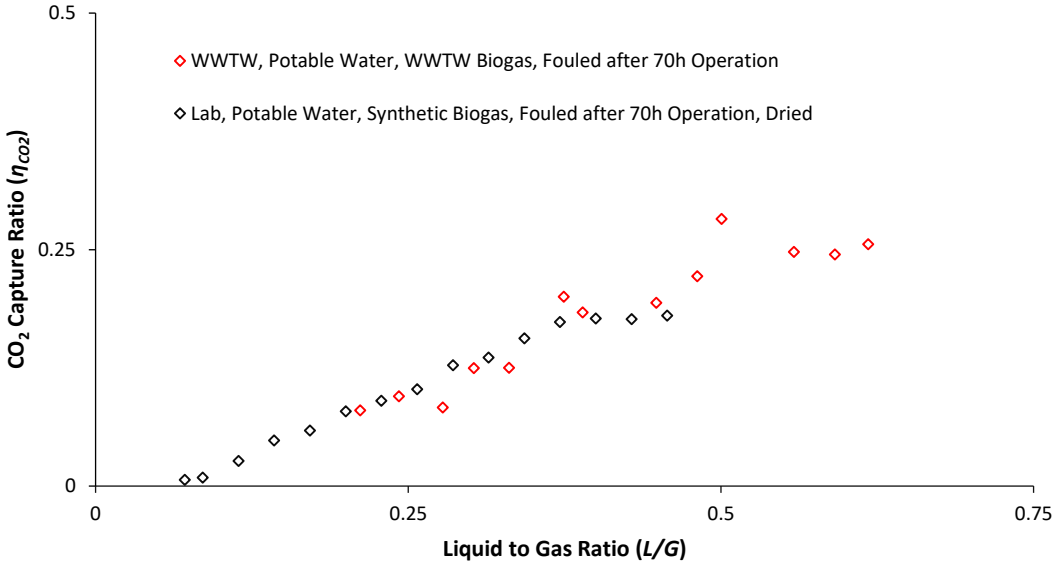

Figure 4.4 The impact of membrane drying on performance recover after potential capillary wetting from gas-phase moisture. Gas flow rate (Q_G) was fixed at 3.5 L $m^{-1}$and liquid flow rate (Q_L) varied between 0.1 and 9.5 L m^{-1}.

4.3.2 Gas-phase characteristics

Raw biogas composition measured through GC-MS analysis (Table 4.1) indicates a 320 mg m^{-3} volatile organic compound (VOC) load and 187 mg m^{-3} total petroleum hydrocarbons (TPH) load entering the upgrading system. Solvent extraction of a visible build-up of a black oily substance on the surface of the SAZ pre-filtration media and GC-MS analysis (Table 4.2) indicates the build-up to consist primarily of siloxanes and short chain hydrocarbons. Octamethylcyclotetrasiloxane (D4) and Decamethylcyclopentasiloxane (D5) comprised 25% of bound compounds, C12-C14 hydrocarbons comprised 55% of bound compounds with the remaining 20% split between other sulphur compounds, terpenes and alcohols.

Table 4.2 GC-MS analysis of biogas contaminants bound to 300g SAZ pre-filtration media

Compound	**mg kg^{-1}**
Cyclic Octatomic Sulphur	2.5
Octamethylcyclotetrasiloxane	1.8
Decamethylcyclopentasiloxane	10
Terpenes	4.93
3,7-Dimethyl-3-octanol	2.6
Total C12-C14 Hydrocarbons	27

A similar visible build-up of a black substance on the surface of absorption column packing material operated on the same WWTW site for one year can be seen in Figure 4.5. Direct exposure of an HFMC to 1.26 Nm^3 unfiltered biogas (Figure 4.3) over 8 hours, following 41 hours of contact with filtered biogas, yielded comparable

performance to averaged module performance from two HFMC exposed to filtered biogas over 76 hours of operation at a fixed L/G (0.29, Q_G = 3.5 L min^{-1} and Q_L = 1 L min^{-1}) with an observed η_{CO2} of 0.17 (Figure 4.3). Gaps in Figure 4.3 represent time where data were not collected, either due to periods of non-continuous reporting or due to operation under different experimental protocol (e.g. contact hours 6-18 and 22-33 are represented in Figure 4.2) where data were gathered at low gas contact hours to ensure potential membrane fouling did not impede comparison with laboratory data. The high TPH, 187 mg m^{-3} detected in the raw biogas and 27 mg kg^{-1} adsorbed to the SAZ filtration indicate the presence of vehicle fuel oil, the presence of which has previously been detected in WWTW derived biogas [20] and attributed to substances present in the AD substrate. Unlike application in CCS [25–28] lumen side ESEM images of fibres taken from the HFMC after exposure to unfiltered biogas do not show any visible particle adsorption to the membrane surface (**Error! Reference source not found.**b) and EDX analysis confirms the elemental composition to be like that of an unused fibre. Subsequent FTIR analysis (Figure 4.) did not indicate the absorption spectra expected of bound siloxanes at 1150–1000 cm^{-1} [33]. GC-MS analysis of prefiltered biogas contaminants (Table 4.1) indicates that sequential and additional inclusion of an ACS and SAZ filters respectively reduces VOC by 69% and THP levels by 81%, with the SAZ filter having the greatest effect on reducing biogas contaminants.

Figure 4.5 Fouling during dispersive, absorption column and non-dispersive, HFMC gas-liquid contacting. The left-hand photograph of liquid-phase fouling shows from left to right: a chemically cleaned, unused and fouled membrane respectively. The right-hand photographs show fouling in full scale column packing material with a visible build-up after a 1-year exposure to 1700 Nm^3 h^{-1} biogas.

4.3.3 Liquid-phase characteristics

A visible greening of a HFMC after 115 days of contact with potable water is shown photographically in Figure 4.5 whilst shell side ESEM images of fibres taken from fouled HFMC indicate a fouling layer (Figure 4.6 b,d & d) in addition to inorganic build-up. FTIR analysis of fibres taken from the same membrane (Figure 4.7) details absorption peaks at 1540 cm^{-1} and 1650 cm^{-1} and are attributed to Amide II and Amide I stretches respectively, indicative of protein fouling [34] with subsequent EDX analysis identifying oxygen, sulphur and copper as the primary inorganic foulants. Absorbent sampled from an HFMC after lying stagnant for 5 days had a turbidity of 29 FTU, compared to an IBC sample reading of 1.4 FTU. As such, the fouling layer is attributed primarily to liquid-phase biological fouling. Performance deterioration after 70h of operation on pre-filtered WWTW derived biogas and 115 days contact with potable water is measured between 25% and 50% relative to a clean HFMC (Figure 4.8). Complete performance recovery after chemical cleaning of the module shell side is shown in Figure 4.8 whilst Figure 4.5 photographically details the reduction in visible membrane greening after chemically cleaning with FTIR analysis of the chemically cleaned HFMC notable for the disappearance of the two absorption peaks at 1540 cm^{-1} and 1650 cm^{-1} relative to a fouled HFMC (Figure 4.7).

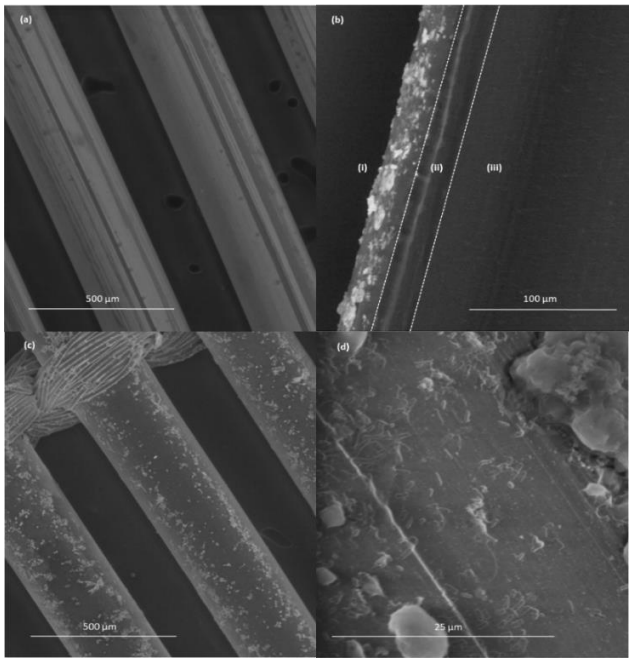

Figure 4.6 Backscatter ESEM images of hollow fibres extracted from a membrane module (a) exposed to synthetic biogas and potable water (b) a fouled fibre after 115 days of potable water contact and 77 hours gas contact (i) fibre shell-side (ii) fibre wall (iii) fibre lumen-side (c) a fouled fibres after 115 days of potable water contact (d) a 25µm scale image of a fouled shell-side fibre with extensive surface fouling.

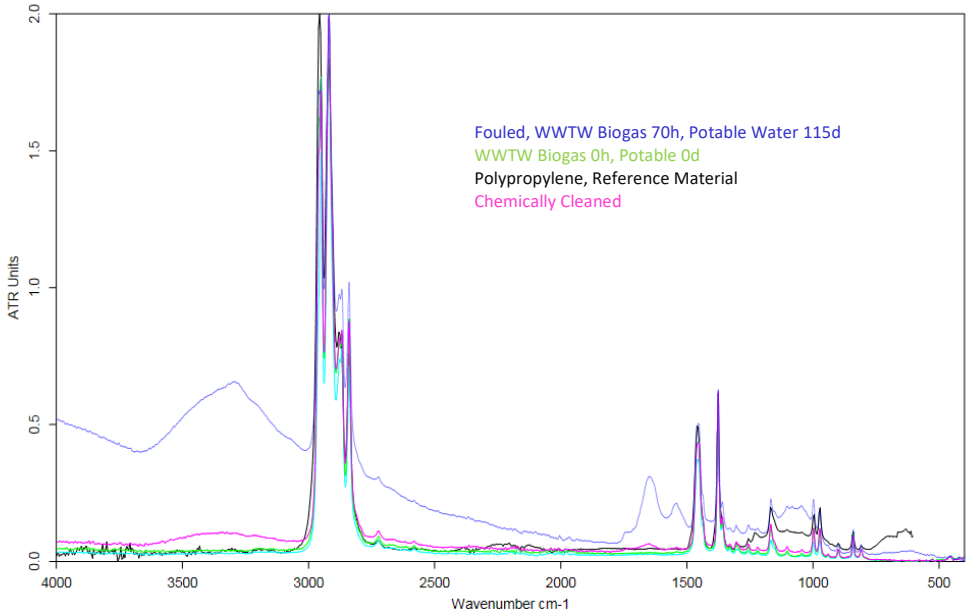

Figure 4.7 FTIR spectra detailing surface bound functional groups present on polypropylene (PP) hollow fibres pre and post shell-side chemical clean. Additional peaks at 1542 cm^{-1} and 1647 cm^{-1} are attributed to Amide II and Amide I stretches respectively [34] whilst the stretch from 3100 cm^{-1} downwards is attributed to water [35].

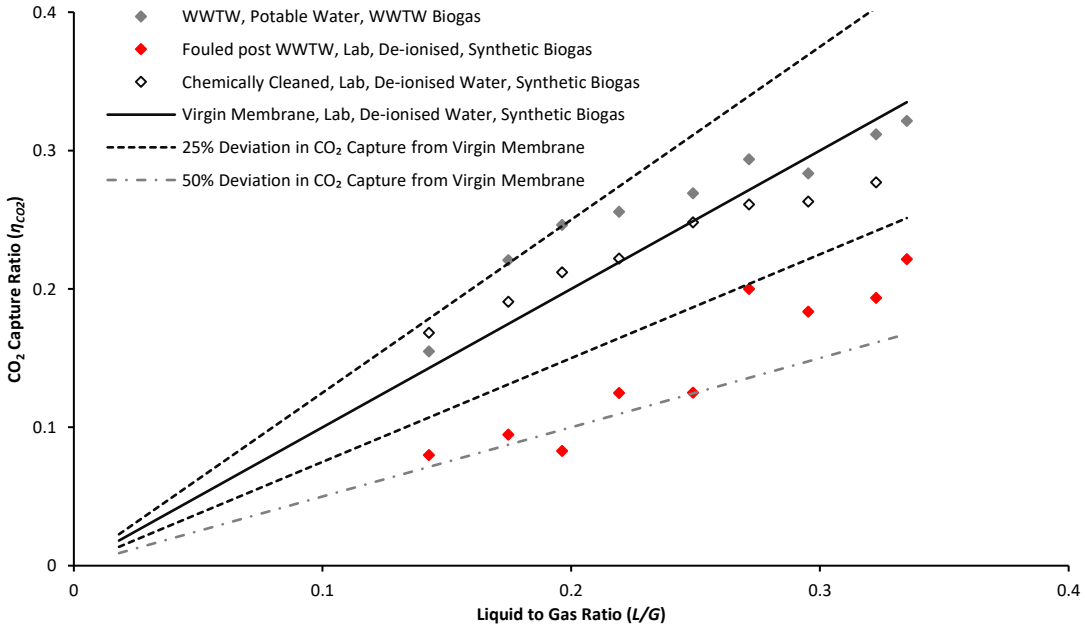

Figure 4.8 Performance recovery parity of a fouled membrane after chemical cleaning of the membrane shell. Gas flow rate (Q_G) was fixed at 3.5 L m^{-1} and liquid flow rate (Q_L) varied between 0.5 and 1.2 L m^{-1}, inlet gas comprised 60/40 CO_2/CH_4 and P_G 0.5 BarG and potable water at 20°C.

4.4 Discussion

In this study, consistent CO_2 mass transfer has been identified for a HFMC applied in an industrial setting to biogas produced at a centralised sewage treatment works (Figure 4.2) which contradicts observations from industrial flue gases [25,26,28], where gas phase contaminants were identified to contribute to fouling, resulting in a loss of CO_2 flux (Figure 4.). Three gas-phase mechanisms are thought to reduce CO_2 flux during industrial operation: accumulation of particulate matter (channel clogging), surface adsorption [26,28] and capillary wetting [24,36]. The unfiltered biogas composition was comparable to literature (Table 4.2) [21,22], comprising organosilicon compounds (siloxanes, D4 and D5) which are characterised by a high octanol-water partitioning coefficient [37], indicating their affinity for adsorption [44,45], VOCs such as Terpenes, which were characterised in the bulk gas and identified through analysis of the SAZ filtration media (Table 4.2), are frequently associated with biogas arising from WWTW [20] and landfills [22,38,39], in addition to gas phase humidity approaching saturation. However, after 77 hours of direct contact with the gas phase, in addition to a further eight hours of direct contact with unfiltered gas, diagnostic investigation using environmental SEM imaging, indicated negligible deposition on the lumen side of the fibre where gas passed (Figure 6b). This is in contrast to observed particulate build-up after 7 hours following HFMC operation on unfiltered industrial flue gas from a coal fired power station [26–28]. Gas-phase particulates were not explicitly measured in this study, and whilst deposition on the prefiltration media was observed, recent studies suggest that the particulate concentration of biogas is relatively low, even before filtration which may explain the disparity between investigations [40]. Compositional analysis of the membrane lumen-side provided confirmation of negligible particulate deposition or adsorption as the elemental composition was comparable to that of a virgin fibre. Introduction of membrane drying also did not recover CO_2 flux (Figure 4.4), which we propose implies that capillary wetting is not the primary mechanism, which has been previously identified as an effective strategy for recovery of progressively wetting membranes after 7 days of operation [41,42]. As such, performance degradation is not attributed to capillary wetting.

Using FTIR to investigate shell-side membrane surface chemistry, amide functional groups were evidenced which was coincident with the build-up of a green deposition (Figure 4.5 and Figure 4.7), indicative of biologically derived organics. We suggest that it was this deposition which contributed to a 50% reduction in CO_2 flux (Figure 4.8). Biological fouling has been previously reported within absorption columns

for biogas upgrading and is attributed to methanotropes (type I and II), gram negative bacteria, gram positive bacteria, actinomyces and fungi [23], despite the use of potable water as the absorption fluid and can be ascribed to its application in a closed loop, which will quickly consume the disinfection residual. In this study, potable water was maintained within the HFMC for 115 days, with significant periods of cessation which provided a sufficient residence time for regrowth and was evidenced by an increase in absorbent turbidity from 1.4 to 29 FTU. We therefore propose that the primary mechanism for HFMC fouling in biogas upgrading is a combination of adsorption and clogging of the shell-side, which once fouled will reduce the efficacy of liquid-phase distribution (channelling), leading to a dissipation in membrane performance [43,44] and would appear consistent to the observations of Vogler et al. [29]. Due to the adsorptive potential of biopolymers which can possess strong lipophilic affinity, desorption can expectedly be thermodynamically unfavourable, thus chemical cleaning methods are preferred to physical methods [44,45]. Polypropylene does not favour oxidants [45] due to their impact upon mechanical strength, specifically fibre tensile strength and elongation values [31]. In this study, an alkali-acid chemical cleaning cycle demonstrated almost complete flux recovery, indicating the organic fraction to be strongly reversible (Figure 4.7 and Figure 4.8).

Importantly, this study demonstrated that comparable CO_2 separation performance could be achieved for synthetic gas and actual biogas which comprises a more complex gas mixture (Figure 4.2), which simplifies considerations for scale-up. This is comparable to earlier observation of HFMC applied to flue gas [17,25]. Slight variations can be accounted for by the transient in the temperature of both fluids. At full-scale, this can be accounted for through feed-back control using the outlet gas-quality as the set-point [46]. Whilst a η_{CO2} of 0.98 was demonstrated to be attainable on synthetic biogas in a single module (Figure 4.2), the limited gas pressure (equivalent to the overpressure from the anaerobic digester) also limited the gas phase flowrates that could be practically achieved. Pressurisation of HFMC to analogous pressures presently used for packed-columns of around 7 BarG has been demonstrated in the literature [11,44,46], which will guarantee that the process intensification provided by HFMC technology will result in next generation biogas plants of considerably smaller process scale and demanding considerably lower pressure drops [17,25,29,49–51]. For reference, Vogler et al. [29] evaluated HFMC in an absorption-desorption arrangement at a similar feed pressure to this study (<100mBar) [29]. Despite the low pressure, the authors reported an energy requirement of 0.3 kWh Nm^{-3} raw biogas which is comparable to the 0.23 - 0.3 kWh Nm^{-}

^{3} reported for gas-liquid absorption columns, and will inevitably reduce considerably once pressurisation has been introduced [7]. Pre-filtration with SAZ reduced the trace contaminants in the gas phase by between 70 and 80%. Present biogas upgrading systems comprising packed columns are ordinarily integrated with adsorption technology to remove this organic fraction and are sited either upstream or downstream of the packed column, dependent upon the installation. It is recommended that when incorporating HFMC, there could be synergistic advantage in the long-term by siting adsorption technology for VOC removal upstream. Present gas-liquid packed column installations are designed based on a single-stage solution [7]. However, on-site experience has shown that reactive maintenance due to biological fouling occurs frequently and can require down-time of up to two-weeks, which limits asset availability and reduces profitability [23]. Due to the reduction in process scale, and relatively low cost of the membrane material [52,53], a duty-standby system could be implemented to ensure 100% asset availability. Furthermore, due to the comparatively smaller volume of the reactor zone, the incorporation of proactive chemical maintenance would be considerably easier to implement.

4.5 Conclusions

In this study, demonstration scale operation of a commercial transverse flow HFMC on industrial biogas at a WWTW has evidenced the robustness of the technology to impurities within industrial biogas. Additionally, flux data gathered on synthetic biogas is comparable to flux data gathered from industrial biogas, indicating the suitability of simplified systems in predicting performance for industrial use. Importantly, performance identified on synthetic biogas can be expected to hold true for industrial application. From the study several further conclusions can be drawn:

- Adsorption and clogging of the shell-side resulting from biological fouling seeded from the absorbent is the primary source of membrane fouling, which due to low membrane cost can be controlled through the introduction of a duty-standby system, ensuring 100% asset availability.
- Biological fouling experienced at a WWTW is readily reversible by standard membrane alkali-acid wash protocols. However, due to the nature of biological fouling and limited resistance of membrane material to oxidants, alternate cleaning methods are not recommended.
- Gas-phase pre-filtration had no impact in protecting from capillary wetting and particulate fouling, which were found not to occur even in the absence of pre-filtration.

The membrane modules can be expected to offer robustness which may be further enhanced by siting VOC removal systems upstream of the upgrading process.

Acknowledgements

The authors would like to thank Anglian Water, Northumbrian Water and Severn Trent Water for their practical and financial support. We are also grateful for funding from the Engineering and Physical Sciences Research Council (EPSRC) which was provided through the STREAM Industrial Doctorate Centre. Enquiries for access to the data referred to in this article should be directed to: researchdata@ cranfield.ac.uk.

References

[1] G. Silvestre, B. Fernández, A. Bonmatí, Significance of anaerobic digestion as a source of clean energy in wastewater treatment plants, Energy Convers. Manag. 101 (2015) 255–262.

[2] D. Thrän, E. Billig, J. Daniel-Gromke, J. Ponitka, M. Seiffert, T. Persson, M. Svensson, J. Balswin, L. Kranzl, F. Schipfer, J. Matzenberger, N. Devriendt, M. Dumont, J. Dahl, G. Bochmann, Biomethane Status and Factors Affecting Market Development and Trade, 2014. https://www.ieabioenergy.com/publications/biomethane-status-and-factors-affecting-market-development-and-trade/.

[3] Anaerobic Digestion and Biogas Association (ADBA), Anaerobic Digestion Market Report, London, 2015. http://adbioresources.org/library/market-report-july-2015.

[4] P.M. Connor, L. Xie, R. Lowes, J. Britton, T. Richardson, The development of renewable heating policy in the United Kingdom, Renew. Energy. 75 (2015) 733–744.

[5] IPPT Associates, United Kingdom Anaerobic Digestion Market Report, 2017. https://anaerobic-digestion.com/downloads/free-downloads/uk-anaerobic-digestion-market-report-2017.

[6] J. Baldwin, UK Biomethane Market: Market Update and the Capacity Question, (2017). [Presentation] http://www.cngservices.co.uk/images/BiomethaneDay/2017/John-Baldwin--%0AUK-Biomethane-Market--the-Capacity-Question.pdf. (accessed January 10, 2019)

[7] F. Bauer, C. Hulteberg, T. Persson, D. Tamm, Biogas upgrading – Review of commercial technologies, 2013.

http://www.sgc.se/ckfinder/userfiles/files/SGC270.pdf. (accessed January 10, 2019).

[8] Z. Cui, D. DeMontigny, Part 7: A review of CO_2 capture using hollow fiber membrane contactors, Carbon Manag. 4 (2014) 69–89.

[9] S. Heile, S. Rosenberger, A. Parker, B. Jefferson, E.J. McAdam, Establishing the suitability of symmetric ultrathin wall polydimethylsiloxane hollow-fibre membrane contactors for enhanced CO_2 separation during biogas upgrading, J. Memb. Sci. 452 (2014) 37–45.

[10] J. Elhajj, M. Al-hindi, F. Azizi, A Review of the Absorption and Desorption Processes of Carbon Dioxide in Water Systems, Ind. Eng. Chem. Res. 53 (2014) 2–22.

[11] B. Belaissaoui, J. Claveria-Baro, A. Lorenzo-Hernando, D. Albarracin, E. Chabanon, C. Castel, S. Rode, D. Roizard, E. Favre, Potentialities of a dense skin hollow fiber membrane contactor for biogas purification by pressurized water absorption, J. Memb. Sci. 513 (2016) 236–249.

[12] D.A. Zaidiza, B. Belaissaoui, S. Rode, E. Favre, Intensification potential of hollow fiber membrane contactors for CO_2 chemical absorption and stripping using monoethanolamine solutions, Sep. Purif. Technol. 188 (2017) 38–51.

[13] S. Zhao, P.H.M. Feron, L. Deng, E. Favre, E. Chabanon, S. Yan, J. Hou, V. Chen, H. Qi, Status and progress of membrane contactors in post-combustion carbon capture : A state-of-the-art review of new developments, J. Memb. Sci. 511 (2016) 180–206.

[14] O. Falk-Pedersen, M.S. Grønvold, P. Nøkleby, F. Bjerve, H.F. Svendsen, CO_2 Capture with Membrane Contactors, Int. J. Green Energy. 2 (2004) 157–165.

[15] O. Falk-Pedersen, Y. Bjerve, G. Glittum, S. Rønning, Separation of Carbon Dioxide from Offshore Gas Turbine Exhaust, Energy Convers. Manag. 36 (1995) 393–396.

[16] H. Herzog, O. Falk-pedersen, The Kvaerner membrane contactor: lessons from a case study in how to reduce capture costs, in: Greenh. Gas Control Technol. Proc. 5th Int. Conf. Greenh. Gas, 2001. 121–125.

[17] A. Comite, C. Costa, M. Demartini, R. Di, M. Oliva, Exploring CO_2 capture from pressurized industrial gaseous effluents in membrane contactor-based pilot plant, Int. J. Greenh. Gas Control. 67 (2017) 60–70.

[18] R. Klaassen, Achieving flue gas desulphurization with membrane gas absorption, Filtr. Sep. 40 (2003) 26–28.

[19] G.L. Noble, D. Broomhall, M. Maple, L. Shelenko, J. Truong, Hazards arising from the conveyance and use of gas from Non-Conventional Sources (NCS), 2011. http://www.hse.gov.uk/research/rrpdf/rr882.pdf. (accessed January 10, 2019).

[20] K. Arrhenius, U. Johansson, Characterisation of contaminants in biogas before and after upgrading to vehicle gas, 2012. http://www.sgc.se/ckfinder/userfiles/files/SGC246_eng.pdf. (accessed January 15, 2019)

[21] S. Rasi, A. Veijanen, J. Rintala, Trace compounds of biogas from different biogas production plants, Energy. 32 (2007) 1375–1380.

[22] S. Rasi, J. Läntelä, J. Rintala, Trace compounds affecting biogas energy utilisation - A review, Energy Convers. Manag. 52 (2011) 3369–3375.

[23] A. Håkansson, Preventing microbial growth on pall-rings when upgrading biogas using absorption with water wash, 2006. http://www.sgc.se/ckfinder/userfiles/files/SGC166.pdf. (accessed November 20, 2018)

[24] H. Yu, J. Thé, Z. Tan, X. Feng, Modeling SO_2 absorption into water accompanied with reversible reaction in a hollow fiber membrane contactor, Chem. Eng. Sci. 156 (2016) 136–146.

[25] C.A. Scholes, A. Qader, G.W. Stevens, S.E. Kentish, Membrane Gas-Solvent Contactor Pilot Plant Trials of CO_2 Absorption from Flue Gas, Sep. Sci. Technol. 49 (2014) 2449–2458.

[26] L. Zhang, R. Qu, Y. Sha, X. Wang, L. Yang, Membrane gas absorption for CO_2 capture from flue gas containing fine particles and gaseous contaminants, Int. J. Greenh. Gas Control. 33 (2015) 10–17.

[27] L. Zhang, B. Hu, H. Song, L. Yang, L. Ba, Colloidal Force Study of Particle Fouling on Gas Capture Membrane, Sci. Rep. 7 (2017) 1–11.

[28] L. Zhang, J. Li, L. Zhou, R. Liu, X. Wang, L. Yang, Fouling of Impurities in Desulfurized Flue Gas on Hollow Fiber Membrane Absorption for CO_2 Capture, Ind. Eng. Chem. Res. 55 (2016) 8002–8010.

[29] S. Vogler, A. Braasch, G. Buse, S. Hempel, J. Schneider, M. Ulbricht, Biogas conditioning using hollow fiber membrane contactors, Chemie-Ingenieur-Technik. 85 (2013) 1254–1258.

[30] A. Sengupta, P.A. Peterson, B.D. Miller, J. Schneider, C.W. Fulk, Large-scale application of membrane contactors for gas transfer from or to ultrapure water, Sep. Purif. Technol. 14 (1998) 189–200.

[31] Liqui-Cel, Cleaning Guidelines, (2013) 1–24. https://www.3m.com/3M/en_US/liquicel-us/resources/operating-and-technical-guides/. (accessed February 05, 2016)

[32] E. Chabanon, D. Roizard, E. Favre, Modeling strategies of membrane contactors for post-combustion carbon capture: A critical comparative study, Chem. Eng. Sci. 87 (2013) 393–407.

[33] C.A. Hepburn, P. Vale, A.S. Brown, N.J. Simms, E.J. McAdam, Development of on-line FTIR spectroscopy for siloxane detection in biogas to enhance carbon contactor management, Talanta. 141 (2015) 128–136.

[34] A. Zarebska, Á.C. Amor, K. Ciurkot, H. Karring, O. Thygesen, T.P. Andersen, M.B. Hägg, K.V. Christensen, B. Norddahl, Fouling mitigation in membrane distillation processes during ammonia stripping from pig manure, J. Memb. Sci. 484 (2015) 119–132.

[35] M.J. Luján-Facundo, J.A. Mendoza-Roca, B. Cuartas-Uribe, S. Álvarez-Blanco, Evaluation of cleaning efficiency of ultrafiltration membranes fouled by BSA using FTIR-ATR as a tool, J. Food Eng. 163 (2015) 1–8.

[36] H. Mahmud, A. Kumar, R.M. Narbaitz, T. Matsuura, A study of mass transfer in the membrane air-stripping process using microporous polyproplylene hollow fibers, J. Memb. Sci. 179 (2000) 29–41.

[37] L. Xu, Y. Shi, N. Liu, Y. Cai, Methyl siloxanes in environmental matrices and human plasma/fat from both general industries and residential areas in China, Sci. Total Environ. 505 (2015) 454–463.

[38] M.R. Allen, A. Braithwaite, C.C. Hills, Trace organic compounds in landfill gas at seven U.K. waste disposal sites, Environ. Sci. Technol. 31 (1997) 1054–1061.

[39] B. Eklund, E.P. Anderson, B.L. Walker, D.B. Burrows, Characterization of landfill gas composition at the Fresh Kills municipal solid-waste landfill, Environ. Sci. Technol. 32 (1998) 2233–2237.

[40] R. Högström, H. Vesala, M. Heinonen, Particulate content of biogas, 18th Int. Congr. Meterology. 08002 (2017).

[41] M. Mavroudi, S.P. Kaldis, G.P. Sakellaropoulos, A study of mass transfer resistance in membrane gas-liquid contacting processes, J. Memb. Sci. 272 (2006) 103–115.

[42] V. Fougerit, V. Pozzobon, D. Pareau, M. Théoleyre, M. Stambouli, Gas-liquid absorption in industrial cross-flow membrane contactors : Experimental and numerical investigation of the influence of transmembrane pressure on partial

wetting, Chem. Eng. Sci. 170 (2017) 561–573.

[43] N.M. D'Souza, A.J. Mawson, Membrane cleaning in the dairy industry: A review, Crit. Rev. Food Sci. Nutr. 45 (2005) 125–134.

[44] X. Shi, G. Tal, N.P. Hankins, V. Gitis, Fouling and cleaning of ultrafiltration membranes: A review, J. Water Process Eng. 1 (2014) 121–138.

[45] N. Porcelli, S. Judd, Chemical cleaning of potable water membranes: A review, Water Res. 71 (2010) 137–143.

[46] F. Bauer, T. Persson, C. Hulteberg, D. Tamm, Biogas upgrading - technology overview, comparison and perspectives for the future, Biofuels, Bioprod. Biorefining. 7 (2013) 499–511.

[47] B. Belaissaoui, E. Favre, Evaluation of a dense skin hollow fiber gas-liquid membrane contactor for high pressure removal of CO_2 from syngas using Selexol as the absorbent, Chem. Eng. Sci. 184 (2018) 186–199.

[48] V.Y. Dindore, D.W.F. Brilman, P.H.M. Feron, G.F. Versteeg, CO_2 absorption at elevated pressures using a hollow fiber membrane contactor, J. Memb. Sci. 235 (2004) 99–109.

[49] B. Belaissaoui, E. Favre, Novel dense skin hollow fiber membrane contactor based process for CO_2 removal from raw biogas using water as absorbent, Sep. Purif. Technol. 193 (2018) 112–126.

[50] E. Chabanon, E. Kimball, E. Favre, O. Lorain, E. Goetheer, D. Ferre, A. Gomez, P. Broutin, Hollow Fiber Membrane Contactors for Post-Combustion CO_2 Capture: A Scale-Up Study from Laboratory to Pilot Plant, Oil Gas Sci. Technol. – Rev. d'IFP Energies Nouv. 69 (2014) 1035–1045.

[51] E. Kimball, A. Al-azki, A. Gomez, E. Goetheer, N. Booth, D. Adams, D. Ferre, Hollow Fiber Membrane Contactors for CO_2 Capture : Modeling and Up-Scaling to CO_2 Capture for an 800 MW e Coal Power Station, Oil Gas Sci. Technol. – Rev. d'IFP Energies Nouv. 69 (2014) 1047–1058.

[52] S. Boributh, W. Rongwong, S. Assabumrungrat, N. Laosiripojana, R. Jiraratananon, Mathematical modeling and cascade design of hollow fiber membrane contactor for CO_2 absorption by monoethanolamine, J. Memb. Sci. 401–402 (2012) 175–189.

[53] S. Boributh, S. Assabumrungrat, N. Laosiripojana, R. Jiraratananon, Effect of membrane module arrangement of gas-liquid membrane contacting process on CO_2 absorption performance: A modeling study, J. Memb. Sci. 372 (2011) 75–86.

5 Hollow fibre membrane contactors and absorption columns as crystallising reactors for a biogas upgrading – ammonium bicarbonate recovery system

Hollow fibre membrane contactors and absorption columns as crystallising reactors for a biogas upgrading – ammonium bicarbonate recovery system

S. Houlker[a], M.Hermassi[a], A. Brookes[b], A. Moore[c], P. Vale[d], M. Pidou[a], E.J. McAdam[a,*]

[a]Cranfield Water Science Institute, Cranfield University, Bedfordshire, UK
[b]Anglian Water, Thorpewood House, Peterborough, UK
[c]Northumbrian Water, Boldon House, Pity Me, Durham, UK
[d]Severn Trent Water, Coventry, UK
*Corresponding author: e.mcadam@cranfield.ac.uk

Abstract

Ammonia is recognised as an emerging high capacity chemically enhanced absorbent for biogas upgrading. Precipitation of ammonium bicarbonate as the reaction product of ammonia and carbon dioxide is undertaken in absorption columns to increase the solvent loading rate and reduce the specific heat energy demand of regeneration. However, ammonium bicarbonate recovery has value as a recoverable product at a wastewater treatment works (WWTW), where high concentration ammonia waste is available as an environmental source of absorbent. Previous studies have demonstrated controlled crystallisation and recovery of ammonium bicarbonate in single fibre hollow fibre membrane contactors (HFMC), exploiting the membrane surface as a nucleation substrate and by limiting ammonia volatility through chilling, applying low concentration NH_3 and recycling absorbents to shift equilibria in favour of non-volatile ammonium. This study achieves industrially relevant product gas quality (≥98% CH_4) whilst sustaining crystallisation within a commercially configured module to evidence capability. In addition to evidencing that controlled crystallisation and recovery in gas-liquid absorption columns as a current generation industrial bulk gas separation technology is not practical. An absorption column and commercially available HFMC are compared during physical absorption and chemically enhanced absorption with a low concentration (3.3 mol L^{-1}) ammonia solution, demonstrating comparable performance. Subsequent ammonium bicarbonate crystallisation in both absorber types demonstrates that a high specific nucleation rate and agglomeration in the column leads to flooding whilst high ammonia slip reduces reaction yield. HFMC in contrast demonstrated an 87% chemical reduction of the nitrogen load, biogas upgrading to industrial standard (≥98% CH_4) and protection from system blocking by the low specific nucleation rate and preferential crystal growth.

Keywords: membrane crystallisation, biogas upgrading, absorption column, ammonia

5.1 Introduction

The application of gas-liquid contacting technology to the selective separation of CO_2 from a multi component gas has been extensively studied for bulk gas separation processes [1–5]. For example, absorption columns have been extensively applied at full-scale for biogas upgrading with the International Energy Association reporting 56% of known installations as employing this technology [6]. However, as columns rely on dispersive gas-liquid contact they suffer from practical limitations such as flooding, channelling, entrainment and foaming [7] which limit their operational range. Furthermore, their low interfacial area, coupled with the common use of water as the solvent, constrains absorption capacity and subsequently mass transfer [7,8]. Hollow fibre membrane contactors (HFMC) are an alternative gas-liquid separation technology which employ an analogous absorption mechanism to columns, where the microporous membrane facilitates CO_2 diffusion from the gas phase through the micropores of a hydrophobic membrane into the absorbent [9]. The membrane therefore establishes non-dispersive contact between the two fluids, and with interfacial areas an order of magnitude higher that traditional absorption columns, an intensification factor of 15 times can be achieved [8,10].

In Carbon Capture and Storage (CCS), and biogas upgrading, amines such as Monoethanolamine (MEA) with a high absorption capacity of around 0.55 $kgCO_2\,kgMEA^{-1}$ [1] have been applied to bring about process intensification, reduce methane slip [11] and pressure reduction [2,11,12] relative to physical absorption. This reduces the specific power consumption from 0.22 – 0.3 kWh Nm^{-3} biogas for physical absorption to 0.12 – 0.14 kWh Nm^{-3} biogas for chemical absorption [2,12]. However, absorbent regeneration introduces an additional specific heat demand of 0.55 kWh Nm^{-3} biogas [2], and chemical losses are also realised (up to 6.5 kgMEA tCO_2 [13]) due to solvent degradation [2,10,11]. Aqueous free ammonia (NH_3) is an alternative chemical absorbent which increases absorption capacity to 1.76 $kgCO_2\ kgNH_3$ [10,13], eliminates solvent degradation [10] and is non-corrosive [14]. The cost of ammonia can be further obviated through sustainably sourcing from high concentration wastewaters, and has been demonstrated for the recovery of NH_3 absorbents ranging up to 6 mol L^{-1}in concentration [15]. Studies applying HFMC for CCS have applied ammonia absorbents up to 3 mol L^{-1}, demonstrating the intensification potential of HFMC over absorption columns [13,16]. However, the formation of ammonium bicarbonate salts in the gas phase causes blocking of the fibre lumen leading to cessation of gas flow [13,16]. In commercial CCS in absorption columns, the formation of ammonium bicarbonate precipitates in the

absorbent (10M NH_3) have been exploited to increase CO_2 loading, and reduce the subsequent regenerative heat demand, releasing carbon dioxide as a recoverable product during regeneration [17]. However, demonstration trials have noted ammonium salt precipitation leading to column blocking and loss of function [18,19], thus on-going research commonly focuses on limiting precipitation [20–22].

To facilitate continuous operation during biogas upgrading, without process blockage, chemically reactive membrane crystallisation reactors (CR-MCr) have been developed to control the recovery of crystalline ammonium bicarbonate precipitate in the aqueous phase [15,23]. Shell-side (aqueous phase) crystallisation is preferentially achieved by limiting ammonia slip into the gas-phase. Recycling a low concentration (3.3 mol L^{-1}) ammonia absorbent, limits ammonia slip into the gas phase by shifting ammonia-ammonium equilibrium toward non-volatile ammonium [15,23]. Ammonia vapour pressure is further minimised through absorbent temperature reduction and NH_3 concentration restriction, obviating breakthrough, and adoption of smaller pore sizes limit wetting which constrains crystallisation development [15,23]. Surface scaling is controlled by slowing the nucleation rate through limiting the free ammonia concentration and reducing the availability of the bicarbonate ion (HCO_3^-) [15]. The high contact angle of the hydrophobic membrane surface reduces surface free energy and due to the lower activation energy, in combination with the counter-current diffusion of CO_2 and NH_3 into the concentration boundary layer, primary heterogeneous nucleation is favoured at the gas-liquid interface of the membrane surface [15,23]. The kinetics of nucleation in HFMC may therefore progress very differently to that for absorption columns [23,24].

Mani et al. [25] report an optimal concentration (2.5M NH_3) for absorption columns with respect to limiting ammonia slip and maximising CO_2 capacity, similar to that reported as the free ammonia concentration threshold at which solvent reactivity becomes independent of concentration [15]. Bavarella [15] reports that for low NH_3 solution concentrations, a reduction in pH on CO_2 absorption shifts reaction equilibrium in favour of ammonium and carbonic acid, inhibiting absorbent reactivity and nucleation. Interestingly the application of a lower concentration ammonia solution might be expected to reduce the nucleation rate and hence crystal number in solution, limiting agglomeration and process blocking during column operation.

Applied for industrial CO_2 separation, a binary gas such as biogas (50/50 CH_4/CO_2) can be expected to reduce CO_2 partial pressure and the diffusion rate of CO_2 into the boundary layer, leading to a further decrease in nucleation rate. Under these conditions, controlled crystallisation might be achieved in both columns and HFMC

systems. However, the increased surface area and pore sites as nucleating loci in a multi-fibre bundle can be expected to increase the nucleation rate [15]. Control of the competing mechanisms will be important in preventing blocking of a multi-fibre bundle within a commercial module.

Whilst the CR-MCR concept has been successfully evaluated, the previous literature has focussed on single hollow fibre membranes using pure carbon dioxide. However, to progress the technology toward realisation, the membrane configuration must be scalable, indicating considerably higher hollow fibre packing fractions, and must be able to achieve gas separation to the required standard whilst simultaneously crystallising the reaction product. Biogas is a binary gas which during the selective separation of CO_2 will undergo a reduction in CO_2 partial pressure from 0.5 (50% CO_2) to 0.02 (2% CO_2) after upgrading, introducing a reducing CO_2 flux along the membrane, limiting the availability of CO_2 as reactant in the absorption fluid. This study has therefore sought to assess a multi-fibre membrane, analogous to those used in industry, as the crystallising substrate in a low concentration ammonia solution (3.3 mol L^{-1} NH_3) and reduced CO_2 partial pressure (50/50 CH_4/CO_2) synthetic biogas relative to crystallisation in an absorption column, as current generation industrial upgrading technology, whilst maintaining an industrially relevant gas purity (>98% CH_4). Specific objectives are to: (i) Characterise mass transfer during column and HFMC mediated gas-liquid separation to intimate the impact of contacting mechanism and CO_2 partial pressure on chemical enhancement arising from a low concentration ammonia solution (3.3 mol L^{-1}) (ii) Identify the impact of controlled crystallisation, absorbent recycle, low temperature (5°C) and low concentration ammonia solution (3.3 mol L^{-1}) on nucleation and growth kinetics for both absorber types (iii) demonstrate the co-production of NH_4HCO_3 and ≥98% CH_4 from a synthetic biogas employing an HFMC mediated process design.

5.2 Materials and methods

5.2.1 Experimental set-up

The performance of HFMC gas-liquid contacting technology during physical absorption (water) and chemically reactive absorption (3.3 mol L^{-1} NH_3) was assessed utilising two commercial HFMC, a small-scale parallel flow and larger-scale transverse flow module (3M Industrial Group, Charlotte, USA). The fibre bundles of both modules were comprised of polypropylene X50 fibres with an outer diameter and inner diameter of 300 µm and 240 µm respectively. Interfacial area was increased from 0.5m^2 in the parallel flow module to 1.2m^2 in the transverse flow module by increasing fibre length from 0.13m

to 0.16m and fibre number from 7400 to 10200 respectively. Due to the high absorptive capacity of NH_3, a low absorption flow rate (0.1 – 0.4 L min^{-1}) was required to create both low and high solvent loading rates, parallel flow modules were applied with a lower contact area to lower the risk of crystal formation in single pass. Parallel flow modules, geometrically structured like shell-and-tube heat exchanger designs, suffer shell-side maldistribution due to non-uniform fibre packing. As such, the absorbent was applied to the well distributed lumen side. Comparison of contacting mechanism, dispersive or non-dispersive, was achieved by subjecting a bespoke absorption column to the same operating conditions as the parallel flow module. A 0.3 m acrylic absorption column (Figure 5.1) of 0.05 m diameter was filled with 0.005 m diameter borosilicate glass raschig rings with a specific surface area of 984 m^2m^3 (Hilgenberg GmbH, Malsfeld, Germany) to yield an interfacial area of 0.5m^2. Interfacial contact area and operational conditions were uniform between column and membrane, enabling any disparity in performance to be ascribed to the impact of membrane resistance. Absorption solvent was stored in an 85 L PVC tank and was pumped counter current to the gas using a peristaltic pump (up 2000mL min^{-1}, 530S, Watson-Marlow Ltd, Falmouth, UK). Physical absorption was evaluated using 15.0 MΩ cm^{-1} de-ionised water, and for chemical absorption, a chemically reactive absorbent was developed using 3.3 mol L^{-1} NH_3 solution (Fisher Chemicals, Loughborough, UK). Absorbent was applied from the top of the absorption column, and flowed counter-current to the gas phase. All experiments were undertaken in a temperature-controlled environment (20°C). Synthetic biogas, comprising a 0.5 BarG, 50/50 CH_4/CO_2 mixture, was prepared in-line by mixing carbon dioxide (CO_2, 99.7%) and methane (CH_4, 99.995%) (BOC gases, Ipswich, UK) using mass flow controllers (0.01 - 5.0 L min^{-1}, Roxspur Measurement and Control Ltd., Sheffield, UK) to provide combined flow rates between 0.05 and 4 L min^{-1}.

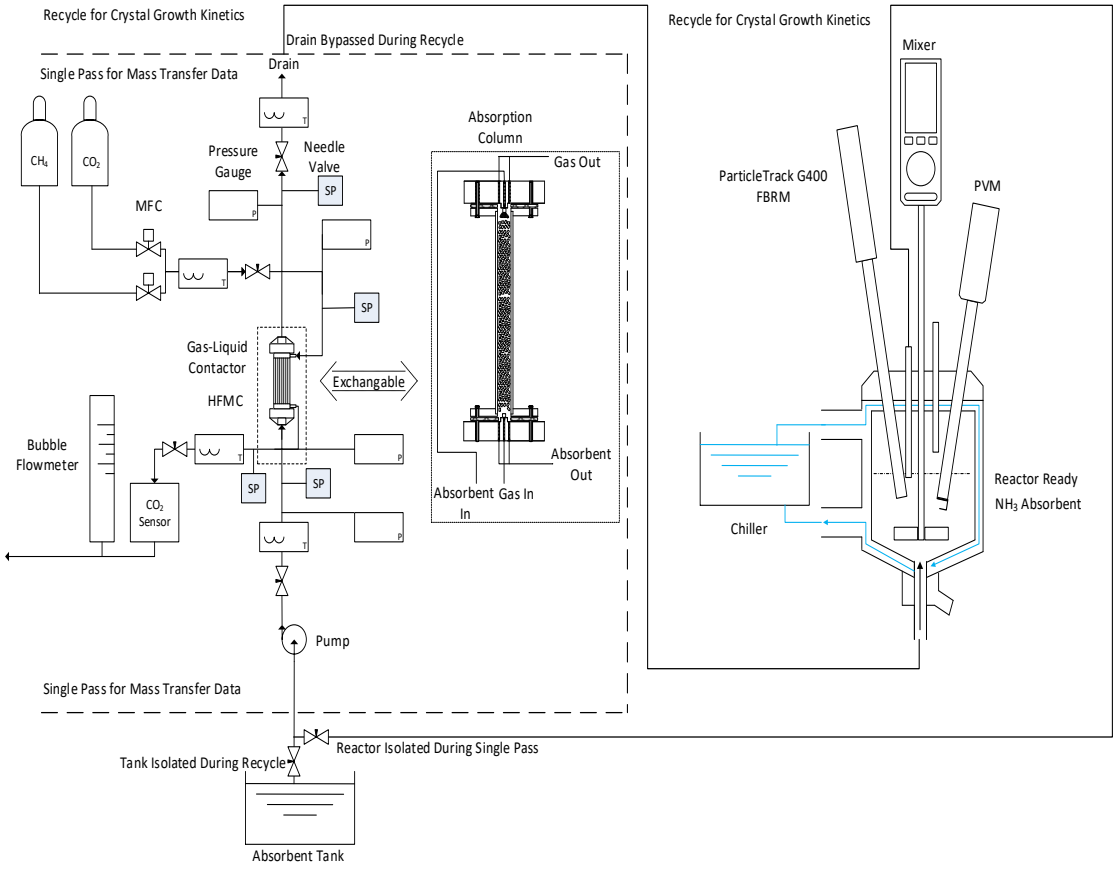

Figure 5.1 Schematic of experimental set up for the determination of CO_2 capture, K_{OV} and E under differing L/G set points, in addition to log G in dispersive (absorption column) and non-dispersive (HFMC) gas-liquid contacting technologies.

However, crystallisation must be undertaken shell side to prevent lumen blocking [15,23]. Ammonium bicarbonate crystallisation was therefore undertaken shell-side in a transverse flow module which exploits a central baffle to overcome maldistribution experienced in the parallel flow module and is representative of the internal architecture of industrial modules [27]. The supersaturation ratio of carbon dioxide (C/C*), defined as the ratio between the CO_2 absorbed in solution and the CO_2 required to form ammonium bicarbonate at the solubility limit was varied in both the transverse flow module and absorption column to assess crystallisation. $Q_{G,in}$ and absorbent flow rate ($Q_{L,in}$) were fixed at 2 L min^{-1} respectively during HFMC operation, with $Q_{L,in}$ operated as recycling batch flow, whilst $Q_{G,in}$ and Q_{Lin} were fixed at 2 L min^{-1} and 0.7 L min^{-1} respectively during column operation due to column hold up at higher $Q_{L,in}$. The ammonia absorbent volume was 0.6L for both column and HFMC. Absorbent temperature was maintained with a circulating chiller (R1 series, Grant Instruments Ltd., Cambridge, UK) at an average of 4.9°C (σ = 1.4) during HFMC operation but 6°C (σ = 1.45) during column operation due

to increased process volume and heat gain. The gas-phase inlet temperature was 20°C, gas and liquid phase temperatures were measured during operation (K-type thermocouples, Thermosense Ltd., Bucks, UK). Absorbent pH was 13 (10°C) for both column and HFMC and monitored using a Jenway epoxy bodied pH electrode (Jenway 4330, Cole-Parmer, Stone, UK). Bicarbonate concentration in solution was determined by UV absorbance at 215 nm (Jenway 6715, Cole-Parmer, Stone, UK), corresponding to the absorption region for bicarbonate [15,27].

5.2.2 Analysis

Mettler-Toledo Focused Beam Reflectance Measurement (FBRM®) G400 and ParticleView (V19®) with PVM (Particle Vision and Measurement) probes provide determination of crystallisation in-situ and in real time (Figure 5.1). FBRM detection of nucleation represents an approximation as crystal nuclei must reach a detectable size and number [28]. The FBRM employs a laser beam, rotated with high speed optics set at 2m s^{-1}, to scan a circular path in the flow, with particles measured via diffuse backscattered light at a rate of five measurements per second, to provide a robust particle chord length distribution (CLD) measurement at a measurement frequency of 15 s. Two particle detection settings were employed, fine (Primary), which yields an enhanced sensitivity to fine particles and coarse (Macro), with a higher sensitivity to large particles. Stuck particle correction was employed to mitigate background noise due to sensitivity to impeller agitation, yielding a background count of from 0-0.05 counts s^{-1}. Crystal size measurements at increasing levels of supersaturation were based on an average of the Macro (number weighted) and Primary (number weighted) CLD, to ensure coverage from small nucleating crystals through to larger crystals. The CLD was determined with iC FBRM® software using a window size of 10 sample smoothing correspond to a 50 bins number for a range of 1-100 microns with logarithmic regulation spacing applied. The ParticleView V19 immersion probe-based video microscope utilises reflected light illumination to collect high-resolution images of liquid suspensions under harsh conditions with respect to temperature and pressure with a field of view 1300 µm x 890 µm (± 50 µm).

Gas flow rate was measured by means of a bubble flow meter (up to 300 mL min^{-1}, 50 mL, error ±2%, Restek, Bellefonte, USA; from 300-3000 mL min^{-1}, 1000 mL, Model 311, error ±2%, Blandford Forum, UK) and gas composition determined using an in-line infrared CO_2 analyser (BCP-CO_2, accuracy <0.5% full-scale, Bluesens gas sensor GmbH, Herten, Germany). A gas phase mass-balance was completed according to [29]:

$$\eta = \frac{[(Q_{G,in} \times C_{G,in}) - (Q_{G,out} \times C_{G,out})]}{(Q_{G,in} \times C_{G,in})} \quad \text{(Equation 5.1)}$$

where η is the dimensionless CO_2 capture ratio, $Q_{G,in}$ and $Q_{G,out}$ are inlet and outlet gas flow rates respectively ($m^3\ s^{-1}$), and $C_{G,in}$ and $C_{G,out}$ are inlet and outlet gas phase concentrations respectively (mol m^{-3}). Carbon dioxide flux (J_{CO2}, mol $m^{-2}\ s^{-1}$) was calculated using:

$$J_{CO2} = \frac{[(Q_{G,in} \times C_{G,in}) - (Q_{G,out} \times C_{G,out})] \times 273.15 \times 1000}{(22.4 \times A_m \times T_G)} \quad \text{(Equation 5.2)}$$

Where A_m refers to available membrane surface area for absorption (m^2) and T_G is gas temperature (K)[30]. Chemical enhancement of J_{CO2} was characterised using the 'enhancement factor' (E) [31] :

$$E = \frac{J_{CO2}(chemical)}{J_{CO2}(physical)} \quad \text{(Equation 5.3)}$$

The CO_2 absorption rate and the enhancement factor are dependent on reaction and diffusion rates in the liquid film, often expressed as the Hatta number, the ratio of maximum reactive conversion rate to the maximum diffusion mass transfer rate is defined as [32]:

$$Ha = \frac{\sqrt{k_{2,NH3} D_{CO2,L} C_{NH3}}}{k_{L,ext}} \quad \text{(Equation 5.4)}$$

where $k_{2,NH3}$ ($m^3\ kmol^{-1}\ s^{-1}$) is the second-order reaction rate constant as taken from Liu et al. [33], and C_{NH3} is the NH_3 concentration (kmol m^{-3}). $k_{L,ext}$ (m s^{-1}) is the liquid phase mass transfer coefficient, which during liquid phase control, a non-wetted membrane and the presence of 100% CO_2 is equivalent to the overall mass transfer coefficient, K_{OV} (m s^{-1}) [32], and experimentally measured as [29,34]:

$$\eta = 1 - exp\left(\frac{-K_{OV} aL}{V_G}\right) \quad \text{(Equation 5.5)}$$

where V_G, L and a are the superficial gas velocity (m s^{-1}), fibre length (m) and interfacial area ($m^2\ m^{-3}$) respectively. Crystal nucleation kinetics (Equation 5.7) and growth (Equation 5.6) in a supersaturated solution for both dispersive and non-dispersive contacting was undertaken according to the methodology proposed by Chen et al. [35]:

$$G = K_G (c_{fm} - c^*)^g \quad \text{(Equation 5.6)}$$

$$B = K_B G^b$$ (Equation 5.7)

Where K_G is the kinetic rate constant for crystal growth ($kg^{-g}\ m^{3g+1}\ s^{-1}$), K_B the nucleation rate constant (No $m^{-3-b}\ s^{-1+b}$), and *g* and *b* exponent constants. The parameters c_{fm} and c^* (kg m^{-3}) represent the CO_2 (aq) concentrations adjacent to the membrane surface and the equilibrium-saturated concentration at the membrane wall temperature T_{fm}. Defining the crystal growth rate as the size variation from *L* (m) at time *t* to $L+\Delta L$ at $t+\Delta t$, allows the average crystal growth rate G, over Δt (s), to be calculated through the linear equation [37]:

$$G(L,t) = \Delta L/\Delta t$$ (Equation 5.8)

When experimentally determining *G* at different experimental time intervals and converting Equation 5.8 into its logarithmic form:

$$\log G = \log K_G + g \log(c_{fm} - c^*)$$ (Equation 5.9)

The crystal growth rate constant K_G and the exponent *g* can be derived from the intercept and slope of the linear regression respectively.

5.3 Results and discussion

5.3.1 Chemical reactivity is comparable for CO_2 separation with HFMC and column technology

Absorber performance was evaluated applying water as a physical absorbent in counter current operation within a column and HFMC, of 0.5m^2 interfacial area respectively. During HFMC operation, gas flow was passed to the module shell-side. The influence of contacting mechanism on the CO_2 capture (η_{CO2}) attained under variable liquid-to-gas ratios (*L/G*) was assessed at differing gas flow rates by initially fixing Q_G and subsequently varying liquid flow rate for both absorber types (Figure 5.2). A comparable impact of the *L/G*, as indicator of absorbed CO_2 load, is observed as a log-linear relationship with η_{CO2} (Figure 5.2), with both absorbers reaching a target 0.98 η_{CO2} at a *L/G* of 8.2, as demanded as an industrial biomethane standard [10]. Parity is demonstrated across the operational spectrum of both absorber types (Figure 5.2), evidenced from the lower to upper boundary conditions, as limited by gas-phase bubbling into the liquid-phase (HFMC) and entrainment (column) at the lower boundary and maximum mass transfer (HFMC) and flooding at the upper boundary. As consequence of performance parity between the two absorber types, comparable K_{OV} values (Equation

5.5) are expected at identical flow conditions. This corroborates previous literature assertions that intensification factors favouring HFMC over columns [7,8,10,46,47] can be attributed to increased interfacial area.

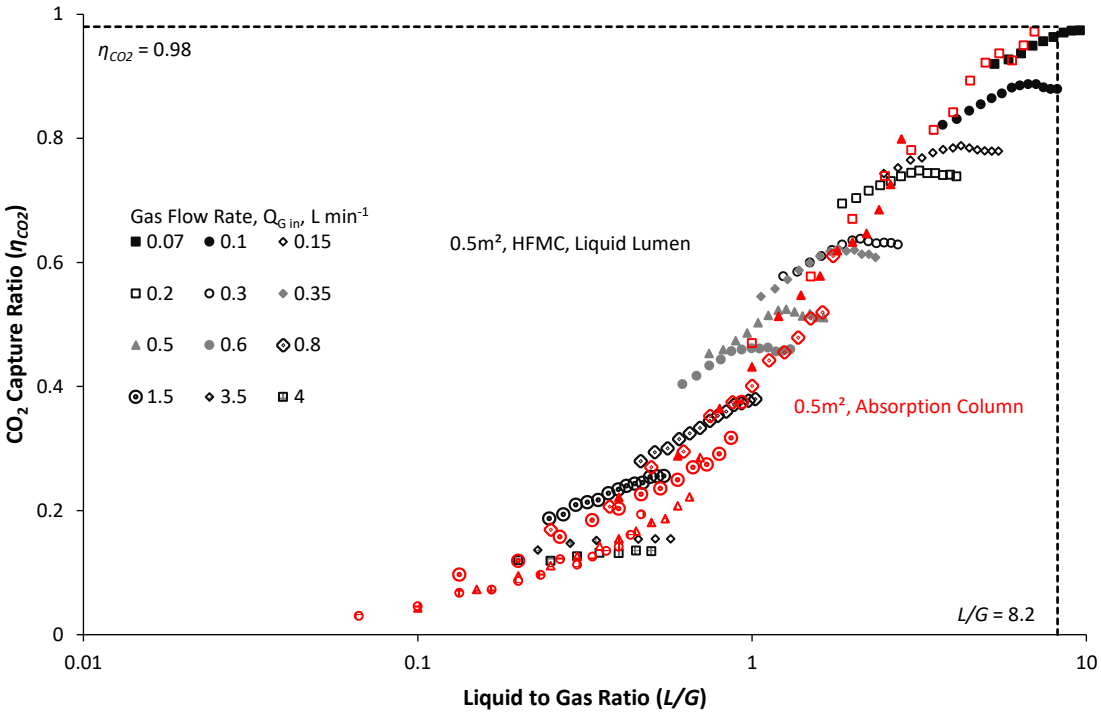

Figure 5.2 The response of the dimensionless capture ratio (η_{CO2}) to hydrodynamic conditions (liquid-to-gas ratio) for physical absorption under dispersive and non-dispersive gas-liquid contacting. Gas inlet, 50/50 CO_2/CH_4 at a P_G of 0.5 BarG with deionised water applied as absorbent (20°C) with Q_G fixed between 0.05 and 4 L m^{-1} and at each Q_G, Q_L was varied between 0.1 and 2 L m^{-1}.

Transition to a CO_2–NH_3–H_2O chemically reactive system (Figure 5.3a) yields comparable performance at *L/G* above 0.1 for both absorber types (Figure 5.3b). CO_2 separation (η_{CO2}) was evaluated using 3.3 mol L^{-1} NH_3 solution to drive a chemical reaction. For comparison, reactive absorption during column contacting (Figure 5.3b) maintains the linear relationship down to an *L/G* of 0.03, the lower boundary condition as dictated by column entrainment at higher gas flow, indicative of a single primary contributor to resistance to mass transfer. However, a log-linear relationship between the *L/G* and η_{CO2} is only partially observed for HFMC operation from an L/G of 0.1 upwards (Figure 5.3a), in contrast to physical absorption (Figure 5.2 and Figure 5.3), indicating more than one contributor to mass transfer resistance.

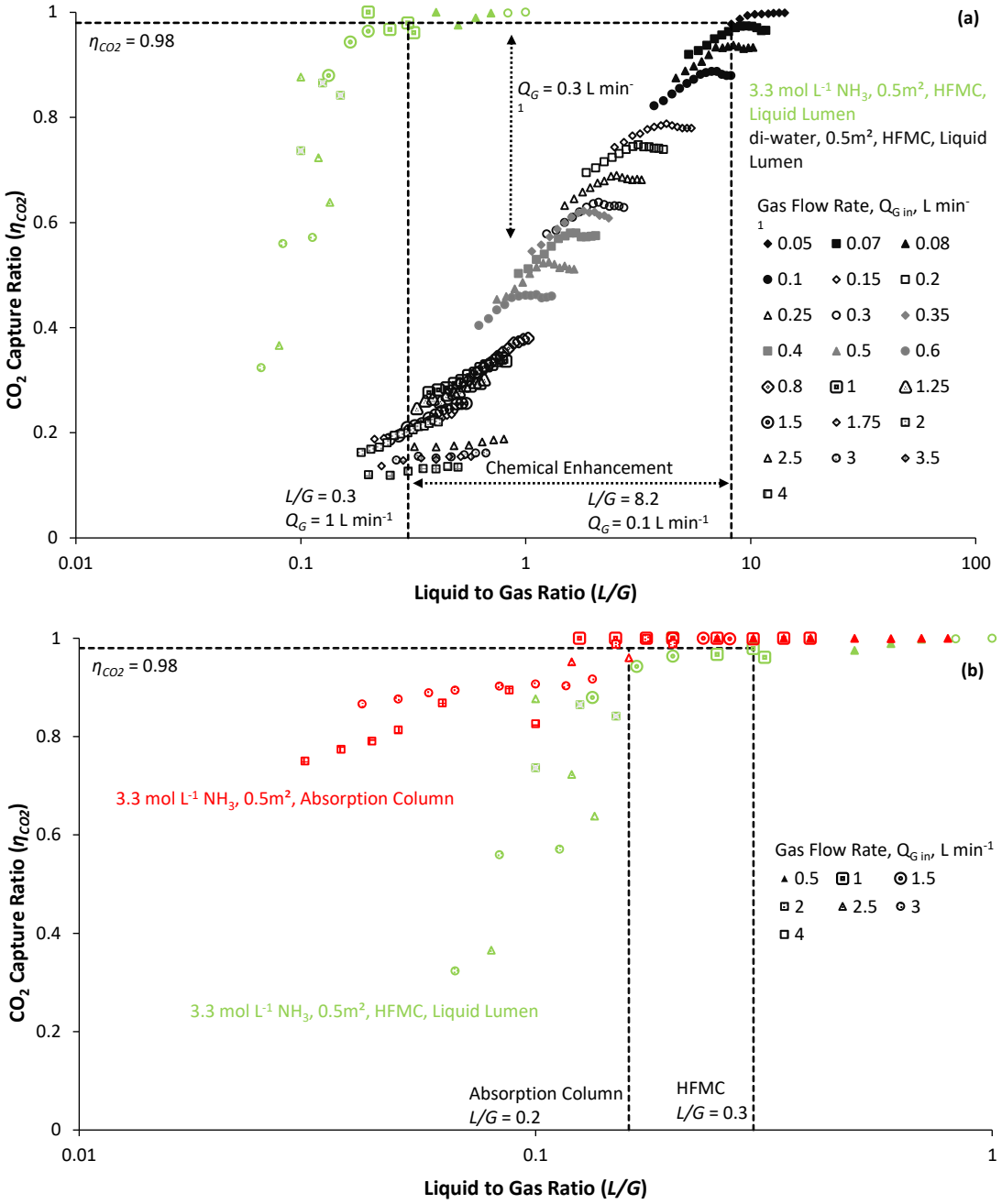

Figure 5.3 The impact of chemical enhancement (3.3 mol L^{-1} NH_3) on the dimensionless capture ratio (η_{CO2}) (a) The liquid to gas ratio needed to achieve a η_{CO2} of 0.98 during non-dispersive (HFMC) gas-liquid absorption (b) The impact of dispersive (absorption column) and non-dispersive (HFMC) contacting. Q_G was fixed between 0.05 and 4 L m^{-1} and at each fixed Q_G liquid flow rate was varied between 0.2 and 0.6 L m^{-1}.

The likely cause of deviation from a linear relationship is increased membrane wetting [16,43], due to ammonia as a low surface tension solution (65.8 mN m^{-1} [48] relative to a surface tension of 72.3 mN m^{-1} for water [49]) reducing breakthrough pressure [44]. This is evidenced by membrane resistance as measured by Wilson Plot

analysis increasing from 120 s m^{-1} at higher *L/G* (0.17 – 1) to 600 s m^{-1} at lower *L/G* (0.07 – 0.17). During HFMC operation, to prevent bubbling of the gas-phase into the absorbent, the absorbent must remain at a higher pressure than the gas-phase, however low enough to prevent pore wetting. As consequence of pressure drop the pressure differential varies with module length and due to counter-current operation, gas and liquid pressure loss is greatest at opposing ends. Lumen-side pressure drop as experienced by the liquid-phase is greater than shell-side pressure drop as experienced by the gas-phase, introducing a pressure differential favouring pore infiltration at the liquid inlet. Wetting is a common issue with HFMC [40–44] and typically mitigated through control of transmembrane pressure during pressure transients [37–39]. The use of composite dense membrane layers have been proposed and demonstrated to eliminate wetting without significant loss of mass transfer [13,45]. The impact of membrane wetting is limited at the *L/G* ratio (0.2 - 0.3) required for a 0.98 η_{CO2}, with both absorbers displaying comparable performance. Chemically reactive absorption reduced the operational *L/G* required to reach η_{CO2} 0.98 from an *L/G* of 8.2 for physical absorption to an *L/G* of 0.3 and increased the gas loading within the example system from a Q_{Gin} of 0.08L min^{-1} for physical absorption to a Q_{Gin} of 1L min^{-1} for reactive absorption, a 12.5-fold increase in treatment capacity.

Intermediary CO_2 diffusion across a membrane barrier (HFMC) introduces an additional resistance to mass transfer relative to direct diffusion into the absorbent (column). During non-wetted operation it is expected to contribute less than 1% of total resistance to mass transfer [50]. The gas-phase is expected to contribute between 6 and 12% of overall resistance to mass transfer [50,51], whilst not representing the dominant phase, reduced CO_2 partial pressure (0.02) achieved at low gas velocities when producing a high purity gas product (>98% CH_4) [52,53] limits CO_2 flux [54] and increases the relative contribution of membrane resistance to mass transfer [50]. As example, CO_2 flux reduces from 13 x10^{-4} mol m^2 s^{-1} to 2 x10^{-4} mol m^2 s^{-1} when decreasing Q_G from 3 to 0.3 L min^{-1}. A reduced CO_2 flux can be expected to limit the enhancement to mass transfer attained through chemically reactive absorption [54].

Enhancement of mass transfer (Equations 5.2 & 5.3) through chemical reaction was determined for both configurations and compared through application of the Hatta number (Figure 5.4, inset) to describe the impact of reducing CO_2 flux at lower gas velocity (high product purity) on the reactive conversion rate.

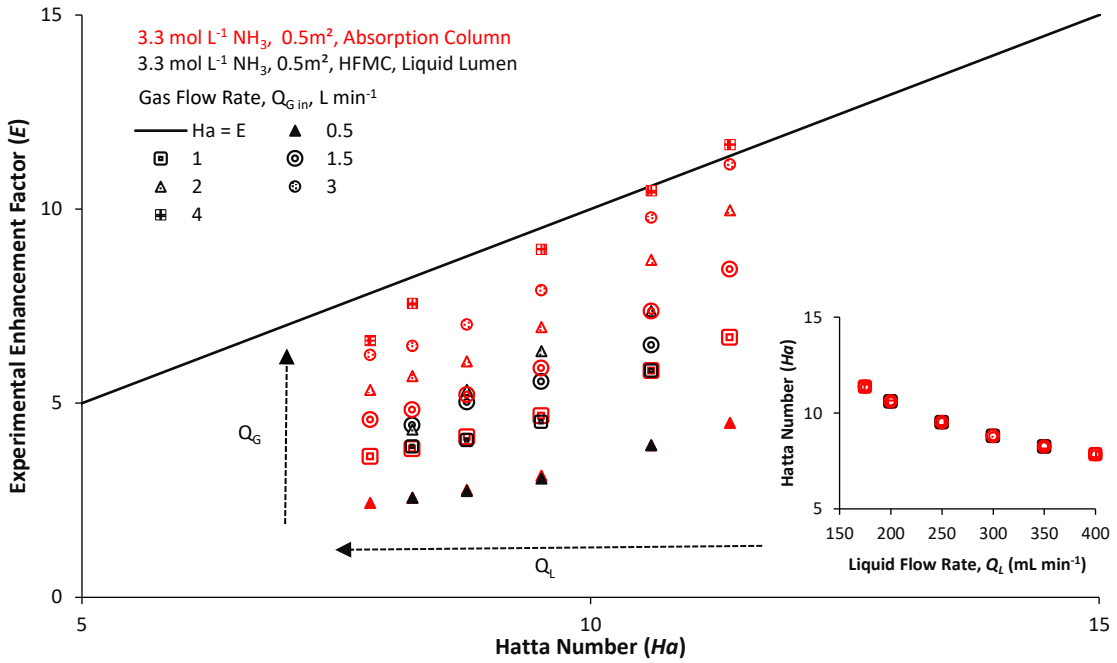

Figure 5.4 The impact of chemically enhanced absorption described by an approximate solution to mass transfer enhancement (*E*) where the enhancement factor is equal to the modified Hatta number (*Ha*), comparing response during dispersive and non-dispersive gas-liquid contacting. The inlet gas is 50/50 CO_2/CH_4 at a P_G of 0.5 BarG (20°C) with 3.3 ml L^{-1} NH_3 applied as absorbent in single pass with Q_L fixed between 0.15 and 0.4 L m^{-1}, at each fixed Q_L, Q_G was varied between 0.5 and 4 L m^{-1}. Inset is the response of *Ha* to increasing Q_L for both absorbers, the inlet gas is 100% CO_2 at a Q_G of 1.2 L min^{-1}.

The Hatta number (*Ha*) as the ratio of maximum reactive conversion rate to the maximum diffusion mass transfer rate, and enhancement factor (*E*) are expected to display parity at *Ha* >3 [55,56] (Figure 5.4). This relationship is borne out across both absorber types at a Q_{Gin} of 4 L min^{-1} displaying parity between *Ha* and *E*, however this corresponds to a η_{CO2} of 0.79. To achieve a η_{CO2} of 0.98 required for biogas upgrading, a Q_G of 1 L min^{-1} is needed, the expected *Ha* and *E* parity is no longer observed. As example, at a *Ha* of 9.5 the corresponding *E* is 5.9, 62% of expected. Disparity between *Ha* and experimental *E* (Figure 5.4) at reducing Q_G is therefore attributed to the observed high (>0.98) η_{CO2} (Figure 5.3) and reduction in CO_2 flux. However, a corresponding reduction in *E* at comparable *Ha* is evident in both absorber types (Figure 5.4) for Q_G of 0.5 – 1.5 L min^{-1}. Membrane wetting occurred at higher Q_G due to the induction of gas phase bubbling and subsequent pressure transient during compensation of the liquid-phase pressure. This indicates the system to be influenced by absorbent choice and not the dispersive or non-dispersive contacting mechanism, as corroborated in the literature by the wide spread use of Hatta number estimations of mass transfer enhancement in both absorption columns [52,57] and HFMC modelling studies [10,58,59].

The transverse flow HFMC ordinarily applied in industry, use liquid on the shell-side to reduce pressure drop [26]. In this study, the 0.5m^2 parallel flow HFMC modules passed liquid through the lumen which may have exacerbated 'wetting' due to the raised pressure. Furthermore, the housing was constructed of polycarbonate, which is not compatible with aqueous ammonia. Consequently, for the assessment of crystallisation, transverse flow modules with a surface area of 1.2m^2 were used. Relative performance (Figure 5.5) of 1.2m^2 shell-side NH_3 > 0.5m^2 lumen-side NH_3 > 0.5m^2 shell-side is in-line with previous literature of enhanced mass transfer at scale, particularly in the presence of enhanced liquid phase distribution during transverse flow [26].

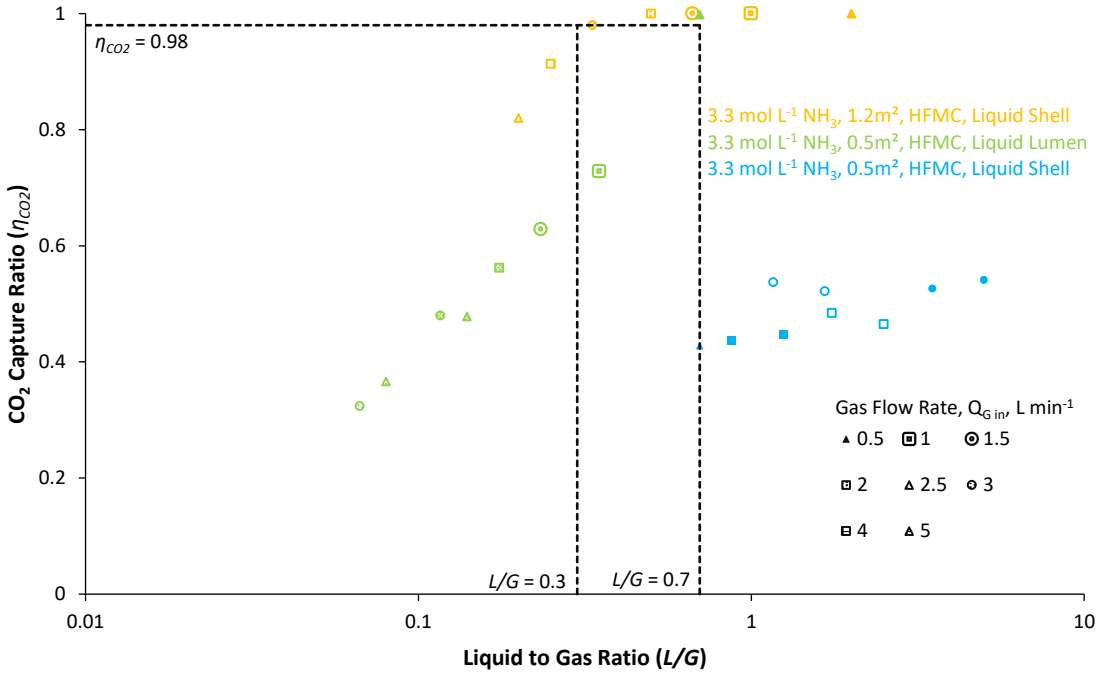

Figure 5.5 The impact of lumen-side liquid flow, in-parallel liquid shell-side flow and transverse shell-side liquid flow and contact area (0.5 or 1.2 m^2) under chemical enhancement (3.3 mol L^{-1} NH_3) on the liquid to gas ratio needed to achieve a η_{CO2} of 0.98 during wetted non-dispersive gas-liquid absorption. Absorbent was applied in single pass and Q_L was fixed between 0.2 and 1 L m^{-1}, at each fixed Q_L gas flow rate was varied between 0.1 and 5 L m^{-1} with the inlet gas as 50/50 CO_2/CH_4 at a P_G of 0.5 BarG (20°C).

5.3.2 Lower nucleation rates in HFMC sustain CO_2 separation during crystal growth

Integration of the CO_2–NH_3–H_2O system within HFMC as CR-MCr for the precipitation of NH_4HCO_3 from ammonia solution was previously demonstrated by Mcleod et al.[23] and Bavarella [15], the studies focused on the nucleation kinetics at the local gas-liquid interfacial contact zone of the shell-side micropore entrance and within a stirred

dispersive batch reaction volume [15,23]. The studies note that the disconnection of nucleation from growth in the membrane system is expected to limit intra-fibre clogging by limiting crystal size. This assertion is borne out by this study with crystal growth kinetics measured during batch operation of both absorber types (Table 5.1). FBRM derived chord length distributions at increasing supersaturation levels for column contacting (Figure 5.6a) and HFMC contacting (Figure 5.6b) were evaluated utilising the primary setting to detect small particulates, corresponding to crystal nucleation and macro for larger particle growth and agglomeration.

Table 5.1 Ammonium bicarbonate reaction efficiency, kinetics and crystal growth rates for dispersive and non-dispersive gas-liquid contacting

Contacting Technology	Absorption Fluid pH	Initial Ammonium Concentration (mol L^{-1})	Final Ammonium Concentration (mol L^{-1})	Reaction Efficiency (%)	Kinetic Rate Constant, Log K*G*	Maximum Grow Rate, *G* (m s^{-1})	Exponent, g
HFMC	13	3.32	2.34	41.8	50.1	3.2 x10^{-9}	-44.3
Column	13	3.32	2.54	30	60.9	6.1 x10^{-9}	-45.3

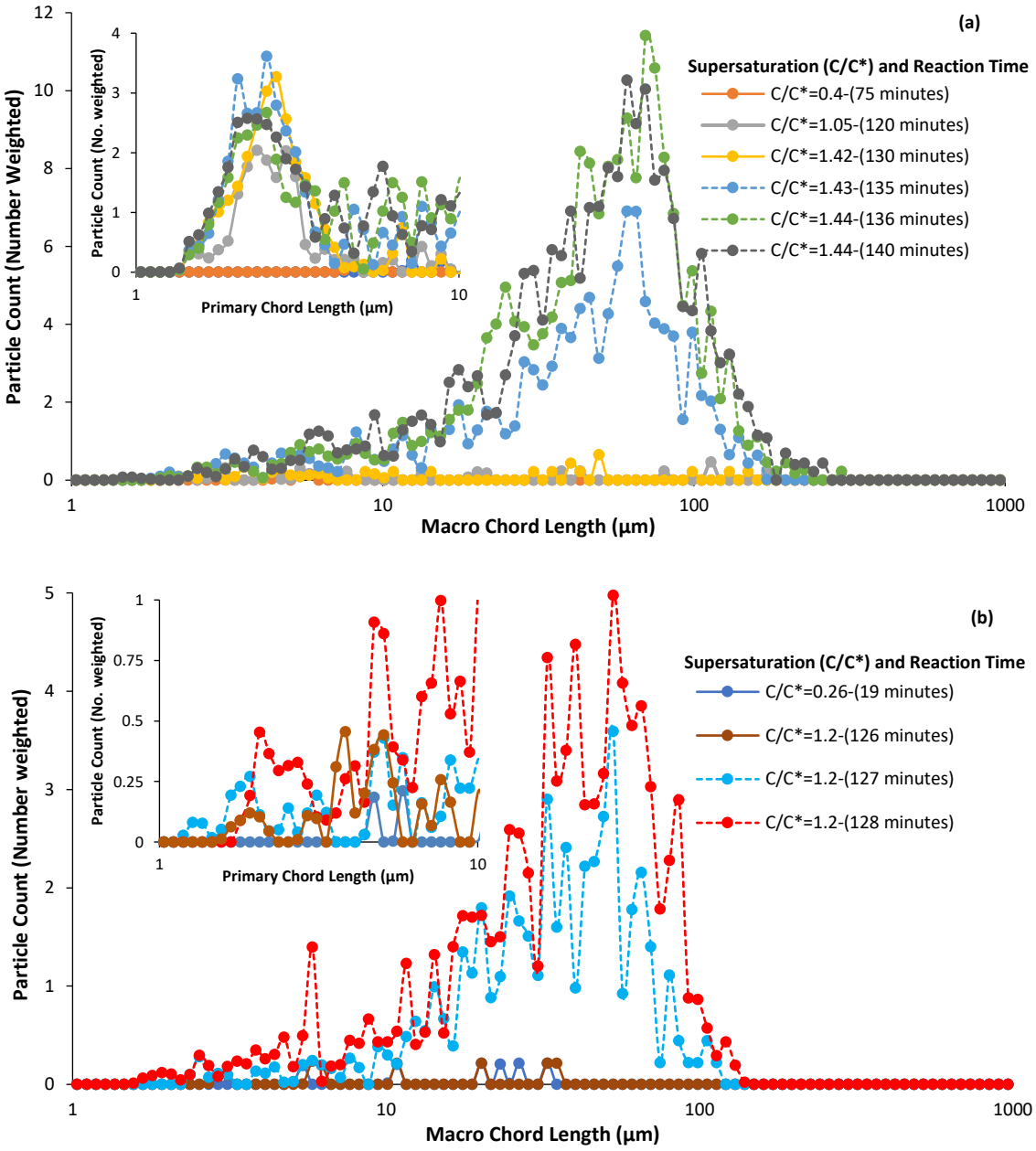

Figure 5.6 Chord length distribution as measured by FBRM for dispersive and non-dispersive chemically reactive crystallisation reactors during supersaturation. (a) Absorption column, inset is primary chord length (b) HFMC, inset is primary chord length. The inlet gas was 50/50 CO_2/CH_4 at a P_G of 0.5 BarG (20°C) and Q_G of 2 L min^{-1} whilst the 3.3M NH_3 reaction volume was a chilled (5°C) 0.6L with a Q_L of 1 L min^{-1} and 0.7 L min^{-1} during HFMC and column operation respectively, limited by column flooding.

HFMC contacting does not evidence an elevated particle count expected of newly nucleated crystals in the sub 10µm region (Figure 5.6b, inset) around the C/C* = 1 expected to initiate crystallisation [15,60]. A subsequent increase in particle count within the 10-100 µm range at a C/C* of 1.2 and above (Figure 5.6b) is however evidenced. This contrasts with dispersive column contacting (Figure 5.6a, inset) which evidences

both sub 10 µm and post 10 µm CLD particle count increase after a C/C* 1.05 reaction initiation point, indicating concurrent nucleation and growth within the system. This intimates that the increased interfacial area offered by a fibre bundle relative to a single fibre and development of a concentration boundary layer may slow reaction development. The comparatively slower rate of supersaturation as the reaction slows on bulk ammonia consumption limits the nucleation rate, and instead favours growth of fewer, larger crystals [15]. This is evidenced by the decrease in number weight particle count and mean weight particle size at reaction end time, C/C* = 1.2 for HFMC and C/C* = 1.44 for column (Figure 5.6a&b). During column operation, mean weight particle size reached 58 µm and weighted count of 12 whereas during membrane operation, mean weight particle size reached 40 µm and a weighted count of 5. This corresponds to a 2.6-fold reduction in nucleation rate based on particle count in HFMC relative to the absorption column, when considering a specific nucleation rate per unit area the increase in interfacial area, 0.5m^2 for the absorption column to 1.2 m^2 for the HFMC, reduces nucleation rate by a further factor of 2.2. The crystal growth rate constant K_G, of $5.7x10^{21}$ kg^{-g} m^{3g+1} s^{-1}, maximum growth rate of 3.2 $x10^{-9}$ m s^{-1}, and exponent *g*, of -45.3 (Table 5.1) during HFMC operation indicate a crystal growth rate slower than the K_G, $2.8x10^{26}$ kg^{-g} m^{3g+1} s^{-1}, maximum growth rate of 6.1 $x10^{-9}$ m s^{-1} and decreased exponent *g*, of -45.3 (Table 5.1) for column operation. Whilst the specific nucleation rate is reduced 4.8-fold during HFMC crystallisation, the crystal growth rate is only reduced by a factor of 2.

Bavarella [15], demonstrates a nucleation rate five orders of magnitude greater during contacting in a stirred batch reaction relative to membrane assisted contacting. Primarily laminar flow conditions at a membrane surface favours heterogenous nucleation with secondary nucleation and growth downstream in the bulk solution, whereas turbulent flow during the stirred reaction favours homogenous nucleation and growth in the same system [15]. The difference in nucleation rate is attributed to the stochastic nature of homogenous nucleation in a bulk solution relative to heterogenous nucleation with a constrained number of nucleating loci (micropores) available during membrane assisted contacting [15]. This is corroborated in the literature by the suspected crystallisation mechanism, where the membrane material itself acts as a substrate for nucleation [15,23], the local conditions of supersaturation at the micropore gas-liquid interface induce nucleation, limited growth occurs until enough shear is induced to initiate crystal detachment [15,23].

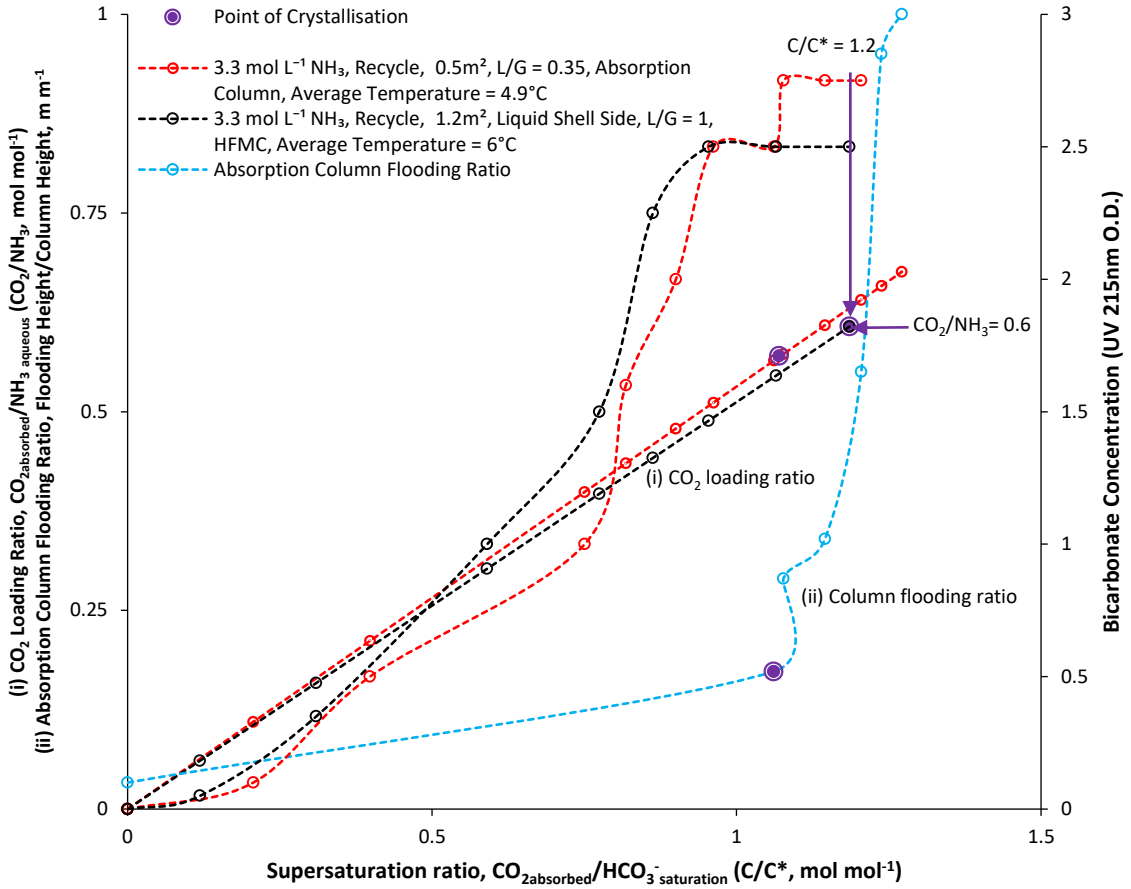

Figure 5.7 The impact of dispersive and non-dispersive gas-liquid contacting on NH_4HCO_3 crystallisation under conditions of supersaturation in a chilled (5°C) 0.6L, 3.3 mol L^{-1} NH_3 reaction solution (i) CO_2 loading ratio, bicarbonate concentration at supersaturation and observed point of crystallisation with FBRM (ii) the effect of supersaturation on column flooding. Inlet gas is 50/50 CO_2/CH_4 at a P_G of 0.5 BarG (20°C), gas flow rate (Q_G) was fixed at 2 L min^{-1} and liquid flow rate (Q_L) was fixed in recycle at 2 L min^{-1} in the membrane and 0.7 L min^{-1} in the absorption column.

The increased nucleation rate in the gas-liquid column resulted in the agglomeration of crystalline reaction product (Figure 5.8c&d) and detrimental precipitation with the absorber packing material (Figure 5.9) leading to column flooding (Figure 5.7). This is evidenced by the detection of primary nucleation within the reaction volume (Figure 5.6a, inset) at a C/C* of 1.05 which corresponds with the initiation of column flooding (Figure 5.7) at a C/C* of 1.06, indicating that column blockage precedes crystal growth. Further rapid growth and formation of aggregates of the entrained crystals consequently accounts for the rapid process blockage by a C/C* of 1.27 (Figure 5.7), close to the C/C* of 1.2 at which crystallisation is detected within the HFMC system (Figure 5.6). Agglomeration is evidenced by PVM imaging (Figure 5.8c&d). In contrast during HFMC crystallisation, the observed particle size (40 µm) is smaller than the

interstitial fibre spacing (180µm [61]) present in the fibre bundle, indicating that process blockage is unlikely to occur. This is further evidenced by the preference for single crystal growth in HFMC visualised using PVM (Figure 5.8a&b). The reduction in specific nucleation rate and preferential crystal growth in HFMC therefore protects the system from blocking by the reaction product. In contrast the high specific nucleation rate and subsequent agglomeration of the reaction product induces process blocking during column operation.

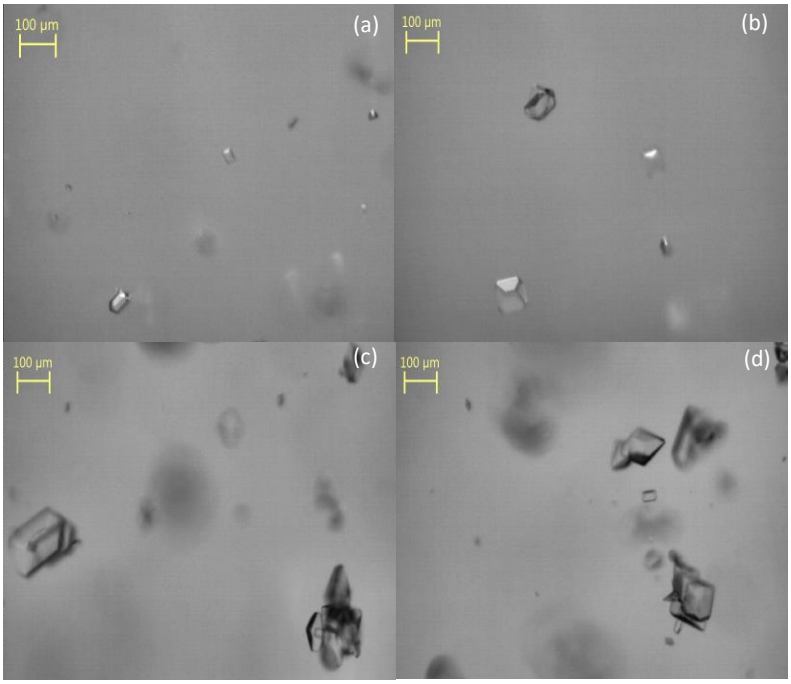

Figure 5.8 Crystal formation and aggregation as photographed in the reactor volume by insitu particle view microscopy (PVM) at reaction end point during HFMC crystallisation (a,b) and absorption column crystallisation (c,d) (a) C/C*= 1.2 (127 minutes) (b) C/C*= 1.2 (130 minutes) (c) C/C*= 1.44 (137 minutes) (d) C/C*= 1.44 (140 minutes)

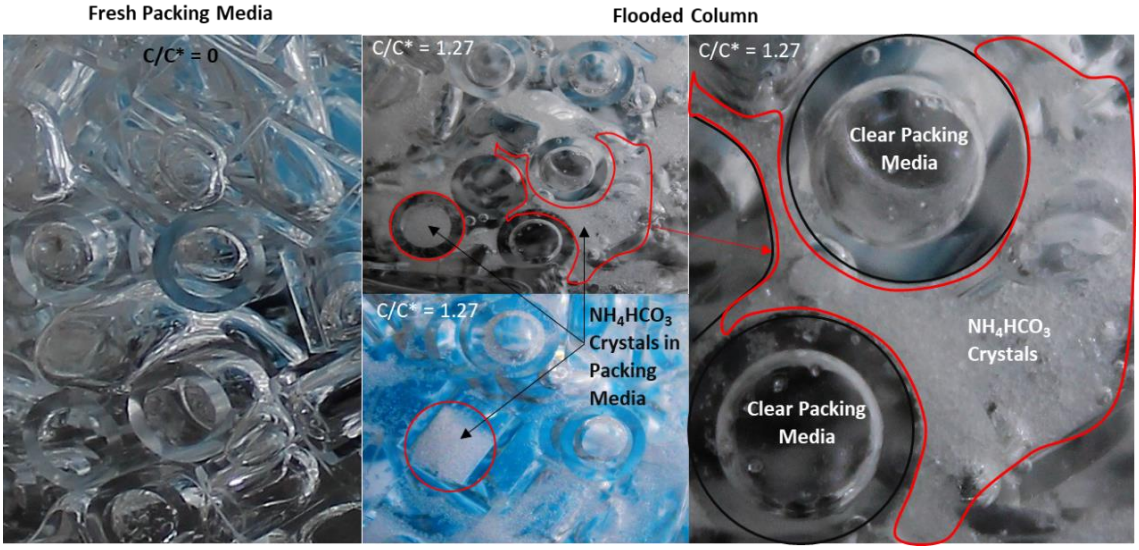

Figure 5.9 NH_4HCO_3 visible as a white precipitate in absorption column packing media (5mm glass Raschig rings) at a C/C* of 1.27. The left-hand panel shows fresh media at experimental initiation (flooding ratio = 0.03) and the three right hand panels show precipitate at a C/C* of 1.27 (flooding ratio = 1), the blue colour is caused by the gas diffusor.

A further consideration is reaction yield, at 5°C, a 3.3 mol L^{-1} NH_3 absorbent at pH 13 has an ammonium bicarbonate solubility limit of 1.7 mol kg^{-1} [28], enabling a maximum reaction yield of 48.5%. The obtained reaction yield of 41.8% (Table 5.1) by the HFMC represents an 87% yield relative to the solubility limit of ammonium bicarbonate, a significant increase over the 1.9% previously attained by Bavarella [15] employing 3.3 mol L^{-1} NH_3 at a pH of 10, where the reduced pH limited the relative abundance of HCO_3^- in favour of H_2CO^3. The increase in yield is attributed to both increased pH and subsequent elimination of bicarbonate transition into carbonic acid and the increased interfacial area of a multi-fibre bundle and hence nucleation rate relative to the single fibre of the Bavarella [15] study. Bavarella [15] further reports increased ammonia slip during dispersive gas-liquid contacting (non-membrane) which contributes to a reduction in reaction yield relative to HFMC, this is corroborated by this study (Table 5.1) which evidenced a 30% (63% of solubility limit) reaction yield during dispersive contacting within an absorption column. This is compounded by the occurrence of process flooding (Figure 5.7) reducing the available interfacial area in which additional CO_2 could be absorbed into the system (Table 5.1). Column blockage is readily noted in the literature [18,19] and research undertaken to limit ammonium salt precipitates [20–22], however should the technology be applied as a crystallising reactor, the formation of process blocking precipitates at a low C/C* and immediate column flooding will limit attainable K_{OV} values at the point of product formation, as such a separate crystallising

reactor would be required to ensure process size and hence cost does not increase to compensate for the loss of function. Ammonia slip, reaction yield reduction and process blocking therefore limit the potential for current generation absorption columns at WWTW in operating as crystallising reactors.

5.3.3 In-series HFMC can achieve simultaneous gas separation and crystallisation

To take advantage of greater reaction yield and lack of process blocking available through HFMC, a design for a biogas upgrading-CR-MCr process based on a crystallising-purity membrane cascade for in-series gas-phase contacting is demonstrated (Figure 5.10). To facilitate crystallisation, the ammonia absorbent requires a CO_2/NH_3 loading ratio of 0.6 and a recycling batch volume to selectively control crystallisation on the shell-side, under these conditions the reactivity of the absorbent is diminished resulting in minimal CO_2 transport from the gas. A second absorber is required to ensure adequate gas quality. The crystallising membrane exploits the elevated CO_2 partial pressure present in untreated biogas to maintain higher rates of mass transfer whilst an independent recycling absorbent reservoir (0.6L) ensures the 0.6 CO_2/NH_3 loading ratio required for precipitation (Figure 5.7) can be quickly met. The purity membrane employs a second larger recycling absorbent reservoir (2L) to ensure a low CO_2/NH_3 loading ratio to maintain a concentration gradient against the reduced CO_2 partial pressure in the partially treated biogas (Figure 5.10) without losing absorbed CO_2. Once crystallisation is initiated, careful control of the crystallising reaction volume at a 0.6 CO_2/NH_3 loading ratio through in-line UV_{215} absorbance and continued feed of partially saturated absorbent from the purity module would facilitate process control [15]. To demonstrate the co-production of high purity CH_4 and NH_4HCO_3 within an HFMC cascade, two chilled ammonia batches (5°C) were applied to the shell-side of two separate 1.2m^2 HFMC, creating two independent ammonia reservoirs. The inlet gas flow was passed sequentially from the upfront crystallising HFMC to a secondary gas purity module with an integrated gas-phase CO_2 mass balance completed over reaction time, and bicarbonate concentration (UV_{215nm}) measured at each supersaturation point (Figure 5.10) for the crystallising module and the crystallising-purity module cascade.

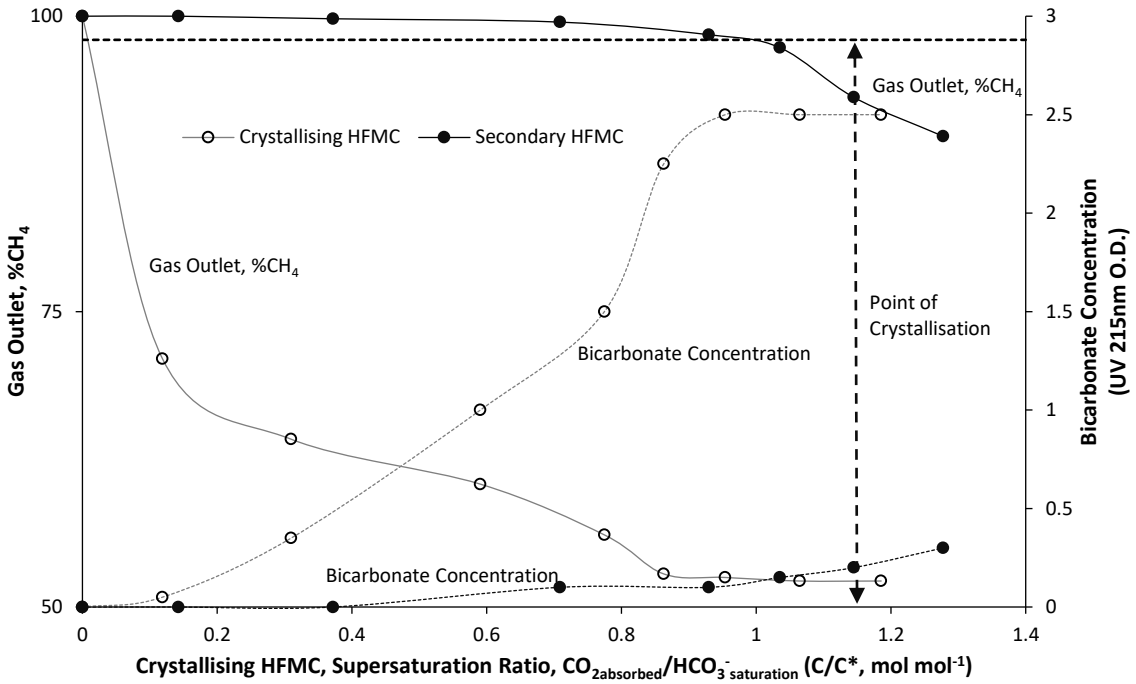

Figure 5.10 Co-production of ammonium bicarbonate and high purity (≥98%) CH_4. Two in-series 1.2 m^2 HFMCs operated liquid shell-side under conditions of independent absorbent recycle with gas flow passed successively between modules. The crystallising HFMC had an ammonia recycle volume of 0.6L whilst the secondary HFMC had an ammonia recycle volume of 4L. Inlet gas was 50/50 CO_2/CH_4 at a P_G of 0.5 BarG (20°C) with 3.3 mol L^{-1} NH_3 used as absorbent (5°C). Gas flow rate (Q_G) was fixed at 2 L min^{-1}. Liquid flow rate (Q_L) was fixed in recycle at 2 L min^{-1}.

As a function of the supersaturation ratio (C/C*) and CO_2 loading ratio (CO_2/NH_3), the point of crystallisation measured through FBRM is C/C* = 1.18, CO_2/NH_3 = 0.61 and C/C* = 1.05, CO_2/NH_3 = 0.64 for HFMC and column contacting respectively, coincident with a maximum absorbance reading of 2.5 to 2.75 (Figure 5.7). As per the outcome of Bavarella [15] and this study (Figure 5.7) the UV_{215} absorbance was used as a surrogate for assessing crystal nucleation at supersaturation. The concurrence of 98% CH_4 and a maximum absorbance reading at a C/C* of 1 indicative of the co-production of high purity CH_4 and precipitation of NH_4HCO_3 is indicated in Figure 5.10. However, at the observed point of crystallisation, C/C* = 1.2 (Figure 5.6b) the outlet gas purity was measured at 95% CH_4. An increased ammonia volume of the purity module is required to decrease the CO_2/NH_3 loading and maintain a higher gas purity (≥98% CH_4). This process has demonstrated chemical reduction of the nitrogen load of the solution through an 87% reaction yield, upgrading of biogas and process intensification through chemical enhancement, representing a viable process for cost reduction and increase in resource recovery if applied at a WWTW.

5.4 Conclusions

In this study, the reduction in specific nucleation rate and preferential crystal growth in HFMC protects the system from blocking by the reaction product, in contrast the high specific nucleation rate and subsequent agglomeration of the reaction product induces process blocking during column operation. Operation of current generation gas-liquid absorption columns as crystallising reactors is limited by the inability to control crystal nucleation and ammonia slip into the gas-phase. As consequence, a design for a biogas upgrading-CR-MCr process based on a crystallising-purity membrane cascade for in-series gas-phase contacting is demonstrated. The process demonstrated an 87% chemical reduction of the nitrogen load, biogas upgrading to industrial standard (≥98% CH_4) and process intensification through chemical enhancement, representing a viable process for cost reduction and increase in resource recovery if applied at a WWTW. Further conclusion that can be drawn from this study are:

- Membrane resistance does not have a significant impact on overall resistance to mass transfer during physical absorption, as consequence intensification factors between HFMC and absorption columns can be ascribed to the increased interfacial area of HFMC relative to absorption columns.
- Chemical enhancement is influenced by absorbent choice and not the dispersive or non-dispersive contacting mechanism.

Acknowledgements

The authors would like to thank Anglian Water, Northumbrian Water and Severn Trent Water for their practical and financial support. We are also grateful for funding from the Engineering and Physical Sciences Research Council (EPSRC) which was provided through the STREAM Industrial Doctorate Centre. Enquiries for access to the data referred to in this article should be directed to: researchdata@ cranfield.ac.uk.

References

[1] A. Mcleod, B. Jefferson, E.J. McAdam, Biogas upgrading by chemical absorption using ammonia rich absorbents derived from wastewater, Water Res. 67 (2014) 175–186.

[2] F. Bauer, T. Persson, C. Hulteberg, D. Tamm, Biogas upgrading - technology overview, comparison and perspectives for the future, Biofuels, Bioprod. Biorefining. 7 (2013) 499–511.

[3] E. Chabanon, E. Kimball, E. Favre, O. Lorain, E. Goetheer, D. Ferre, A. Gomez,

P. Broutin, Hollow Fiber Membrane Contactors for Post-Combustion CO_2 Capture: A Scale-Up Study from Laboratory to Pilot Plant, Oil Gas Sci. Technol. – Rev. d'IFP Energies Nouv. 69 (2014) 1035–1045.

[4] B. Belaissaoui, E. Favre, Novel dense skin hollow fiber membrane contactor based process for CO_2 removal from raw biogas using water as absorbent, Sep. Purif. Technol. 193 (2018) 112–126.

[5] V. Telikapalli, F. Kozak, J.F. Leandri, B. Sherrick, J. Black, D. Muraskin, M. Cage, M. Hammond, G. Spitznogle, CCS with the Alstom Chilled Ammonia Process Development Program - Field Pilot Results, Energy Procedia. 4 (2011) 273–281.

[6] International Energy Association Task 37, IEA Bioenergy Task 37 Upgrading Plant List 2017, (2017). http://task37.ieabioenergy.com/plant-list.html (accessed November 17, 2018).

[7] D. deMontigny, P. Tontiwachwuthikul, A. Chakma, Comparing the Absorption Performance of Packed Columns and Membrane Contactors, Ind. Eng. Chem. Res. 44 (2005) 5726–5732.

[8] B. Belaissaoui, J. Claveria-Baro, A. Lorenzo-Hernando, D. Albarracin, E. Chabanon, C. Castel, S. Rode, D. Roizard, E. Favre, Potentialities of a dense skin hollow fiber membrane contactor for biogas purification by pressurized water absorption, J. Memb. Sci. 513 (2016) 236–249.

[9] S. Heile, S. Rosenberger, A. Parker, B. Jefferson, E.J. McAdam, Establishing the suitability of symmetric ultrathin wall polydimethylsiloxane hollow-fibre membrane contactors for enhanced CO_2 separation during biogas upgrading, J. Memb. Sci. 452 (2014) 37–45.

[10] S. Rode, P.T. Nguyen, D. Roizard, R. Bounaceur, C. Castel, E. Favre, Evaluating the intensification potential of membrane contactors for gas absorption in a chemical solvent: A generic one-dimensional methodology and its application to CO_2 absorption in monoethanolamine, J. Memb. Sci. 389 (2012) 1–16.

[11] F. Bauer, C. Hulteberg, T. Persson, D. Tamm, Biogas upgrading – Review of commercial technologies, 2013. http://www.sgc.se/ckfinder/userfiles/files/SGC270.pdf. (accessed January 10, 2019)

[12] I. Ullah Khan, M. Hafiz Dzarfan Othman, H. Hashim, T. Matsuura, A.F. Ismail, M. Rezaei-DashtArzhandi, I. Wan Azelee, Biogas as a renewable energy fuel – A review of biogas upgrading, utilisation and storage, Energy Convers. Manag. 150 (2017) 277–294.

[13] C. Makhloufi, E. Lasseuguette, J.C. Remigy, B. Belaissaoui, D. Roizard, E. Favre, Ammonia based CO_2 capture process using hollow fiber membrane contactors, J. Memb. Sci. 455 (2014) 236–246.

[14] W.M. Budzianowski, Benefits of biogas upgrading to biomethane by high-pressure reactive solvent scrubbing, Biofuels, Bioprod. Biorefining. 6 (2012) 12–20.

[15] S. Bavarella, Chemically reactive membrane crystallisation reactor for CO_2 separation and ammonia recovery, PhD theis, Cranfield University, 2018.

[16] Z. Cui, D. deMontigny, Experimental study of carbon dioxide absorption into aqueous ammonia with a hollow fiber membrane contactor, J. Memb. Sci. 540 (2017) 297–306.

[17] O. Augustsson, B. Baburao, S. Dube, S. Bedell, P. Strunz, M. Balfe, O. Stallmann, Chilled Ammonia Process Scale-up and Lessons Learned, Energy Procedia. 114 (2017) 5593–5615.

[18] H. Yu, G. Qi, S. Wang, S. Morgan, A. Allport, A. Cottrell, T. Do, J. Mcgregor, L. Wardhaugh, P. Feron, Results from trialling aqueous ammonia-based post-combustion capture in a pilot plant at Munmorah Power Station : Gas purity and solid precipitation in the stripper, Int. J. Greenh. Gas Control. 10 (2012) 15–25.

[19] F. Kozak, A. Petig, E. Morris, R. Rhudy, D. Thimsen, Chilled Ammonia Process for CO_2 Capture, Energy Procedia. 1 (2009) 1419–1426. 1.186.

[20] D. Sutter, M. Gazzani, M. Mazzotti, Formation of solids in ammonia-based CO_2 capture processes — Identification of criticalities through thermodynamic analysis of the CO_2–NH_3–H_2O system, Chem. Eng. Sci. 133 (2015) 170–180.

[21] M. Gazzani, D. Sutter, M.M. Mazzotti, Improving the efficiency of a chilled ammonia CO_2 capture plant through solid formation: A thermodynamic analysis, Energy Procedia. 63 (2014) 1084–1090.

[22] P. Versteeg, E.S. Rubin, A technical and economic assessment of ammonia-based post-combustion CO_2 capture at coal-fired power plants, Int. J. Greenh. Gas Control. 5 (2011) 1596–1605.

[23] A. Mcleod, P. Buzatu, O. Autin, B. Jefferson, E. McAdam, Controlling shell-side crystal nucleation in a gas–liquid membrane contactor for simultaneous ammonium bicarbonate recovery and biogas upgrading, J. Memb. Sci. 473 (2015) 146–156.

[24] W.M. Budzianowski, Mitigating NH_3 vaporization from an aqueous ammonia process for CO_2 capture, Int. J. Chem. React. Eng. 9 (2011) 58–60.

[25] F. Mani, M. Peruzzini, P. Stoppioni, CO_2 absorption by aqueous NH_3 solutions:

speciation of ammonium carbamate, bicarbonate and carbonate by a 13C NMR study, Green Chem. 8 (2006) 995–1000.

[26] A. Sengupta, P.A. Peterson, B.D. Miller, J. Schneider, C.W. Fulk, Large-scale application of membrane contactors for gas transfer from or to ultrapure water, Sep. Purif. Technol. 14 (1998) 189–200.

[27] N.S. Wilson, R. Morrison, J.W. Dolan, Buffers and Baselines. LC-GC Europe. 1, (2001) 1–3.

[28] D. Sutter, M. Mazzotti, Solubility and Growth Kinetics of Ammonium Bicarbonate in Aqueous Solution, Cryst. Growth Des. 17 (2017) 3048–3054.

[29] E. Chabanon, D. Roizard, E. Favre, Modeling strategies of membrane contactors for post-combustion carbon capture: A critical comparative study, Chem. Eng. Sci. 87 (2013) 393–407.

[30] S. Atchariyawut, R. Jiraratananon, R. Wang, Separation of CO_2 from CH_4 by using gas–liquid membrane contacting process, J. Memb. Sci. 304 (2007) 163–172.

[31] V.Y. Dindore, D.W.F. Brilman, G.F. Versteeg, Hollow fiber membrane contactor as a gas–liquid model contactor, Chem. Eng. Sci. 60 (2005) 467–479.

[32] W. Rongwong, S. Assabumrungrat, R. Jiraratananon, Rate based modeling for CO_2 absorption using monoethanolamine solution in a hollow fiber membrane contactor, J. Memb. Sci. 429 (2013) 396–408.

[33] J. Liu, S. Wang, G. Qi, B. Zhao, C. Chen, Kinetics and mass transfer of carbon dioxide absorption into aqueous ammonia, Energy Procedia. 4 (2011) 525–532.

[34] B.W. Reed, M.J. Semmens, E.J. Cussler, Membrane contactors, in: R.D. Nobel, A.S. Stern (Eds.), Membr. Sep. Technol. Princ. Appl., Elsevier, 1995: pp. 467–498.

[35] G. Chen, Y. Lu, X. Yang, R. Wang, A.G. Fane, Quantitative Study on Crystallization-Induced Scaling in High- Concentration Direct-Contact Membrane Distillation, Ind. Eng. Chem. Res. 53 (2014) 15656–15666.

[36] O.S. Söhnel, M. Bravi, A. Chianese, B. Mazzarotta, Growth kinetics of sodium perborate from batch crystallization, 160 (1996) 355–360.

[37] N. Nishikawa, M. Ishibashi, H. Ohta, N. Akutsu, H. Matsumoto, T. Kamata, H. Kitamura, CO_2 removal by hollow-fibre gas-liquid contactor, Energy Convers. Manag. 36 (1995) 415–418.

[38] H.A. Rangwala, Absorption of carbon dioxide into aqueous solutions using hollow fiber membrane contactors, J. Memb. Sci. 112 (1996) 229–240.

[39] J.G. Lu, Y.F. Zheng, M.D. Cheng, Wetting mechanism in mass transfer process

of hydrophobic membrane gas absorption, J. Memb. Sci. 308 (2008) 180–190.

[40] M. Shuangchen, S. Huihui, Z. Bin, C. Gongda, Experimental study on additives inhibiting ammonia escape in carbon capture process using ammonia method, Chem. Eng. Res. Des. 91 (2013) 2775–2781.

[41] A. Mansourizadeh, A.F. Ismail, Hollow fiber gas – liquid membrane contactors for acid gas capture : A review, J. Hazard. Mater. 171 (2009) 38–53.

[42] Y. Lv, X. Yu, S.T. Tu, J. Yan, E. Dahlquist, Wetting of polypropylene hollow fiber membrane contactors, J. Memb. Sci. 362 (2010) 444–452.

[43] V. Fougerit, V. Pozzobon, D. Pareau, M. Théoleyre, M. Stambouli, Gas-liquid absorption in industrial cross-flow membrane contactors : Experimental and numerical investigation of the influence of transmembrane pressure on partial wetting, Chem. Eng. Sci. 170 (2017) 561–573.

[44] M. Mavroudi, S.P. Kaldis, G.P. Sakellaropoulos, A study of mass transfer resistance in membrane gas-liquid contacting processes, J. Memb. Sci. 272 (2006) 103–115.

[45] R. Wang, H.Y. Zhang, P.H.M. Feron, D.T. Liang, Influence of membrane wetting on CO_2 capture in microporous hollow fiber membrane contactors, Sep. Purif. Technol. 46 (2005) 33–40.

[46] C.A. Scholes, A. Qader, G.W. Stevens, S.E. Kentish, Membrane Gas-Solvent Contactor Pilot Plant Trials of CO_2 Absorption from Flue Gas, Sep. Sci. Technol. 49 (2014) 2449–2458.

[47] C.A. Scholes, J. Bacus, G.Q. Chen, W.X. Tao, G. Li, A. Qader, G.W. Stevens, S.E. Kentish, Pilot plant performance of rubbery polymeric membranes for carbon dioxide separation from syngas, J. Memb. Sci. 389 (2012) 470–477.

[48] H. Herzog, O. Falk-pedersen, The Kvaerner membrane contactor: lessons from a case study in how to reduce capture cost, in: Greenh. Gas Control Technol. Proc. 5th Int. Conf. Greenh. Gas, 2001. 121–125.

[49] B. Belaissaoui, E. Favre, Evaluation of a dense skin hollow fiber gas-liquid membrane contactor for high pressure removal of CO_2 from syngas using Selexol as the absorbent, Chem. Eng. Sci. 184 (2018) 186–199.

[50] S. Boributh, W. Rongwong, S. Assabumrungrat, N. Laosiripojana, R. Jiraratananon, Mathematical modeling and cascade design of hollow fiber membrane contactor for CO_2 absorption by monoethanolamine, J. Memb. Sci. 401–402 (2012) 175–189.

[51] S. Boributh, S. Assabumrungrat, N. Laosiripojana, R. Jiraratananon, Effect of

membrane module arrangement of gas-liquid membrane contacting process on CO_2 absorption performance: A modeling study, J. Memb. Sci. 372 (2011) 75–86.

[52] G. Versteeg, J. Kuipers, F. Beckum, W. Van Swaaij, Mass transfer with complex reversible chemical reactions - I: Single reversible chemical reaction, Chem. Eng. Sci. 44 (1989) 2295–2310.

[53] H. Zhang, R. Wang, D. Tee, J. Hwa, Modeling and experimental study of CO_2 absorption in a hollow fiber membrane contactor, J. Memb. Sci. 279 (2006) 301–310.

[54] H.Y. Zhang, R. Wang, D.T. Liang, J.H. Tay, Modeling and experimental study of CO_2 absorption in a hollow fiber membrane contactor, J. Memb. Sci. 279 (2006) 301–310.

[55] G.F. Versteeg, J.A.M. Kuipers, F.P.H. Van Beckum, W.P.M. Van Swaaij, Mass transfer with complex reversible chamical reactions - II. Parallel reversible chemical reactions, Chem. Eng. Sci. 45 (1990) 183–197.

[56] W.P.M. van Swaaij, G.F. Versteeg, Mass Transfer Accompanied With Complex Reversible Chemical Reactions In Gas - Liquid Systems: An Overview, Chem. Eng. Sci. 47 (1992) 3181–3195.

[57] K.R. Putta, F.A. Tobiesen, H.F. Svendsen, H.K. Knuutila, Applicability of enhancement factor models for CO_2 absorption into aqueous MEA solutions, Appl. Energy. 206 (2017) 765–783.

[58] P.S. Kumara, J.A Hogendoorn, P.H.M. Feron, G.F. Versteeg, Approximate solution to predict the enhancement factor for the reactive absorption of a gas in a liquid flowing through a microporous membrane hollow fiber, J. Memb. Sci. 213 (2003) 231–245.

[59] W. Rongwong, C. Fan, Z. Liang, Z. Rui, R.O. Idem, P. Tontiwachwuthikul, Investigation of the effects of operating parameters on the local mass transfer coefficient and membrane wetting in a membrane gas absorption process, J. Memb. Sci. 490 (2015) 236–246.

[60] F. Kozak, A. Petig, E. Morris, R. Rhudy, D. Thimsen, Chilled Ammonia Process for CO_2 capture, Energy Procedia. 1 (2009) 1419–1426.

[61] G.C. Bue, L.A. Trevino, G. Tsioulos, J. Settles, A. Colunga, M. Vogel, W. Vonau, J.S. Center, Hollow Fiber Spacesuit Water Membrane Evaporator Development and Testing for Advanced Spacesuits, 40th Int. Conf. Environ. Syst. (2011) 1–15.

6 Renewable energy policy and innovation in the UK biomethane sector

Renewable energy policy and innovation in the UK biomethane sector

S. Houlker[a], A. Brookes[b], A. Moore[c], P. Vale[d], M. Pidou[a], E.J. McAdam[a,*]

[a]Cranfield Water Science Institute, Cranfield University, Bedfordshire, UK
[b]Anglian Water, Thorpewood House, Peterborough, UK
[c]Northumbrian Water, Boldon House, Pity Me, Durham, UK
[d]Severn Trent Water, Coventry, UK
*Corresponding author: e.mcadam@cranfield.ac.uk

Abstract

Biogas upgrading to biomethane is a growing market sector in the United Kingdom (UK) driven by government incentivisation with the potential to reduce greenhouse gas emissions, increase energy independence, decarbonise the natural gas grid and to encourage innovative renewable energy cost reduction. Within this study the impact of renewable energy source (RES) policy in the UK on the replacement of natural gas with biomethane as a renewable heat source is assessed with respect to biogas upgrading technology choice, treatment capacity, site-specific innovation and likely future trends. The UK biomethane sector currently favours small to medium scale facilities driven by the low specific investment cost of membrane separation technology with value realised through the Renewable Heat Incentive (RHI) Tier 1 remuneration scheme. Whilst process innovation is realised in myriad ways to introduce complementary value, no single process innovation is capable of compensating for reducing RHI value beyond Tier 1. To realise government RES policy aims, increased biogas upgrading capacity is required and the Renewable Transport Fuel Obligation (RTFO) may provide an opportunity to encourage capacity beyond that driven by RHI.

Keywords: renewable energy policy, biogas, biomethane, renewable heat incentive, renewable transport fuel obligation, biomethane innovation

6.1 Renewable energy policy in the UK

The general aims of UK renewable energy policy are to reduce greenhouse gas emissions, to enhance energy security, to create new employment opportunities and to stimulate innovation and technological development [1]. The United Kingdom has a historic reliance on fossil fuels, in 2010 the UK energy mix consisted of; natural gas 42%, oil 31%, coal 15%, nuclear 8% and less than 4% from renewables [2]. Heating accounts for up to 48% of energy consumption in Europe [1,3] and estimated to account for 47% of UK energy consumption in 2012 [1], of which natural gas accounted for 80% [4]. However, UK renewable energy source (RES) policy has historically focused on renewable electricity (RES-E) [5], introducing one of the first mechanisms to stimulate RES-E production [6]. The need for a mechanism to stimulate renewable energy heat sources (RES-H) was not realised until the introduction of the Renewable Energy Directive 2020 (RED2020) which stipulated renewable energy production in the European Union (EU) to reach 20% by 2020 [4,7] and a legally binding 15% target for the UK [8,9]. Within the UK, reliance on natural gas has created an extensive transmission and distribution network, 85% of the domestic market and 95% of industry is connected to the natural gas grid [10]. The UK is unusual as less than one quarter of its energy demand comes from the industrial sector [2], transmission of RES-H from the site of production to domestic consumers is vital. Biomethane production from biogas represents an RES-H source with the potential to displace 48%–72% of natural gas in the domestic supply [11] and reduce greenhouse gas emissions by 64% to 80% [11]. The introduction of the Renewable Heat Incentive (RHI) within the 2008 Energy Act [4,12,13], a tariff mechanism for the financial remuneration of RES-H, incentivises the transmission of biomethane [14] as renewable heat source in the national gas grid [15] over utilisation as RES-E [16–18]. Additional policies complement RHI: the Climate Change Levy as a fossil fuel tax for commercial entities valued at £10 $tonne^{-1}$ [4], the Renewables Obligation which indirectly supported RES-H by supporting RES-E from biomass but came to an end in 2017, in favour of Contracts for Difference [4] and the Energy Companies Obligation requiring large electricity suppliers to reduce domestic consumer emissions [4]. An important feature of the RHI is the tariff guarantee [19] which guarantees remuneration, initially set at 7.5 p kWh^{-1} in 2014 [4] a tariff regression mechanism has reduced the value to 5.6 p kWh^{-1} by 2018 [20], intended to reflect the reduction of technology cost on market maturation [4]. As consequence of the regressive mechanism, innovative implementation to reduce cost as well as innovative technology to reduce cost is encouraged, delivering new capacity at lower cost [1].

However, the RHI tariff guarantee for large scale plants ends 31st December 2019 [19] alternative mechanisms such as the Renewable Transport Fuel Obligation (RTFO), for the incentivisation of biomethane production will gain significance. Gaseous biofuels such as biomethane have been shown more environmentally beneficial than liquid biofuels [21] and in the UK, Renewable Transport Fuel Certificates (RTFC) are awarded per kg of renewable fuel (biomethane) produced [22,23], valued up to £0.35 kg^{-1} [21] the mechanism awards 1.9 RTFC for biomethane and further doubling to 3.8 RTFC for the use of a source of waste, to limit competition between food and fuel [24]. This represents a potential remuneration value of 12 p kWh^{-1}. The main disadvantage of implementing biomethane as vehicle fuel is its gaseous form at ambient temperature and pressure, requiring additional infrastructure for compression and storage. If implemented through compressed tank storage, more stringent upgrading processes are required to prevent water and hydrogen sulphide contaminants from corroding storage units [25]. Currently, no site in the UK operates biogas upgrading for use as vehicle fuel [26] however vehicle fuel as a value recovery mechanism is expected to become a future driver for growth [27]. This study has therefore focused on the impact of UK renewable energy policy on the biogas upgrading market for injection into the natural gas network and compression for vehicle fuel by investigating technology choice and innovative implementation for reducing capital (CAPEX) and operational (OPEX) expenditure in addition to novel payback mechanisms.

6.2 Biogas upgrading technology choice

The specific investment cost for a biomethane facility is the highest of any RES-H technology, at £ 3,300K MW^{-1} it is £ 567K MW^{-1} greater than a large biogas facility as the next highest specific investment cost [28]. However, in 2015, the UK had 405 sites operating Anaerobic Digestion (AD) for the production of biogas [16] of which 29 upgraded to biomethane [16]. At the end of 2017, the International Energy Association (IEA) reported the number of biomethane producing sites had increased to 96, the second largest in Europe [26]. On introduction of the RHI mechanism in late 2011 for non-domestic use [4], the IEA reports a single biogas upgrading facility in the UK, by the end 2014, a further 25 were operating, a significant increase in a little over 2 years. Of the 96 UK biogas upgrading facilities listed by the IEA in 2017, 70 report on technology type, with an average treatment capacity of 700 Nm^3 h^{-1} biogas. Physical absorption columns applying water (water scrubbers) as absorbent account for 30%, permeation membranes account for 66% and chemically enhanced absorption columns (chemical

scrubbers) account for 4%. Permeation membranes offer the lowest specific investment cost up to a treatment capacity of 700 $Nm^3\ h^{-1}$ biogas [29,30] , accounting for their prevalence in the UK for small to midscale capacities. Interestingly, 700 $Nm^3\ h^{-1}$ biogas represents an annual energy production capacity of 36,000 MWh, close to the limits of an RHI Tier 1 payment mechanism for the first 40,000 MWh produced, after which the RHI value reduces by 58% in Tier 2 (next 40,000 MWh) and by a further 13% in Tier 3 (remaining MWh) [20]. Installed water wash columns in the UK have an average treatment capacity of 900 $Nm^3\ h^{-1}$ biogas [26] despite the specific investment cost only becoming competitive above 1500-2000 $m^3\ h^{-1}$ [29,31]. As a consequence of the tariff regression mechanism, which offers greater financial reward to early adopters, water wash columns as a historically proven technology [29,31–35] represented low risk investment and fit for immediate purpose [35], despite disadvantages such as high CAPEX and high OPEX. This is evidenced in the UK water sector, a historically risk averse sector, where water wash columns account for 85% of the reported biomethane installations despite an average treatment capacity of 880 $Nm^3\ h^{-1}$ biogas [26]. This is in contrast to Germany as the leading producer of biomethane with 200 facilities [26]. The German tariff system introduced in 2008 (EEG 2009) stipulates that to qualify for remuneration, methane losses must not exceed 0.5%, chemical scrubbers are consistently able to meet this demand [21]. As such, Germany has 55 sites operating chemical scrubbers, more than any other IEA member [26] despite high specific investment costs [29,31]. Interestingly, the RHI does not stipulate gas quality standards, instead the local gas distribution network (of which there are 4 in the UK [36]) imparts gas quality standards, the level of injected gas quality therefore varies between facilities.

It is therefore suggested that the UK biogas upgrading market is primarily driven by low cost technologies and RHI remuneration, a view upheld by government response to consultation [19]. For RHI as an incentivisation mechanism to increase capacity beyond Tier 1 per installation, a complementary technology or implementation cost reduction will need to be realised to ensure economic viability. An interesting method is the diversification of payback mechanisms claimed, with the introduction of Renewable Transport Fuel Certificates (RTFC) and the reduction of RHI value at higher tariffs, larger facilities may benefit to switching to RTFCs over RHI at Tier 2 or 3 payback. An example of a diversified payback mechanism is given by an ‘Energy Park’ established at a wastewater treatment works, where investment in a 600 $Nm^3\ h^{-1}$ treatment upgrading facility [26], combined heat and power (CHP), solar photovoltaics, hydroelectric

generation, and wind generation [37] achieves resilience and energy self-sufficiency in addition to RHI remuneration.

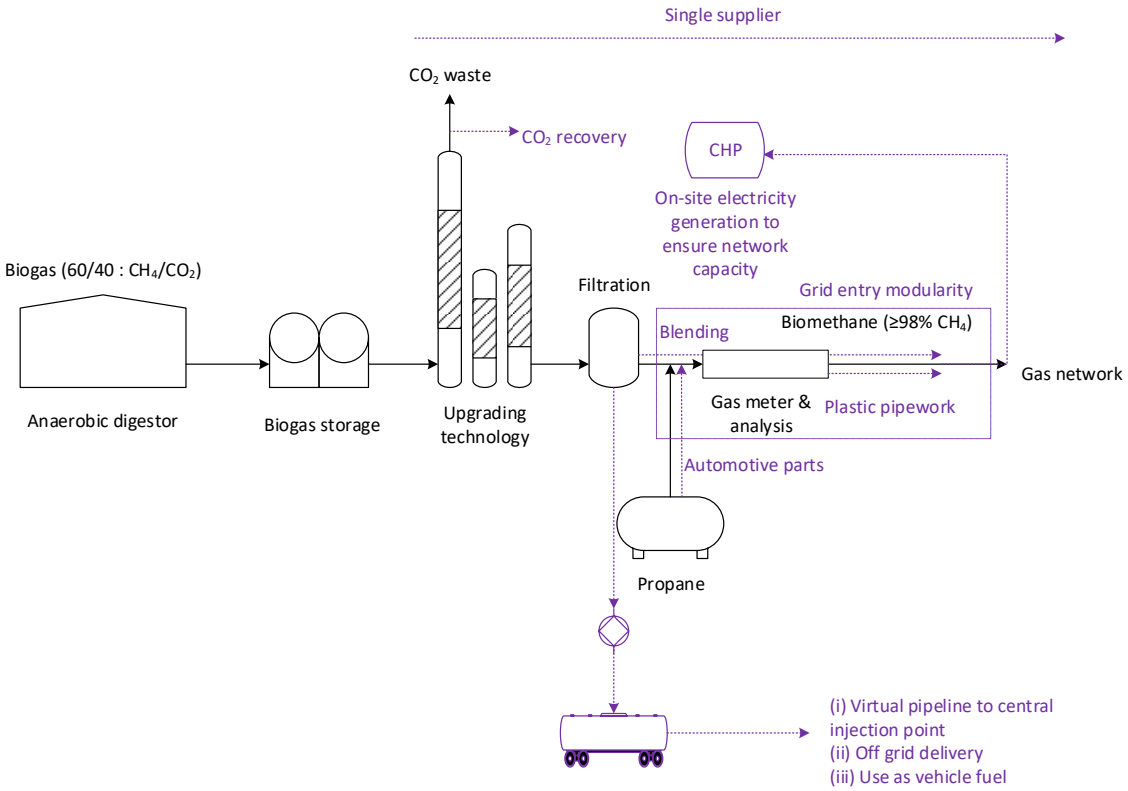

Figure 6.1 Represented in black is a schematic of a typical biogas upgrading process and represented in purple are innovative solutions to reducing OPEX and CAPEX currently in place in the UK.

6.3 Innovations in networks and distribution

To enable biomethane injection, a network entry agreement (NEA) is required with the local gas distribution network (GDN) [38,39]. At the point of injection into the network, a grid entry unit (GEU) is required to monitor gas quality and a remotely operated valve linked to the GDN to enable remote closure should gas quality fail [36]. Currently connections to the GDN or National Transition System (NTS) take up to 3 years and cost £2M for lower flow gas connections [40]. The national grid is making available above ground injection points and modularised telemetry kiosks (Figure 6.1) combined with remote operated valves, intending to reduce connection to 1 year and cost below £1M [40], encouraging predictability. Various engineering solutions to reduce the cost of grid connection have been realised, at an agricultural site with a biogas treatment capacity of 600 $Nm^3\ h^{-1}$ [26], the UKs first self-lay pipeline to a Local Transmission System (LTS) was implemented, enabling biomethane injection at a site distant from the gas network, further cost saving was enabled by employing a single principle contractor [41]. Another

agricultural site with a biogas treatment capacity of 1000 Nm^3 h^{-1} [26], implemented a similar solution but employed a 7km private pipeline to enable injection into the nearest LTS [41]. A self-lay pipe line at further agricultural site with a biogas treatment capacity of 500 Nm^3 h^{-1} [26] was later adopted by the National Grid [36], reducing maintenance cost of the connection. An agricultural site with a biogas treatment capacity of 550 Nm^3 h^{-1} [26] reduced the cost of a private pipeline by employing a 1.4 km Hexel One pipeline, a high pressure polyethylene pipe, cheaper than the standard steel pipelines [41] (Figure 6.1). Additionally, the construction time was reduced by minimising pipeline joins (supplied in 140m lengths) and easy installation into trenches [41]. An alternative avenue for innovation is to either share a GEU or to eliminate the connection point entirely. A remote grid entry hub and virtual pipeline developed by a local Gas Distribution Network in the south of England, has a 6,000 Nm^3 h^{-1} injection capacity split between 5 download bays [38,42]. Biomethane producers compress their product and transport in 250 Bar tankers to the central injection site, creating a virtual gas pipeline by road transport (Figure 6.1). The concept enables sites with a high biomethane potential but limited access to the NTS access to the biomethane market. Ancillary benefits include the obviation of propane cost as the biomethane is blended into a high capacity main, expedition of the time required to get a grid connection, reduced grid connection cost and reduced OPEX through the sharing of injection equipment [38,42]. Interestingly, download time into the gas network is effected by biomethane quality, encouraging the production of high purity biomethane, as such the first site entering into agreement with the GDN employed a chemical scrubber [38,42]. Transport companies are available to manufacture bespoke compression tankers to facilitate a virtual pipeline [43], as consequence a biomethane facility can choose to compress, transport to an injection site and access RHI remuneration for biomethane production or compression as vehicle fuel and access remuneration through the RTFO, increasing revenue flexibility and de-risking investment. However, trials at an international beverage company into replacing diesel vehicles with biomethane gas vehicles demonstrated a 12% decrease in fuel cost favouring biomethane but a 15% increase in CAPEX associated with vehicle purchase [44], demand for biomethane as a renewable transport fuel is likely to require further equipment cost reduction. The need for an injection point into the NTS can be avoided by liquefying biomethane and transporting directly to customers without grid access [45,46].

Network capacity is an emerging problem for biogas upgrading, the UK transmission network is designed for transmission from high pressure gas mains to low

pressure local gas networks [47], the system is not optimised for distributed biomethane production [47]. A proposed solution is to employ the 6,000 km of local transmission system (LTS) as a transport system for compressed natural gas (CNG) [48], immediate value lying in the lack of gas leaks in the LTS and OPEX reduction relative to compression to form a typical 200 mBar gas grid [48]. The idea is being realised in Ireland as part of the €25 million Causeway Project for the first national CNG network with 14 CNG filling stations and a biomethane injection facility [49]. Indirect value can be found by increasing and maintaining demand on the gas network, increasing and stabilising network capacity.

An alternative value mechanism linked to network capacity is the nature of biomethane within the national grid as a store of renewable energy, biomethane can be injected into national grid and extracted at a point and time distant from injection [50]. Such renewable energy storage is valuable in balancing the electricity grid, RES-E for solar and wind is periodic and unsuited for demand balancing [51]. Biomethane is available for combustion in CHP engines at periods of electricity demand, enabling cost recovery mechanisms to be more closely linked to electricity price and less reliant on incentives. An example is the use of CHP in London, the extensive natural gas network in the city has encouraged local CHP generation for heating, electricity and cooling at office buildings however, the use of biomethane as a RES-H and RES-E is currently limited compared to natural gas consumption [51].

6.4 Identifying synergies with existing infrastructure to maximise value

The manner of site operation can influence OPEX. As example, propane blending is typically required to maintain the calorific value of injected gas, however a wastewater treatment works (WWTW) with a biogas treatment capacity of 900 $Nm^3\ h^{-1}$ [26] has employed biomethane blending directly into a high pressure gas main, reducing propane cost [52]. However, the solution is only applicable for high pressure gas mains [53]. A novel solution proposed to reduce the capital cost of propane blending at small scale, low pressure (≤100 $Nm^3\ h^{-1}$, 2 Bar) facilities is to utilise automotive parts, manufactured to a high quality and in large quantity to construct a blending system, replacing expensive bespoke propane blending systems and reducing cost [54]. The conversion of existing assets at an existing biogas producing AD facility can introduce further benefits. As example, a WWTW with a biogas treatment capacity of 1500 $Nm^3\ h^{-1}$ [26] converted an existing biogas facility with electrical production through combined heat and power engines (CHP) [55] to biogas upgrading [56]. The site is connected by an intermediate

pressure main to an area of low gas demand, with minimal demand during the summer. To maintain gas demand and sustain the business case, the biomethane injected into the network is taken out locally and combusted in CHP engines to generate the onsite electricity demand of the WWTW. As consequence of the higher gas quality of upgraded biomethane relative to biogas, the CHP engines also operate at a higher efficiency [56]. Such operation enables the site to meet its own electricity demand whilst ensuring capacity and demand in the local gas network. Project cost and perceived project risk can be reduced using a single process provider for biogas upgrading, injection facilities and continued support [27]. As example, the upgrader supplier awarded the contract to construct an agricultural upgrading facility with a biogas treatment capacity of 700 Nm^3 h^{-1} [26,57] was chosen due to their ability to support the project from construction to ongoing operation [58].

6.5 Opportunities for the co-production of new materials through biogas upgrading

A typical biogas upgrading facility (Figure 6.1) will collect low pressure (20 mBar) biogas from anaerobic digestion process, pressurise (6-8 Bar) and pass to an upgrading process i.e. water wash or membrane separation, perform an extra filtration step to remove contaminants such as particulates or hydrogen sulphide prior to blending with propane to ensure calorific value, odourising and finally injection into the natural gas network [29,31]. However, innovation can be realised within such a process.

The IEA lists 8 sites in the UK that combine membrane separation for biogas upgrading with cryogenic recovery of CO_2 [16]. Operation of a multi-stage membrane system in combination with a cryogenic recovery step enables biogas upgrading with minimal methane slip and liquid CO_2 to be recovered as a secondary product [59] (Figure 6.1). As example two agricultural sites, one a small scale producer and one a larger centralised facility employ a biogas upgrading-CO_2 recovery system [60,61]. The small scale agricultural site has a biogas treatment capacity of 500 Nm^3 h^{-1} [26] and an annual CO_2 recovery capacity of 3,000 tonnes [60], value is realised by utilising recovered CO_2 on-site. The site produces tomatoes, by controlling dosing of recovered CO_2, optimal growth is assured and tomato output is increased by 15% [60]. In contrast the larger centralised facility employs innovation through two different drivers. The first driver was the reduction in arable crop value and increased export cost for processing, as consequence six local farmers in conjunction with a local grain storage company invested in a centralised AD facility to ensure stable value through energy production, 53 farms export crops to the facility for a biogas treatment capacity of 1050 Nm^3 h^{-1} [26]

and an annual CO_2 recovery capacity of 6,900 tonnes [61]. The second driver was a local industrial gases company investing in transport cost reduction by sourcing CO_2 locally, ensuring a market for the recovered CO_2 [61]. An innovative method to further exploit CO_2 is proposed for distilleries on the north east coast of Scotland, where waste CO_2 from a cluster of local distilleries would be transported to a central facility where the Sabatier process ($CO_2 + 4H_2 \underset{Pressure}{\overset{400°C}{\longrightarrow}} CH_4 + 2H_2O$) powered by RES-E derived from windfarms would enable conversion to CH_4, converting a waste into energy [59]. Within the water sector, the co-production of biomethane for grid injection and for vehicle fuel has been demonstrated, with a local bus company operating a 'biobus' on the recovered biomethane, with value lying in reduced emissions relative to diesel [62].

6.6 Identifying new value propositions through exporting to new markets

Complementary to innovative implementation is realising the value of green energy credentials. Green Gas Certification and virtual trading enable biomethane producers to realise value by trading green credentials with corporate entities seeking to reduce the carbon intensity of their gas supply. As example, a medium size agricultural site producing 800 $Nm^3\ h^{-1}$ biogas [26] entered into a supply agreement with Barrow Green Gas as a UK Gas Shipper [63,64] to supply an annual 70 million units (1 unit = 1kWh) of certified Green Gas under the Renewable Energy Assurance Limited (REAL) Green Gas Certification Scheme (GGCS). In 2016 the site announced a partnership with a national supermarket chain to supply six per cent of the company's total gas use [65]. As of 2017, the REAL GGCS had a registered 47 producers with a combined 2.5 TWh capacity supplying 87 consumers, primarily corporate consumers [66]. Continued expansion of the scheme has the potential to foster the value of green energy credentials and compensate the reduction in financial value available through a regressing RHI. A recent proposal is to open EU biomethane trade through the European Renewable Gas Registry (ERGaR), enabling the European natural gas network to act as a single logistical system for green gas trading [67].

6.7 Conclusions

To realise government policy aims of reducing greenhouse gas emissions and increasing energy security via RES-H, biomethane production capacity is required. Remuneration through the Renewable Heat Incentive and minimal specific investment cost is the primary driver for membranes as upgrading technological choice. However, increased biogas plant capacity is limited by the RHI Tier 2 tariff reduction, leading to a proliferation

of small to medium size facilities. Further capital and operational cost reduction can be realised by novel process implementation or recovery of secondary produces such as liquid CO_2 but does not offer enough value to increase capacity, further cost reduction is required. Alternative remuneration through the Renewable Transport Fuel Obligation is likely to gain value in the future as both a mechanism for increasing network capacity, such as in Ireland [49], and for incentivising larger facilities beyond RHI Tier 1 whereas complementary mechanisms such as the GGCS are likely to increase value outside of government remuneration, laying the groundwork for sector sustaining economic viability without remuneration.

Acknowledgements

The authors would like to thank Anglian Water, Northumbrian Water and Severn Trent Water for their practical and financial support. We are also grateful for funding from the Engineering and Physical Sciences Research Council (EPSRC) which was provided through the STREAM Industrial Doctorate Centre. Enquiries for access to the data referred to in this article should be directed to: researchdata@ cranfield.ac.uk.

References

[1] P. Connor, B. Veit, L. Beurskens, K. Ericsson, C. Egger, Devising renewable heat policy : Overview of support options, Energy Policy. 59 (2013) 3–16.

[2] International Energy Association, Energy Policies of IEA Countries: The United Kingdom 2012 Review, 2012. https://webstore.iea.org/energy-policies-of-iea-countries-the-united-kingdom-2012-review. (accessed February 1, 2019)

[3] G. Wood, S. Dow, What lessons have been learned in reforming the Renewables Obligation? An analysis of internal and external failures in UK renewable energy policy, Energy Policy. 39 (2011) 2228–2244.

[4] P.M. Connor, L. Xie, R. Lowes, J. Britton, T. Richardson, The development of renewable heating policy in the United Kingdom, Renew. Energy. 75 (2015) 733–744.

[5] C. Mitchell, P. Connor, Renewable energy policy in the UK 1990-2003, Energy Policy. 32 (2004) 1935–1947.

[6] C. Mitchell, The England And Wales Non-Fossil Fuel Obligation: History and Lessons, Annu. Rev. Energy Environ. 25 (2000) 285–312.

[7] European Parliament, Directive 2009/28/EC of the European Parliament and of the Council of 23 April 2009, Off. J. Eur. Union. 140 (2009) 16–62.

[8] Department of Energy and Climate Change, National Renewable Energy Action Plan for the United Kingdom, 2009. https://www.gov.uk/government/publications/national-renewable-energy-action-plan. (accessed February 9, 2019)

[9] Department of Energy and Climate Change, The UK Renewable Energy Strategy, 2009. http://www.decc.gov.uk/en/content/cms/what_we_do/uk_supply/energy_mix/renewable/res/res.aspx. (accessed February 9, 2019)

[10] J. Baldwin, UK Biomethane Market: Market Update and the Capacity Question, (2017). [Presentation] http://www.cngservices.co.uk/images/BiomethaneDay/2017/John-Baldwin--%0AUK-Biomethane-Market--the-Capacity-Question.pdf. (accessed February 12, 2019)

[11] T. Fubara, F. Cecelja, A. Yang, Techno-economic assessment of natural gas displacement potential of biomethane: A case study on domestic energy supply in the UK, Chem. Eng. Res. Des. 131 (2018) 193–213.

[12] T. Patterson, S. Esteves, R. Dinsdale, A. Guwy, An evaluation of the policy and techno-economic factors affecting the potential for biogas upgrading for transport fuel use in the UK, Energy Policy. 39 (2011) 1806–1816.

[13] T. Horschig, P.W.R. Adams, M. Röder, P. Thornley, D. Thrän, Reasonable potential for GHG savings by anaerobic biomethane in Germany and UK derived from economic and ecological analyses, Appl. Energy. 184 (2016) 840–852.

[14] S.H. Abu-bakar, F. Muhammad-sukki, R. Ramirez-iniguez, T. Kumar, C. Mclennan, A. Bakar, S. Hajar, M. Yasin, R. Abdul, Is Renewable Heat Incentive the future?, Renew. Sustain. Energy Rev. 26 (2013) 365–378.

[15] D. Thrän, E. Billig, J. Daniel-Gromke, J. Ponitka, M. Seiffert, T. Persson, M. Svensson, J. Balswin, L. Kranzl, F. Schipfer, J. Matzenberger, N. Devriendt, M. Dumont, J. Dahl, G. Bochmann, Biomethane Status and Factors Affecting Market Development and Trade, 2014. https://www.ieabioenergy.com/publications/biomethane-status-and-factors-affecting-market-development-and-trade/.

[16] Anaerobic Digestion and Biogas Association (ADBA), Anaerobic Digestion Market Report, London, 2015. http://adbioresources.org/library/market-report-july-2015.

[17] P.L. McCarty, J. Bae, J. Kim, Domestic Wastewater Treatment as a Net Energy Producer - Can This be Achieved?, Environ. Sci. Technol. 45 (2011) 7100–7106.

[18] K. Mizuta, M. Shimada, Benchmarking energy consumption in municipal wastewater treatment plants in Japan, Water Sci. Technol. 62 (2010) 2256–2262.

[19] Department for Business Energy & Industrial Strategy, The Renewable Heat Incentive: A Reformed Scheme, 2016. https://www.gov.uk/government/uploads/system/uploads/attachment_data/file/577024/RHI_Reform_Government_response_FINAL.pdf. (accessed February 12, 2019)

[20] Ofgem, Non-Domestic RHI tariff rates, Non-Domestic RHI Tarif. Rates. (2018). https://www.ofgem.gov.uk/environmental-programmes/non-domestic-rhi/contacts-guidance-and-resources/tariffs-and-payments-non-domestic-rhi (accessed September 9, 2018).

[21] T. Patterson, S. Esteves, R. Dinsdale, A. Guwy, An evaluation of the policy and techno-economic factors affecting the potential for biogas upgrading for transport fuel use in the UK, Energy Policy. 39 (2011) 1806–1816.

[22] Department for Transport, Renewable transport fuel obligation, 2017. http://www.dft.gov.uk/topics/sustainable/biofuels/rtfo.

[23] Department for Transport, Renewable Transport Fuel Obligation Guidance Part One Process Guidance, 2018. https://www.gov.uk/government/publications/renewable-transport-fuel-obligation-rtfo-guidance-year-11.

[24] C. Whittaker, M.C. McManus, G.P. Hammond, Greenhouse gas reporting for biofuels: A comparison between the RED, RTFO and PAS2050 methodologies, Energy Policy. 39 (2011) 5950–5960.

[25] W.M. Budzianowski, M. Brodacka, Biomethane storage: Evaluation of technologies, end uses, business models, and sustainability, Energy Convers. Manag. 141 (2017) 254–273.

[26] International Energy Association Task 37, IEA Bioenergy Task 37 Upgrading Plant List 2017, (2017). http://task37.ieabioenergy.com/plant-list.html (accessed November 17, 2018).

[27] J. Baldwin, Grid Injection Regime Lessons Learned from GB and Recommendations for Northern Ireland Lessons Learned from GB – Good Stuff, (2018). [Presentation] http://www.cngservices.co.uk/index.php/news/cng-events/158-northern-ireland-biomethane-seminar. (accessed February 12, 2019)

[28] Renewable Energy Association, Renewable Energy Review, 2015.

[29] F. Bauer, T. Persson, C. Hulteberg, D. Tamm, Biogas upgrading - technology

overview, comparison and perspectives for the future, Biofuels, Bioprod. Biorefining. 7 (2013) 499–511.

[30] F. Bauer, C. Hulteberg, T. Persson, D. Tamm, Biogas upgrading – Review of commercial technologies, 2013. http://www.sgc.se/ckfinder/userfiles/files/SGC270.pdf.

[31] M. Miltner, A. Makaruk, M. Harasek, Review on available biogas upgrading technologies and innovations towards advanced solutions, J. Clean. Prod. 161 (2017) 1329–1337.

[32] E. Ryckebosch, M. Drouillon, H. Vervaeren, Techniques for transformation of biogas to biomethane, Biomass and Bioenergy. 35 (2011) 1633–1645.

[33] R. Muñoz, L. Meier, I. Diaz, D. Jeison, A review on the state-of-the-art of physical/chemical and biological technologies for biogas upgrading, Rev. Environ. Sci. Biotechnol. 14 (2015) 727–759.

[34] I. Ullah Khan, M. Hafiz Dzarfan Othman, H. Hashim, T. Matsuura, A.F. Ismail, M. Rezaei-DashtArzhandi, I. Wan Azelee, Biogas as a renewable energy fuel – A review of biogas upgrading, utilisation and storage, Energy Convers. Manag. 150 (2017) 277–294.

[35] Q. Sun, H. Li, J. Yan, L. Liu, Z. Yu, X. Yu, Selection of appropriate biogas upgrading technology-a review of biogas cleaning, upgrading and utilisation, Renew. Sustain. Energy Rev. (2015) 521–532.

[36] J. Baldwin, UK Biomethane Market The last 12 Months, (2016). http://www.cngservices.co.uk/index.php/news/cng-events/125-biomethane-day-2017.

[37] A. Dixon, Five Fords WwTW, (2016). http://www.waterprojectsonline.com/publication_date/2016.htm.

[38] A. Midwinter, Scotia Gas Networks - Commercial Services SGN Gas Network, (2014). http://www.cngservices.co.uk/index.php/news/cng-events/35-uk-biomethane-day-2014.

[39] L. Nattrass, L. Hopwood, M. Goldsworthy, J. Baldwin, L. Firth, R. McKeon, Biogas networks, 2013. http://www.wrap.org.uk/sites/files/wrap/NNFCC and CNG Services Ltd - DIAD 2 feasibility study.pdf. (accessed February 12, 2019)

[40] C. Gumbley, Project CLoCC Customer Low Cost Connections, (2018). [Presentation] http://www.cngservices.co.uk/index.php/news/cng-events/137-biomethane-day-2018. (accessed February 12, 2019)

[41] J. Baldwin, Biomethane Project Innovation, (2015). [Presentation]

http://www.cngservices.co.uk/index.php/news/cng-events/35-uk-biomethane-day-2015. (accessed February 12, 2019)

[42] A. Midwinter, The Virtual Gas Pipeline, (2015). [Presentation] http://www.cngservices.co.uk/index.php/news/cng-events/35-uk-biomethane-day-2015. (accessed February 12, 2019)

[43] Calvera, Refuelling on the go, AD&BIORESOURCES NEWS. (2018) 30.

[44] S. Carrol, The Coca-Cola Enterprises Biomethane Trial Report, Anaerob. Dig. BBoresources Assoc. (2012). http://adbioresources.org/wp-content/uploads/2012/05/CCE-biomethane-trial-report-1_3.pdf?_ga=2.259976012.710664460.1549009481-1688060882.1548144459 (accessed February 1, 2019).

[45] AD&BIORESOURCES, Awards Winners, AD&BIORESOURCES NEWS. (2018) 26–28.

[46] Cryo Pur, Technology, (2019). http://www.cryopur.com/en/technology/ (accessed January 30, 2019).

[47] J. Baldwin, UK Biomethane Market Market Update and the Capacity Question, (2017). [Presentation] http://www.cngservices.co.uk/images/BiomethaneDay/2017/John-Baldwin--%0AUK-Biomethane-Market--the-Capacity-Question.pdf. (accessed February 12, 2019)

[48] K. Zennaro, REView 2016: Biomethane-to-grid is heating up, Renew. Energy Assoc. Rev. 2016. (2016). https://www.r-e-a.net/blog/review-2016-biomethane-to-grid-is-heating-up-14-06-2016 (accessed February 1, 2019).

[49] J. Browne, Cush RNG Injection Project, (2018). [Presentation] http://www.cngservices.co.uk/index.php/news/cng-events/137-biomethane-day-2018. (accessed February 12, 2019)

[50] S. Farris, Severn Trent Biogas Development, (2017). [Presentation] http://www.cngservices.co.uk/index.php/news/cng-events/125-biomethane-day-2017. (accessed February 12, 2019)

[51] J. Baldwin, Briefing on GB Biomethane Market, (2018). [Presentation] http://www.cngservices.co.uk/index.php/news/cng-events/158-northern-ireland-biomethane-seminar. (accessed February 12, 2019)

[52] S. Farris, Minworth Biomethane Injection Plant, (2015). [Presentation] http://www.waterprojectsonline.com/water_companies/Severn_Trent_Water.htm#Renewable Energy. (accessed February 12, 2019)

[53] S. Farris, Minworth Sewage Treatment Works, (2013). [Presentation] http://www.cngservices.co.uk/index.php/news/cng-events/38-uk-biomethane-day-2013. (accessed February 12, 2019)

[54] T. Williamson, Propane blending system for biomethane to grid applications, 2013. http://www.wrap.org.uk/search-results#stq=biomethane&stp=1. (accessed February 13, 2019)

[55] D. Rawlinson, S. Coverdale, B. Oliver, J. Ord, B.S. Stws, Howdon & Bran Sands STWs, (2012). http://www.waterprojectsonline.com/water_companies/Northumbrian_Water.htm. (accessed February 2, 2019)

[56] L. Yingjian, Q. Qi, H. Xiangzhu, L. Jiezhi, Energy Use Project and Conversion Efficiency Analysis on Biogas Produced in Breweries, Ind. Energy Effic. (2011) 1489–1496.

[57] IEA Bioenergy Task 37, an Integrated Farm Enterprise, (2018). http://task37.ieabioenergy.com/case-stories.html. (accessed February 2, 2019)

[58] EnviTec, EnviTec Biogas, EnviTec Webpage. (2015). https://www.envitec-biogas.co.uk/references/references-biomethane/ (accessed February 1, 2019).

[59] Pentair, Biomethane & Green CO_2, 2016. https://foodandbeverage.pentair.com/en/products/haffmans-biogas-upgrading-technology (accessed February 1, 2019).

[60] Pentair, HAFFMANS BIOGAS UPGRADING SPRINGHILL FARMS , UK, 2013. https://foodandbeverage.pentair.com/en/products/haffmans-biogas-upgrading-technology. (accessed February 2, 2019)

[61] Pentair, HAFFMANS BIOGAS UPGRADING WIGHT FARM ENERGY LLP, 2016. https://foodandbeverage.pentair.com/en/products/haffmans-biogas-upgrading-technology. (accessed February 2, 2019)

[62] S. Carver, Avonmouth Biomethane Project, UK Water Proj. Online. (2015). http://www.waterprojectsonline.com/case_studies/2015/Wessex_Avonmouth_Biomethane_2015.pdf. (accessed August 2, 2019)

[63] S. Thomas, Barrow green gas, (2015). [Presentation] http://www.cngservices.co.uk/index.php/news/cng-events/35-uk-biomethane-day-2015. (accessed February 2, 2019)

[64] T. Davis, Biomethane Production Review, [Presentation] (2018). http://www.cngservices.co.uk/index.php/news/cng-events/(accessed February 2, 2019)137-biomethane-day-2018.

[65] W. Farms, T. Grocer, Wyke Farms – leading the way in creating a sustainable energy future, Barrow Green Gas Website. (2014). http://www.barrowgreengas.co.uk/case-studies-1/ (accessed February 1, 2019).

[66] J. Scharf, Green Gas Certification Scheme, (2018). [Presentation] http://www.cngservices.co.uk/index.php/news/cng-events/137-biomethane-day-2018. (accessed February 2, 2019)

[67] A. Kovacs, ERGaR : Tool for cross border transfer and mass balancing biomethane within the European natural gas network, (2017). [Presentaion] http://www.cngservices.co.uk/index.php/news/cng-events/125-biomethane-day-2017. (accessed February 2, 2019)

7 Discussion

7.1 Discussion

The constituent chapters of this thesis have collectively tested the initial hypothesis that 'HFMC are a successor technology to existing gas-liquid absorption columns for industrial biogas upgrading by exploiting modularity to enhance performance'. Further exploitative advantages of the thesis have enabled the translatability of performance data across scale to inform process design and incorporate the recovery of ammonium bicarbonate that provides new value streams. To contextualise the impact of the research toward an implementable solution, the contribution to knowledge is explored around a set of four operational questions.

1. Can membranes compete on scale and cost with absorption columns?

Commercial scale HFMC are sized through the volumetric mass transfer coefficient ($K_{OV}a$) as the product of the mass transfer coefficient (m s^{-1}) and specific surface area (m^2 m^{-3}) to estimate total membrane volume [1,2]. Variable membrane geometries and interfacial areas are available within a commercial range up to 330m^2 of membrane area, the required surface area is dependent on desired performance (treatment capacity and $K_{OV}a$). Each membrane module can operate as a standalone absorption unit or the absorption process can be broken up between multiple modules [3], introducing economies of scale available within a commercial module range (i.e. multiple unit scales available to produce multiple configuration choices). The process length (L) is reached by supplementing individual transfer units (*HTU*) (HFMC modules) with additional transfer units (*NTU*) [4–6]. The choice of *HTU* (individual module size) is predicated on attainable $K_{OV}a$ values at the desired treatment capacity weighted against capital and operational cost. The primary advantage of HFMC over absorption column is the substantial increase in specific surface area (a) in membrane contactors (around 7500 m^2 m^{-3}) versus packed columns (around 250 m^2 m^{-3}) [7,8]. deMontigny et al. [9] report comparable performance between columns and HFMC but favourable $K_{OV}a$ in HFMC, similar results are obtained in this thesis (Chapter 5). Further studies by deMontigny et al. [10] and Belaissaoui et al. [7] comparing a single HFMC and absorption column attribute a 15 fold intensification factor to HFMC [7]. To demonstrate the impact of intensified mass transfer, a capital cost comparison (packing material and absorber casing) of a biogas upgrading process employing HFMC and absorption columns based on the outcomes of Chapter 2 is undertaken, the translatability and accuracy of estimations of mass transfer at scale being demonstrated in Chapter 3, indicating that membrane size does not impact process design principles. Obtained $K_{OV}a$ values of 18.3

– 42.2 x10^3 (s^{-1}) for HFMC operation are congruent with literature values [11] whilst absorption column $K_{OV}a$ values, 0.8 – 2.2 x10^3 (s^{-1}), are representative of those reported in the literature for column operation [12,13]. Optimal $K_{OV}a$ values are estimated at 42.2 x10^{-3} (s^{-1}) for HFMC and 2.2 x10^{-3} (s^{-1}) for absorption columns for an operational set point (*L/G*) of 0.8. Applying an empirical relationship reported by Brunazzi et al. [8] for the capital cost of an absorption column:

$$C_{col} = 583.6 \times d^{0.675} \times h \times F_{mat} \times \left(\frac{p \times 14.5}{50}\right)^{0.44} \quad \text{(Equation 7.1)}$$

Where C_{col} is column capital cost in Euros, *d* the column diameter (m), *h* column height (m), *p* is pressure (kPa) and F_{mat} a column material correction factor taken as 1.7 [8]. Column material is assumed stainless steel 304 and operated at ambient pressure (Chapter 4), enabling comparable absorber performance. Taking a representative £1,291 m^{-3} for 2" Raschig rings as an industry standard packing material [8], with an *a* of 100 m^2 m^{-3} [8], capital cost is estimated to be £15,328. In comparison, a membrane material with an *a* of 3600 m^2 m^{-3} (Chapter 2) and cost of £40 m^{-2} [14] is taken, and the methodology of Shao et al. [15] applied to estimate casing cost:

$$C_{cas} = \left[\frac{1000 \times (A_1 + A_2)}{60} + \frac{80 \times A_3}{30}\right] \times \frac{1}{25 \times 365 \times 24} \quad \text{(Equation 7.2)}$$

Where C_{cas} is casing cost (US$ h^{-1}) and A_1, A_2 and A_3 are contact area (m^2) of the membrane stages. For the costing a single membrane stage was considered of 1000 US$ pc^{-1} [15].

Table 7.1 A capital costing exercise of absorber design

Gas-Liquid Absorber	$K_{ov}a$ (s^{-1})	*HTU* (*m*)	Process Volume (m^3)	*L* (*m*)	Q_L (L min^{-1})	Q_G (L min^{-1})	Absorber Cost (£)	Contacting Media (£)	CAPEX (£)
HFMC	42.2	0.113	0.001	0.9	0.8	1	70	160	230
Column	2.2	0.3	0.02	2.4	0.8	1	15,276	52	15,328
Volume and CAPEX Reduction Factor			19						36.3

Whilst factors associated with economies of scale will likely reduce costs of the column, which in industry achieve an optimum at 1500-2000 Nm^3 h^{-1} treatment flow relative to the lower flow 700 Nm^3 h^{-1} breakpoint of permeation membranes [16], the two

orders of magnitude difference in cost between the two studies emphasises the potential for CAPEX reduction available through high specific surface area technology. The capital expenditure can be expected to reduce by a factor of 36, in line with the reduction of process volume (Table 7.1). In term of operational costs, to enable a $K_{OV}a$ amenable to process intensification, absorption columns are operated under pressure, typically 6-10 Bar [16], for a process capacity of 1000 m^3 h^{-1} biogas a 210-230 m^3 h^{-1}, 20°C Q_L is required at a gas pressure of 8 Bar, and accounts for 0.10-0.15 kWh Nm^{-3} [16], or 50% of the total 0.2-0.3 kWh Nm^{-3} energy demand [17]. Due to the vertical positioning of absorption columns, hydraulic pressure is required to pump absorbent to the top of the column, compounding pressurisation needs, HFMC in comparison can be operated horizontally and thus limit additional pressurisation to overcoming friction losses. Gas phase pressure drop across each small scale HFMC (Chapter 2) was measured at 1 mBar and up to 33 mBar (Chapter 4) at industry, HFMC can facilitate an industrially relevant 0.98 η_{CO2} [18] (Chapter 3 & 4) with minimal pressurisation (0.5 BarG). However, previous studies have successfully pressurised HFMC up to 60 Bar [7,19–21] through correctly balancing the pressure differential across the membrane. Minimally pressurised operation (2 Bar) would reduce process scale whilst allowing for direct biomethane injection into low pressure local transmission systems, key to maintaining network capacity for distributed small-scale upgrading facilities favoured through RHI remuneration (Chapter 6). The primary operational cost would then lie in the 0.05-0.10 kWh Nm^{-3} water pumping cost [16] adopting the industry practice of applying final effluent as a free source of absorbent [16,22]. However, by phase separation in HFMC, this can be further reduced through horizontal operation whereby pressurisation is limited to friction losses across the module length. This reduces associated issues with planning permission and should further process intensification be desired, pressurisation in line with current column operation can be expected to reduce process scale by a further order of magnitude.

Whilst mass transfer can be described as gas-phase controlled when producing a high purity methane product (Chapter 2) at laboratory scale, the dominance of gas-phase resistance can be ascribed to fibre non-uniformity and shell-side maldistribution present in small-scale parallel flow modules, whereby increasing gas-phase velocity overcomes increased local pressure drop induced by a higher local packing fraction. Within larger-scale transverse flow modules, enhanced shell-side distribution encourages application of shell-side absorbents and a lumen side gas phase, as such the distribution of the gas-phase is increased relative to shell-side parallel flow,

accounting for the reduction in the gas-phase contribution to mass transfer at lower gas velocities (Chapter 3). As example, when maintaining the mass transfer characteristics, $K_{OV}a$ = 0.042 s^{-1} for physical absorption with water as absorbent, at ambient pressure and temperature and translating to a larger scale 104 m^2 HFMC within the same commercial range [1], a biogas treatment capacity of 8.7 m^3 h^{-1} can be achieved at ambient pressure. Further scaling into the upper range of industrial ranges would require further module geometric information.

2. How should the membrane system be configured?

Modularity can be implemented in two ways (i) optimisation of a single module and employing multiple in-parallel modules to reach a desired treatment capacity (ii) a membrane cascade of multiple in-series modules with treatment capacity reached by the cascades end. Boributh et al. [20] and [21] demonstrated in terms of contact area (m^2), stage number (*NTU*) and J_{CO2} the positive benefit of an in-series module cascade with individually controlled transfer units on process intensification over individual module operation [23,24]. This is corroborated by this thesis (Chapter 2) where an in-series design is demonstrated to deliver gas quality targets with a lower total membrane area. In this theoretical example, the absorber design (Table 7.1) utilise HFMC within an in-series design (Figure 7.1). A single HFMC has a maximum treatment capacity of 0.05 L min^{-1} and requires an *L/G* of 8.9 where as an in-series design has a maximum treatment capacity of 1 L min^{-1} and requires an *L/G* of 8.9. To reach a 1 L min^{-1} treatment capacity, in-parallel operation would require 20 modules, in-series operation can achieve the same treatment capacity with a 60% reduction in absorber number and a 91% reduction in absorbent flow. In practice, further refinement in the economics can be realised with transverse flow due to an enhancement in mixing (Chapter 3), and an increase in fibre number (equal to modules in parallel) and an increase in fibre length (equal to an increase in modules in series), which would inevitably simplify module specification. Due to the reduction in process scale, and relatively low cost of the membrane material [23,24], a duty-standby system could be implemented to ensure 100% asset availability. Typical availability in absorption columns stands at 95% [16], at a site producing 3,400 m^3 h^{-1} raw biogas, the 5% is valued at 0.3 M £ y^{-1}, additional revenue that could cover the cost of installation.

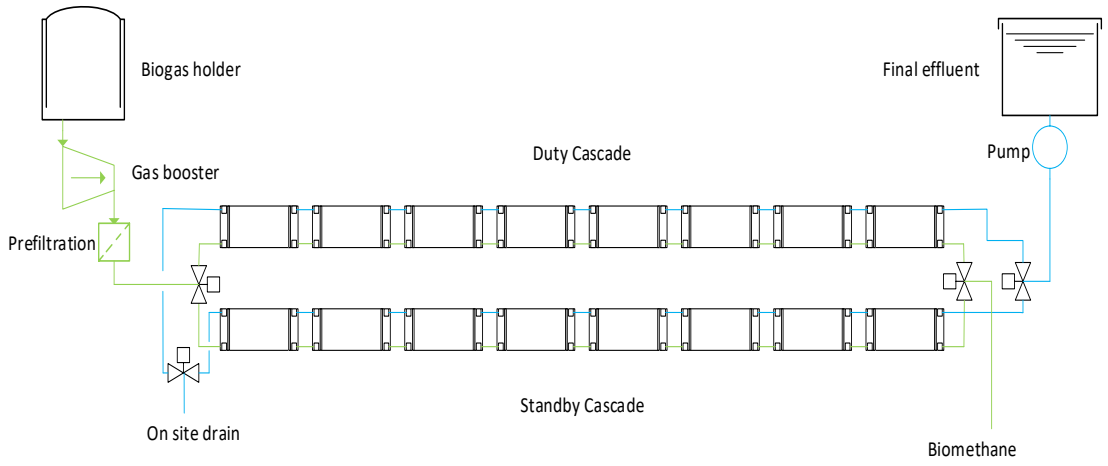

Figure 7.1 Process design, including duty standby for physical absorption in an HFMC cascade.

When transitioning to a CO_2–NH_3–H_2O system, the in-series design detailed in Table 7.1 could be expected to experience an enhancement factor to mass transfer of 4 (Chapter 5) at Q_L of 0.8 L min^{-1}, reducing the needed NTU from 8 to 2, a significant reduction in process scale and capital investment (Figure 7.2). Within transverse modules applied at scale, the primary resistance to mass transfer lies in the liquid-phase (Chapter 3) when applying a physical absorbent. On transition to chemical enhancement the liquid phase resistance to mass transfer is reduced however previous literature has demonstrated the gas-phase contribution to remain similar [23–25] with estimation of the enhancement factor being well described by the Hatta number providing complete CO_2 capture is not achieved i.e. η_{CO2} ≤0.98 (Chapter 5), ensuring a consistent contribution of the gas-phase to overall resistance to mass transfer. The co-production of high purity methane and NH_4HCO_3 necessitates a two-module arrangement to maintain a high solvent loading rate for crystallisation and a low solvent loading rate to enable maximum mass transfer and hence gas quality (Chapter 5), with an upfront crystallising membrane exploiting the elevated CO_2 partial pressure present in untreated biogas to maintain higher rates of mass transfer whilst an independent recycling absorbent reservoir ensures the 0.6 CO_2/NH_3 loading ratio required for precipitation can be quickly met. The purity membrane employs a second larger recycling absorbent reservoir to ensure a low CO_2/NH_3 loading ratio to maintain a concentration gradient against the reduced CO_2 partial pressure in the partially treated biogas without losing absorbed CO_2. At the point of crystallisation, the crystallising membrane is removing negligible carbon dioxide from the gas stream (Chapter 5). To achieve removal in the example system, two purity membranes would be required, for a total membrane cascade of 3 modules. The cascade could be reduced to two modules by limited pressurisation in the purity module.

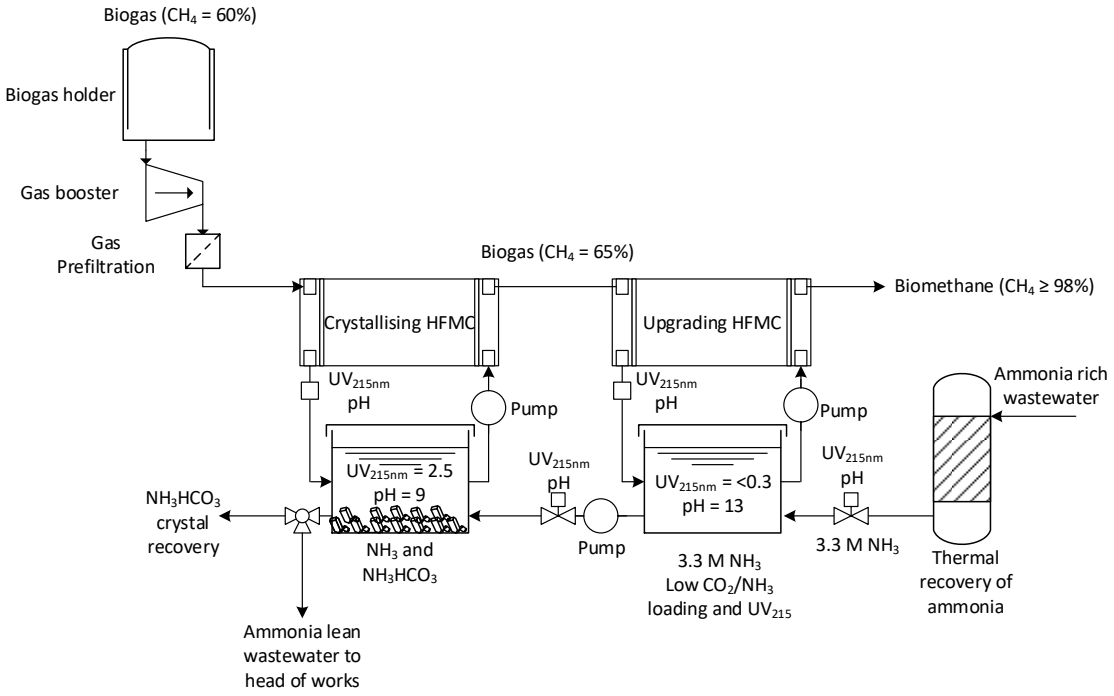

Figure 7.2 Process design for the co-production of high a high purity methane gas product and recovery of ammonium bicarbonate.

3. How should the membrane system be operated?

Recovered ammonia represents a sustainable endogenous source of chemical enhancement [14] that because of continuous production obviates the specific heat demand of 0.55 kWh Nm^{-3} biogas [17] of traditional chemically enhanced absorption columns. Without the additional heat demand, chemically enhanced absorption columns would have the lowest specific investment cost of commercial upgrading technologies [16,17] however are susceptible to process blocking if applied as crystallising reactors (Chapter 5). Should HFMC be implemented at an existing biogas upgrading facility, the transition from absorption columns would enable the current desorption column for CO_2 rich water regeneration to be applied for the thermal stripping of ammonia from return liquor, equivalent in process complexity. Bavarella [26] considering a WWTW that treats 500,000 m^3 d^{-1} influent (50 gH_4^+-N m^{-3}) and produces 3,400 m^3 h^{-1} raw biogas (60/40 CH_4/CO_2), demonstrate that the heat demand for thermal stripping can be met by available on-site heat. The process has the potential to recover 25,000 kg of N, with a biogas treatment capacity of 100,000 m^3, more than the 3,400 m^3 h^{-1} raw biogas produced. The value of produced biogas under current practices, (scenario 1) is given in Table 7.3 as 16.2 M £ y^{-1}. However, current generation WWTW require the maintenance of a nitrogen balance across the works to maintain biological process for the removal of

phosphates [23]. Partial nitrogen removal could be readily achieved from sludge return liquors (827 m^3 d^{-1} at 2kg NH_4-N m^{-3}), 1700 kg of nitrogen would be available, with a biogas treatment capacity of 280 m^3 h^{-1}. Once integrated into the crystallising-purity cascade, careful control of the crystallising reaction volume at a 0.6 CO_2/NH_3 loading ratio through in-line UV_{215} absorbance and continued feed of partially saturated absorbent from the purity module would facilitate process control [26]. Ammonia recovered from the return liquors would be fed to the purity module, maintaining a minimal UV_{215} absorbance.

The inclusion of a desorption unit in absorption columns can lead to biological and inorganic fouling through contacting solubilised H_2S with air leading to oxidation to elemental sulphur, whilst bacterial colonisation can be seeded by the strip gas in the desorption unit [22]. Removal of the desorption step in favour of NH_4HCO_3 recovery in HFMC reduces the risk of process fouling. This thesis has demonstrated that biological fouling from the liquid phase (Chapter 5) is the primary mechanism behind the loss of membrane function with time but demonstrated readily recoverable by chemical cleaning. Fouling prevention might be further achieved by the ammonia absorbent itself, by inducing alkaline hydrolysis and electrostatic repulsion by raising pH above the isoelectric point [28]. Ammonia has previously demonstrated a 90% performance recovery of reverse osmosis membranes fouled by whey protein [29] and apple juice [30] with a 2 mol L^{-1} NH_3 solution evidencing bacteriostatic properties in ammonia resistant bacteria [31]. In this fashion ammonia could act to both enhance rates of mass transfer and as chemical cleaning agent, increasing asset availability

4. What is the perceived value of the end products?

Value recovery mechanisms are considered in Table 7.2 for an example WWTW that treats 500,000 m^3 d^{-1} influent. Technology type (HFMC or columns) is not considered as capital and operational costs universally favour HFMC over absorption columns. Direct government incentivisation through the Renewable Heat Incentive (RHI) offers greatest recovery value, however due to tariff regression the mechanism by 2018 lost 28% of its value over 2014. In addition the guarantee for large scale plants ends 31st December 2019 [32], increasing risk beyond 2019. An alternative mechanism is available through the Renewable Transport Fuel Obligation (RTFO) where Renewable Transport Fuel Certificates (RTFC) are awarded per kg of renewable fuel (biomethane) produced. The mechanism awards 1.9 RTFC for biomethane and further doubling to 3.8 RTFC for the

use of a source of waste, yielding an annual value comparable to that of 2018 RHI tariff values (Table 7.1).

Table 7.2. Value recovery mechanisms for an annual energy production of 1.73 x10^8 kWh y^{-1} (3,400 m^3 h^{-1} Biogas)

Source of Value	Value	Unit	Reference	Value (M £ y^{-1})
Ammonium Bicarbonate (AB)[a]	9	p kg^{-1}	[36]	2.5
Ammonium Aeration Saving (AAS)[b]	31.8	p kg N^{-1}	[14]	2.9
Network Gas Value (NGV)	1.6	p kWh^{-1}	[37]	2.8
RHI Value (2014)	7.77	p kWh^{-1}	[38]	13.4
RHI Value (2018)	5.6	p kWh^{-1}	[38]	9.7
RTFO (2018) [c]	5.5	p kWh^{-1}	[39]	9.5
CfD (2nd allocation round)[d]	11.5	p kWh^{-1}	[40]	7.9

[a] Assumes 100% NH_4 use (3.3 mol NH_3 L^{-1}), where 1.5mol NH_3 L^{-1} saturated absorbent leaves the upgrading system and is redirected towards aeration due to NH_4HCO_3 solubility limit [41]
[b] Aeration cost based on nitrification demand using 4.34 kgO_2 kgN^{-1}, oxygen transfer efficiency 15%, water depth 5 m [14]
[c] 1 RTFC kg^{-1} valued at 20p with biomethane entitled to 1.9 RTFC, with a two-fold multiplier for energy production from waste (3.8 RTFC total) [39]
[d] Assumes an electrical conversion efficiency of 40% during CHP generation [42]

However, RTFO obviates revenue value from wholesale gas values arising from the sale of biomethane in the national gas network. Value recovery scenario 4 (Table 7.3) demonstrates a 30% value reduction relative to a 2018 RHI tariff recovery mechanism (scenario 3). Short term investment projects would favour RHI. However, the RTFO requires that fuel suppliers provide 12.4% of their fuel from renewable means by 2032, with a reduction from 4% in 2018 to 2% in 2032 of the proportion provided by food crops, increasing the proportion provided from waste. The long-term availability of the mechanism minimises risk and encourages investment in biogas upgrading technology. Sale of ammonium bicarbonate as an industrial fertiliser has been demonstrated in China [33] where market regulation stipulates that ammonium bicarbonate should contain 17% N with less than 5% hygroscopic water to qualify as a commercial product [29]. However, the poor physical properties of the ammonium bicarbonate powder result in a tendency to cake, this is overcome by pressing the powder into pills, imparting stability and crush resistance [34]. In such a form, the pills might be controllably blended into digestate sold to farmers to enable precise control of the nitrogen load applied to land. The European Union ‘end of waste’ criteria stipulate that a fertiliser derived from waste retains the same status as the input material and cannot gain a CE marking [35]. However, the European commission has recently adopted a new Circular Economy Package where exemption from ‘end of waste’ criteria for Struvite and other recoverable phosphorous salts from waste is proposed on the basis of product purity [35], with the UK already allowing its

use as a fertiliser [35]. Bavarella [26] has previously demonstrated that ammonium bicarbonate formed from the reaction between CO_2 and ammonia thermally recovered from wastewater return liquors to be of good quality. As such, if ammonium bicarbonate were eligible under the same rules it would qualify for direct fertiliser use or as a component material for organo-material fertilisers [35].

Table 7.3 Value recovery scenarios for an annual energy production of 1.73 x10^8 kWh y^{-1} (3,400 m^3 h^{-1} Biogas)

Value Recovery Scenario	M £ y^{-1}	Net Gain (M £ y^{-1})
(1) 2014 RHI[1] + NGV[2]	16.2	0.0
(2) 2014 RHI + NGV + AAS[3] + AB[4]	21.6	5.4
(3) 2018 RHI + NGV	12.4	-3.7
(4) 2018 RTFO	9.5	-6.7
(5) 2018 RHI + NGV + AAS	15.3	-0.8
(6) 2018 RTFO + AAS + AB	14.9	-1.3
(7) 2018 RHI + NGV + AAS + AB	17.8	1.7
(8) CfD[5] + AAS + AB	13.3	-2.8

[1]Renewable Heat Incentive, [2]Network Gas Value, [3]Ammonium Aeration Saving, [4]Ammonium Bicarbonate, [5]Renewable Transport Fuel Obligation, [6]Contracts for Difference

The implementation of chemical enhancement through ammonia recovery offers significant value (Table 7.3). Scenario 2 considers retrofit at an existing biogas upgrading facility, the additional value of ammonia recovery increases the process value by 33%. From an implementation perspective, the repurposing of existing absorption or desorption processes for the thermal recovery of ammonia would minimise capital expenditure. Scenario 7 considering a new build facility, indicates that ammonia recovery and 2018 RHI tariff mechanisms could outperform current practices (Scenario 1) by 1.7 M £ y^{-1}, offering compensation for the reduction in RHI. This outperforms scenario 6, a new build facility recovering value through the RTFO. A final comparison is given in scenario 8, which considers electrical generation in combined heat and power (CHP) engines. The net gain for such a scenario is negative, however within the context of market regulation by the water services regulation authority, Ofwat [37] and the PR 19 emphasis on the role of future challenges, in particular to the environment, resilience, innovation and affordability [43], it gains value. The scenario facilitates on site production of sustainable renewable electricity, capable of powering the whole site assuming an upper energy consumption value of 2.07 kWh m^{-3} influent [44], generates excess waste heat during CHP operation utilisable in the thermal recovery of ammonia and enables electrical self-sufficiency. During implementation of the most cost-effective scenarios (1 and 7) it may be worth designing the processes with the intention to convert to scenario

8 should regulatory value increase. However, consistent across all scenarios is the net gain of 5.4 M £ y^{-1} enabled through incorporating an ammonium bicarbonate recovery system, such value will help extend the economic feasibility of biogas upgrading, ensuring longevity for the nascent biomethane market sector outside of government remuneration.

References

[1] A. Sengupta, P.A. Peterson, B.D. Miller, J. Schneider, C.W. Fulk, Large-scale application of membrane contactors for gas transfer from or to ultrapure water, Sep. Purif. Technol. 14 (1998) 189–200.

[2] E. Chabanon, D. Roizard, E. Favre, Modeling strategies of membrane contactors for post-combustion carbon capture: A critical comparative study, Chem. Eng. Sci. 87 (2013) 393–407.

[3] J.L. Li, B.H. Chen, Review of CO_2 absorption using chemical solvents in hollow fiber membrane contactors, Sep. Purif. Technol. 41 (2005) 109–122.

[4] B.W. Reed, M.J. Semmens, E.J. Cussler, Membrane contactors, in: R.D. Nobel, A.S. Stern (Eds.), Membr. Sep. Technol. Princ. Appl., Elsevier, 1995: pp. 467–498.

[5] S. Zhao, P.H.M. Feron, L. Deng, E. Favre, E. Chabanon, S. Yan, J. Hou, V. Chen, H. Qi, Status and progress of membrane contactors in post-combustion carbon capture : A state-of-the-art review of new developments, J. Memb. Sci. 511 (2016) 180–206.

[6] D. Albarracin Zaidiza, J. Billaud, B. Belaissaoui, S. Rode, D. Roizard, E. Favre, Modeling of CO_2 post-combustion capture using membrane contactors, comparison between one- and two-dimensional approaches, J. Memb. Sci. 455 (2014) 64–74.

[7] B. Belaissaoui, J. Claveria-Baro, A. Lorenzo-Hernando, D. Albarracin, E. Chabanon, C. Castel, S. Rode, D. Roizard, E. Favre, Potentialities of a dense skin hollow fiber membrane contactor for biogas purification by pressurized water absorption, J. Memb. Sci. 513 (2016) 236–249.

[8] E. Brunazzi, G. Nardini, A. Pagliani, An economical criterion for packed absorption column design, Chem. Biochem. Eng. Q. 15 (2002) 199–206.

[9] D. deMontigny, P. Tontiwachwuthikul, A. Chakma, Comparing the Absorption Performance of Packed Columns and Membrane Contactors, Ind. Eng. Chem. Res. 44 (2005) 5726–5732.

[10] D. deMontigny, A. Aboudheir, P. Tontiwachwuthikul, A. Chakma, Using a packed-column model to simulate the performance of a membrane absorber, Ind. Eng. Chem. Res. 45 (2006) 2580–2585.

[11] A. McLeod, B. Jefferson, E.J. McAdam, Quantifying the loss of methane through secondary gas mass transport (or 'slip') from a micro-porous membrane contactor applied to biogas upgrading, Water Res. 47 (2013) 3688–3695.

[12] V. Evren, T. Çağatay, A.R. Özdural, Carbon dioxide-air mixtures: Mass transfer in recycling packed-bed absorption columns operating under high liquid flow rates, Sep. Purif. Technol. 17 (1999) 89–96.

[13] J. Elhajj, M. Al-hindi, F. Azizi, A Review of the Absorption and Desorption Processes of Carbon Dioxide in Water Systems, Ind. Eng. Chem. Res. 53 (2014) 2–22.

[14] A. Mcleod, B. Jefferson, E.J. McAdam, Biogas upgrading by chemical absorption using ammonia rich absorbents derived from wastewater, Water Res. 67 (2014) 175–186.

[15] P. Shao, M. Dal-Cin, A. Kumar, H. Li, D.P. Singh, Design and economics of a hybrid membrane–temperature swing adsorption process for upgrading biogas, J. Memb. Sci. 413–414 (2012) 17–28.

[16] F. Bauer, C. Hulteberg, T. Persson, D. Tamm, Biogas upgrading – Review of commercial technologies, 2013. http://www.sgc.se/ckfinder/userfiles/files/SGC270.pdf.

[17] F. Bauer, T. Persson, C. Hulteberg, D. Tamm, Biogas upgrading - technology overview, comparison and perspectives for the future, Biofuels, Bioprod. Biorefining. 7 (2013) 499–511.

[18] E. Ryckebosch, M. Drouillon, H. Vervaeren, Techniques for transformation of biogas to biomethane, Biomass and Bioenergy. 35 (2011) 1633–1645.

[19] G. Kang, Z.P. Chan, S.B.M. Saleh, Y. Cao, Removal of high concentration CO_2 from natural gas using high pressure membrane contactors, Int. J. Greenh. Gas Control. 60 (2017) 1–9.

[20] B. Belaissaoui, E. Favre, Evaluation of a dense skin hollow fiber gas-liquid membrane contactor for high pressure removal of CO_2 from syngas using Selexol as the absorbent, Chem. Eng. Sci. 184 (2018) 186–199.

[21] V.Y. Dindore, D.W.F. Brilman, P.H.M. Feron, G.F. Versteeg, CO_2 absorption at elevated pressures using a hollow fiber membrane contactor, J. Memb. Sci. 235 (2004) 99–109.

[22] A. Håkansson, Preventing microbial growth on pall-rings when upgrading biogas using absorption with water wash, 2006. http://www.sgc.se/ckfinder/userfiles/files/SGC166.pdf.

[23] S. Boributh, S. Assabumrungrat, N. Laosiripojana, R. Jiraratananon, Effect of membrane module arrangement of gas-liquid membrane contacting process on CO_2 absorption performance: A modeling study, J. Memb. Sci. 372 (2011) 75–86.

[24] S. Boributh, W. Rongwong, S. Assabumrungrat, N. Laosiripojana, R. Jiraratananon, Mathematical modeling and cascade design of hollow fiber membrane contactor for CO_2 absorption by monoethanolamine, J. Memb. Sci. 401–402 (2012) 175–189.

[25] S. Boributh, S. Assabumrungrat, N. Laosiripojana, R. Jiraratananon, A modeling study on the effects of membrane characteristics and operating parameters on physical absorption of CO_2 by hollow fiber membrane contactor, J. Memb. Sci. 380 (2011) 21–33.

[26] S. Bavarella, Chemically reactive membrane crystallisation reactor for CO_2 separation and ammonia recovery, PhD thesis, Cranfield University, 2018.

[27] T. Yamashita, R. Yamamoto-Ikemoto, Nitrogen and phosphorus removal from wastewater treatment plant effluent via bacterial sulfate reduction in an anoxic bioreactor packed with wood and iron, Int. J. Environ. Res. Public Health. 11 (2014) 9835–9853.

[28] X. Shi, G. Tal, N.P. Hankins, V. Gitis, Fouling and cleaning of ultrafiltration membranes: A review, J. Water Process Eng. 1 (2014) 121–138.

[29] S.S. Madaeni, Y.M. Mansourpanah, Chemical cleaning of reverse osmosis membranes fouled by whey, Desalination. 161 (2004) 13–24.

[30] S.S. Madaeni, A. Sasanihoma, S. Zereshki, Chemical cleaning of reverse osmosis membrane fouled by apple juice, J. Food Process Eng. 34 (2011) 1535–1557.

[31] T. Müller, B. Walter, A. Wirtz, A. Burkovski, Ammonium toxicity in bacteria, Curr. Microbiol. 52 (2006) 400–406.

[32] Department for Business Energy & Industrial Strategy, The Renewable Heat Incentive: A Reformed Scheme, 2016. https://www.gov.uk/government/uploads/system/uploads/attachment_data/file/577024/RHI_Reform_Government_response_FINAL.pdf.

[33] A. Bouwman, L.J. Boumans, Estimation of global NH_3 volatilization loss from synthetic fertilizers and animal manure applied to arable lands and grasslands, Glob. Biochem. Cycles. 16 (2002) 1–11.

[34] C.-K. Li, R.-Y. Chen, Ammonium bicarbonate used as a nitrogen fertilizer in China, Fertil. Res. 1 (1980) 125–136.

[35] D. Huygens, H. Saveyn, P. Eder, L. Delgado Sancho, DRAFT STRUBIAS Technical Proposals, 2017. https://phosphorusplatform.eu/images/download/STRUBIAS-draft-report-24-5-17-I.pdf.

[36] W.M. Budzianowski, Mitigating NH_3 vaporization from an aqueous ammonia process for CO_2 capture, Int. J. Chem. React. Eng. 9 (2011) 58–60.

[37] Ofgem, Wholse Sale Market Indicators, Whole Sale Price Trends. (2019). https://www.ofgem.gov.uk/data-portal/wholesale-market-indicators (accessed January 22, 2019).

[38] Ofgem, Non-Domestic RHI tariff rates, Non-Domestic RHI Tarif. Rates. (2018). https://www.ofgem.gov.uk/environmental-programmes/non-domestic-rhi/contacts-guidance-and-resources/tariffs-and-payments-non-domestic-rhi (accessed September 9, 2018).

[39] Department for Transport, Renewable Transport Fuel Obligation Annual Report 2012-13, (2013) 14. https://www.gov.uk/government/uploads/system/uploads/attachment_data/file/307437/impact-assessment-pir.pdf. (accessed January 22, 2019).

[40] BEIS, Contracts for Difference Second Allocation Round Results, (2017) 1–3. https://www.gov.uk/government/uploads/system/uploads/attachment_data/file/643560/CFD_allocation_round_2_outcome_FINAL.pdf. (accessed January 22, 2019).

[41] D. Sutter, M. Mazzotti, Solubility and Growth Kinetics of Ammonium Bicarbonate in Aqueous Solution, Cryst. Growth Des. 17 (2017) 3048–3054.

[42] D. Mikielewicz, J. Mikielewicz, A thermodynamic criterion for selection of working fluid for subcritical and supercritical domestic micro CHP, Appl. Therm. Eng. 30 (2010) 2357–2362.

[43] Ofwat, Delivering Water 2020 : Our final methodology for the 2019 price review, Birmingham, 2017. https://www.ofwat.gov.uk/publication/delivering-water-2020-final-methodology-2019-price-review/. (accessed January 22, 2019).

[44] Y. Gu, Y. Li, X. Li, P. Luo, H. Wang, X. Wang, J. Wu, F. Li, Energy Self-sufficient Wastewater Treatment Plants: Feasibilities and Challenges, Energy Procedia. 105 (2017) 3741–3751.

8 Conclusions and further work

8.1 Conclusions

The presented thesis has demonstrated a hollow fibre membrane contactor multi-module design for physical gas-liquid separation (biogas upgrading) with the potential to offer the same performance as current generation absorption columns with a 19-fold intensification factor, reducing CAPEX and OPEX. Further integration of ammonia as a chemically reactive absorbent and ammonium bicarbonate recovery is preferentially carried out in HFMC, enabling further intensification, cost reduction and ammonia recovery.

1. Mass transfer can be described as gas phase controlled when modules are configured for high gas product quality in a CO_2 containing binary gas. Consequently, a simplified mass transfer model, based on the overall mass transfer coefficient, can be used to determine gas product quality, process scale and membrane configuration for water scrubbing of CO_2 from biogas (Objective 1).

2. Configuring hollow fibre membrane contactors in series for binary gas separation is advantageous for capital cost, as an enhancement in mass transfer is evidenced that is greater than the sum of the membrane material added (Objective 1).

3. Mass transfer data can be translated across module scale when reconciling maldistribution with a description of parallel flow, representing a powerful tool for module sizing, the development of cascade design and choice of optimal operational set points at industrial scale (Objective 2).

4. Comparable CO_2 separation performance can be achieved for synthetic gas and industrial biogas which comprises of a more complex gas mixture, which simplifies considerations for scale-up (Objective 3).

5. The primary mechanism for HFMC fouling in biogas upgrading is a combination of biological adsorption and clogging of the shell-side, which is readily reversible through chemical cleaning (Objective 3).

6. The impact of a 3.3 mol L^{-1} NH_3 reactive absorbent on mass transfer enhancement is comparable between absorption columns and HFMC, however the development of a concentration gradient and explicitly a clearly defined counter-current concentration gradient at a well-defined membrane surface area encourages crystal growth over nucleation in HFMC (Objective 4).

7. Absorption columns as current generation gas-liquid contacting technology suffer process blocking at the point of NH_4HCO_3 crystallisation whereas multi-fibre HFMC can maintain continued crystallisation without suffering process blocking (Objective 4).

8. Employing a two-module cascade design, an initial crystallising module and secondary gas purity module can co-produce NH_4HCO_3 and a high purity gas product from biogas (Objective 4).

8.2 Further work

Areas where further research would be beneficial have been identified and summarised as follows:

1. In this work wetting was an issue, dense skin hollow fibre membrane contactors coat the microporous structure of an HFMC with a thin dense layer, eliminating direct phase contact. They have demonstrated remarkable resistance to wetting and the ability to withstand a high transmembrane pressure. Investigation into replacing HFMC contactors with dense skin HFMC may obviate the practical disadvantages of the current system. However, the impact of total phase separation imparted by a thin dense membrane barrier on controlled crystallisation at a micropore entrance needs to be investigated.
2. The mass transfer correlation developed in this study was applied to a single membrane material. However, membrane characteristics, such as pore size influence the nucleation rate and ammoniacal nitrogen recovery. To fully optimise the process, it may be necessary to specify a crystallising membrane material i.e. microporous hollow fibre and upgrading material resistant to wetting i.e. dense skin. To translate design, the impact of changing membrane material needs to be investigated with regards to predicting mass transfer and crystallisation.
3. Investigation into the scaling of the combined biogas upgrading & ammonium bicarbonate recovery system is required to ensure that continuous operation can be achieved over the long-term.
4. The viability of developing UV_{215nm} detection as a surrogate for bicarbonate concentration together with on-line pH for use as automatic process control in future industrial application needs investigation
5. Membrane assisted crystallisation has been undertaken with a synthetic biogas mixture, the impact of industrial biogas on the chemical composition of recovered crystalline precipitate remains unclear.

6. Ammonia solution was created in batch, investigation into the integration of a continual ammonia thermal ammonia recovery step into a continually operating system is required prior to commercialisation.